Durham E-Theses

Simplified Models and Effective Theories in Searches for New Physics

WANG, QI

Simplified Models and Effective Theories in Searches for New Physics

Qi Wang

A Thesis presented for the degree of

Doctor of Philosophy

Institute for Particle Physics Phenomenology

Department of Physics

University of Durham

England

February 2018

Dedicated to my parents

Simplified Models and Effective Theories in Searches for New Physics

Qi Wang

Submitted for the degree of Doctor of Philosophy

February 2018

Abstract

In this thesis two different types of effective field theories (EFTs) have been considered to give an interpretation to effects of physics beyond the Standard Model. The first type of EFT is a so-called Simplified Models, in which the Standard Model is extended by new scalar degrees of freedom A (CP-odd) and S (CP-eve), which give rise to interactions of the type $t\bar{t}S$ and $t\bar{t}A$ with subsequent decay of $S/A \to b\bar{b}$. We study the phenomenology of these processes at the LHC and find that the production of $t\bar{t}A$ is suppressed compared to that of $t\bar{t}S$. Using the Weyl-van-der-Waerden spinor formalism we analyse the helicity amplitudes in order to explain this phenomenon.

In the second part of this thesis, we focus on the dimension-six Standard Model Effective Field Theory (SMEFT) to calculate the next-to-leading order (NLO) electroweak corrections to the forward-backward asymmetry in the process $e^+e^- \to b\bar{b}$. We find that the NLO EFT corrections can not be neglected compared to the LO EFT contributions. We show that relevant numerical results have been obtained, which can be used to constrain the Wilson Coefficients involved in this process. We calculate the amplitude of the $Z \to b\bar{b}$ process and renormalise it together with the $e^+e^- \to b\bar{b}$ process. We have also analysed the NLO EFT corrections to the cross-section of the $e^+e^- \to b\bar{b}$ process, which can be used to set limits on the Wilson coefficients with future collider experiments.

Declaration

The work in this thesis is based on research carried out in the Institute for Particle Physics Phenomenology, Department of Physics at Durham University. No part of this thesis has been submitted elsewhere for any degree or qualification.

The work presented in Chapter 3 is part of the research undertaken by the author in collaboration with Matthew J. Dolan, Michael Spannowsky and Zhao-Huan Yu. The original work can be found in:

Determining the Quantum Numbers of Simplified Models in $t\bar{t}X$ production at the LHC

Matthew J. Dolan, Michael Spannowsky, Qi Wang, Zhao-Huan Yu

Phys. Rev. D 94, 015025

The work of Chapter 4 which involves NLO calculations of the forward-backward asymmetry in the dimension-six SMEFT framework. It was undertaken by the author in collaboration with Rhorry Gauld, Michael Spannowsky and Ben Pecjak. The results have not been published on the date of submission of this thesis.

Acknowledgements

I have had a very memorisable time during the past few years in which I carried on my research work included in this thesis. The words are always too limited to express the human emotions and feelings. There are too many people I want to thank in a short acknowledgement.

First and foremost I offer my sincerest gratitude to my supervisor, Michael Spannowsky, who has guided me and encouraged me during my PhD period with his rich knowledge and patience. What's more, the freedom he gave me that allow me to work in my own way is very precious. I would also like to thank Ben Pecjak and Rhorry Gauld, who provided me a lot of help in my research. All the people in IPPP are very nice and they deserve my regards.

Special thanks to my friends Yang Lei, Xin Tang, Yan Xu and Ye-Ling Zhou for friendship and accompany, and all the good memories. Finally, I want to thank my parents who allow me to pursue my degree in a foreign country especially in the hard times.

Contents

List of Figures

List of Tables

Chapter 1

An introduction to the Standard Model of particle physics

1.1 Gauge Symmetries and Lagrangian

The Standard Model of particle physics (SM) describes the fundamental fields and forces in the framework of quantum field theory (QFT) [1–3]. In realistic field theories, the laws of physics can be expressed in terms of a least-action principle. The symmetry principle requires the action of a field to remain unchanged under certain transformations. As a relativistic theory, the Lagrangian should be invariant under Lorentz transformations. As a result, the laws of conservation of momentum and energy can be obtained through Noether's theorem [4].

For a free matter field (fermion) the Lagrangian include a mass and kinetic term. It can be written as

$$L_0 = \bar{\psi} \left(i\slashed{\partial} - m \right) \psi, \tag{1.1.1}$$

where $\slashed{\partial} = \gamma^\mu \partial_\mu$. It can be easily verified that this Lagrangian is a scalar under Lorentz transformations. The relativistic wave equation for all fermion fields, known as the Dirac equation, can be deduced from the Euler-Lagrange equation directly. If we impose an additional global symmetry $U(1)$ on a Dirac field, the Lagrangian should be invariant under a phase transformation

$$\psi(x) \rightarrow \psi' = e^{iq\theta}\psi\left(\mathrm{x}\right), \tag{1.1.2}$$

where q is a constant factor which can be different for different types of particles. According to Noether's theorem, associated with this global symmetry, there should be a conserved current $\boldsymbol{j}^\mu = q\bar{\psi}\gamma^\mu\psi$ and a corresponding constant charge $Q = \int d^3x\ \boldsymbol{j}^0$. In Quantum electrodynamics (QED), a gauge or local symmetry $U(1)$ is required. Similar to the global case, the transformation of a local $U(1)$ symmetry could be expressed as

$$\psi(x) \to \psi' = e^{iq\theta(x)}\psi(x),\tag{1.1.3}$$

where the phase $\theta(x)$ is no longer a constant but a function of the space-time coordinate. Under this local transformation, the Lagrangian 1.1.1 is no longer a scalar. To keep the Lagrangian invariant locally, the derivative in the kinetic term has to be replaced by a covariant derivative

$$\partial_\mu \to \mathrm{D}_\mu = \partial_\mu + ieqA_\mu,\tag{1.1.4}$$

where a auxiliary gauge field $A_\mu(x)$ is introduced. Under this local symmetry, the gauge field $A_\mu(x)$ transforms like

$$\mathrm{A}_\mu(x) \to \mathrm{A}_\mu(\mathrm{x})' = \mathrm{A}_\mu(x) - \frac{1}{eq}\partial_\mu\theta(x).\tag{1.1.5}$$

The introduction of the covariant derivative will give birth to a interaction term in the Lagrangian:

$$L_{\mathrm{int}} = -eq\bar{\psi}\gamma^\mu\psi A_\mu,\tag{1.1.6}$$

in which e and q is respectively the interaction coupling and the charge. The gauge field $\mathrm{A}_\mu(x)$ is thus deemed as the force carrier that mediates the interaction under the local $U(1)$ symmetry. A complete Lagrangian should include all possible terms that obey the symmetry principle. In the local $U(1)$ case, a gauge invariant kinetic term of the gauge field should be included into the Lagrangian. The complete Dirac Lagrangian with interactions reads:

$$L_0 = \bar{\psi}(i\slashed{D} - m)\psi - \frac{1}{4}\mathrm{F}_{\mu\nu}\mathrm{F}^{\mu\nu},\tag{1.1.7}$$

where $\slashed{D} = \gamma^\mu\mathrm{D}_\mu$ and the field strength tensor $\mathrm{F}_{\mu\nu} = \partial_\mu A_\nu - \partial_\nu A_\mu$. Note that the mass term of the gauge field is not included in 1.1.7, as such a term will break the $U(1)$ local symmetry:

$$\frac{1}{2}M_A^2 A_\mu A^\mu \to \frac{1}{2}M_A^2(A_\mu - \frac{1}{eq}\partial_\mu\theta)(A^\mu - \frac{1}{eq}\partial^\mu\theta) \neq \frac{1}{2}M_A^2 A_\mu A^\mu.\tag{1.1.8}$$

In the $U(1)$ example, as shown above, the requirement of gauge symmetry brings interactions to the theory. Actually, this feature holds for all gauge symmetries, which explains why symmetry principles play a core role in QFT. The property of gauge symmetries can be described by group theory concepts. A general gauge symmetry group G is an N-dimensional compact Lie group:

$$\omega \in G, \ \omega_a(\theta) = e^{-iT_a\theta^a(x)}, \ a = 1, 2, ...N, \tag{1.1.9}$$

in which, $\theta^a(x)$ is a real number, and the hermitian quantity T_a is the generator of the group. The number of generators in this Lie group is $N^2 - 1$. These generators obey the Lie algebra

$$[T_a, T_b] = if_{abc}T_c, \tag{1.1.10}$$

where f_{abc} is named as the structure constant. If $f_{abc} = 0$, the group is abelian, otherwise it is non-abelian. In a gauge field theory, every field must belong to a certain representation of the gauge group. In QED, the Dirac field transforms in the fundamental representation of $U(1)$. In a general non-abelian $SU(N)$ gauge theory, corresponding to N generators, N auxiliary gauge fields need to be introduced to retain the gauge symmetry invariance. We denote each gauge field as $\mathbf{A}_\mu^a$, where $a = 1, 2, ...N$. Neglecting the coupling and charge, the associated gauge covariant derivative can be defined as

$$D_\mu\psi = \partial_\mu\psi + igA_\mu\psi, \tag{1.1.11}$$

where $A_\mu = \mathbf{A}_\mu^a \cdot T_a$ and g is the coupling constant. Under the gauge transformation, the covariant derivative transforms as

$$D_\mu\psi(x) \to \omega(x)D_\mu\psi(x), \tag{1.1.12}$$

and A_μ has to transform homogeneously as

$$A_\mu \to A'_\mu = \omega A_\mu \omega^{-1} - i\frac{1}{g}\omega\partial_\mu\omega^{-1} \tag{1.1.13}$$

to make sure that the covariant derivative transforms correctly. In the first term of 1.1.13, we recognize that the gauge field transforms according to the adjoint representation of $SU(N)$.

The non-abelian gauge theory is known as Yang-Mills theory [5]. The Lagrangian including the covariant derivative is also called the Yang-Mills Lagrangian. We denote a generic $SU(N)$ gauge field as W_μ^i, then the Lagrangian can be written as

$$L_{\text{YM}} = -\frac{1}{4} F_{\mu\nu}^a F^{a,\mu\nu}, \tag{1.1.14}$$

where the eld strength tensor $F_{\mu\nu}^a$ is given by

$$F_{\mu\nu}^a = \partial_\mu W_\nu^a - \partial_\nu W_\mu^a + g f_{abc} W_\mu^b W_\nu^c. \tag{1.1.15}$$

After the expansion, the Yang-Mills Lagrangian can be divided into three parts:

$$
\begin{aligned}
L_{\text{kin}} &= -\frac{1}{4}(\partial_\mu W_\nu^a - \partial_\nu W_\mu^a)(\partial^\mu W^{a,\nu} - \partial^\nu W^{a,\mu}), \\
L_{\text{cubic}} &= -\frac{1}{2} g f_{abc}(\partial_\mu W_\nu^a - \partial_\nu W_\mu^a) W^{b,\mu} W^{c,\nu}, \\
L_{\text{quartic}} &= -\frac{1}{4} g^2 f_{abe} f_{cde} W_\mu^a W_\nu^b W^{c,\mu} W^{d,\nu},
\end{aligned}
\tag{1.1.16}
$$

where L_{cubic} and L_{quartic} are self-interaction terms. Such terms do not exist in abelian gauge theories.

Now we are ready to write down all symmetry groups in the Standard Model, which are

$$U(1)_Y \otimes SU(2)_L \otimes SU(3)_c, \tag{1.1.17}$$

where the subscript Y represents the hyper charge, L refers to the left-handed chiral component, and c stands for color. The $U(1)_Y$ is a an abelian group, while $SU(2)_L$ and $SU(3)_c$ are non-abelian groups. It needs to be emphasized that the left-handed and right-handed components of fermions are treated differently in the Standard Model. For a fermion field ψ, chiral fields could be obtained through the projection operators as

$$\psi_L = P_L \psi = \frac{1 - \gamma^5}{2} \psi, \quad \psi_R = P_R \psi = \frac{1 + \gamma^5}{2} \psi, \tag{1.1.18}$$

in which, ψ_L is a doublet under $SU(2)_L$ transformations with an isospin charge $I = \frac{1}{2}$, while ψ_R is a singlet with $I = 1$. Using the property of these projection operators, it is easy to verify that

$$\bar{\psi}_L \psi_L = \bar{\psi}_R \psi_R = 0. \tag{1.1.19}$$

The fermion mass term can then be expressed in the helicity states:

$$-m_f \bar{\psi}\psi = -m_f \left(\bar{\psi}_R + \bar{\psi}_L\right)\left(\psi_L + \psi_R\right) = -m_f \left(\bar{\psi}_R \psi_L + \bar{\psi}_L \psi_R\right), \tag{1.1.20}$$

which are not invariant under the gauge transformation of $SU(2)_L$. As a consequence, all fermions in the gauge field theory have to be massless, which is obviously not confirmed by experimental observation. However, the problem can be solved through the Higgs Mechanism, which will be introduced in 1.2.

Applying the knowledge of abelian and non-abelian gauge theories, we can write down the Yang-Mills part of the Standard Model Lagrangian:

$$\begin{aligned}
L_{\text{gauge}} = &-\frac{1}{4}(\partial_\mu B_\nu - \partial_\nu B_\mu)(\partial^\mu B^\nu - \partial^\nu B^\mu) \\
&-\frac{1}{4}(\partial_\mu W_\nu^a - \partial_\nu W_\mu^a + g_2 f_{abc} W_\mu^b W_\nu^c)(\partial^\mu W^{a,\nu} - \partial^\nu W^{a,\mu} + g_2 f_{abc} W^{b,\mu} W^{c,\nu}) \\
&-\frac{1}{4}(\partial_\mu G_\nu^A - \partial_\nu G_\mu^A + g_s f_{ABC} G_\mu^B G_\nu^C)(\partial^\mu G^{A,\nu} - \partial^\nu G^{A,\mu} + g_s f_{ABC} G^{B,\mu} G^{B,\nu}),
\end{aligned} \tag{1.1.21}$$

where B_μ, W_μ^a $a = 1, 2, 3$ and G_μ^A $A = 1, 2, ...8$ are respectively associated with $U(1)_Y$, $SU(2)_L$ and $SU(3)_c$.

Corresponding to the three $SU(2)$ bosons, there are 3 generators $T^a = \frac{\sigma^a}{2}$, where the 2×2 matrices σ^a are Pauli matrices that are defined as:

$$\sigma^1 = \begin{pmatrix} 0 & 1 \\ 1 & 0 \end{pmatrix} \qquad \sigma^2 = \begin{pmatrix} 0 & -i \\ i & 0 \end{pmatrix} \qquad \sigma^3 = \begin{pmatrix} 1 & 0 \\ 0 & -1 \end{pmatrix}. \tag{1.1.22}$$

And in the $SU(3)$ case, $T^A = \frac{\lambda^A}{2}$, where the 3×3 matrices σ^A are Gell-Mann matrices [6] that are defined as:

$$\lambda^1 = \begin{pmatrix} 0 & 1 & 0 \\ 1 & 0 & 0 \\ 0 & 0 & 0 \end{pmatrix} \qquad \lambda^2 = \begin{pmatrix} 0 & -i & 0 \\ i & 0 & 0 \\ 0 & 0 & 0 \end{pmatrix} \qquad \lambda^3 = \begin{pmatrix} 1 & 0 & 0 \\ 0 & -1 & 0 \\ 0 & 0 & 0 \end{pmatrix}$$

$$\lambda^4 = \begin{pmatrix} 0 & 0 & 1 \\ 0 & 0 & 0 \\ 1 & 0 & 0 \end{pmatrix} \qquad \lambda^5 = \begin{pmatrix} 0 & 0 & -i \\ 0 & 0 & 0 \\ i & 0 & 0 \end{pmatrix} \qquad \lambda^6 = \begin{pmatrix} 0 & 0 & 0 \\ 0 & 0 & 1 \\ 0 & 1 & 0 \end{pmatrix} \tag{1.1.23}$$

$$\lambda^7 = \begin{pmatrix} 0 & 0 & 1 \\ 0 & 0 & -i \\ 0 & i & 0 \end{pmatrix} \qquad \lambda^8 = \begin{pmatrix} \frac{1}{\sqrt{3}} & 0 & 0 \\ 0 & \frac{1}{\sqrt{3}} & 0 \\ i & 0 & -\frac{2}{\sqrt{3}} \end{pmatrix}.$$

Recall that fermions live in the fundamental representation of the gauge symmetries. Specifically, all the left-handed fermions in the Standard Model, i.e. quarks and leptons, are doublets under $SU(2)_L$ transformations, and all the right-handed fermions are singlets. In the $SU(3)_c$ case, quarks are triplets while leptons do not take part in strong interactions governed by the $SU(3)_c$ symmetry. Accordingly, a quark and lepton field transforming under $SU(2)_L$ can be separately expressed as

$$Q_L = \begin{pmatrix} u_L \\ d_L \end{pmatrix}, \quad u_R, d_R \qquad L_L = \begin{pmatrix} \nu_L \\ e_L \end{pmatrix}, \quad e_R. \qquad (1.1.24)$$

According to the Standard Model, there are three generations of fermions, each generation contains two types of quarks and two types of leptons as shown in 1.1.24. We write down the three generations fields as follows:

$$\begin{pmatrix} u_L \\ d_L \end{pmatrix}, \quad u_R, d_R \qquad \begin{pmatrix} c_L \\ s_L \end{pmatrix}, \quad c_R, s_R \qquad \begin{pmatrix} t_L \\ b_L \end{pmatrix}, \quad t_R, b_R$$

$$\begin{pmatrix} \nu_L^e \\ e_L \end{pmatrix}, e_R \qquad \begin{pmatrix} \nu_L^\mu \\ \mu_L \end{pmatrix}, \quad \mu_R \qquad \begin{pmatrix} \nu_L^\tau \\ \tau_L \end{pmatrix}, \quad \tau_R. \qquad (1.1.25)$$

The electric charges are different for the two fermions in each generation, and their masses can be different as well. The mass gap between fermions in different generations is very large. Unfortunately, The Standard Model does neither provide an answer to the existence of three chiral generations nor to the mass gap between different generations.

Note that there is no ν_R term that represents the right-handed neutrino in 1.1.25, since in the Standard Model the right-handed neutrino does not exist. However, according to neutrino oscillation experiments, the three neutrinos should have very small masses. New methods like the so-called seesaw mechanism have been introduced in order to solve this problem [7]. However, the details of such mechanisms would not be introduced in this thesis, since they are not important to our work.

All gauge fields mentioned above are Lorentz invariant, which means one can not a Lorentz gauge transformation on a gauge field can not affect the physical state of the gauge field. For example, in QED we can take the gauge Lagrangian

$$L_{gauge} = -\frac{1}{4} F_{\mu\nu} F^{\mu\nu} - \frac{1}{2\xi} (\partial_\mu A^\mu)^2 \qquad (1.1.26)$$

According to the Lorentz gauge condition [8], $\partial_\mu A^\mu = 0$. As a result, we can choose the value of ξ arbitrarily. Different choices of ξ lead to different "gauges". Specifically, $\xi = 0$ refers to "Landau Gauge" and $\xi = 1$ is called "Feynman Gauge". Another common choice $\xi \to \infty$ is known as "Unitary Gauge".

Until now we have introduced all the gauge symmetries in the Standard Model and obtained the associated Lagrangian. In QFT, by computing the correlation functions, one can translate the Lagrangian into Feynman rules that can be directly used to calculate the probability amplitudes order by order in perturbation theory.

1.2 Spontaneous Symmetry Breaking and Electroweak Theory

In the Standard Model, the $U(1)_Y \otimes SU(2)_L$ gauge theory provides a unified description for the electromagnetic and weak interactions. However, these symmetries must be broken through some physical mechanism to generate the masses of fermions and gauge bosons. According to the Standard Model, such a mechanism is known as Higgs mechanism [9]. As shown in 1.1, mass terms in the Yang-Mills Lagrangian would break gauge symmetries. The solution provided by the Higgs mechanism is to introduce a new complex scalar field which Lagrangian is $U(1)_Y \otimes SU(2)_L$ invariant, but with a non-zero vacuum expectation value that is not invariant under the gauge symmetry, so that the electroweak symmetry would be broken spontaneously. The process is thus called spontaneous symmetry breaking. Obeying the symmetry principle, under the $SU(2)_L$ transformation, the complex scalar field must be a doublet:

$$H = \begin{pmatrix} \phi^+ \\ \phi^0 \end{pmatrix}, \tag{1.2.27}$$

where ϕ^+ and ϕ^0 are a charged and neutral goldstone boson respectively. And the Higgs potential for this complex scalar field is

$$V(H) = -\mu^2 H^\dagger H + \lambda(H^\dagger H)^2, \tag{1.2.28}$$

where μ and λ are positive real numbers. Using the Euler-Lagrange equations, we can obtain the Klein-Gordon equation for the free scalar field. It can be verified

that the minimum of this potential is not at $\langle H \rangle = 0$, but at the point $\langle H \rangle = \frac{v}{\sqrt{2}} = \sqrt{\frac{\mu^2}{2\lambda}}$. Since this potential depends only on the product $H^+ H$, any global phase transformation on H will not affect the physical result. Therefore, one can rotate the direction of the Higgs doublet arbitrarily. For convenience, a special choice for the direction is adopted, where the vacuum expectation value (vev) of the Higgs doublet can be written as

$$\langle 0|H|0 \rangle = \frac{1}{\sqrt{2}} \begin{pmatrix} 0 \\ v \end{pmatrix}. \tag{1.2.29}$$

$\phi^+ \phi^- = 0$ has been used to deduce 1.2.29, which means that in this direction choice, the vev of the charged scaler is 0, while the neutral scalar ϕ^0 obtains a non-zero vev. Thereby the generic form of Higgs doublet can be expressed as

$$H = \frac{1}{\sqrt{2}} \begin{pmatrix} \phi^+ \\ h + v + i\phi^0 \end{pmatrix}, \tag{1.2.30}$$

in which $\phi^\pm$ and ϕ^0 are known as goldstone fields. In 1.2.30, the vev is extracted from the original neutral scalar ϕ^0, and ϕ^0 is split into a real part and an imaginary part, both of which has a zero vev. Due to the symmetry of the Higgs potential, we can express the Higgs doublet as a simple form without including the goldstone bosons in the unitary gauge:

$$H = \frac{1}{\sqrt{2}} \begin{pmatrix} 0 \\ h + v \end{pmatrix}, \tag{1.2.31}$$

where a special choice of direction has been made for the Higgs field, which violates three global initial symmetries of the Lagrangian, leaving only one remaining.

Now we are ready to write down the Higgs Lagrangian, which should include a kinetic term besides the potential term. The Lagrangian is

$$\mathrm{L_{Higgs}} = (\mathrm{D}_\mu H)^\dagger \mathrm{D}^\mu H - V(H), \tag{1.2.32}$$

where the covariant derivative D_μ is associated with the electroweak symmetry:

$$\mathrm{D}_\mu H = (\partial_\mu + ig_2 T^a W_\mu^a + ig_1 y_\psi B_\mu)H, \ a =, 1, 2, 3, \tag{1.2.33}$$

in which the gauge boson W_μ^a belongs to the $SU(2)_L$ representation and B_μ) belongs to the $U(1)_Y$ representation, and $y_\psi = \frac{1}{2}$ in the convention we adopt. After the expansion, we can express the kinetic term specifically as:

$$(\mathrm{D}_\mu H)^\dagger (\mathrm{D}^\mu H) = \frac{v^2}{8} \left| \begin{pmatrix} g_2 W_\mu^1 - i g_2 W_\nu^2 \\ -g_2 W_\mu^3 - i g_1 B_\nu \end{pmatrix} \right|^2 \qquad (1.2.34)$$

$$= \frac{v^2}{8} \left[g_2^2 \left(W_\mu^{1,2} + W_\mu^{2,2} \right) + (g_2 W_\mu^3 - g_1 B_\mu)^2 \right].$$

Observing equation 1.2.34 more closely, we find that the kinetic term has been turned into a mass term. Consequently, we obtain three physical gauge bosons which are combinations of the original gauge bosons:

$$W_\mu^\pm \equiv \frac{1}{2}(W_\mu^1 \mp i W_\mu^2),$$
$$Z_\mu \equiv \frac{1}{\sqrt{g_1^2 + g_2^2}} \left(g_2 W_\mu^3 - g_1 B_\mu \right), \qquad (1.2.35)$$

where $W_\mu^\pm$ are charged bosons, while Z_μ^0 is a neutral boson. Their masses can be directly read off from 1.2.34, which are

$$M_W = \frac{g_2 v}{2}, \quad M_Z = \frac{v}{2} \sqrt{g_1^2 + g_2^2}. \qquad (1.2.36)$$

As expected, in the broken phase three non-physical massless Goldstone fields each with one degree of freedom disappear in the Lagrangian, while a real scalar Higgs field h with only one degree of freedom survives. The 3 non-physical degrees of freedom belonging to Goldstones are "eaten" by three massive gauge bosons: the $W^\pm$ and the Z, so that the total degrees of freedom remain unchanged. Besides the three massive bosons, there is still another physical massless boson, which is defined as

$$A_\mu \equiv \frac{1}{\sqrt{g_1^2 + g_2^2}}(g_1 W_\mu^3 + g_2 B_\mu). \qquad (1.2.37)$$

The relation between the physical bosons and the original bosons can be written in a more compact way in the matrix language as follow:

$$\begin{pmatrix} W_\mu^3 \\ B_\mu \end{pmatrix} = \begin{pmatrix} \cos\theta_w & \sin\theta_w \\ -\sin\theta_w & \cos\theta_w \end{pmatrix} \begin{pmatrix} Z_\mu \\ A_\mu \end{pmatrix}, \qquad (1.2.38)$$

where the rotation angle θ is known as the Weinberg angle [10] or the weak mixing angle. It is defined as

$$\cos\theta_w = \frac{g_2}{\sqrt{g_1^2 + g_2^2}}. \qquad (1.2.39)$$

The Weinberg angle is very important in electroweak physics, many observables are very sensitive to it, e.g., the forward-backward asymmetry that we will introduce in the next section in this chapter. In particle physics we tend to express quantities in terms of the observables that could be determined experimentally. In terms of the masses of bosons, the cosine of the Weinberg angle is expressed as

$$\cos\theta_w = \frac{M_W}{M_Z}. \tag{1.2.40}$$

So far, through the Higgs mechanism, gauge bosons have obtained their masses that are associated with the vacuum expectation value of Higgs field. If we check the symmetries after the above operation, we will find that the original symmetries are no longer obeyed strictly, while a new abelian symmetry $U(1)$ appears. It will be more clear if we write down the covariant derivative in terms of the new physical fields that are the eigenstates of the masses:

$$\begin{aligned}
\mathrm{D}_\mu = {} & \partial_\mu + ig_2\sin\theta_w(T^3 + Y)A_\mu - i\frac{g_2}{\cos\theta_w}\left(T^3 - g_2(T^3 + Y)\sin^2\theta_w\right)Z_\mu \\
& - ig_2\sqrt{2}(\frac{1}{2}(T^1 - iT^2)W_\mu^+ + \frac{1}{2}(T^1 + iT^2)W_\mu^-),
\end{aligned} \tag{1.2.41}$$

where Y is the Hyper charge, T^1, T^2 and T^3 is the first, second and third component of the weak isospin respectively. For convenience, we define $Q_f \equiv T^3 + Y$. In equation 1.2.41 Q_f plays exactly the role of a transformation phase factor of the $U(1)$ symmetry. To see that this $U(1)$ is still valid in the broken phase, we consider the following transformations

$$H \to H' = e^{i\alpha Q_f}H. \tag{1.2.42}$$

Note That

$$Q_f H = (T^3 + Y)H = \begin{pmatrix} 1 & 0 \\ 0 & 0 \end{pmatrix}\begin{pmatrix} 0 \\ v + h \end{pmatrix} = 0, \tag{1.2.43}$$

we can conclude that after spontaneous symmetry breaking, the system still has an abelian symmetry $U(1)$. This $U(1)$ symmetry turns out to be exactly the gauge symmetry $U(1)$ in QED, which governs the electromagnetic interactions. And the electric charge e in QED is expressed as $e = g\sin\theta_w$ in accordance with the electroweak theory. Correspondingly, Q_f is supposed to be the electric charge.

As shown above, in the electroweak theory, the Higgs mechanism yields the following symmetry breaking scheme:

$$U(1)_Y \otimes SU(2)_L \to U(1)_{\text{EM}}. \tag{1.2.44}$$

We now turn to investigate the behavior of fermions in the electroweak theory. The interaction term in the Lagrangian of a gauge field theory is obtained by imposing the covariant derivative on fermions. Taking a quark field q for example, the interaction term can be written as

$$\frac{g}{\sqrt{2}}(J^{-,\mu}W_\mu^+ + J^{+,\mu}W_\mu^-) + \frac{g}{\cos\theta_w}(J^{3,\mu} - \sin^2\theta_w J^{\text{EM},\mu})Z_\mu + eJ^{\text{EM},\mu}A_\mu, \tag{1.2.45}$$

in which we have made the following definitions:

$$\begin{aligned}
J^{\pm,\mu} &\equiv \bar{u}_L\gamma^\mu T^\pm d_L, \\
J^{3,\mu} &\equiv \bar{q}_L T^3 q_L = \bar{u}_L\gamma^\mu u_L - \bar{d}_L\gamma^\mu d_L, \\
J^{\text{EM},\mu} &\equiv \bar{q}T^3 q = \bar{q}\gamma^\mu Q_f q.
\end{aligned} \tag{1.2.46}$$

Both $J^{\pm,\mu}$ and $J^{3,\mu}$ are weak currents that only include the left-handed sector of q. $J^{\pm,\mu}$ describes a charged weak interaction and $J^{3,\mu}$ describes a neutral weak interaction. The other current in 1.2.46 is the electromagnetic current $J^{\text{EM},\mu}$ that includes both left-handed and right-handed fermions.

In 1.2.45 and 1.2.46, one finds that the left-handed and right-handed fermions are treated differently in $Zf\bar{f}$ interactions, since J^3 in this interaction only contains left-handed fermions. As a consequence, the left-handed and the right-handed couplings g_L and g_R are different as well. They are given as

$$\begin{aligned}
g_L &= \frac{T^3 - Q_f\sin^2\theta_w}{2\sin\theta_w\cos\theta_w} \\
g_R &= \frac{-Q_f\sin^2\theta_w}{2\sin\theta_w\cos\theta_w}.
\end{aligned} \tag{1.2.47}$$

We can express the $Zf\bar{f}$ couplings in terms of vector and axial-vector couplings g_V and g_A. The relations between the two types of couplings are

$$\begin{aligned}
g_V &= g_L + g_R, \\
g_A &= g_L - g_R.
\end{aligned} \tag{1.2.48}$$

The asymmetry of chiral couplings will obviously affect Z-boson phenomenology. The simplest example is a decay process $Z \to f\bar{f}$. In this process, an asymmetry named polarization asymmetry [11] arises, which is defined as

$$A_{\mathrm{LR}} = \frac{\Gamma_{Z \to f_L \bar{f}_R} - \Gamma_{Z \to f_R \bar{f}_L}}{\Gamma_{Z \to f_L \bar{f}_R} + \Gamma_{Z \to f_R \bar{f}_L}}. \tag{1.2.49}$$

In the lowest order of perturbative theory, this asymmetry can be directly expressed in terms of the chiral couplings:

$$A_{\mathrm{LR}}^{\mathrm{LO}} = \frac{g_L^2 - g_R^2}{g_L^2 + g_R^2}. \tag{1.2.50}$$

Another asymmetry named forward-backward asymmetry, arising from the same origin, will be discussed in Sec. 1.3.

Up to now, the origin of the fermion masses is still not introduced. In order to solve this problem, an interaction between the Higgs doublet H and a Dirac field Ψ known as Yukawa interaction was introduced into Electroweak theory [12]. Following the symmetry principle, terms like $\bar{\Psi}_L \Psi_R$ that break the gauge symmetry are forbidden in the Lagrangian. In general, the gauge invariant Yukawa Lagrangian can be constructed as follows:

$$L_{\mathrm{Yukawa}} = -\lambda_f \left[\bar{\Psi}_L H \Psi_R + \bar{\Psi}_R H^\dagger \Psi_L \right], \tag{1.2.51}$$

where λ_f is known the Yukawa coupling. Specifically, for leptons and quarks, the Yukawa Lagrangian after spontaneous symmetry breaking can be expressed as:

$$
\begin{aligned}
& -\lambda_d \left(\bar{u}_L \bar{d}_L \right) \frac{1}{\sqrt{2}} \begin{pmatrix} 0 \\ v + h \end{pmatrix} d_R - \lambda_d \left(\bar{u}_L \bar{d}_L \right) \frac{1}{\sqrt{2}} \begin{pmatrix} 0 \\ v + h \end{pmatrix} u_R \\
& -\lambda_l \left(\bar{\nu}_L \bar{e}_L \right) \frac{1}{\sqrt{2}} \begin{pmatrix} 0 \\ v + h \end{pmatrix} e_R.
\end{aligned}
\tag{1.2.52}
$$

After reduction, this Lagrangian takes the form

$$L_{\mathrm{Yukawa}} = -\frac{1}{\sqrt{2}} (v + h) \left(\lambda_d \bar{d}_L d_R + \lambda_u \bar{u}_L u_R + \lambda_l \bar{l}_L l_R \right), \tag{1.2.53}$$

in which we can clearly see the mass terms for leptons and quarks. Through the Yukawa couplings, every fermion f can obtain a mass

$$m_f = \lambda_f \frac{v}{\sqrt{2}}, \tag{1.2.54}$$

where λ_f is the Yukawa coupling constant of f. While the right-handed neutrino is an exception in the SM, its Yukawa-mass term is not forbidden by the electroweak theory. If right handed neutrinos do exist, they can also acquire a mass through Higgs-Yukawa couplings. It is worth to emphasize that besides mass terms, interaction terms like $-\lambda_d h \bar{d} d$ can be found in 1.2.53 as well.

In 1.2.54, the mixing between the three generations of quarks, as observed experimentally [13], is not taken into consideration for simplicity's sake. In fact, the mass eigenstates of quarks are not equal to the weak eigenstates, but connected via transformation matrix

$$
\begin{pmatrix} d' \\ s' \\ b' \end{pmatrix} = \begin{pmatrix} V_{(ud)} & V_{(us)} & V_{(ub)} \\ V_{(cd)} & V_{(cs)} & V_{(cb)} \\ V_{(td)} & V_{(ts)} & V_{(tb)} \end{pmatrix} \begin{pmatrix} d \\ s \\ b \end{pmatrix}, \tag{1.2.55}
$$

which is known as Cabibbo-Kobayashi-Maskawa matrix, or CKM matrix in short. The Yukawa couplings in this case are no longer numbers, but group into two 3×3 matrices: Y_u^{ij} and Y_d^{ij}, where $i, j = 1, 2, 3$. The masses of quarks are then obtained by diagonalising $Y_{u,d}^{ij}$. And the weak charged current for quarks appearing in 1.2.46 can be accordingly written in terms of these mass eigenstates:

$$
J^{\pm,\mu} = \bar{u}_L^i \gamma^\mu T^\pm V_{ij} d_L^j. \tag{1.2.56}
$$

This charged current couples to the $W^\mp$ in the Lagrangian. Physical processes due to this interaction will obviously violate the flavor symmetry since the $SU(2)_L$ doublets of quarks are no longer physical eigenstates. Similar mixing might exist in the lepton case. Actually, a mixing matrix known as Pontecorvo-Maki-Nakagawa-Sakata matrix for neutrinos had been introduced to explain neutrino oscillations [14].

1.3 Two Processes in Electroweak Physics

1.3.1 $e^+ e^- \to b\bar{b}$

The first scattering process in this section we consider is $e^+ e^- \to f\bar{f}$ whose diagram are shown in Fig. 1.1, in which the photon-mediated reaction and Z-mediated reaction are separately the basic process in QED and Electroweak Physics.
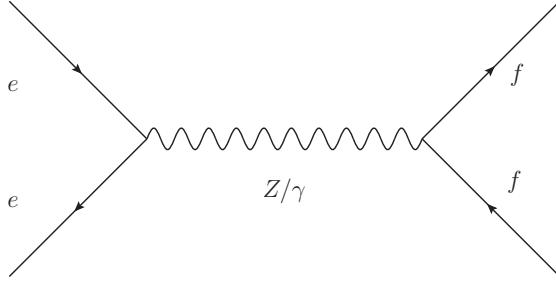
Figure 1.1 The tree-level diagram for $e^+e^- \to Z/\gamma \to ff$ reactions

In the Z-mediated case, the Vertex on the right side of this diagram is exactly the chiral coupling $Zf\bar{f}$ introduced in 1.1. In order to gain a deep understanding of this process, we need to calculate its polarised cross-section. This first step is to calculate the born amplitude for each reaction using the Feynman rules in helicity states. The trivial amplitude for each reaction is written respectively as

$$A_Z = \frac{\sqrt{2}G_F M_Z}{s - M_Z^2}[g_L^f \bar{f}_L \gamma \mu f_L + g_R^f \bar{f}_R \gamma \mu f_R][g_L^e \bar{e}_L \gamma \mu e_L + g_R^e \bar{e}_R \gamma \mu e_R],$$
$$A_\gamma = \frac{e^2}{s}[\bar{f}\gamma^\mu f][\bar{e}\gamma^\mu e],$$

(1.3.57)

where the chiral coupling constants g_L and g_R are adopted, and the G_F is the Fermi coupling constant which will be introduced in 1.3.2. Then the differential cross-sections can be obtained by calculating squared matrix elements. The result can be expressed in a compact form as:

$$\frac{d\sigma}{d\Omega}\left(e_L^- e_R^+ \to f_L \bar{f}_R\right) = \frac{\alpha}{4s}(1 + \cos\theta)^2|1 + rg_L^e g_L^f|^2,$$
$$\frac{d\sigma}{d\Omega}\left(e_L^- e_R^+ \to f_R \bar{f}_L\right) = \frac{\alpha}{4s}(1 - \cos\theta)^2|1 + rg_L^e g_R^f|^2,$$
$$\frac{d\sigma}{d\Omega}\left(e_R^- e_L^+ \to f_L \bar{f}_R\right) = \frac{\alpha}{4s}(1 - \cos\theta)^2|1 + rg_R^e g_L^f|^2,$$
$$\frac{d\sigma}{d\Omega}\left(e_R^- e_L^+ \to f_R \bar{f}_L\right) = \frac{\alpha}{4s}(1 + \cos\theta)^2|1 + rg_R^e g_R^f|^2,$$

(1.3.58)

where r is the ratio of coefficients of A_Z and A_γ, and σ is the scattering angle. Note that the ratio r has an imaginary part on the M_Z resonance due to the pole in the Z propagator. Combining all four possible helicity amplitudes and simplifying the formula, we have:

$$\frac{d\sigma}{d\Omega}(e^- e^+ \to f\bar{f}) = \frac{\alpha}{4s}[(A_0(1 + \cos\theta^2) + A_1\cos\theta],$$

(1.3.59)

in which $\alpha = e^2/4\pi$ is the famous fine structure constant, and we have defined

$$A_0 = 1 + 2\operatorname{Re}[r]\, g_V^2 + |r|^2(g_V^2 + g_A^2) \qquad\qquad A_1 = 4\operatorname{Re}[r]\, g_A^2 + 8|r|^2 g_A^2 g_V^2.$$
(1.3.60)

In order to obtain the total cross-section, one needs to perform an integration over the scattering angle θ. Note that the $\cos\theta$ term vanishes in the integration while the $\cos\theta$ term survives. As a consequence, the integration of the forward hemisphere would not be equal to the backward-hemisphere one. This difference leads to an asymmetry in collider detections, which is called as forward-backward asymmetry. It is defined as:

$$A_{\text{fb}} = \frac{\int_0^1 \frac{d\sigma}{d\Omega}d\Omega - \int_{-1}^0 \frac{d\sigma}{d\Omega}d\Omega}{\int_0^1 \frac{d\sigma}{d\Omega}d\Omega + \int_{-1}^0 \frac{d\sigma}{d\Omega}d\Omega}.$$
(1.3.61)

It is easy to verify that

$$A_{\text{fb}} = \frac{3A_1}{8A_0}.$$
(1.3.62)

At the low energy scale $s \ll M_Z^2$, the ratio $|r| \ll 1$, where the photon diagram dominates, the forward-backward asymmetry is small. However, near the Z resonance $s = M_Z^2$, where the Z diagram dominates, the asymmetry will be much bigger due to the small denominator in the propagator and should reach its maximum at the peak. The denominator gets smaller near the resonance, so the total amplitude gets bigger. Actually, A_{fb} was measured at The Large Electron-Positron Collider (LEP) on the M_Z resonance [15]. However, to calculate A_{fb} on the resonance the pole needs to be disposed, as is done in Breit-Wigner distribution formula [16].

Here we will introduce the Breit-Winger formula in a very physical way. For a stable massive particle that oscillates with a frequency in its rest frame, the on-shell time-depended wave function is

$$\psi(t) \propto e^{-ip_\mu x^\mu} = e^{-iMt},$$
(1.3.63)

where M is the mass of the particle. In this case, the probability to detect the particle is always 1 in the whole space. But for an unstable particle with the same mass, the probability of finding the particle will decrease exponentially according to its decay width Γ

$$\psi(t) \propto e^{-ip_\mu x^\mu} = e^{-iMt}e^{-i\Gamma\frac{t}{2}} = e^{-i(M - i\frac{\Gamma}{2})t},$$
$$P(\psi(t)) = |\psi(t)|^2 \propto e^{-\Gamma t},$$
(1.3.64)

In the equation 1.3.64, the unstable particle can been effectively deemed as having a "complex mass" $M - i\frac{\Gamma}{2}$, where the imaginary part is the decay width. In quantum field theory, a free stable "Z" boson propagator could be expressed in the momentum space as:

$$\frac{g_{\mu\nu}}{k^2 - M_Z^2}, \tag{1.3.65}$$

while the real Z boson is not stable, whose propagator can then be expressed as:

$$\frac{g_{\mu\nu}}{k^2 - (M_Z - i\frac{\Gamma}{2})^2} \approx \frac{g_{\mu\nu}}{k^2 - M_Z^2 - i\Gamma M_Z}. \tag{1.3.66}$$

And the cross-section for a relating process is proportional to its value squared:

$$\sigma \propto \frac{g_{\mu\nu}}{s - M_Z^2 - i\Gamma M_Z} \left(\frac{g^{\mu\nu}}{s - M_Z^2 - i\Gamma M_Z} \right)^* \propto \frac{1}{(s - M_Z^2)^2 - \Gamma^2 M_Z^2}. \tag{1.3.67}$$

Note that in the amplitude of $e^+ e^- \to f\bar{f}$, the propagator of Z boson is

$$\frac{1}{s - M_Z^2 - i\Gamma_Z M_Z}, \tag{1.3.68}$$

where Γ_Z is the decay width of Z boson.

In the Standard model, using the Breit-Winger formula, the forward-backward asymmetry at the Z peak can be written in terms of the polarization asymmetry in the $Z \to f\bar{f}$ process. It is

$$A_{fb} = \frac{3}{4} A_{LR}^e A_{LR}^f. \tag{1.3.69}$$

However, this feature does not hold in the Standard Model Effective Theory, which will be introduced in Chapter 2. The details of the next-to-leading order calculation of the forward-backward asymmetry for $e^+ e^- \to b\bar{b}$ on the M_Z resonance in the Standard Model will be given in Chapter 4. As one of the precision electroweak measurements, the forward-backward asymmetry is a very important experiment measurement that can test new physics beyond the Standard Model [17–19].

1.3.2 The Muon Decay

The other important reaction in this thesis are muon decay process $\mu^- \to e^- + \nu_\mu + \bar{\nu}_e$ which are related to the charged weak couplings. Through this reaction, the muon decay to the lightest massive lepton electron and two neutrinos. The decay of a muon

is a purely leptonic process which is very clean experimentally and theoretically, and thus can be measured very precisely. The tree-level diagram of this decay process in given in Fig. 1.2.
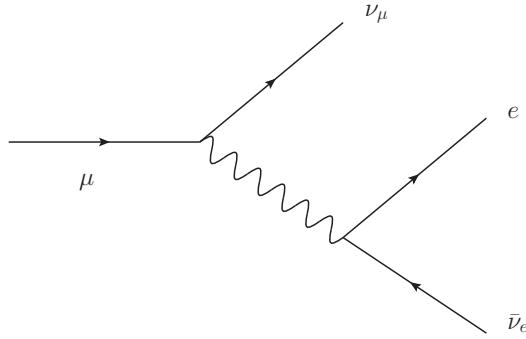
Figure 1.2 The tree level diagram for μ decay process in the Standard Model

According to the Feynman rules, we can obtain the Born amplitude:

$$A_W = -\frac{g^2}{8} \left(\bar{u}(\nu_e)\gamma^\mu \left(1 - \gamma^5\right) u(e^+) \right) \frac{-g_{\mu\nu}}{s - M_W^2} \left(\bar{u}(\bar{\nu}_\mu)\gamma^\nu \left(1 - \gamma^5\right) u(\mu^+) \right).$$
(1.3.70)

In the low transverse momentum region $s \ll M_W^2$, obviously the matrix element can be simplified as

$$A_W = -\frac{g^2}{8} \left(\bar{u}(\nu_e)\gamma^\mu(1 - \gamma^5)u(e^+) \right) \frac{g_{\mu\nu}}{M_W^2} \left(\bar{u}(\bar{\nu}_\mu)\gamma^\nu(1 - \gamma^5)u(\mu^+) \right),$$
(1.3.71)

in which case the whole process can be effectively viewed as a four-fermion interaction with a coupling constant

$$G_F = \frac{g^2}{4\sqrt{2}M_W^2}.$$
(1.3.72)

Actually, G_F is famously known as the Fermi Coupling Constant, which value can be determined very precisely by measuring the lifetime of the Muon, therefore the Fermi Coupling constant is usually used as one of the input parameters in Particle Physics. The four-fermion interaction appearing in 1.3.71 can not be renormalised in the framework of the Standard Model, that is the reason why it is viewed as an effective interaction. This effective interaction was firstly suggested by Fermi to explain the nuclear beta decay before the discovery of W boson [20].

1.4 Divergences and Renormalisation

1.4.1 Introduction

Historically, when people tried to calculate the one-loop Feynman diagrams in perturbative quantum field theory, divergent terms appeared. The divergences could be divided into two categories: Infrared(IR) divergences and Ultraviolet(UV) divergences. The IR divergence only appears when a particle is massless, e.g., the exchange or emission of a photon in the low energy limit $k \to 0$, where k is the momentum transfer in the loop diagram. On the other hand, in measurements involving charged particles, countless numbers of soft photons with arbitrary small energy might exist in the final states that could escape detection. If we consider diagrams for those processes, there is a divergence term too. According to the Kinoshita-Lee-Nauenberg theorem [21, 22], the IR divergences arising from virtual correction can be exactly cancelled by the real soft photon emission processes. In this thesis we mainly focus on the UV divergences arising at the high-energy scale. The UV divergence is ubiquitous in the one-loop corrections. For example, in the ϕ^4 theory, the one-loop transition amplitudes for the $\phi_i \to \phi_j$ process is

$$\frac{(-i\lambda)^2}{2} \int \frac{d^4k}{(2\pi)^2} \frac{i}{k^2 - m^2 + i\epsilon} \frac{i}{(k-p)^2 - m^2 + i\epsilon}, \qquad (1.4.73)$$

where p is the total incoming momentum, and k is the loop momentum that should be integrated over from $0 \to \infty$. In the large momentum transfer limit $m^2 \ll k^2$, the mass could be neglected and the integral behaves like

$$\sim \int \frac{d^4k}{k^4}, \qquad (1.4.74)$$

which is obviously divergent as $k \to +\infty$, known as UV divergence. The divergence comes from the short distance scale that we lack knowledge of. When the UV divergence was firstly discovered in QED, a lot of physicists believed that to eliminate the divergences, fundamental principles of physics had to be modified. However, it turns out there is a way out by the methods of regularization and renormalisation [23, 24].

Since the divergence comes from the high energy limit $k \to +\infty$, we can make a "cutoff" operation at the scale Λ, so that the ultraviolet divergences at short

distances are sensitive to the "regulator" Λ, in which case the physical quantities go to infinity when $\Lambda \to +\infty$. There are many other regularization schemes, amongst which the dimensional regularization scheme is the most widely used one, introduced by Giambiagi and Bolling [25]. The dimensional regularization scheme parameterises the UV divergence by a dimensional regulator $\epsilon = d - 4$. However, the choice of regularization schemes will not affect the non-trivial structure of loop diagrams. We will use dimensional regularization in our work in Chapter 4.

In a renormalizable quantum field theories, analyses of the one-loop corrections show that the divergent part of all of the diagrams always has the structure of a polynomial of the momentum, just as the tree-level contribution in the Lagrangian. So by redefining the original coupling constants by infinite shifts, we are able to absorb the divergences that parameterized in terms of the regulator into redefinitions of physical quantities. We can finally obtain physically reasonable finite results in the calculation of higher-order Feynman diagrams.

For a long time, the physical meaning of renormalisation was a mystery until K.G. Wilson and John B. Kogut published their profound paper in 1974 [26]. In Wilson's view, renormalisation is not only a technical tool to deal with the infinite quantities, but also explains why the nature is described by renormalizable theories. Through the renormalisation procedure, high energy effects can be parameterized in a low energy theory that we have knowledge of, like we have seen in the Fermi four-fermion example in 1.3. In this sense, the Standard Model itself can be viewed as an effective field theory too, which is exactly the case in the Standard Model Effective Field theory that will be introduced in Chapter 2.

1.4.2 Renormalisation in Electroweak Standard Model

In this part we will introduce the renormalisation procedure in the electroweak Standard Model which we are interested in. As it is mentioned above, the first step is to express the bare quantities in the Lagrangian in terms of renormalised

constants. The related terms are defined as follows:

$$M_W^0 = M_W + \delta M_W,$$

$$M_Z^0 = M_Z + \delta M_Z,$$

$$M_H^0 = M_H + \delta M_H, \tag{1.4.75}$$

$$M_f^0 = M_f + \delta M_f,$$

$$e^0 = e + \delta e,$$

where the bare quantities are denoted by an index 0, m_f is the generic fermion mass. Besides, because the radiative corrections add an infinite contribution to the normalization of the fields, the fields need to be renormalised as well:

$$W^{\pm,0} = Z_W^{1/2} W^{\pm}$$

$$\begin{pmatrix} Z^0 \\ A^0 \end{pmatrix} = \begin{pmatrix} Z_{ZZ}^{1/2} & Z_{ZA}^{1/2} \\ Z_{AZ}^{1/2} & Z_{AA}^{1/2} \end{pmatrix} \begin{pmatrix} Z \\ A \end{pmatrix}$$

$$H^0 = Z_H^{1/2} \tag{1.4.76}$$

$$f^{L,0} = Z_{fL}^{1/2} f^L$$

$$f^{R,0} = Z_{fR}^{1/2} f^R.$$

In the perturbative theory, the generic renormalised constant Z could be expanded as:

$$Z = 1 + \delta Z + (\delta Z)^2. \tag{1.4.77}$$

Since we only consider the leading order virtual corrections in this thesis, higher-order corrections expressed by $(\delta Z)^2$ will be neglected. In this case, all the renormalised constants can be split into two parts. Consequently, the bare Lagrangian can be divided into a renormalised Lagrangian and a counterterm Lagrangian as follow:

$$L^0 = L + \delta L, \tag{1.4.78}$$

where the renormalised Lagrangian L has exactly the same form as L^0, with the physical quantities and fields replaced by the renormalised ones. The counterterm δL can be translated into Feynman diagrams that are known as counterterm diagrams, which contribute to the virtual corrections too.

The UV divergent field renormalisation constants and the mass renormalisation constants can be determined by calculating the one-particle irreducible two-point functions that represent quantum corrections to a propagator so that the UV divergent terms in the two-point function can be cancelled by the counterterms. The function $\Sigma(p)$, as a polynomial in momentum, is known as the self-energy. Then by choosing the renormalisation schemes, the finite part of the field renormalisation constants and the mass renormalisation constants can be fixed. In QED, external electrons and photons are on their mass shell, so it is natural to imposing the on-shell condition to the external particles. But in other cases, like QCD, because of the color confinement, there is no such natural choice. As a result, we are free to choose a different renormalisation scheme. If we can calculate the perturbation theory up to infinite order, different renormalisation schemes can give the same finite result for any physical process in principle, though the definition of the renormalised constants are different. However, since in practice we can only do the computation up to a few loops, different physical predictions are produced from different renormalisation schemes. In the electroweak Standard Model, the on-shell renormalisation scheme turns out to be a very successful renormalisation scheme due to its impressive agreement with experiments [27]. In Chapter 4, as the energy scale we are interested in is the electroweak scale, we will implement the on shell scheme as well.

In order to renormalise the qft, one needs to calculate the transition amplitudes for the $f_i \to f_j$ process, where f_i represents for any field, i.e. the one-particle irreducible two-point functions. In Feynman Gauge, those two-point functions in electroweak theory can be parameterised as follows [28]:

$$\Gamma_{\mu\nu}^{W}(p) = -ig_{\mu\nu}\left(p^2 - M_W^2\right) - i\left(g_{\mu\nu} - \frac{p_\mu p_\nu}{p^2}\right)\Sigma_L^{W}\left(p^2\right) - i\frac{p_\mu p_\nu}{p^2}\Sigma_T^{W}\left(p^2\right),$$

$$\Gamma_{\mu\nu}^{ab}(p) = -ig_{\mu\nu}\left(p^2 - M_a^2\right)\delta_{ab} - i\left(g_{\mu\nu} - \frac{p_\mu p_\nu}{p^2}\right)\Sigma_L^{ab}\left(p^2\right) - i\frac{p_\mu p_\nu}{p^2}\Sigma_T^{ab}\left(p^2\right),$$

$$\Gamma_{\mu\nu}^{H}(p) = i\left(p^2 - M_H^2\right)\delta_{ab} + i\Sigma^{H}\left(p^2\right),$$

$$\Gamma_{\mu\nu}^{f}(p) = i\left(\not{p} - M_f\right) + i\left[\not{p}\left(P_L\Sigma_L^{f}\left(p^2\right) + P_R\Sigma_R^{f}\left(p^2\right)\right) + M_f\left(P_L\Sigma_{S*}^{f}\left(p^2\right) + P_R\Sigma_R^{f}\left(p^2\right)\right)\right],$$

$$(1.4.79)$$

where $a, b = A, Z$ and $M_A = 0$. Next we should impose the renormalisation condi-

tions for the external physical fields [28]:

$$\widetilde{\mathrm{Re}}\Gamma^W_{\mu\nu}(p)\,\varepsilon^\nu(p)\,|_{p^2=M_W^2}=0,$$

$$\mathrm{Re}\,\Gamma^{ZZ}_{\mu\nu}(p)\,\varepsilon^\nu(p)\,|_{p^2=M_Z^2}=0, \qquad\qquad \mathrm{Re}\,\Gamma^{ZA}_{\mu\nu}(p)\,\varepsilon^\nu(p)\,|_{p^2=M_Z^2}=0,$$

$$\Gamma^{AZ}_{\mu\nu}(p)\varepsilon^\nu(p)\,|_{p^2=0}=0, \qquad\qquad \Gamma^{AA}_{\mu\nu}(p)\varepsilon^\nu(p)\,|_{p^2=0}=0,$$

$$\lim_{p^2\to M_W^2}\frac{1}{p^2-M_W^2}\widetilde{\mathrm{Re}}\Gamma^W_{\mu\nu}(p)\,\varepsilon^\nu(p)=-i\varepsilon_\mu,$$

$$\lim_{p^2\to M_Z^2}\frac{1}{p^2-M_Z^2}\,\mathrm{Re}\,\Gamma^{ZZ}_{\mu\nu}(p)\,\varepsilon^\nu(p)=-i\varepsilon_\mu, \quad \lim_{p^2\to 0}\frac{1}{p^2}\,\mathrm{Re}\,\Gamma^{AA}_{\mu\nu}(p)\,\varepsilon^\nu(p)=-i\varepsilon_\mu$$

$$\mathrm{Re}\,\Gamma^H(p)|_{p^2=M_H^2}=0, \qquad\qquad \lim_{p^2\to M_H^2}\frac{1}{p^2-M_H^2}Re\Gamma^H(p)=i,$$

$$\widetilde{\mathrm{Re}}\Gamma^f(p)\,u(p)\,|_{p^2=m_f^2}=0, \qquad\qquad \widetilde{\mathrm{Re}}\bar{u}(p')\,\Gamma^f(p)\,|_{p'^2=m_f^2}=0,$$

$$\lim_{p^2\to m_f^2}\frac{\not{p}+m_f}{p^2-m_f^2}\widetilde{\mathrm{Re}}\Gamma^f(p)\,u(p)=iu(p), \quad \lim_{p^2\to m_f^2}\bar{u}(p')\widetilde{\mathrm{Re}}\Gamma^f(p')\frac{\not{p}+m_f}{p'^2-m_f^2}=i\bar{u}(p'),$$

$$(1.4.80)$$

where $\epsilon^\mu(p)$ is the polarization vectors, and $u(p)$ and $\bar{u}(p')$ are the spinors of the external fermion fields. $\widetilde{\mathrm{Re}}$ takes the real part of the loop integrals in the self energies without including the quark mixing matrix elements. Thus the mass counterterms in the on-shell scheme could be deduced as follows:

$$\delta m_f=\frac{m_f}{2}\widetilde{\mathrm{Re}}\left(\Sigma^f_L\left(m_f^2\right)+\Sigma^f_R\left(m_f^2\right)+\Sigma^f_S\left(m_f^2\right)+\Sigma^f_{S*}\left(m_f^2\right)\right),$$

$$\frac{\delta M_W}{M_W}=\widetilde{\mathrm{Re}}\frac{\Sigma^W_T(M_W^2)}{2M_W^2}.$$

$$(1.4.81)$$

And the counterterms from field renormalisation take the form [28]

$$\delta Z_f^L = -\widetilde{\text{Re}} \left(\Sigma_L^f \left(m_f^2 \right) + \Sigma_S^f \left(m_f^2 \right) - \Sigma_{S*}^f \left(m_f^2 \right) \right)$$
$$- m_f^2 \frac{\partial}{\partial p^2} \left(\Sigma_L^f \left(m_f^2 \right) + \Sigma_R^f \left(m_f^2 \right) + \Sigma_S^f \left(m_f^2 \right) + \Sigma_{S*}^f \left(m_f^2 \right) \right) |_{p^2 = m_f^2},$$

$$\delta Z_f^R = -\widetilde{\text{Re}} \Sigma_R^f \left(m_f^2 \right)$$
$$- m_f^2 \frac{\partial}{\partial p^2} \left(\Sigma_L^f \left(m_f^2 \right) + \Sigma_R^f \left(m_f^2 \right) + \Sigma_S^f \left(m_f^2 \right) + \Sigma_{S*}^f \left(m_f^2 \right) \right) |_{p^2 = m_f^2},$$

$$\delta Z_W = -\text{Re} \frac{\partial \Sigma_T^W \left(p^2 \right)}{\partial p^2} |_{p^2 = m_W^2}, \qquad (1.4.82)$$

$$\delta Z_{ZZ} = -\text{Re} \frac{\partial \Sigma_T^{ZZ} \left(m_Z^2 \right)}{\partial p^2} |_{p^2 = m_Z^2},$$

$$\delta Z_{AA} = -\frac{\partial \Sigma_T^{AA} (p^2)}{\partial p^2} |_{p^2 = 0},$$

$$\delta Z_{ZA} = 2 \frac{\Sigma_T^{AZ} \left(p^2 \right)}{M_Z^2} |_{p^2 = 0},$$

$$\delta Z_H = -\text{Re} \frac{\partial \Sigma_T^H \left(m_H^2 \right)}{\partial p^2} |_{p^2 = m_H^2}.$$

At last, the counterterms from the renormalisation of the electric charge in the on-shell scheme can be formulated by the field renormalisation constants as:

$$\delta Z_e = -\frac{1}{2} \delta Z_{AA} - \frac{\sin \theta_w}{2 \cos \theta_w} \delta Z_{ZA}. \qquad (1.4.83)$$

As mentioned above, there are other renormalisation schemes that could be used. As the only physical renormalisation scheme, the on-shell scheme has the advantage that in all orders of perturbative expansion of Feynman diagrams, the basic renormalised constants like m_f and e corresponds to their measured value. But calculations of the finite terms are very complicated in some cases. Thus, it is more convenient to adopt other renormalisation scheme like the minimal subtraction (MS) scheme [29], and modified minimal subtraction scheme, called $\overline{\text{MS}}$ scheme [30], especially for QCD, in which case the mass eigenstates of quarks could not be measured directly. In the MS scheme proposed by 't Hooft, the renormalised constants are chosen to be completely infinite to chop off the divergent poles $\frac{1}{\epsilon}$ arising from the dimensional regularization. Because the finite counterterms in MS is just zero, compared to the on-shell scheme, the MS scheme is much simpler to calculate since its finite parts of counterterms are just zero. People then find that the poles $\frac{1}{\epsilon}$ are always a combination of two constants: γ_E and $\ln 4\pi$. So in the modified MS scheme,

we make the replacement:

$$\frac{1}{\epsilon} \rightarrow \frac{1}{\bar{\epsilon}} = \frac{1}{\epsilon} + \gamma_E + \ln 4\pi. \tag{1.4.84}$$

Correspondingly, the finite terms in $\overline{\text{MS}}$ scheme have fixed finite parts. As a result, in the MS and $\overline{\text{MS}}$ schemes, the renormalised masses for the external fields are no longer equal to the physical mass, but depend on the renormalisation scale μ, which would be affected by high-orders radiative correction.

1.5 Outline of the Thesis

The main goal of this thesis is to probe the new physics beyond the SM using effective field theories. In the example of Fermi's four-fermion effective interaction, introduced in this chapter, it has been shown that non-SM effective Lagrangians that encode the unknown high energy physics could be used to describe the low energy interactions. The same approach can be used to explore the impact of new physics. In the present situation, the data obtained from high-energy experiments does not suffice to deduce the theory underlying the Standard Model of particle physics, we are parametrising our ignorance using an effective field theory approach, which allows to parameterise deviations from the Standard Model in a fairly model-independent way. In Chapter 2, two kinds of effective field theories are introduced, i.e. the dimension-six Standard Model effective field (SMEFT) theories and Simplified Models with dark sectors. In the SMEFT part, a short review of the Higgs and electroweak phenomenology in tree-level SMEFT is given which will be used in Chapter 4. And in the Simplified Model part, a simple dark matter Simplified Model is introduced. In Chapter 3, four simple effective operators are defined to introduce interactions between a new (pseudo-)scalar particle and the SM top quark. Such interactions are motivated by scalar mediators between the SM and a dark sector. In this chapter, we study the ability of the LHC to probe the spin and parity quantum numbers of a new light scalar resonance X which couples predominantly to the third generation quarks in a variety of simplified models through the $t\bar{t}X$ interaction. In chapter 4, the NLO correction to the forward-backward asymmetry for $e^+e^- \rightarrow b\bar{b}$ process in the framework of dimension-six Standard Model Effective field theory

(SMEFT). Numerical results are presented to show the influence of EFT corrections on the phenomena. Finally, a conclusion is made in Chapter 5 by summing up the main findings at the end of this thesis.

Chapter 2

Effective Field Theories

The Standard Model has been found to be a very successful theory in explaining all experimental results obtained at collider experiments and in predicting a wide range of phenomena such as the existence of W boson and Z boson in electroweak physics. After the discovery of the Higgs boson by ATLAS and CMS at the LHC in 2012 [31, 32], all particles predicted by the Standard Model have been found. However, there are still phenomena, such as the matter/anti-matter asymmetry, the Standard Model cannot fully explain. Yet, no new particles beyond the Standard Model have been discovered so far.

The ultimate goal of modern physics is to describe all observed phenomena in the framework of one theory that is valid up to arbitrary high energies, in which different kinds of interactions can be unified as one. Such a theory can be called a fundamental theory. Correspondingly, a theory that is only valid up to a finite energy scale is called an effective field theory. Just as the name implies, an effective field theory can only describe physics below some scale Λ. Specifically, these scales are the masses of the heavy particles in the effective field theory. In the example of Fermi's four-fermion effective theory that has been introduced in Chapter 1, we know that it will no longer be effective beyond the electroweak scale, and one has $\Lambda = M_W$. In fact, all field theories we have are effective theories. For the SM, the situation is the same. Though we still don't know the correct Λ for the SM, since new particles beyond SM have not been found yet. Actually, it took a long time for physicists to realise the SM is also an effective field theory. In effective field theories, like

for example Fermi's four-fermion theory, the effects at the scale Λ are suppressed by a factor $\frac{E}{\Lambda}$, where E is the characteristic energy of the process considered in the effective theory. Due to this factor, physics at a very high energy scales or regimes of very small distance will not be important for the phenomenology at low energy scales. Consequently, the parameter space of the world could be divided into different regions, in each region with a different energy scale. The physics at each scale is relatively independent from each other so that we can explain the physical phenomena at certain scales we are interested in without a real fundamental theory that can explain the physics at all scales in principle.

2.1 Standard Model Effective Fields Theory

If we view the Standard Model as an effective field theory that can be decoupled from the new physics scale, it is a reasonable choice to build higher dimensional effective operators using the Standard Model fields assuming the same symmetry groups of the SM. Such a theory is called Standard Model Effective Field Theory (SMEFT) [33]. In SMEFT we assume that the $SU(2)_L \otimes U(1)_Y$ symmetry is spontaneously broken to $U(1)_{\text{EM}}$ via the Higgs mechanism. To keep the Lagrangian dimensionless, the operators in SMEFT should be multiplied by couplings with a negative mass dimension, which are known as the Wilson Coefficients [34]. For a d dimension operator, the corresponding Wilson Coefficient C_i should have a dimension $4 - d$. We can also express the Wilson coupling as a dimensionless coupling divided by the cut-off scale as $\widetilde{C}^i = \frac{C^i}{\Lambda^{d-4}}$. These operators are the low-energy remnants of the heavy new physics integrated out at the scale Λ, which appears then as the scale suppressing the effects of these operators at lower scales.

A generic SMEFT Lagrangian can be written as following:

$$\mathcal{L}_{\text{SMEFT}} = \mathcal{L}_{\text{SM}} + \sum_d \mathcal{L}_d, \qquad d = 5, 6, 7, \dots \quad , \tag{2.1.1}$$

where the d dimensional effective Lagrangian $\mathcal{L}_d = C_i^d Q_i^d$. In the limit $\Lambda \to +\infty$, SMEFT can be reduced to the normal SM. The first EFT Lagrangian arises at dimension five, denoted as $\mathcal{L}_5$, and contains only a lepton-number violating operator [35]. In the dimension-six SMEFT, all the operators obey the law of conservation

of lepton number, however, there could be baryon-number violating operators [36]. In the dimension-five SMEFT, the left-handed neutrinos have Majorana masses [36], which would be considerably suppressed by the small-neutrino-mass restriction from Neutrino oscillation experiments. Thus, the suppression scale of the dimension-five operator is usually deemed to be much larger than the scale Λ that suppresses the dimension-six operators. Through the power counting in the SMEFT, higher dimension operators are suppressed more severely due to the Λ^{d-4} in the denominator so that they have less impact on the low-energy scale. Therefore in our work in Chapter 4, we will only consider the dimension-6 operators and assume the conservation of baryon number.

Since no new gauge symmetries beyond the SM are imposed, we are free to construct any operators that obey those symmetries. Though the amount of all possible operators is very large, the number can be reduced according to the Equations of motion of the fields since these operators are not independent from each other. Thus we can choose a basis in which operators are independent. Actually, there are different basis schemes that are identical in physics. Among them, assuming the baryon number conservation, an irreducible basis with 59 operators was proposed in [36], known as "Warsaw Basis". These 59 operators are categorized into 8 classes, which can be found in A.1 in the Appendix. In chapter 4, we choose to work in the "Warsaw Basis" since it has been studied much better than any other basis.

2.1.1 Higgs and Electroweak Phenomenology in the Tree-Level Dimension-six SMEFT

Since all the interactions in the SMEFT are built from the SM particles, a large number of SM processes might be influenced by the EFT operators [33]. The SMEFT could be viewed as a perturbative theory. For example, the next-to-leading order corrections in dimension-six SMEFT have the same power counting as the dimension-eight SMEFT. In this section, we are mainly interested in the electroweak phenomena that are related to the Dimension-six SMEFT. Only the basic tree-level effects of the SMEFT will be introduced, which means that the $O(\frac{1}{\Lambda^4})$ effects are neglected.

To understand the spontaneous symmetry breaking process in the SMEFT, we need to introduce the new Higgs potential. In the dimension-six SMEFT, it can be written as

$$V(H) = V_{SM}(H) - C_H (H^\dagger H)^3$$
$$= \lambda (H^\dagger H - \frac{1}{2}v^2)^2 - C_H (H^\dagger H)^3, \tag{2.1.2}$$

which is altered by only one Wilson Coefficient C_H. The new vev could be obtained by solving the minimum of the potential

$$v_T = \left(1 + \frac{3C_H v_T^2}{8\lambda}\right)\hat{v}_T, \tag{2.1.3}$$

where v_T is the new vev and $\hat{v}_T$ is the original SM one. The 'hat' symbol will be used to characterise the SM quantities in what follows.

Furthermore, the Higgs doublet field receives corrections from the EFT kinetic Wilson Coefficients C_{HD} and $C_{H\square}$. Consequently, the Higgs doublet in dimension-six SMEFT in the unitary gauge take the form

$$H = \begin{pmatrix} 0 \\ (1 + (C_{H\square} - \frac{1}{4}C_{HD})v_T^2)h + v_T \end{pmatrix}. \tag{2.1.4}$$

Using 2.1.3 on 2.1.4, we can obtain the mass of the Higgs boson:

$$M_H^2 = 2\lambda \left(1 - \frac{3C_H v^2}{2\lambda} + 2\left(C_{H\square} - \frac{1}{4}C_{HD}\right)v_T^2\right)v_T^2. \tag{2.1.5}$$

Then we move on to the operators that are connected with electroweak gauge terms. The Class 4 operators in the Warsaw Basis contribute to the $SU(2)_L \otimes U(1)_Y$ gauge kinetic terms and mass terms in the broken phase:

$$L_{\text{EW}}^{(6)} = \frac{1}{2}v_T^2 C_{HW} W_{\mu\nu}^a W^{a,\mu\nu} + \frac{1}{2}v_T^2 C_{HB} B_{\mu\nu} B^{\mu\nu} + \frac{1}{2}v_T^2 C_{HWB} W_{\mu\nu}^3 B^{\mu\nu}, \tag{2.1.6}$$

and

$$L_{\text{EW}}^{mass,(6)} = \frac{1}{16}v_T^4 \left(g_2 W_\mu^3 - g_1 B_\mu\right)^2. \tag{2.1.7}$$

Correspondingly, the gauge fields can be redefined as

$$W_\mu^a = \mathcal{W}_\mu^a \left(1 + C_{HW} v_T^2\right), \ B_\mu^a = \mathcal{B}_\mu \left(1 + C_{HB} v_T^2\right), \tag{2.1.8}$$

and the related gauge coupling is shifted as

$$\bar{g}_2 = g_2(1 + C_{HW} v_T^2), \ \bar{g}_1 = g_1(1 + C_{HB} v_T^2). \tag{2.1.9}$$

So that we can express the electroweak gauge Lagrangian in terms of the mass eigenstates:

$$\mathcal{W}^{\pm} = \frac{1}{2}(\mathcal{W}_{\mu}^1 \mp i\mathcal{W}_{\mu}^2),$$

$$\begin{pmatrix} \mathcal{W}_{\mu}^3 \\ \mathcal{B}_{\mu} \end{pmatrix} = \begin{pmatrix} \cos\bar{\theta}_w & \sin\bar{\theta}_w \\ -\sin\bar{\theta}_w & \cos\bar{\theta}_w \end{pmatrix} \begin{pmatrix} \mathcal{Z}_{\mu} \\ \mathcal{A}_{\mu} \end{pmatrix}, \qquad (2.1.10)$$

in which the Weinberg angle is replaced by a effective one

$$\sin\bar{\theta} = \frac{\bar{g}_1}{\bar{g}_1^2 + \bar{g}_2^2}\left(1 + \frac{v_T^2}{2}\frac{\bar{g}_2}{\bar{g}_1}\frac{\bar{g}_2^2 - \bar{g}_1^2}{\bar{g}_1^2 + \bar{g}_1^2}C_{HWB}\right). \qquad (2.1.11)$$

The trigonometric function of Weinberg angle $\sin\theta_w$ and $\cos\theta_w$ has been replaced with $\hat{s}_w$ and $\hat{c}_w$ respectively for convenience's sake. From now on all the original SM quantities will we be denoted as hatted symbols and the EFT quantities will be denoted as barred symbols in this thesis.

In the dimension-six SMEFT, the covariant derivative can be written as

$$D_{\mu} = \partial_{\mu} + i\frac{\bar{g}_2}{\sqrt{2}}\left(\mathcal{W}^+T^+\mathcal{W}^-T^-\right) + ig_Z(\bar{g}_2^2 + \bar{g}_1^2)\left[T^3 - \bar{s}_w^2\right]\mathcal{Z}_{\mu} + i\bar{e}Q_f\mathcal{A}_{\mu}, \qquad (2.1.12)$$

where $Q = T^3 + Y$ as in the SM. Accordingly, the electric coupling and the neutral weak effective coupling need to be redefined as

$$\bar{e} = \frac{\bar{g}_1\bar{g}_2}{\sqrt{\bar{g}_1^2 + \bar{g}_2^2}}\left[1 - \frac{\bar{g}_1\bar{g}_2}{\bar{g}_1^2 + \bar{g}_2^2}v_T^2 C_{HWB}\right]$$

$$\bar{g}_Z = \sqrt{\bar{g}_1^2 + \bar{g}_2^2} + \frac{\bar{g}_1\bar{g}_2}{\sqrt{\bar{g}_1^2 + \bar{g}_2^2}}v_T^2 C_{HWB}. \qquad (2.1.13)$$

The masses of the electroweak bosons can be directly read off from the Lagrangian:

$$M_W^2 = \frac{\bar{g}_2^2 v_T^2}{2},$$

$$M_Z^2 = \frac{v_T^2}{4}\left(\bar{g}_2^2 + \bar{g}_1^2\right) + \frac{v_T^4}{8}C_{HD}\left(\bar{g}_2^2 + \bar{g}_1^2\right) + \frac{v_T^4}{2}\bar{g}_2\bar{g}_1 C_{HWB}. \qquad (2.1.14)$$

As is shown above, the dimension-six SMEFT always refines the quantities by adding some terms proportional to $\frac{1}{\Lambda^2}$ at tree level.

Finally, the fermion masses also need to be shifted to their EFT forms. In dimension-six SMEFT, fermions acquire their masses through Yukawa couplings and additional EFT terms that include three Higgs doublets, one left-handed fermion doublet and one right-handed fermion:

$$C_{\Psi H}(H^{\dagger}H)\left(\bar{\Psi}_L H\Psi_R\right) + h.c.. \qquad (2.1.15)$$

In the broken phase this generates an interaction term that couples two fermions with one Higgs boson. Together with the normal SM Yukawa terms, this leads to a generic fermion mass matrix

$$M_\Psi^{ij} = \frac{v_T}{\sqrt{2}} \left(Y_\Psi^{ij} - \frac{1}{2} v^2 C_{\Psi H}^* \right). \tag{2.1.16}$$

Consequently, the Yukawa coupling Y_Ψ obtains a correction due to the redefinition of the Higgs doublet together with corrections from $C_{\Psi H}^*$:

$$Y_\Psi^{ij} = \frac{1}{\sqrt{2}} \left(Y_\Psi^{ij} \left(1 + C_{H\Box} - \frac{1}{4} C_{HD} \right) v^2 \right) - \frac{3}{2} v^2 C_{\Psi H}^{*ij} \tag{2.1.17}$$

Recall that in the SM the Fermi coupling constant G_F is directly related to a four-fermion interaction that is exactly a dimension-six operator. Now in the SMEFT,

$$G_F = \frac{1}{\sqrt{2} v_t^2} + \frac{1}{\sqrt{2}} \left(C_{\underset{\mu e e \mu}{ll}} + C_{\underset{e \mu \mu e}{ll}} \right) - \frac{1}{2\sqrt{2}} \left(C_{\underset{ee}{Hl}}^{(3)} + C_{\underset{\mu\mu}{Hl}}^{(3)} \right), \tag{2.1.18}$$

in which the four fermion operators appear again. In 2.1.18, besides the four-fermion operators, there is another operator $C_{Hl}^{(3)}$ that influence the $\mu^- \to e^- + \nu_\mu + \bar{\nu}_e$ decay process by altering the electroweak charged current coupling.

2.2 Simplified Models

The LHC has been demonstrated to be a very powerful collider at detecting the fundamental physics at the electroweak scale. Therefore physicists are now aiming to discover new physics in the ongoing and upcoming runs of the LHC at higher energy scales. Benefiting from its collision energy of $\sqrt{s} = 14$ TeV, the LHC has the potential to detect new physics that might exist at $\mathcal{O}(\text{TeV})$ scale. Furthermore, there might be some unknown particles at the electroweak scale that escape the detection of current experiments, e.g., a possible dark matter candidate with a mass of a few hundreds GeV. To find the signals that might contain such kinds of new physics beyond the Standard Model(BSM), we need a theory framework to deal with the complex data gathered by the multi-purpose experiments. Many specific models to extend the SM have been built, such as SUSY [37] or GUTs [38]. However, even if a new signal is captured by the LHC, it is still not easy to identify the theory behind

it, as the signal can be generated in many ways in different models [39, 40]. Thus, the situation gets worse as the phenomenon might depend on a great number of free parameters. Based on phenomenological considerations, it is useful to characterize special BSM processes in terms of an effective Lagrangian as a starting point, as it is done in Simplified Models.

Simplified models are also effective field theories, but with an extended particle content and/or gauge group compared to the SM. A Simplified Model only contains a few new particles and interactions rather than including all possible interactions. The new interactions in Simplified Models are directly related to the physics observables in collider experiments. As a result, the new process appearing in the signal only depends on a small number of parameters. Physicists are free to choose different effective interaction operators according to their needs, and the results obtained in the Simplified Models can be matched onto more specific models which can give rise to the same topologies.

Different kinds of Simplified models can be applied for different purposes. In this chapter I will focus on the simplified Dark Matter (DM) models which are used to analyse the possible DM candidates and their influences on the Collider experiments [41, 42]. The center-of-mass energy at the LHC has successfully reached 13 TeV in 2015. This increases the sensitivity to detect DM directly and indirectly in searches performed at the LHC, which might open a new window for us to improve our understanding of the universe.

Three kinds of models could be used in the DM case. General models can afford the task to provide different kinds of DM candidates, like the weakly interacting massive particles (WIMP) in supersymmetry theories. However, the details of such BSM theories are still unknown to us, this leads to a large number of free parameters in the general models. For example, in the analysis of DM in the framework of Minimal Supersymmetric Standard Model (MSSM), more than 20 relevant free parameters will cause too much uncertainties, and lead to varieties of DM versions [39]. As a result, from a finite amount of data that we might have in the foreseeable future, a complete DM model is usually not a suitable choice due to too many underlying unknown dynamics though in principle it can explain all questions about

DM.

Effective field theories provide alternative frameworks on the simple assumption that the DM candidate might be the only accessible state to our experiments. In such a DM effective field theory, the interactions between the possible DM candidate and the SM particles could be expressed as effective operators, suppressed by a high energy cut off scale Λ. All phenomena caused by the heavy states of the dark sector are thus now encoded in the relevant operator coefficients. In such a way, all possible kinematically inaccessible particles could be disposed in the EFT framework in a general way. Many related works had been done and it is shown that the LHC Run I data provides strict restrictions on the BSM scale Λ [43–45].

As phenomenon oriented theories, Simplified Models provide us very good tools to analyse the collider signals related to the dark sector. In Simplified Models we are not limited to assume that the DM candidate might be the only accessible state in our experiments. Alternatively, the most important mediators that couples the DM particle with the SM particles are also introduced in Simplified Models, together with the DM candidates themselves. The mediators could be SM particles or BSM particles, since in Simplified Models the DM particles do not interact with SM particles directly. The number of new parameters of the dark sector could be more than one. However, this number is usually not as large as it is in the full theory, therefore it does not cause too much trouble in the calculation. The results obtained from the DM simplified Models could be compared with the LHC data to learn the basic features of the DM sector.

To ensure that the results of a DM Simplified Models is meaningful, the model should be simple enough so that it can be extended to a general model that can explain the physical mechanism behind the effective operators. For example, the light sectors in Simplified Models should only include the lightest DM fields that are stable enough. Furthermore, to compare the data with the predictions of Simplified Models, these models should be complete in explaining the relevant phenomena at the energies that Colliders are able to probe. It is worth to emphasize that if the mass of the mediator(s) is sufficiently heavy, then the relevant process will be suppressed by the squared mass(es), and we return to the SMEFT case.

Generally, the stable DM sectors in Simplified Models are responsible for explaining the DM, and the mediator(s) connecting DM sectors and SM sectors are responsible to provide the expected SM particle excess at the LHC experiments. Meanwhile, to satisfy all non high-p_T constraints from the data, when building the Lagrangians, one should follow some extra criteria. First, all gauge invariant and gauge invariant terms should be included in the Lagrangian to ensure the completeness of the model. Second, the interaction terms between DM sector and SM sector should respect the exact and approximate accidental global symmetries of the SM. Consequently, lepton number violating and baryon number violating terms are forbidden in the Lagrangian. Meanwhile, the custodial and flavor symmetries of the SM should not be broken strongly. These criteria are discussed in detail in [42].

Now the problem is how to control the new Lagrangian terms so that it would not break the custodial and flavor symmetries severely. New physics are required to respect the exact symmetries but not the approximate global accidental symmetries in full theories. Any accidental symmetries violating terms would be severely constrained by the electroweak data, since the experimental data in electroweak scale fits the SM expectation very well. One smart way to solve the problem is to let the new physics break the flavor symmetry as similar as the SM. A method called Minimal Flavour Violation (MFV) [46–49] assumption is deliberately developed for this purpose. In the SM, the non-diagonalizable CKM matrix leads to the fact that the flavor eigenstates are not the mass Eigenstates. Correspondingly, in the MFV scheme only two kinds of new interactions are permitted in the Lagrangians: those which are invariant under the global SM flavor group $G_q = U(3)_q \otimes U(3)_u \otimes U(3)_d$ and those break the flavor symmetry that are associated with the quark Yukawa couplings Y_u and Y_d.

A simple example of Simplified Models is given in [42] to show how the MFV requirement restricts the construction of Simplified Models. In this example, the DM candidate is chosen to be a real scalar under gauge and flavor symmetry, denoted as χ, and the mediator is set to be the SM-like higgs doublet under $SU(2)$ gauge symmetry, denoted as H'. The interaction between the DM and the mediator opens a portal from the SM to the DM sector, which is simply given as $\chi^2 |H'|^2$.

As in the SM case, we suppose that the new Higgs-like mediator interacts with quarks in the SM. Now we pretend that we do not know the interaction between the SM Higgs doublet and quarks, but following the instruction of MFV procedure to construct the corresponding Lagrangian. The left-handed and the right-handed quarks transforming under the flavour symmetry could be expressed as $q_L \sim (3, 1, 1)$, $u_R \sim (1, 3, 1)$ and $d_R \sim (1, 1, 3)$ respectively. It is can be easily seen that $\bar{q}_L u_R$ breaks the $U(3)_q \otimes U(3)_u$, and $\bar{q}_L d_R$ breaks $U(3)_q \otimes U(3)_d$, when they interact with Higgs doublet, $SU(2)_L$ symmetry can be obeyed. The other possible combination terms that couple with Higgs doublet even break $SU(2)_L$ gauge symmetry, which are definitely not allowed. So we have to connect the two flavour symmetry breaking terms with the Yukawa couplings. Hence we have the following Lagrangian:

$$\mathcal{L} = -\sum_{i,j} \left(Y_u^{i,j} \bar{q}^i H' u^j + Y_d^{i,j} \bar{q}^i \varepsilon_{ab} H'^a d^j + h.c. \right), \qquad (2.2.19)$$

where ε_{ab} with $a, b = 1, 2$ is Levi-Civita symbol. We can find that this Lagrangian is exactly the same as the Yukawa sector of quarks in the SM.

Chapter 3

Simplified Models in searches for dark sectors

3.1 Motivation and Introduction

As it is mentioned in Chapter 2, physicists expect to make new discoveries of physics beyond the Standard Model in future high-energy experiments. The main focus of attention has been put on the heavy new particles at high energy scale. However, some light resonances could have escaped notice through some unknown mechanism from previous colliders such as LEP and the Tevatron, and may be discovered in the large datasets which the LHC will accrue in coming years.

Astronomical Observations are important sources for testing the fundamental particles physics models. With the help of the Fermi Large Area Telescope, an excess of γ-rays at energies of a few GeV was observed in the region around the Galactic Center [50], which is called as GCE for short. The excess can not be explained by the SM but might implicate the existence of dark matter [51]. This has been an area of particular interest due to the Galactic Centre excess of diuse gamma-rays, which may be explained by dark matter (DM) annihilating via a light mediator into Standard Model (SM) particles [5, 7, 8] [52–54]. Simplified Models are very suitable for characterizing these data in a simple way with only a few parameters. In this case, effective mediators can be considered to generate the dark matter particle. According to some studies, the mediators in the annihilating process might be a

scalar [55], pseudoscalar [56], or a vector boson [57, 58]. The collider sensitivity to these mediators have been explored in a series of papers under the assumption that the mediator couples to the quarks and DM [59–65]. Since some analyses of the GC excess suggest that DM annihilation into b quarks provides a particularly good fit, some studies have assumed the mediator predominantly couples to the third generation quarks. In that case an important collider signal is associated production with a pair of top or bottom quarks [66–68], particularly for spin-1 mediators where LHC production via gluon fusion is forbidden by the Landau-Yang theorem [69, 70]. There has also been model building interest recently in top-philic Z' bosons in the context of a slight excess in $t\bar{t}h$ searches for SM Higgs boson production [71]. Some recent work has studied searches for $t\bar{t}$ resonances in the context of two Higgs doublet models [72–74], and on searches for top-philic dark matter mediators [75]. However, these works focus on the heavier resonances. It is therefore important to understand the ability of the LHC to discover and measure the properties of light new resonances with strong couplings to the third generation.

If such a new light (i.e. $m_X \lesssim 100$ GeV) resonance X is discovered in Run 2 of the LHC, a first priority will be the characterisation of its quantum numbers. In the context of resonances with strong coupling to top quarks studies have already been made in $t\bar{t}X$ production [68, 76, 77], focussing on the semi- and di-leptonic top decay channels, where either one or both tops decay leptonically. In the case of di-leptonic top decays, it is known (building upon older work on spin-polarisation in $t\bar{t}$ production [78]) that the azimuthal angle between the leptons encodes much of the relevant CP information. Related work has focussed on dijet angular correlations in $pp \rightarrow jjX$ [79], as well as extending results to NLO accuracy [80, 81].

In this work we seek to extend these previous works in a number of ways. We explore other angular variables which may be of use in pinning down the quantum numbers of top-philic resonances at the LHC. Where most other works have focussed on the di-leptonic final state (with some exceptions [68, 82]) we perform a detector-level analysis of the semi-leptonic final states. We find that although the SM backgrounds are challenging, this final state will indeed be useful in the discovery and characterisation of new light resonances.

We study the phenomenology of a variety of simplified models [83] with a new neutral resonance which we assume to be an eigenstate of parity and charge conjugation. Its couplings are restricted to the third generation quarks (bottoms and tops) only. For a scalar resonance S and a pseudoscalar resonance A, we assume the following CP-conserving interaction Lagrangians:

$$\mathcal{L}_S = -\sum_{q=b,t} \frac{g_q y_q}{\sqrt{2}} S \bar{q} q,$$
$$\mathcal{L}_A = -\sum_{q=b,t} \frac{g_q y_q}{\sqrt{2}} A i \gamma^5 \bar{q} q,$$

(3.1.1)

where y_q is the SM Yukawa couplings. We also study a vector resonance $Z'_{\rm V}$ and an axial vector resonance $Z'_{\rm A}$ with interaction Lagrangians given by

$$\mathcal{L}_S = -\sum_{q=b,t} g_q y_q Z'^\mu_V \bar{q} \gamma_\mu q,$$
$$\mathcal{L}_A = -\sum_{q=b,t} g_q y_q Z'^\mu_A \bar{q} \gamma_\mu \gamma^5 \bar{q} q.$$

(3.1.2)

In all these cases the decay width of the resonance is set to its natural width calculated from the theory parameters at tree level. We do not include any interactions between X and possible dark matter candidates, focussing on its interactions with the SM (equivalently, there may be a coupling between X and dark matter, but we study the parameter space where $m_X > 2m_{DM}$). In the case that the resonance is lighter than $2m_t$ it must decay into a pair of b quarks with a branching ratio equal to one (neglecting three-body decays). While these Lagrangians will also lead to dimension-five interactions with gluons for the scalar and pseudoscalar (whose CP properties can be probed in di-jet angular correlations for instance [84]), in this work we exclusively focus on what can be gleaned from associated production with tops.

We have implemented these models in `FeynRules` [85] which allows us to generate simulated events at the LHC using `MadGraph` [86] via the `UFO` [87] format.
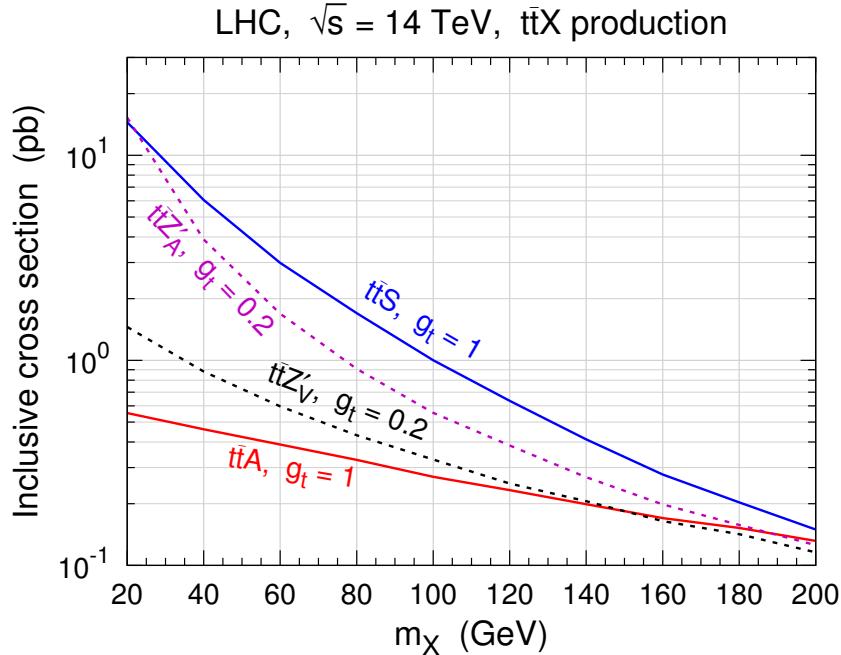
Figure 3.1   This figure shows the $t\bar{t}X + jets$ ($X = S, A, Z'_V, or Z'_A$) production cross sections as functions of m_X at the 14 TeV LHC for the four simplified models.

In 3.1 we show the behaviour of the cross-sections for the four simplified models as functions of the resonance mass m_X. As has been demonstrated before [68], for low masses (below around GeV) the $t\bar{t}A$ production cross section is quite suppressed relative to that of $t\bar{t}S$, and is smaller by over an order of magnitude below 40 GeV. We also observe similar behaviour (although not as extreme) in the $t\bar{t}Z'^{\mu}_V$ versus $t\bar{t}Z'^{\mu}_A$ cross sections. The differences between the cross sections become smaller as m_X increases, and are all within a factor of two at $m_X = 200$ GeV. To attempt to understand this, in the next section we will calculate the helicity amplitudes for $t\bar{t}A$ and $t\bar{t}S$ production, using the Weyl-van-der-Waerden spinor formalism for the case of massive particles.

3.2   The Amplitudes in the WvdW Formalism

All diagrams contributing to the $gg \rightarrow tH\bar{t}$ due to the scalar operator at tree-level are given in 3.2, and diagrams due to the pseudoscalar operator have exactly the same topologies as the scalar case, which could be easily seen from their Lagrange
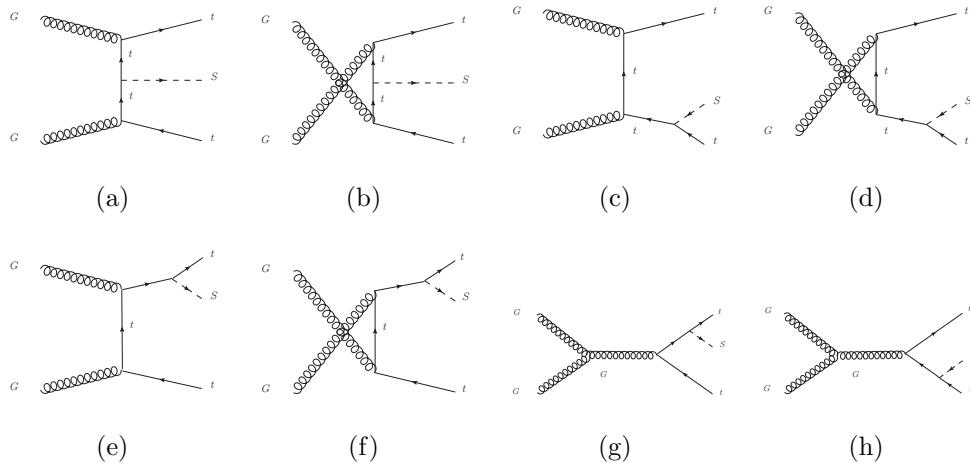
Figure 3.2 LO ggtHt diagrams

terms. Therefore these diagrams will not be listed here anymore.

For convenience, in the following calculation in this section, we set $-\frac{g_q y_q}{\sqrt{2}} = 1$, which would not affect the comparison between the amplitudes in the scalar and pseudoscalar case.

3.2.1 A Brief Introduction to the Weyl-van-der-Waerden Spinor Technique

In perturbative quantum field theory, the probability amplitude is directly connected with the cross-section that can be measured in the experiment. Hence a important step from theories to observables is the calculation of the cross-section at the lowest order. For the $1 \rightarrow 2$ decay process and $2 \rightarrow 2$ scattering process, tree-level results are easy to compute. However, when the number of final states increases to 3 or more, the situation will become very complicated due to the uncontrolled increment of the amount of involved Feynman diagrams. The traditional method of calculating the cross-section is squaring the total scattering amplitude of all the relevant diagrams followed by summing over the spins. However, these amplitudes interfere with each other. Therefore for N diagrams, the number of squared elements is N^2. One of the solutions is to employ the helicity amplitude technique. In the helicity eigenstates, polarized scattering amplitudes could be decoupled with each other. Accordingly, the scattering amplitudes could be decoupled into helicity

components that are independent from each other. Consequently, if each amplitude has m helicity components, the number of total squared elements would be equal to mN rather than N^2. In the large N case, the advantage of helicity amplitude technique is very clear.

A variety of spinor techniques has been developed in the past years. At first, only the spin-1 massless fields like photons and gluons are transversely polarized [88], which cause many cancellations in the calculation but leave the Dirac spinor unchanged. Since the light-like Dirac fields are naturally the helicity states, a more general spinor technique was then formulated to include both polarization vectors, and massless Dirac spinors [89, 90], in which the Dirac spinors are split into two two-component Weyl-van-der-Waerden (WvdW) spinors [91]. The WvdW spinor technique was then extended to be compatible with massive Dirac fields. Furthermore, the Weyl-van der Waerden spinor technique for spin-3/2 fermions was proposed in [92]. In this section, the WvdW spinor technique including the massive polarized spin-1/2 fermions will be adopted.

As a starting point, we should introduce the basic elements, which include Minkowski 4-vector momentum, massless spin-1 boson vector, and the massive spin-1/2 Dirac field in terms of WvdW spinors. According to the WvdW formalism, ψ_A and $\psi^{\dot{A}}$ are introduced to represent WvdW covariant and contravariant spinors respectively. Complex conjugation is consistently indicated by dotting (undotting) indices, i.e.

$$\psi_{\dot{A}} = (\psi_A)^*, \ \psi^{\dot{A}} = \left(\psi^A\right)^*. \tag{3.2.3}$$

And we have the relation

$$\psi^A = \epsilon^{AB}\psi_B, \ \psi^{\dot{A}} = \epsilon^{\dot{A}\dot{B}}\psi_{\dot{B}},$$
$$\psi_A = \psi^B\epsilon_{BA}, \ \psi_{\dot{A}} = \psi_{\dot{B}}\epsilon^{\dot{B}\dot{A}}, \tag{3.2.4}$$

in which,

$$\epsilon^{AB} = \epsilon^{\dot{A}\dot{B}} = \epsilon_{AB} = \epsilon_{\dot{A}\dot{B}} = \begin{pmatrix} 0 & +1 \\ -1 & 0 \end{pmatrix}. \tag{3.2.5}$$

Any terms in the Lagrangian should be Lorentz-invariant. The Lorentz-invariant

spinor products could be built as

$$\langle\phi\psi\rangle = \phi_A\psi^A = \phi_1\psi_2 - \psi_2\phi_1,$$
$$\langle\phi\psi\rangle^* = \phi_{\dot{A}}\psi^{\dot{A}} = (\phi_1\psi_2 - \psi_2\phi_1)^*. \tag{3.2.6}$$

For a Minkowski 4-vector k^μ, after projecting into the spinor basis, it is related to a 2×2 matrix

$$K_{\dot{A}B} = k^\mu\sigma_{\dot{A}B} = \begin{pmatrix} k^0 + k^3 & k^1 + ik^2 \\ k^1 - ik^2 & k^0 - k^3 \end{pmatrix}, \tag{3.2.7}$$

which can be factorized into a product of two spinors

$$K_{\dot{A}B} = k^\mu\sigma_{\dot{A}B} = k_{\dot{A}}k_B, \quad k_A = \sqrt{2k^0}\begin{pmatrix} e^{-i\phi}\cos\frac{\theta}{2} \\ \sin\frac{\theta}{2} \end{pmatrix}. \tag{3.2.8}$$

The Lorentz-invariant spinor products including Minkowski 4-vector can be built similarly, e.g.,

$$\langle\phi K\psi\rangle = \left\langle\phi_A k^{\dot{A}}k^B\psi_{\dot{B}}\right\rangle. \tag{3.2.9}$$

Dirac spinors belong to the representation $D(\frac{1}{2},0) \oplus D(0,\frac{1}{2})$ and could be written into WvdW spinors as

$$\Psi = \begin{pmatrix} \phi_A \\ \psi^{\dot{A}} \end{pmatrix}. \tag{3.2.10}$$

To be more specific, for the Dirac spinor of the outgoing fermion with helicity σ,

$$\bar{\Psi}_{p,i}^{(+)} = \left(\psi_A, \phi^{\dot{A}}\right) \tag{3.2.11}$$

with

$$\begin{cases} (\kappa_1, -\kappa_2) & i = 1\,(\sigma = +) \\ (\kappa_2, \kappa_1) & i = 2\,(\sigma = -) \end{cases}, \tag{3.2.12}$$

in which,

$$\kappa_1 = \sqrt{p^0 + |\mathbf{p}|}\begin{pmatrix} e^{-i\phi}\cos\frac{\theta}{2} \\ \sin\frac{\theta}{2} \end{pmatrix}$$
$$\kappa_2 = \sqrt{p^0 - |\mathbf{p}|}\begin{pmatrix} \sin\frac{\theta}{2} \\ -e^{-i\phi}\cos\frac{\theta}{2} \end{pmatrix}. \tag{3.2.13}$$

And for massless spin-1 particles, the polarization vectors could be expressed as:

$$\varepsilon_{+,\dot{A}B}(k) = \frac{\sqrt{2}g_{+,\dot{A}}k_B}{\langle g_+k\rangle^*}, \quad \varepsilon_{-,\dot{A}B}(k) = \frac{\sqrt{2}k_{\dot{A}}g_{-,B}}{\langle g_-k\rangle},$$
$$\varepsilon_{+,\dot{A}B}(k)^* = \frac{\sqrt{2}k_{\dot{A}}g_{+,B}}{\langle g_+k\rangle}, \quad \varepsilon_{-,\dot{A}B}^*(k) = \frac{\sqrt{2}g_{-,\dot{A}}k_B}{\langle g_-k\rangle^*}, \tag{3.2.14}$$

where $g_{\pm,\dot{A}}$ are gauge spinors which can be chosen arbitrarily. In the following calculation in this section, the gauge spinors are deliberately chosen to simplify the algebraic expression.

3.2.2 The T-channels and U-channels Amplitudes

We consider the SM-like diagrams with scalar first. In 3.2, diagrams $a-f$ belong to T-channel or U-channel, and diagrams $g-h$ belong to S-channel. Diagram 3.2(a) and diagram 3.2(b) can be grouped together, since they can be transformed into each other by interchanging the two incoming particles. For the T-channel diagram 3.2(a), in the WvdW Formalism, four independent polarized helicity components of the amplitude can be obtained, which are given as

$$M_a\left(+,+,\sigma,\sigma'\right) = \frac{Q_t e}{\sqrt{2}p_1\cdot k_1}\left\langle k_1\psi\right\rangle\left(k_1^E,0\right)\times$$

$$\left[-\frac{-Q_t e}{2\sqrt{2}\left(p_1\cdot k_2\right)\left(-p_2\cdot k_2\right)}\left\langle k_2\phi'\right\rangle P_{2,E}^i P_{1,iX}\begin{pmatrix}k_2^X\\0\end{pmatrix}\right.$$

$$+\frac{-Q_t e}{2\sqrt{2}\left(p_1\cdot k_2\right)\left(-p_2\cdot k_2\right)}\left\langle k_2\phi'\right\rangle 2\left(p_1\cdot k_2\right)\begin{pmatrix}k_{2,E}\\0\end{pmatrix}$$

$$+\frac{-Q_t e}{2\sqrt{2}\left(p_1\cdot k_2\right)\left(-p_2\cdot k_2\right)}m_f\left\langle\psi'P_1 k_2\right\rangle\begin{pmatrix}k_{2,E}\\0\end{pmatrix}\right]$$

$$=\frac{Q_t^2 e^2}{4\left(p_1\cdot k_1\right)\left(p_1\cdot k_2\right)\left(p_2\cdot k_2\right)}\left(\left\langle k_1\psi\right\rangle\left\langle k_2\phi'\right\rangle\left\langle k_1 P_2 P_1 k_2\right\rangle^*\right.$$

$$-\left(2p_1\cdot k_2\right)\left\langle k_1\psi\right\rangle\left\langle k_2\phi'\right\rangle\left\langle k_1 k_2\right\rangle$$

$$-m_f\left\langle k_1\psi\right\rangle\left\langle\psi'P_1 k_2\right\rangle\left\langle k_1 k_2\right\rangle\right),$$

(3.2.15)

$$M_a\left(-,-,\sigma,\sigma'\right) = \frac{Q_t e}{\sqrt{2}p_1 \cdot k_1} \langle k_1\phi \rangle^* \left(0, k_{1,\dot{E}}\right) \times$$

$$\left[-\frac{-Q_t e}{2\sqrt{2}\left(p_1 \cdot k_2\right)\left(-p_2 \cdot k_2\right)} \langle k_2\psi' \rangle P_2^{\dot{E}J} P_{1,J\dot{X}} \begin{pmatrix} 0 \\ k_2^{\dot{X}} \end{pmatrix} \right.$$

$$+ \frac{-Q_t e}{2\sqrt{2}\left(p_1 \cdot k_2\right)\left(-p_2 \cdot k_2\right)} \langle k_2\psi' \rangle^* 2\left(p_1 \cdot k_2\right) \begin{pmatrix} 0 \\ k_2^{\dot{E}} \end{pmatrix}$$

$$+ \left. \frac{-Q_t e}{2\sqrt{2}\left(p_1 \cdot k_2\right)\left(-p_2 \cdot k_2\right)} \left(-m_f\right) \langle \phi' P_1 k_2 \rangle^* \begin{pmatrix} 0 \\ k_2^{\dot{E}} \end{pmatrix} \right] \tag{3.2.16}$$

$$= \frac{Q_t{}^2 e^2}{4\left(p_1 \cdot k_1\right)\left(p_1 \cdot k_2\right)\left(p_2 \cdot k_2\right)} \left(-\langle k_1\phi \rangle^* \langle k_2\psi' \rangle^* \langle k_1 P_2 P_1 k_2 \rangle \right.$$

$$+ \left(2p_1 \cdot k_2\right) \langle k_1\phi \rangle^* \langle k_2\psi' \rangle^* \langle k_1 k_2 \rangle^*$$

$$- m_f \langle k_1\phi \rangle^* \langle \phi' P_1 k_2 \rangle \langle k_1 k_2 \rangle^* \Big),$$

$$iM_a\left(+,-,\sigma,\sigma'\right) = \frac{Q_t e}{\sqrt{2}p_1 \cdot k_1} \langle k_1\psi \rangle \left(k_1^E, 0\right) \times$$

$$\left[\frac{-Q_t e}{2\sqrt{2}\left(p_1 \cdot k_1\right)\left(-p_2 \cdot k_2\right)} \left(-1\right) \langle \phi' P_1 k_2 \rangle^* P_{2,E}^{\dot{I}} \begin{pmatrix} k_{2,\dot{I}} \\ 0 \end{pmatrix} \right.$$

$$+ \left. \frac{-Q_t e}{2\sqrt{2}\left(p_1 \cdot k_2\right)\left(-p_2 \cdot k_2\right)} m_f \langle k_2\psi' \rangle P_{1,E\dot{X}} \begin{pmatrix} k_{2,\dot{X}} \\ 0 \end{pmatrix} \right] \tag{3.2.17}$$

$$= \frac{Q_t{}^2 e^2}{4\left(p_1 \cdot k_1\right)\left(p_1 \cdot k_2\right)\left(p_2 \cdot k_2\right)} \left(\left(-1\right) \langle k_1\psi \rangle \langle \phi' P_1 k_2 \rangle^* \langle k_1 P_2 k_2 \rangle^* \right.$$

$$+ m_f \langle k_1\psi \rangle \langle k_2\psi' \rangle^* \langle k_1 P_1 k_2 \rangle^* \Big),$$

$$M_a\left(-,+,\sigma,\sigma'\right) = \frac{Q_t e}{\sqrt{2}p_1 \cdot k_1} \langle k_1\phi \rangle^* \left(0, k_{1,\dot{E}}\right) \times$$

$$\left[\frac{-Q_t e}{2\sqrt{2}\left(p_1 \cdot k_2\right)\left(-p_2 \cdot k_2\right)} \left(-1\right) \langle \psi' P_1 k_2 \rangle P_2^{\dot{E}J} \begin{pmatrix} 0 \\ k_{2,J} \end{pmatrix} \right.$$

$$+ \left. \frac{-Q_t e}{2\sqrt{2}\left(p_1 \cdot k_2\right)\left(-p_2 \cdot k_2\right)} \left(-1\right) m_f \langle k_2\phi' \rangle P_{1,\dot{E}X} \begin{pmatrix} 0 \\ k_2^X \end{pmatrix} \right] \tag{3.2.18}$$

$$= \frac{Q_t{}^2 e^2}{4\left(p_1 \cdot k_1\right)\left(p_1 \cdot k_2\right)\left(p_2 \cdot k_2\right)} \left(\left(-1\right) \langle k_1\phi \rangle^* \langle \psi' P_1 k_2 \rangle \langle k_1 P_2 k_2 \rangle \right.$$

$$- m_f \langle k_1\phi \rangle^* \langle k_2\phi' \rangle \langle k_1 P_1 k_2 \rangle \Big).$$

For the U-channel diagram 3.2(b), the helicity amplitudes can be obtained by interchanging the incoming gluons in 3.2(a), we have

$$M_b\left(+,+,\sigma,\sigma'\right) = \frac{Q_t e}{\sqrt{2}p_1\cdot k_2}\left\langle k_2\psi\right\rangle\left(k_2^E,0\right)\times$$

$$\left[\frac{-Q_t e}{2\sqrt{2}\left(p_1\cdot k_1\right)\left(-p_2\cdot k_1\right)}\left(-1\right)\left\langle k_1\phi'\right\rangle P_{2,E}^{\dot{I}}P_{1,\dot{I}X}\begin{pmatrix}k_1^X\\0\end{pmatrix}\right.$$

$$+\frac{-Q_t e}{2\sqrt{2}\left(p_1\cdot k_1\right)\left(-p_2\cdot k_1\right)}\left\langle k_1\phi'\right\rangle 2\left(p_1\cdot k_1\right)\begin{pmatrix}k_{1,E}\\0\end{pmatrix}$$

$$+\frac{-Q_t e}{2\sqrt{2}\left(p_1\cdot k_1\right)\left(-p_2\cdot k_1\right)}m_f\left\langle\psi'P_1k_1\right\rangle\left.\begin{pmatrix}k_{1,E}\\0\end{pmatrix}\right]$$

$$=\frac{Q_t{}^2e^2}{4\left(p_1\cdot k_2\right)\left(p_1\cdot k_1\right)\left(p_2\cdot k_1\right)}\left(\left\langle k_2\psi\right\rangle\left\langle k_1\phi'\right\rangle\left\langle k_2P_2P_1k_1\right\rangle^*\right.$$

$$+\left(2p_1\cdot k_1\right)\left\langle k_2\psi\right\rangle\left\langle k_1\phi'\right\rangle\left\langle k_1k_2\right\rangle$$

$$-m_f\left\langle k_2\psi\right\rangle\left\langle\psi'P_1k_1\right\rangle\left\langle k_1k_2\right\rangle\left.\vphantom{\frac{}{}}\right), \tag{3.2.19}$$

$$M_b\left(-,-,\sigma,\sigma'\right) = \frac{Q_t e}{\sqrt{2}p_1\cdot k_2}\left\langle k_2\phi\right\rangle^*\left(0,k_{2,\dot{E}}\right)\times$$

$$\left[\frac{-Q_t e}{2\sqrt{2}\left(p_1\cdot k_1\right)\left(-p_2\cdot k_1\right)}\left(-1\right)\left\langle k_1\psi'\right\rangle^* P_2^{\dot{E}J}P_{1,J\dot{X}}\begin{pmatrix}0\\k_1^{\dot{X}}\end{pmatrix}\right.$$

$$+\frac{-Q_t e}{2\sqrt{2}\left(p_1\cdot k_1\right)\left(-p_2\cdot k_1\right)}\left\langle k_1\psi'\right\rangle^* 2\left(p_1\cdot k_1\right)\begin{pmatrix}0\\k_1^{\dot{E}}\end{pmatrix}$$

$$+\frac{-Q_t e}{2\sqrt{2}\left(p_1\cdot k_2\right)\left(-p_2\cdot k_2\right)}\left(-1\right)m_f\left\langle\phi'P_1k_1\right\rangle^*\left.\begin{pmatrix}0\\k_2^{\dot{E}}\end{pmatrix}\right]$$

$$=\frac{Q_t{}^2e^2}{4\left(p_1\cdot k_2\right)\left(p_1\cdot k_1\right)\left(p_2\cdot k_1\right)}\left(\left(-1\right)\left\langle k_2\phi\right\rangle^*\left\langle k_1\psi'\right\rangle^*\left\langle k_2P_2P_1k_1\right\rangle\right.$$

$$+\left(2p_1\cdot k_1\right)\left\langle k_2\phi\right\rangle^*\left\langle k_1\psi'\right\rangle^*\left\langle k_2k_1\right\rangle^*$$

$$-m_f\left\langle k_2\phi\right\rangle^*\left\langle\phi'P_1k_1\right\rangle\left\langle k_2k_1\right\rangle^*\left.\vphantom{\frac{}{}}\right), \tag{3.2.20}$$

$$M_b\left(-,+,\sigma,\sigma'\right) = \frac{Q_t e}{\sqrt{2}p_1\cdot k_2}\left\langle k_2\psi\right\rangle\left(k_2^E,0\right)\times$$

$$\left[\frac{-Q_t e}{2\sqrt{2}(p_1\cdot k_1)(-p_2\cdot k_1)}(-1)<\phi'P_1k_1>^*P_{2,E}^i\begin{pmatrix}k_{1,i}\\0\end{pmatrix}\right.$$

$$\left. + \frac{-Q_t e}{2\sqrt{2}\left(p_1\cdot k_2\right)\left(-p_2\cdot k_2\right)}m_f\left\langle k_2\psi'\right\rangle P_{1,E\dot{X}}\begin{pmatrix}k_1^{\dot{X}}\\0\end{pmatrix}\right] \tag{3.2.21}$$

$$= \frac{Q_t{}^2e^2}{4\left(p_1\cdot k_2\right)\left(p_1\cdot k_1\right)\left(p_2\cdot k_1\right)}\left((-1)\left\langle k_2\psi\right\rangle\left\langle\phi'P_1k_1\right\rangle^*\left\langle k_2P_2k_1\right\rangle^*\right.$$

$$\left. + m_f\left\langle k_2\psi\right\rangle\left\langle k_1\psi'\right\rangle^*\left\langle k_2P_1k_1\right\rangle^*\right),$$

$$M_b\left(+,-,\sigma,\sigma'\right) = \frac{Q_t e}{\sqrt{2}p_1\cdot k_2}\left\langle k_2\phi\right\rangle^*\left(0,k_{2,\dot{E}}\right)\times$$

$$\left[\frac{-Q_t e}{2\sqrt{2}\left(p_1\cdot k_1\right)\left(-p_2\cdot k_1\right)}(-1)\left\langle\psi'P_1k_1\right\rangle P_2^{\dot{E}J}\begin{pmatrix}0\\k_{1,J}\end{pmatrix}\right.$$

$$\left. + \frac{-Q_t e}{2\sqrt{2}\left(p_1\cdot k_1\right)\left(-p_2\cdot k_1\right)}(-1)m_f\left\langle k_1\phi'\right\rangle P_{1,\dot{E}X}\begin{pmatrix}0\\k_1^X\end{pmatrix}\right] \tag{3.2.22}$$

$$= \frac{Q_t{}^2e^2}{4\left(p_1\cdot k_2\right)\left(p_1\cdot k_1\right)\left(p_2\cdot k_1\right)}\left((-1)\left\langle k_2\phi\right\rangle^*\left\langle\psi'P_1k_1\right\rangle\left\langle k_2P_2k_1\right\rangle\right.$$

$$\left. - m_f\left\langle k_1\phi\right\rangle^*\left\langle k_2\phi'\right\rangle\left\langle k_2P_1k_1\right\rangle\right).$$

Comparing the amplitudes of diagram 3.2(b) and diagram 3.2(a),we find

$$M_b\left(+,+,\sigma,\sigma'\right) = \underset{k_1\leftrightarrow k_2}{M_a}\left(+,+,\sigma,\sigma'\right),$$

$$M_b\left(-,-,\sigma,\sigma'\right) = \underset{k_1\leftrightarrow k_2}{M_a}\left(-,-,\sigma,\sigma'\right),$$

$$M_b\left(+,-,\sigma,\sigma'\right) = \underset{k_1\leftrightarrow k_2}{M_a}\left(-,+,\sigma,\sigma'\right), \tag{3.2.23}$$

$$M_b\left(-,+,\sigma,\sigma'\right) = \underset{k_1\leftrightarrow k_2}{M_a}\left(+,-,\sigma,\sigma'\right),$$

which are the relations between the amplitudes of T-channel and U-channel for the same process due to the crossing symmetry in the WvdW Formalism. Due to this crossing symmetry, one can directly obtain the U-channel contribution from the corresponding T-channel result. Specifically, for the U-channel diagrams 3.2(d) and

3.2(f), we have

$$M_d\left(-,-,\sigma,\sigma'\right) = \underset{k_1 \leftrightarrow k_2}{M_c}\left(-,-,\sigma,\sigma'\right),$$

$$M_d\left(+,-,\sigma,\sigma'\right) = \underset{k_1 \leftrightarrow k_2}{M_c}\left(-,+,\sigma,\sigma'\right),$$

$$M_d\left(-,+,\sigma,\sigma'\right) = \underset{k_1 \leftrightarrow k_2}{M_c}\left(+,-,\sigma,\sigma'\right),$$

$$M_f\left(+,+,\sigma,\sigma'\right) = \underset{k_1 \leftrightarrow k_2}{M_e}\left(+,+,\sigma,\sigma'\right), \tag{3.2.24}$$

$$M_f\left(-,-,\sigma,\sigma'\right) = \underset{k_1 \leftrightarrow k_2}{M_e}\left(-,-,\sigma,\sigma'\right),$$

$$M_f\left(+,-,\sigma,\sigma'\right) = \underset{k_1 \leftrightarrow k_2}{M_e}\left(-,+,\sigma,\sigma'\right),$$

$$M_f\left(-,+,\sigma,\sigma'\right) = \underset{k_1 \leftrightarrow k_2}{M_e}\left(+,-,\sigma,\sigma'\right).$$

And we only need to calculate the amplitudes for 3.2(c) and 3.2(e). The four independent polarized amplitudes for the Diagram 3.2(c) are listed below:

$$M_c\left(+,+,\sigma,\sigma'\right) = \frac{Q_t e}{\sqrt{2}p_1 \cdot k_1}\left\langle k_1\psi\right\rangle\left(k_1^E,0\right) \times$$

$$\left[\frac{-Q_t e}{\sqrt{2}\left(p_1 \cdot k_2\right)\left(m_f^2 + 2p_1 \cdot p_3\right)}(-1)\left\langle\phi'P_2P_1k_2\right\rangle\begin{pmatrix}k_{2,E}\\0\end{pmatrix}\right.$$

$$+ \frac{-Q_t e}{\sqrt{2}\left(p_1 \cdot k_2\right)\left(m_f^2 + 2p_1 \cdot p_3\right)}(-1)\left\langle\phi'P_3P_1k_2\right\rangle\begin{pmatrix}k_{2,E}\\0\end{pmatrix}$$

$$\left.+ \frac{-Q_t e}{\sqrt{2}\left(p_1 \cdot k_2\right)\left(m_f^2 + 2p_1 \cdot p_3\right)}\left\langle\phi k_2\right\rangle m_f\left\langle\psi'P_1k_2\right\rangle\begin{pmatrix}k_{2,E}\\0\end{pmatrix}\right] \tag{3.2.25}$$

$$= \frac{Q_t^2 e^2}{2(p_1 \cdot k_1)\left(p_1 \cdot k_2\right)\left(m_f^2 + 2p_1 \cdot p_3\right)}\left(\left\langle k_1\psi\right\rangle\left\langle\phi'P_2P_1k_2\right\rangle^*\left\langle k_1k_2\right\rangle\right.$$

$$+ \left\langle k_1\psi\right\rangle\left\langle\phi'P_3P_1k_2\right\rangle^*\left\langle k_1k_2\right\rangle$$

$$\left.- m_f\left\langle k_2\psi\right\rangle\left\langle k_1\psi\right\rangle\left\langle\psi'P_1k_2\right\rangle\left\langle k_1k_2\right\rangle\right),$$

$$M_c\left(-,-,\sigma,\sigma'\right) = \frac{Q_t e}{\sqrt{2}p_1\cdot k_1}\langle k_1\phi\rangle^*\left(0,k_{1,\dot{E}}\right)\times$$

$$\left[\frac{-Q_t e}{\sqrt{2}\left(p_1\cdot k_2\right)\left(m_f^2+2p_1\cdot p_3\right)}\langle\psi'P_2P_1k_2\rangle^*\begin{pmatrix}k_2^{\dot{E}}\\0\end{pmatrix}\right.$$

$$+\frac{-Q_t e}{\sqrt{2}\left(p_1\cdot k_2\right)\left(m_f^2+2p_1\cdot p_3\right)}\langle\psi'P_3P_1k_2\rangle^*\begin{pmatrix}k_2^{\dot{E}}\\0\end{pmatrix}$$

$$+\frac{-Q_t e}{2\sqrt{2}\left(p_1\cdot k_2\right)\left(m_f^2+2p_1\cdot p_3\right)}\langle\phi k_2\rangle\, m_f\,\langle\phi'P_1k_2\rangle*\left.\begin{pmatrix}k_{2,E}\\0\end{pmatrix}\right] \tag{3.2.26}$$

$$=\frac{Q_t{}^2e^2}{2\left(p_1\cdot k_1\right)\left(p_1\cdot k_2\right)\left(m_f^2+2p_1\cdot p_3\right)}\left(\langle k_1\phi\rangle^*\langle\psi'P_2P_1k_2\rangle\langle k_1k_2\rangle^*\right.$$

$$+\langle k_1\phi\rangle^*\langle\psi'P_3P_1k_2\rangle\langle k_1k_2\rangle^*$$

$$\left.-m_f\langle\phi'P_1k_2\rangle^*\langle k_1k_2\rangle^*\right),$$

$$M_c\left(+,-,\sigma,\sigma'\right) = \frac{Q_t e}{\sqrt{2}p_1\cdot k_1}\langle k_1\psi\rangle\left(k_1^E,0\right)\times$$

$$\left[\frac{-Q_t e}{\sqrt{2}\left(p_1\cdot k_2\right)\left(m_f^2+2p_1\cdot p_3\right)}\langle k_2P_2\phi'\rangle\,P_{1,E\dot{X}}\begin{pmatrix}k_2^{\dot{X}}\\0\end{pmatrix}\right.$$

$$+\frac{-Q_t e}{\sqrt{2}\left(p_1\cdot k_2\right)\left(m_f^2+2p_1\cdot p_3\right)}\langle k_2P_3\phi'\rangle\,P_{1,E\dot{X}}\begin{pmatrix}k_2^{\dot{X}}\\0\end{pmatrix}$$

$$+\frac{-Q_t e}{\sqrt{2}\left(p_1\cdot k_2\right)\left(m_f^2+2p_1\cdot p_3\right)}\langle k_2\psi'\rangle^*\,m_f P_{1,E\dot{X}}\left.\begin{pmatrix}k_2^{\dot{X}}\\0\end{pmatrix}\right] \tag{3.2.27}$$

$$=\frac{Q_t{}^2e^2}{2\left(p_1\cdot k_1\right)\left(p_1\cdot p_2\right)\left(m_f^2+2p_1\cdot p_3\right)}\left((-1)\langle k_1\psi\rangle\langle k_2P_2\phi'\rangle\langle k_1P_1k_2\rangle^*\right.$$

$$-\langle k_1\psi\rangle\langle k_2P_3\phi'\rangle\langle k_1P_1k_2\rangle^*$$

$$\left.-m_f<k_1\psi><k_2\psi'>^*<k_1P_1k_2>^*\right),$$

$$M_c\left(-,+,\sigma,\sigma'\right)=\frac{Q_t e}{\sqrt{2}p_1\cdot k_1}\left\langle k_1\phi\right\rangle^*\left(0,k_{1,\dot{E}}\right)\times$$

$$\left[\frac{-Q_t e}{\sqrt{2}\left(p_1\cdot k_2\right)\left(m_f^2+2p_1\cdot p_3\right)}\left(-1\right)\left\langle k_2 P_1\psi'\right\rangle^* P_{1,\dot{E}X}\begin{pmatrix}k_2^X\\0\end{pmatrix}\right.$$

$$+\frac{-Q_t e}{\sqrt{2}\left(p_1\cdot k_2\right)\left(m_f^2+2p_1\cdot p_3\right)}\left(-1\right)\left\langle k_2 P_3\psi'\right\rangle^* P_{1,\dot{E}X}\begin{pmatrix}k_2^X\\0\end{pmatrix}$$

$$+\frac{-Q_t e}{2\sqrt{2}\left(p_1\cdot k_2\right)\left(m_f^2+2p_1\cdot p_3\right)}\left\langle \phi k_2\right\rangle\left(-1\right)m_f\left\langle k_2\phi'\right\rangle P_{1,\dot{E}X}\begin{pmatrix}0\\k_2^X\end{pmatrix}\right] \tag{3.2.28}$$

$$=\frac{Q_t^{\,2}e^2}{2\left(p_1\cdot k_1\right)\left(p_1\cdot k_2\right)\left(m_f^2+2p_1\cdot p_3\right)}\left(\left\langle k_1\phi\right\rangle^*\left\langle k_2 P_1\psi'\right\rangle^*\left\langle k_1 P_1 k_2\right\rangle\right.$$

$$+\left\langle k_1\phi\right\rangle^*\left\langle k_2 P_1\psi'\right\rangle^*\left\langle k_1 P_1 k_2\right\rangle$$

$$+m_f\left\langle k_1\phi\right\rangle^*\left\langle k_2\phi'\right\rangle\left\langle k_1 P_1 k_2\right\rangle\Big).$$

For the last T-channel diagram 3.2(e), one has:

$$M_e\left(+,+,\sigma,\sigma'\right)=\frac{Q_t e}{2\sqrt{2}p_1\cdot k_1 p_1\cdot p_3}\left\langle\psi P_3 P_1 k_1\right\rangle\left(k_1^F,0\right)\times$$

$$\left[\frac{-Q_t e}{2\sqrt{2}\left(p_1\cdot k_2\right)\left(-p_2\cdot k_2\right)}\left\langle k_2\phi'\right\rangle\left(-1\right)\left\langle p_2 P_1 k_2\right\rangle\begin{pmatrix}k_{2,F}\\0\end{pmatrix}\right.$$

$$+\frac{-Q_t e}{2\sqrt{2}\left(p_1\cdot k_2\right)\left(-p_2\cdot k_2\right)}m_f\left\langle\psi' P_1 k_2\right\rangle\begin{pmatrix}k_{2,F}\\0\end{pmatrix}\right] \tag{3.2.29}$$

$$=\frac{Q_t^{\,2}e^2}{8\left(p_1\cdot k_1\right)\left(p_1\cdot p_3\right)\left(p_1\cdot k_2\right)\left(p_2\cdot k_2\right)}$$

$$+\left(\left\langle\psi P_3 P_1 k_1\right\rangle^*\left\langle p_2 P_1 k_2\right\rangle\left\langle k_2\phi'\right\rangle\left\langle k_2 k_1\right\rangle\right.$$

$$-m_f\left\langle\psi P_3 P_1 k_1\right\rangle^*\left\langle\psi' P_1 k_2\right\rangle\left\langle k_2 k_1\right\rangle\Big),$$

$$M_e\left(-,-,\sigma,\sigma'\right) = \frac{Q_t e}{2\sqrt{2}p_1 \cdot k_1 p_1 \cdot p_3} \langle \phi P_3 P_1 k_1 \rangle^* \left(0, k_{1,\dot{F}}\right) \times$$

$$\left[\frac{-Q_t e}{2\sqrt{2}(p_1 \cdot k_2)(-p_2 \cdot k_2)} (-1) \langle k_2 \psi' \rangle^* \langle p_2 P_1 k_2 \rangle^* \begin{pmatrix} p_2^{\dot{F}} \\ 0 \end{pmatrix} \right.$$

$$\left. + \frac{-Q_t e}{2\sqrt{2}(p_1 \cdot k_2)(-p_2 \cdot k_2)} (-m_f) \langle \phi' P_1 k_2 \rangle^* \begin{pmatrix} k_2^{\dot{F}} \\ 0 \end{pmatrix} \right] \qquad (3.2.30)$$

$$= \frac{Q_t^2 e^2}{8(p_1 \cdot k_1)(p_1 \cdot p_3)(p_1 \cdot k_2)(p_2 \cdot k_2)}$$

$$- \left(\langle \phi P_3 P_1 k_1 \rangle \langle p_2 P_1 k_2 \rangle^* \langle k_2 \psi' \rangle^* \langle k_1 p_2 \rangle^* \right.$$

$$\left. - m_f \langle \phi P_3 P_1 k_1 \rangle \langle \phi' P_1 k_2 \rangle^* \langle k_1 k_2 \rangle^* \right),$$

$$M_e\left(+,-,\sigma,\sigma'\right) = \frac{Q_t e}{2\sqrt{2}p_1 \cdot k_1 p_1 \cdot p_3} \langle \psi P_3 P_1 k_1 \rangle \left(k_1^F, 0\right) \times$$

$$\left[\frac{-Q_t e}{2\sqrt{2}(p_1 \cdot k_2)(-p_2 \cdot k_2)} (-1) \langle \phi' P_1 k_2 \rangle^* P_{2,F}^{\dot{i}} \begin{pmatrix} k_{2,\dot{i}} \\ 0 \end{pmatrix} \right.$$

$$\left. + \frac{-Q_t e}{2\sqrt{2}(p_1 \cdot k_2)(-p_2 \cdot k_2)} m_f \langle k_2 \psi' \rangle P_{1,F\dot{X}} \begin{pmatrix} k_2^{\dot{X}} \\ 0 \end{pmatrix} \right] \qquad (3.2.31)$$

$$= \frac{Q_t^2 e^2}{8(p_1 \cdot k_1)(p_1 \cdot p_3)(p_1 \cdot k_2)(p_2 \cdot k_2)}$$

$$- \left(\langle \psi P_3 P_1 k_1 \rangle^* \langle \phi' P_1 k_2 \rangle^* \langle k_1 P_2 k_2 \rangle^* \right.$$

$$\left. + m_f \langle \psi P_3 P_1 k_1 \rangle^* \langle k_2 \psi' \rangle^* \langle k_1 P_1 k_2 \rangle^* \right),$$

$$M_e\left(-,+,\sigma,\sigma'\right) = \frac{Q_t e}{2\sqrt{2}p_1 \cdot k_1 p_1 \cdot p_3} \langle \phi P_3 P_1 k_1 \rangle^* \left(0, k_{1,\dot{F}}\right) \times$$

$$\left[\frac{-Q_t e}{2\sqrt{2}(p_1 \cdot k_2)(-p_2 \cdot k_2)} (-1) \langle \psi' P_1 k_2 \rangle P_2^{\dot{F}J} \begin{pmatrix} 0 \\ k_2^J \end{pmatrix} \right.$$

$$\left. + \frac{-Q_t e}{2\sqrt{2}(p_1 \cdot k_2)(-p_2 \cdot k_2)} (-m_f) \langle k_2 \phi \rangle P_{1,\dot{F}X} \begin{pmatrix} 0 \\ k_2^X \end{pmatrix} \right] \qquad (3.2.32)$$

$$= \frac{Q_t^2 e^2}{8(p_1 \cdot k_1)^2(p_1 \cdot p_2)(p_1 \cdot k_2)(p_2 \cdot k_2)}$$

$$(-1 \langle \phi P_3 P_1 k_1 \rangle \langle \psi' P_1 k_2 \rangle \langle k_1 P_2 k_2 \rangle$$

$$- m_f \langle \phi P_3 P_1 k_1 \rangle \langle k_2 \phi \rangle \langle k_1 P_1 k_2 \rangle).$$

Then we consider the non-SM-like diagrams with pseudoscalars. Note that the

pseudoscalar operator only differ from the scalar operator by a γ^5 factor. Conse-
quently, we find that the amplitudes including pseudoscalars can actually be ex-
pressed in terms of the SM-like amplitudes with scalars.

$$M'_a\left(+,+,\sigma,\sigma'\right) = M_a\left(+,+,\sigma,\sigma'\right), \qquad M'_a\left(-,-,\sigma,\sigma'\right) = -M_a\left(-,-,\sigma,\sigma'\right)$$

$$M'_a\left(+,-,\sigma,\sigma'\right) = M_a\left(+,-,\sigma,\sigma'\right), \qquad M'_a\left(-,+,\sigma,\sigma'\right) = -M_a\left(-,+,\sigma,\sigma'\right)$$

$$M'_b\left(+,+,\sigma,\sigma'\right) = M_b\left(+,+,\sigma,\sigma'\right), \qquad M'_b\left(-,-,\sigma,\sigma'\right) = -M_b\left(-,-,\sigma,\sigma'\right)$$

$$M'_b\left(+,-,\sigma,\sigma'\right) = -M_b\left(+,-,\sigma,\sigma'\right), \qquad M'_b\left(-,+,\sigma,\sigma'\right) = M_b\left(-,+,\sigma,\sigma'\right)$$

$$M'_c\left(+,+,\sigma,\sigma'\right) = M_c\left(+,+,\sigma,\sigma'\right), \qquad M'_c\left(-,-,\sigma,\sigma'\right) = -M_c\left(-,-,\sigma,\sigma'\right)$$

$$M'_c\left(+,-,\sigma,\sigma'\right) = M_c\left(+,-,\sigma,\sigma'\right), \qquad M'_c\left(-,+,\sigma,\sigma'\right) = -M_c\left(-,+,\sigma,\sigma'\right)$$

$$M'_d\left(+,+,\sigma,\sigma'\right) = M_d\left(+,+,\sigma,\sigma'\right), \qquad M'_d\left(-,-,\sigma,\sigma'\right) = -M_d\left(-,-,\sigma,\sigma'\right)$$

$$M'_d\left(+,-,\sigma,\sigma'\right) = -M_d\left(+,-,\sigma,\sigma'\right), \qquad M'_d\left(-,+,\sigma,\sigma'\right) = M_d\left(-,+,\sigma,\sigma'\right)$$

$$M'_e\left(+,+,\sigma,\sigma'\right) = M_e\left(+,+,\sigma,\sigma'\right), \qquad M'_e\left(-,-,\sigma,\sigma'\right) = -M_e\left(-,-,\sigma,\sigma'\right)$$

$$M'_e\left(+,-,\sigma,\sigma'\right) = M_e\left(+,-,\sigma,\sigma'\right), \qquad M'_e\left(-,+,\sigma,\sigma'\right) = -M_e\left(-,+,\sigma,\sigma'\right)$$

$$M'_f\left(+,+,\sigma,\sigma'\right) = M_f\left(+,+,\sigma,\sigma'\right), \qquad M'_f\left(-,-,\sigma,\sigma'\right) = -M_f\left(-,-,\sigma,\sigma'\right)$$

$$M'_f\left(+,-,\sigma,\sigma'\right) = -M_f\left(+,-,\sigma,\sigma'\right) \qquad M'_f\left(-,+,\sigma,\sigma'\right) = M_f\left(-,+,\sigma,\sigma'\right).$$

$$(3.2.33)$$

3.2.3 The S-channel Amplitudes

In this part we consider the S-channel diagrams, which include the SM-like diagrams
3.2(g) and 3.2(h), and their corresponding non-SM-like pseudoscalar diagrams. A-
gain, for the diagram 3.2(g), we can obtain an amplitude including four independent
components, in which a general helicity amplitude can be expressed as

$$M_g\left(\lambda_1,\lambda_2,\sigma,\sigma'\right) = \frac{1}{\left(p_1+p_3\right)^2 - m_f^2}\left(\psi^K,\phi_{\dot{K}}\right)$$

$$\begin{pmatrix} \delta_K^J & 0 \\ 0 & \delta_{\dot{J}}^{\dot{K}} \end{pmatrix} \begin{pmatrix} m_f\delta_J^I & \left(P_1+P_3\right)_{J\dot{I}} \\ \left(P_1+P_3\right)^{\dot{J}I} & m_f\delta_{\dot{I}}^{\dot{J}} \end{pmatrix} \begin{pmatrix} 0 & \delta_{\dot{L}}^{\dot{G}}\delta_I^J \\ \epsilon^{\dot{I}\dot{G}}\epsilon^{LH} & 0 \end{pmatrix} \begin{pmatrix} \phi'_L \\ \psi'^{\dot{L}} \end{pmatrix} \qquad (3.2.34)$$

$$\frac{-2\epsilon_{\dot{E}\dot{G}}\epsilon_{FH}}{2k_1 \cdot k_2}\frac{e}{4}\left(\epsilon^{\dot{A}\dot{C}}\epsilon^{BD}\left(K_1-K_2\right)^{\dot{E}F} + \epsilon^{\dot{C}\dot{E}}\epsilon^{DF}\left(K_2-K_3\right)^{\dot{A}B}\right.$$

$$\left. + \epsilon^{\dot{A}\dot{E}}\epsilon^{BF}\left(K_3-K_1\right)^{\dot{C}D}\right)\varepsilon_{1,\dot{A}B}\varepsilon_{2,\dot{C}D},$$

where λ_1, λ_2, σ and σ' has not been specified. In order to simplify the analysis, we define:

$$
\begin{aligned}
C_1 &= \frac{1}{2\left(p_1 + p_3\right)^2 - m_f^2} \left(\psi^J \left(P_1 + P_3\right)_J^{\dot{G}} \phi'^H \right. \\
&\quad \left. + m_f \psi^H \psi'^{\dot{G}} + \phi_j \left(P_1 + P_3\right)^{J\dot{G}} \psi'^{\dot{G}} + m_f \phi^{\dot{G}} \phi'^H \right) \\
&= C_1' + C_2',
\end{aligned}
\tag{3.2.35}
$$

where

$$
\begin{aligned}
C_1' &= \frac{1}{\left(p_1 + p_3\right)^2 - m_f^2} \left(\psi^J \left(P_1 + P_3\right)_J^{\dot{G}} \phi'^H + m_f \psi^H \psi'^{\dot{G}}\right), \\
C_2' &= \frac{1}{\left(p_1 + p_3\right)^2 - m_f^2} \left(\phi_j \left(P_1 + P_3\right)^{J\dot{G}} \psi'^{\dot{G}} + m_f \phi^{\dot{G}}\right) \phi'^H,
\end{aligned}
\tag{3.2.36}
$$

and

$$
\begin{aligned}
C_2 &= \frac{-e}{4 k_1 \cdot k_2} \left(\epsilon^{\dot{A}\dot{C}} \epsilon^{BD} \left(K_1 - K_2\right)_{\dot{G}H} \right. \\
&\quad \left. + \epsilon_{\dot{G}}{}^{\dot{C}} \epsilon_H{}^D \left(K_2 - K_3\right)^{\dot{A}B} + \epsilon_{\dot{G}}{}^{\dot{A}} \epsilon_H{}^B \left(K_3 - K_1\right)^{\dot{C}D}\right) \varepsilon_{1,\dot{A}B} \varepsilon_{2,\dot{C}D}.
\end{aligned}
\tag{3.2.37}
$$

As a result, we can express $M_g\left(\lambda_1, \lambda_2, \sigma, \sigma'\right)$ in terms of two divided parts as

$$
\begin{aligned}
M_g^{(1)}\left(\lambda_1, \lambda_2, \sigma, \sigma'\right) &= C_1' \cdot C_2, \\
M_g^{(2)}\left(\lambda_1, \lambda_2, \sigma, \sigma'\right) &= C_2' \cdot C_2.
\end{aligned}
\tag{3.2.38}
$$

For the SM-like diagram 3.2(h), the general helicity amplitude takes the form

$$
\begin{aligned}
M_h\left(\lambda_1, \lambda_2, \sigma, \sigma'\right) &= \frac{1}{\left(p_2 + p_3\right)^2 - m_f^2} \left(\psi^I, \phi_{\dot{I}}\right) \\
&\begin{pmatrix} 0 & \delta_j^{\dot{G}} \delta_I^H \\ \epsilon^{\dot{I}\dot{G}} \epsilon^{JH} & 0 \end{pmatrix} \begin{pmatrix} m_f \delta_J^K & \left(P_2 + P_3\right)_{J\dot{K}} \\ \left(P_2 + P_3\right)^{jK} & m_f \delta_{\dot{K}}^j \end{pmatrix} \begin{pmatrix} \delta_K^L & 0 \\ 0 & \delta_{\dot{L}}^{\dot{K}} \end{pmatrix} \begin{pmatrix} \phi'_L \\ \psi'^{\dot{L}} \end{pmatrix} \\
&\frac{-2\epsilon_{\dot{E}\dot{G}} \epsilon_{FH}}{2 k_1 \cdot k_2} \frac{e}{4} \left(\epsilon^{\dot{A}\dot{C}} \epsilon^{BD} \left(K_1 - K_2\right)^{\dot{E}F} \right. \\
&\left. + \epsilon^{\dot{C}\dot{E}} \epsilon^{DF} \left(K_2 - K_3\right)^{\dot{A}B} + \epsilon^{\dot{A}\dot{E}} \epsilon^{BF} \left(K_3 - K_1\right)^{\dot{C}D}\right) \varepsilon_{1,\dot{A}B} \varepsilon_{2,\dot{C}D}.
\end{aligned}
\tag{3.2.39}
$$

If we define

$$
\begin{aligned}
C_3 &= \frac{1}{\left(p_2 + p_3\right)^2 - m_f^2} \left(\psi^H \left(P_2 + P_3\right)^{\dot{G}K} \phi'_K + m_f \phi^{\dot{G}} \phi'^H \right. \\
&\quad \left. + \left(P_2 + P_3\right)^H{}_{\dot{K}} \psi'^{\dot{K}} \phi^{\dot{G}} + m_f \psi^H \phi'^{\dot{G}}\right) \\
&= C_3' + C_4',
\end{aligned}
\tag{3.2.40}
$$

where

$$C_3' = \frac{1}{(p_2 + p_3)^2 - m_f^2} \left(\psi^H (P_2 + P_3)^{\dot{G}K} \phi'_K + m_f \phi^{\dot{G}} \phi'^H \right),$$

$$C_4' = \frac{1}{(p_2 + p_3)^2 - m_f^2} \left((P_2 + P_3)^H{}_{\dot{K}} \psi'^{\dot{K}} \phi^{\dot{G}} + m_f \psi^H \phi'^{\dot{G}} \right).$$

(3.2.41)

Similar to the former case, we find that this T-channel amplitude could be divided into two parts as

$$M_h^{(1)} (\lambda_1, \lambda_2, \sigma, \sigma') = C_3' \cdot C_2$$

$$M_h^{(2)} (\lambda_1, \lambda_2, \sigma, \sigma') = C_4' \cdot C_2$$

(3.2.42)

Next we will consider those non-SM-like pseudoscalar diagrams with the same topology as 3.2(g) and 3.2(h). The general amplitude of the first diagram could be written as

$$M_g' (\lambda_1, \lambda_2, \sigma, \sigma') = \frac{1}{(p_1 + p_3)^2 - m_f^2} \left(\psi^K, \phi_{\dot{K}} \right)$$

$$\begin{pmatrix} \delta_K^J & 0 \\ 0 & -\delta_{\dot{J}}^{\dot{K}} \end{pmatrix} \begin{pmatrix} m_f \delta_J^I & (P_1 + P_3)_{J\dot{I}} \\ (P_1 + P_3)^{\dot{J}I} & m_f \delta_{\dot{I}}^{\dot{J}} \end{pmatrix} \begin{pmatrix} 0 & \delta_{\dot{L}}^{\dot{G}} \delta_I^J \\ \epsilon^{\dot{I}\dot{G}} \epsilon^{LH} & 0 \end{pmatrix} \begin{pmatrix} \phi'_L \\ \psi'^{\dot{L}} \end{pmatrix}$$

(3.2.43)

$$\frac{-2\epsilon_{\dot{E}\dot{G}} \epsilon_{FH}}{2k_1 \cdot k_2} \frac{e}{4} \left(\epsilon^{\dot{A}\dot{C}} \epsilon^{BD} (K_1 - K_2)^{\dot{E}F} \right.$$

$$\left. + \epsilon^{\dot{C}\dot{E}} \epsilon^{DF} (K_2 - K_3)^{\dot{A}B} + \epsilon^{\dot{A}\dot{E}} \epsilon^{BF} (K_3 - K_1)^{\dot{C}D} \right) \varepsilon_{1,\dot{A}B} \varepsilon_{2,\dot{C}D}.$$

If we define

$$C_5 = \frac{1}{(p_1 + p_3)^2 - m_f^2} \left(\psi^J (P_1 + P_3)_J^{\dot{G}} \phi'^H + m_f \psi^H \psi'^{\dot{G}} \right.$$

$$\left. - \phi_{\dot{J}} (P_1 + P_3)^{J\dot{G}} \psi'^{\dot{G}} - m_f \phi^{\dot{G}} \phi'^H \right),$$

(3.2.44)

and it is easy to verify that

$$C_5 = C_1' - C_2'.$$

(3.2.45)

Using the relation in 3.2.44, we find that one can divide $M_g' (\lambda_1, \lambda_2, \sigma, \sigma')$ into two parts that could be expressed by the SM-like amplitudes:

$$M_g'^{(1)} (\lambda_1, \lambda_2, \sigma, \sigma') = C_1' \cdot C_2 = M_g^{(1)} (\lambda_1, \lambda_2, \sigma, \sigma')$$

$$M_g'^{(2)} (\lambda_1, \lambda_2, \sigma, \sigma') = -C_2' \cdot C_2 = -M_g^{(2)} (\lambda_1, \lambda_2, \sigma, \sigma')$$

(3.2.46)

The general helicity amplitude of the second non-SM-like diagram in WvdW Formalism is

$$M_h'\left(\lambda_1, \lambda_2, \sigma, \sigma'\right) = \frac{1}{\left(p_2 + p_3\right)^2 - m_f^2}\left(\psi^I, \phi_{\dot{I}}\right)$$

$$\begin{pmatrix} 0 & \delta_J^{\dot{G}}\delta_I^H \\ \epsilon^{\dot{I}\dot{G}}\epsilon^{JH} & 0 \end{pmatrix} \begin{pmatrix} m_f\delta_J^K & \left(P_2 + P_3\right)_{J\dot{K}} \\ \left(P_2 + P_3\right)^{\dot{J}K} & m_f\delta_{\dot{K}}^{\dot{j}} \end{pmatrix} \begin{pmatrix} \delta_K^L & 0 \\ 0 & -\delta_{\dot{L}}^{\dot{K}} \end{pmatrix} \begin{pmatrix} \phi_L' \\ \psi'^{\dot{L}} \end{pmatrix} \qquad (3.2.47)$$

$$\frac{-2\epsilon_{\dot{E}\dot{G}}\epsilon_{FH}}{2k_1 \cdot k_2}\frac{e}{4}\left(\epsilon^{\dot{A}\dot{C}}\epsilon^{BD}\left(K_1 - K_2\right)^{\dot{E}F}\right.$$

$$\left. + \epsilon^{\dot{C}\dot{E}}\epsilon^{DF}\left(K_2 - K_3\right)^{\dot{A}B} + \epsilon^{\dot{A}\dot{E}}\epsilon^{BF}\left(K_3 - K_1\right)^{\dot{C}D}\right)\varepsilon_{1,\dot{A}B}\varepsilon_{2,\dot{C}D}.$$

If we define

$$C_7 = \frac{1}{\left(p_2 + p_3\right)^2 - m_f^2}\left(\psi^H\left(P_2 + P_3\right)^{\dot{G}K}\phi_K' + m_f\phi^{\dot{G}}\phi'^H\right.$$

$$\left. - \left(P_2 + P_3\right)^H{}_{\dot{K}}\psi'^{\dot{K}}\phi^{\dot{G}} - m_f\psi^H\phi'^{\dot{G}}\right), \qquad (3.2.48)$$

one can find

$$C_7 = C_3' - C_4'. \qquad (3.2.49)$$

Then it turns out that $M_h'(\lambda_1, \lambda_2, \sigma, \sigma')$ t could be split into two parts that can be expressed by SM-like amplitudes as well:

$$M_h'^{(1)}\left(\lambda_1, \lambda_2, \sigma, \sigma'\right) = C_3' \cdot C_2 = M_h^{(1)}\left(\lambda_1, \lambda_2, \sigma, \sigma'\right)$$

$$M_h'^{(2)}\left(\lambda_1, \lambda_2, \sigma, \sigma'\right) = -C_4' \cdot C_2 = -M_h^{(2)}\left(\lambda_1, \lambda_2, \sigma, \sigma'\right). \qquad (3.2.50)$$

In the S-channel case, the relations between SM-like amplitudes and non-SM-like amplitudes as listed as below:

$$M_g'^{(1)}\left(\lambda_1, \lambda_2, \sigma, \sigma'\right) = M_g^{(1)}\left(\lambda_1, \lambda_2, \sigma, \sigma'\right)$$

$$M_g'^{(2)}\left(\lambda_1, \lambda_2, \sigma, \sigma'\right) = -M_g^{(2)}\left(\lambda_1, \lambda_2, \sigma, \sigma'\right)$$

$$M_h'^{(1)}\left(\lambda_1, \lambda_2, \sigma, \sigma'\right) = M_h^{(1)}\left(\lambda_1, \lambda_2, \sigma, \sigma'\right)$$

$$M_h'^{(2)}\left(\lambda_1, \lambda_2, \sigma, \sigma'\right) = -M_h^{(2)}\left(\lambda_1, \lambda_2, \sigma, \sigma'\right). \qquad (3.2.51)$$

From the above calculations above, we find many non-SM-like helicity amplitudes which differ from the corresponding SM-like amplitudes by opposite signs both, together they are

$$M_{a,c,e}'\left(-, -, \sigma, \sigma'\right), \quad M_{a,c,e}'\left(-, +, \sigma, \sigma'\right),$$

$$M_{b,d,f}'\left(-, -, \sigma, \sigma'\right), \quad M_{b,d,f}'\left(+, -, \sigma, \sigma'\right), \qquad (3.2.52)$$

$$M_g'^{(2)}\left(\lambda_1, \lambda_2, \sigma, \sigma'\right), \quad M_h'^{(2)}\left(\lambda_1, \lambda_2, \sigma, \sigma'\right).$$

These helicity amplitudes are responsible for the differences between the cross sections in scalar and pseudoscalar case. However, due to the complicated 3-body phase space for the processes we study it is difficult to leverage these analytic results into an analytic understanding of the origin of the different cross-section values. As one might expect, the presence of the γ^5 appears to be responsible: comparing the scalar and pseudoscalar cases the γ^5 leads to sign change for a number of the helicity amplitudes, suggesting destructive interference in the pseudoscalar scenario.

3.3 Spin and Parity Discriminating Variables

We now turn to the information available in the kinematic distributions which can be formed from the $t\bar{t}X$ final state ($X = S$, A, Z'_{V}, Z'_{A}), focussing on those which have particular sensitivity to the CP and spin properties. For clarity, we present our results in this section at parton level, before providing a full detector-level analysis in Section 3.4.

We show in Figs. 3.3(a) and 3.3(b) the distributions of the di-top invariant mass $m_{t\bar{t}}$ and the transverse momentum of the resonance $p_{\mathrm{T},X}$, for the four simplified models introduced above with the benchmark mass of $m_X = 50$ GeV. The distributions are normalised and hence independent of the coupling g_t, because we are primarily interested in the shape of the distributions rather than the precise values of the production cross sections. Both $m_{t\bar{t}}$ and $p_{\mathrm{T},X}$ (which are correlated) have previously been suggested as variables which may help distinguish between $t\bar{t}S$ and $t\bar{t}A$ production [76,77,82]; here we see that these variables are also sensitive to $t\bar{t}Z'_{\mathrm{V}}$ and $t\bar{t}Z'_{\mathrm{A}}$ production. The distributions are generally quite similar in shape. However, we notice that $t\bar{t}A$ leads to the hardest distributions, with a shift in the peak and a longer tail at large $m_{t\bar{t}}$ and $p_{\mathrm{T},X}$ compared to $t\bar{t}S$. $t\bar{t}Z'_{\mathrm{V}}$ and $t\bar{t}Z'_{\mathrm{A}}$ interpolate between these two behaviours: they lead to spectra which are harder than $t\bar{t}S$, but not so much as $t\bar{t}A$.

It is known that the azimuthal angle distribution between the two top quarks incorporates much information about the quantum numbers of the resonance X. Accessing this information is non-trivial however: the only case where both tops could

(a) Normalised $m_{t\bar{t}}$ distributions

(b) Normalised $p_{\mathrm{T},X}$ distributions

(c) Normalised θ_t^{CM} distributions

(d) Normalised Θ^{CM} distributions
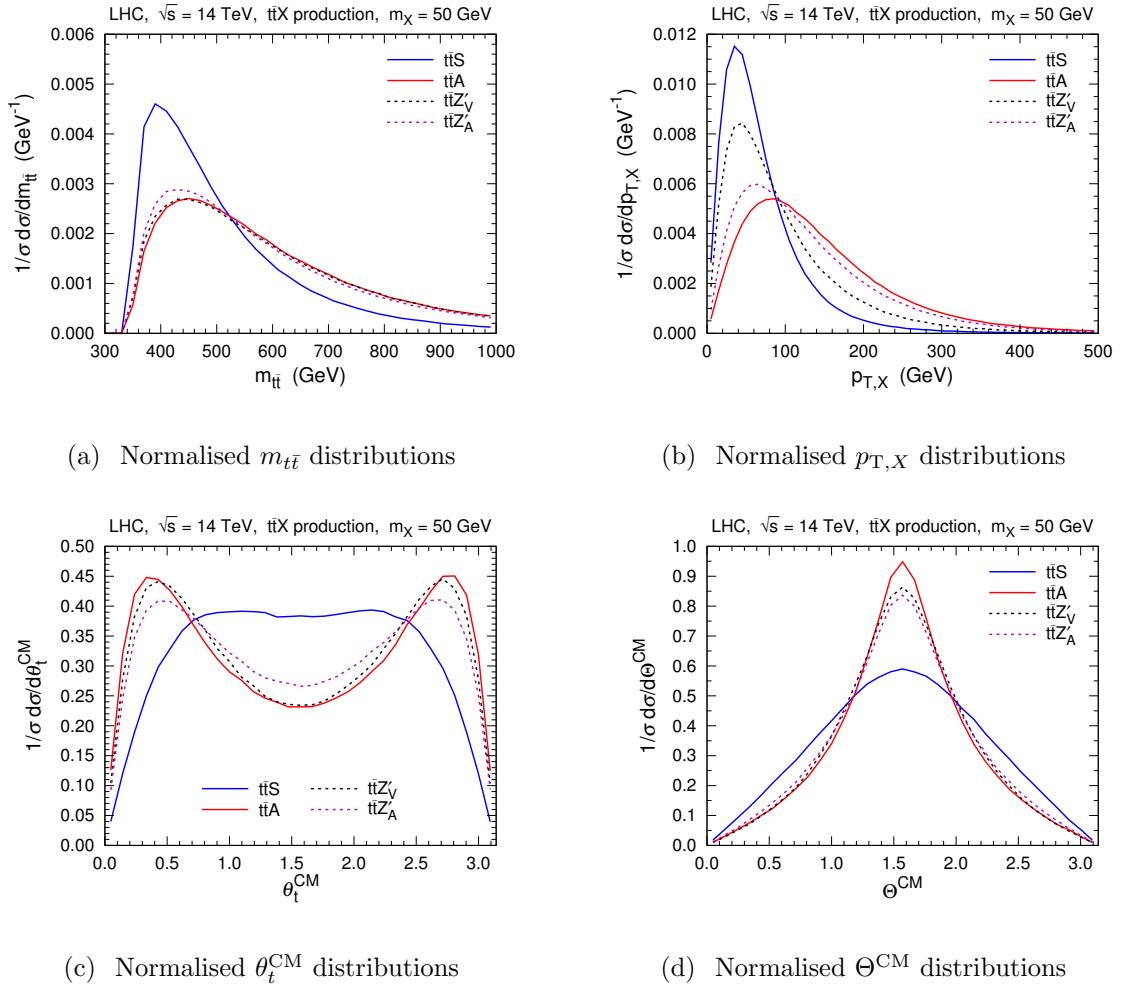
Figure 3.3 This figure shows the normalised distributions of $m_{t\bar{t}}$ (a), $p_{\mathrm{T},X}$ (b), θ_t^{CM} (c) and Θ^{CM} (d) for parton-level $t\bar{t}X$ production with $\sqrt{s} = 14$ TeV and $m_X = 50$ GeV. Here $X = S$, A, Z'_{V}, or Z'_{A}. The angular variables θ_t^{CM} and Θ^{CM} are defined in the CM frame of the $t\bar{t}X$ system. As shown in Fig. 3.4, θ_t^{CM} is the angle between t and the beamline, while Θ^{CM} is the angle between the normal vector to the $t\bar{t}X$ system and the beamline.

in principle be fully reconstructed without missing energy is the fully-hadronic s-cenario, which for any realistic analysis will be plagued by insurmountable QCD backgrounds. This has led Refs. [76, 77] (based on previous work on $t\bar{t}$ spin corre-lations [78, 93]) to explore the fully leptonic case, substituting the azimuthal angle between the leptons for the top quarks, an idea which was met with some success even when X decays to dark matter [77]. They have shown that constraints can be

$t\bar{t}X$ CM frame
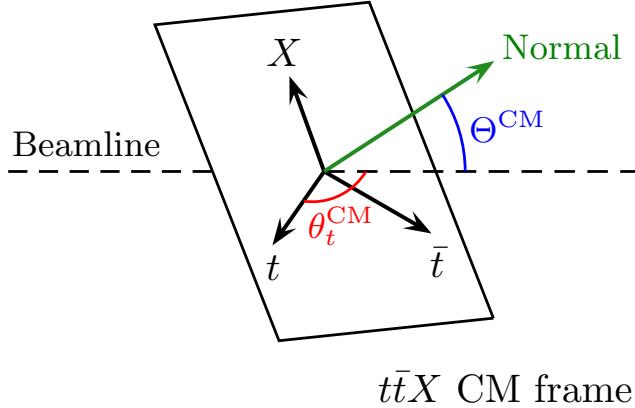
Figure 3.4   This figure shows the definitions of θ_t^{CM} and Θ^{CM} in the CM frame of the $t\bar{t}X$ system. θ_t^{CM} is the angle between the t-quark and the beamline and Θ^{CM} is the angle between the normal vector to the $t\bar{t}X$ system and the beamline.

set on the top-quark Yukawa coupling in associated production towards the end of LHC Run 2 using these techniques.

We therefore consider other angular variables, derived from boosting to the centre-of-mass (CM) frame of the reconstructed $t\bar{t}X$ system. We have investigated a variety of different constructions, and present results for two of the most sensitive that we have found. As illustrated in Fig. 3.4, θ_t^{CM} is the angle between t and the beamline in the CM frame. The normalised θ_t^{CM} distributions are shown in Fig. 3.3(c). We find that this variable is particularly sensitive to $t\bar{t}S$ production, which exhibits a broad plateau at $\pi/2$. The other processes all have a double-peak structure, with $t\bar{t}A$ being the sharpest defined, and $t\bar{t}Z'_{\mathrm{V}}$ and $t\bar{t}Z'_{\mathrm{A}}$ (similar to $m_{t\bar{t}}$ and p_{T} above) interpolating between $t\bar{t}S$ and $t\bar{t}A$.

The other angular variable Θ^{CM} utilises the fact that in the CM frame the $t\bar{t}X$ system forms a plane. We consider the normal vector to this plane, and Θ^{CM} is angle between the normal and the beamline, as explained in Fig. 3.4. Fig. 3.3(d) shows the normalised Θ^{CM} distributions. The shape differences between the scalar and other resonances are not as great in this case, with the distributions for all the simplified models peaking at $\pi/2$. The $t\bar{t}S$ distribution is notable only in that it has the broadest distribution among them. While these variables show good sensitivity
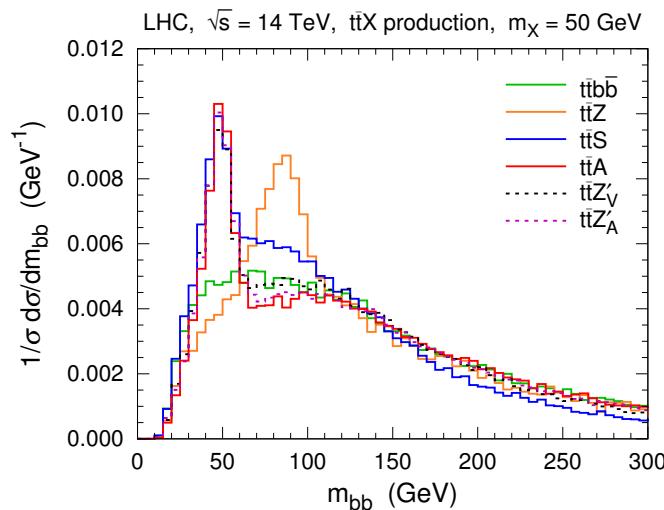
Figure 3.5 This figure shows the normalised m_{bb} distributions after applying all the selection cuts except the cut on m_{bb}. For all the signals we take $m_X = 50$ GeV.

to the properties of the resonance X, a more realistic assessment of their utility requires a full analysis to be performed, which we now turn to.

3.4 Detector-Level Analysis

Previous work has demonstrated that the dominant background in $t\bar{t}X$ final states for low resonance masses comes from $t\bar{t}b\bar{b}$ production [68,94]. While the $t\bar{t}$+light jets rate is significant it is a subdominant background after b-tagging, but with similar kinematics to $t\bar{t}b\bar{b}$ and so will be suppressed by the same analysis cuts. We also include $t\bar{t}Z$ which is more subdominant, but important for a possible data-driven background estimation. We generate background and signal samples with `MadGraph 5.2` [86] before showering them with `PYTHIA 6` [95] and passing them through the `Delphes 3` [96] detector simulation using the default ATLAS detector card. Thus, for jet $p_{\mathrm{T}} = 100$ GeV, the b-tagging efficiency is assumed to be 73%, with the misidentification rates of c-jets and other light jets being 14% and 0.27%, respectively. Jets are clustered using the anti-k_{T} algorithm [97] with an angular distance parameter $R = 0.4$.

Selection cuts are adopted as follows. Firstly we require the selected events

to contain exactly one charged lepton ℓ (electron or muon), exactly four b-tagged jets and at least two light jets. The lepton must be isolated from any jet via the condition $\Delta R > 0.4$. Moreover, the lepton and the jets should have $p_T > 25$ GeV and $|\eta| < 2.5$.

To reconstruct the hadronically decaying top we iterate through the reconstructed light jets and b-jets and find the combination which minimises

$$\chi^2 = \frac{(m_{jj} - m_W)^2}{m_W^2} + \frac{(m_{t,\text{had}} - m_t)^2}{m_t^2} \, , \qquad (3.4.53)$$

where m_{jj} is the invariant mass of two light jets j_1 and j_2, and $m_{t,\text{had}}$ is the invariant mass of j_1, j_2, and a b-jet b_1. After that, to reconstruct the leptonically decaying top we iterate through the remaining b-jets and find the one b_2 which minimises

$$\chi^2 = \frac{(m_{t,\text{lep}} - m_t)^2}{m_t^2} \, , \qquad (3.4.54)$$

where $m_{t,\text{lep}}$ is the invariant mass constructed by b_2, the lepton, and the missing transverse momentum $\not{p}_T$. The remaining b-jets b_3 and b_4 are used to search for the resonance X. We denote their invariant mass as m_{bb} and show the normalised distributions in Fig. 3.5 for our benchmark point with $m_X = 50$ GeV. There is a clear peak at the signal resonance position, and the $t\bar{t}b\bar{b}$ background is flat in the vicinity of the signal. As a reference for calibration, we also show the distribution of the $t\bar{t}Z$ background, which exhibits a clear Z peak. We observe that all signals exhibit long tails in the $b\bar{b}$ invariant mass, due to misattribution of the b's from the tops and the b's from the resonance. Based on experience with the SM Higgs, the use of boosted techniques should ameliorate this.

To further isolate the signal we impose the selection cuts 60 GeV $< m_{jj} <$ 100 GeV, 120 GeV $< m_{t,\text{had}} <$ 200 GeV, 120 GeV $< m_{t,\text{lep}} <$ 220 GeV, and 35 GeV $< m_{bb} <$ 65 GeV. The expected yields per inverse femtobarn for the $t\bar{t}b\bar{b}$ background and the signals after each steps of selection cuts are presented in Table 3.1. These cuts suppress the $t\bar{t}b\bar{b}$ background by a factor of $\sim 5 \times 10^3$. The $t\bar{t}Z$ background is lower than $t\bar{t}b\bar{b}$ by two orders of magnitude.

To estimate the expected exclusion on the signals we carry out a CL$_s$ hypothesis test [98] based on the m_{bb} distributions from 15 GeV to 200 GeV shown in Fig. 3.5. We scale up the $t\bar{t}b\bar{b}$ background by a factor of 1.2 in order to take into account

Table 3.1 Expected background and signal events per fb^{-1} after each step of the selection cuts for $m_X = 50$ GeV. We take $g_q = 1$ $t\bar{t}S$ and $t\bar{t}A$ signals, and $g_q = 0.2$ is assumed for the $t\bar{t}Z'_V$ and $t\bar{t}Z'_A$ signals.

	$t\bar{t}b\bar{b}$	$t\bar{t}S$	$t\bar{t}A$	$t\bar{t}Z'_V$	$t\bar{t}Z'_A$
No cut	24375	4211	428	714	241
1 lepton	4612	744	80.0	132	44.4
4 b-tags	106	33.9	5.15	7.12	27.5
≥ 2 light jets	72.9	22.1	3.51	4.86	18.7
$m_{jj} \in (60, 100)$ GeV	42.0	12.6	2.05	2.82	10.9
$m_{t,\text{had}} \in (120, 200)$ GeV	39.1	11.9	1.92	2.64	10.2
$m_{t,\text{lep}} \in (120, 220)$ GeV	30.2	9.87	1.52	2.09	8.07
$m_{bb} \in (35, 65)$ GeV	4.35	2.33	0.333	0.450	1.78

the remaining backgrounds discussed earlier and assume a flat 10% systematic uncertainty on the total background. The expected 95% CL exclusion limits on the signal strength $\sigma(pp \to t\bar{t}X) \cdot \text{BR}(X \to b\bar{b})$ as functions of the integrated luminosity are shown in in Fig. 3.6. These limits are comparable for the four simplified models due to the similarities in their production kinematics, and with the high-luminosity LHC it should be possible to bound the cross sections to the level of a few hundred femtobarns. For the pseudoscalar this corresponds to g_t just under 1 (*i.e.* essentially no suppression with respect to the SM Yukawa) while for the axial vector we can constrain g_t down to 0.08.

3.4.1 Expected Sensitivity for Discrimination among Simplified Models

Through the above reconstruction procedure, we can construct the 4-momenta of the hadronically decaying top, the leptonically decaying top, and the resonance X

(a) $t\bar{t}S$ production

(b) $t\bar{t}A$ production

(c) $t\bar{t}Z'_{\mathrm{V}}$ production
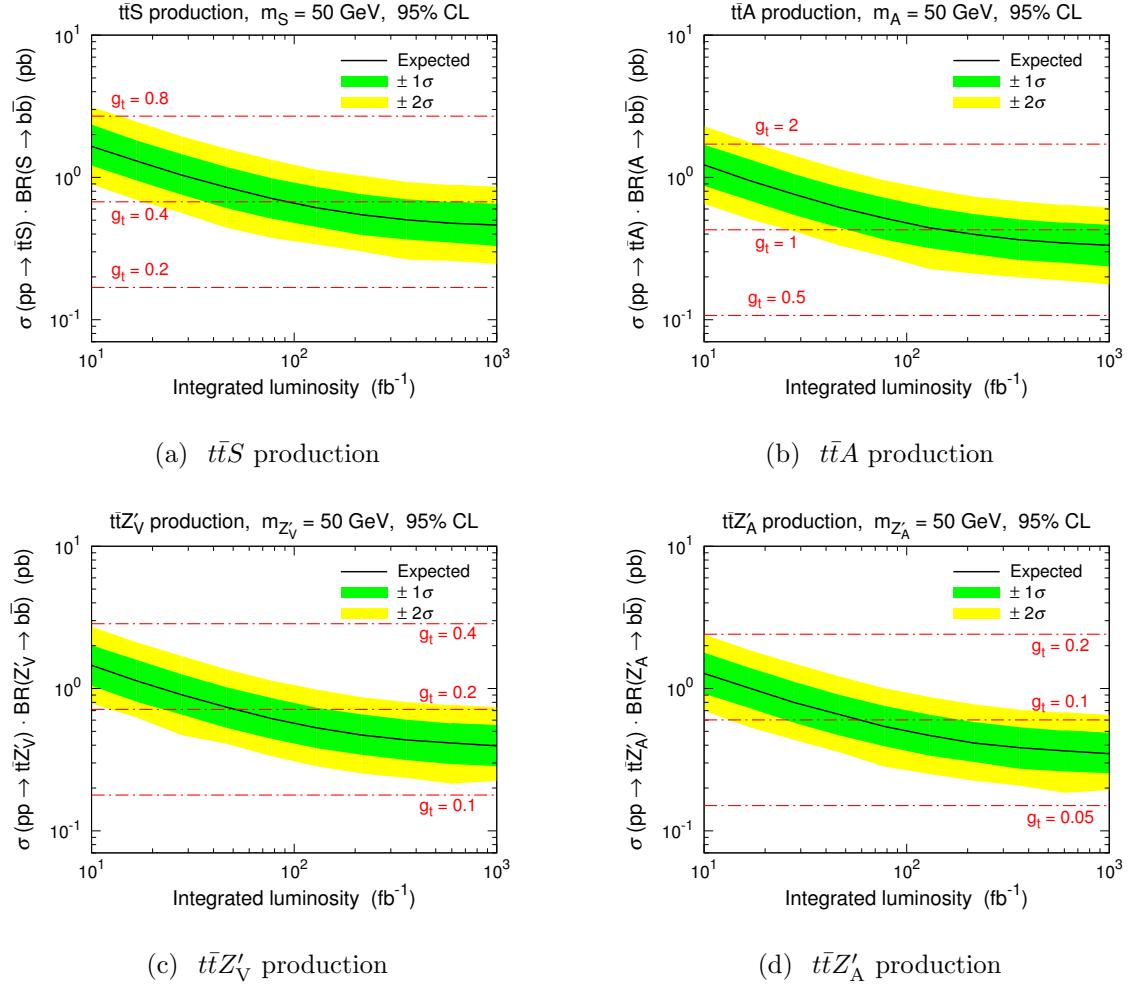
(d) $t\bar{t}Z'_{\mathrm{A}}$ production

Figure 3.6 This figure shows the expected 95% CL exclusion limits on the signal strength $\sigma(pp \to t\bar{t}X) \cdot \mathrm{BR}(X \to b\bar{b})$ with $m_X = 50$ GeV as functions of the integrated luminosity at the 14 TeV LHC for $t\bar{t}S$ (a), $t\bar{t}A$ (b), $t\bar{t}Z'_{\mathrm{V}}$ (c), and $t\bar{t}Z'_{\mathrm{A}}$ (d) production. The dot-dashed lines denote the signal strengths for the g_t values labelled and $\mathrm{BR}(X \to b\bar{b}) = 100\%$.

from the identified jets and lepton:

$$p_{t,\mathrm{had}} = p_{b_1} + p_{j_1} + p_{j_2}, \tag{3.4.55}$$

$$p_{t,\mathrm{lep}} = p_{b_2} + p_\ell + \not{p}_{\mathrm{T}}, \tag{3.4.56}$$

$$p_X = p_{b_3} + p_{b_4}. \tag{3.4.57}$$

The missing momentum $\not{p}_{\mathrm{T}}$ only contains transverse components and hence the reconstructed $p_{t,\mathrm{lep}}$ is not as accurate as $p_{t,\mathrm{had}}$. We can find a CM frame where

(a) Normalised m_{tt} distributions

(b) Normalised $p_{T,X}$ distributions

(c) Normalised $\theta_{t,\mathrm{had}}^{\mathrm{CM}}$ distributions

(d) Normalised Θ^{CM} distributions
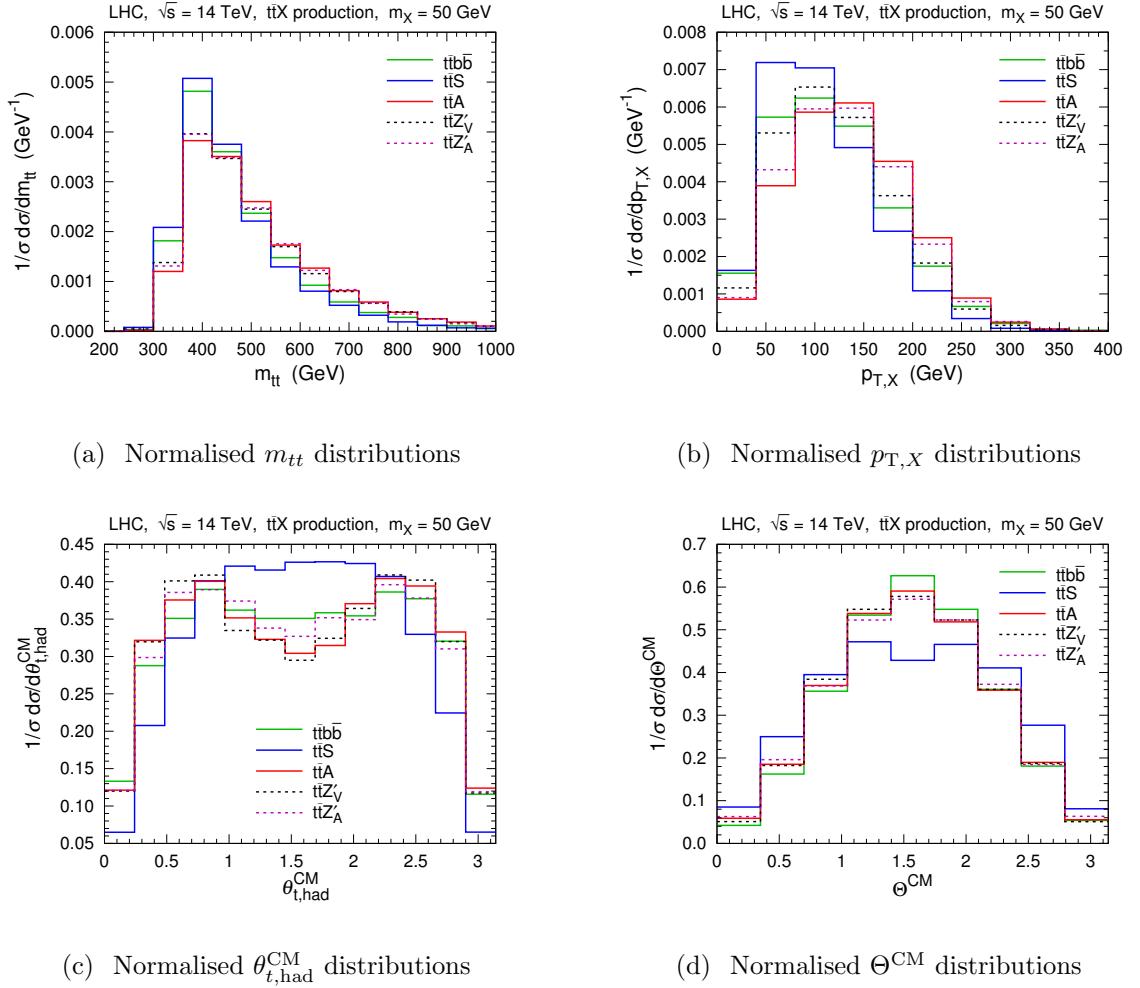
Figure 3.7   This figure shows the normalised distributions of m_{tt} (a), $p_{T,X}$ (b), $\theta_{t,\mathrm{had}}^{\mathrm{CM}}$ (c), and Θ^{CM} (d) at detector level for the 14 TeV LHC and $m_X = 50$ GeV.

$\mathbf{p}_{t,\mathrm{had}} + \mathbf{p}_{t,\mathrm{lep}} + \mathbf{p}_X = 0$. Therefore, these 4-momenta allow us to construct discriminating variables m_{tt}, $p_{T,X}$, $\theta_{t,\mathrm{had}}^{\mathrm{CM}}$, and Θ^{CM} that are equivalent to the parton-level variables discussed in Sec. 3.3. The normalised distributions for the signals and the $t\bar{t}b\bar{b}$ background with all the selection cuts applied are shown in Fig. 3.7. As expected, these detector-level variables catch the basic features of their parton-level counterparts demonstrated in Fig. 3.3. Note that $m_{tt} = (p_{t,\mathrm{had}} + p_{t,\mathrm{lep}})^2$ and $\theta_{t,\mathrm{had}}^{\mathrm{CM}}$ corresponds to the hadronically decaying top. An analogous variable $\theta_{t,\mathrm{lep}}^{\mathrm{CM}}$ can also be constructed from $p_{t,\mathrm{lep}}$, but it is less powerful than $\theta_{t,\mathrm{had}}^{\mathrm{CM}}$ for discrimination among simplified models.

We perform a $\mathrm{CL_s}$ hypothesis test to investigate the discriminating power of

each variable. Analogous to those in the ATLAS [99] and CMS [100] analyses for determining the spin and parity of the SM Higgs, the test statistic is defined as

$$Q = -2\ln\frac{\mathcal{L}(s_2 + b)}{\mathcal{L}(s_1 + b)}, \tag{3.4.58}$$

where $\mathcal{L}(s + b)$ denotes the likelihood for the background b plus a signal hypothesis s. Thus, Q is used to discriminate between signal hypotheses s_1 and s_2. For an observed value Q_{obs}, the exclusion of the hypothesis s_2 in favour of the hypothesis s_1 (denoted as "s_1 vs s_2" below) is evaluated in terms of the modified confidence level

$$\mathrm{CL_s} = \frac{P(Q \geq Q_{\mathrm{obs}}|s_2 + b)}{P(Q \geq Q_{\mathrm{obs}}|s_1 + b)}, \tag{3.4.59}$$

where $P(Q \geq Q_{\mathrm{obs}}|s + b)$ is the probability for $Q \geq Q_{\mathrm{obs}}$ under a hypothesis s.

Fig. 3.8 shows the expected 95% CL exclusion limits on the visible cross section σ_{vis} as functions of the integrated luminosity based on the discriminating variables, assuming 10% systematic uncertainty on the background. Here σ_{vis} is defined as the cross section taking into account the cut acceptance and efficiency. We assume each pair of signal hypotheses yield the same σ_{vis}, and evaluate the exclusion limit of one hypothesis in favour of the other one. In this way, the differences among these limits only come from the different behaviours of the signal hypotheses in the distributions shown in Fig. 3.7. Overall, the $p_{\mathrm{T},X}$ variable seems to be the most powerful one, except for the "A vs Z'_{A}" case, where the $\theta^{\mathrm{CM}}_{t,\mathrm{had}}$ variable is better than $p_{\mathrm{T},X}$ for a high integrated luminosity of $\sim 1\,\mathrm{ab}^{-1}$. The $t\bar{t}S$ production is the easiest to be distinguished from the rest, because its distributions of all the discriminating variables behave most differently from others. The worst case is the discrimination between A and Z'_{A}, which yield similar shapes for every variable.

(a) m_{tt} variable

(b) $p_{\mathrm{T},X}$ variable

(c) $\theta_{t,\mathrm{had}}^{\mathrm{CM}}$ variable

(d) Θ^{CM} variable
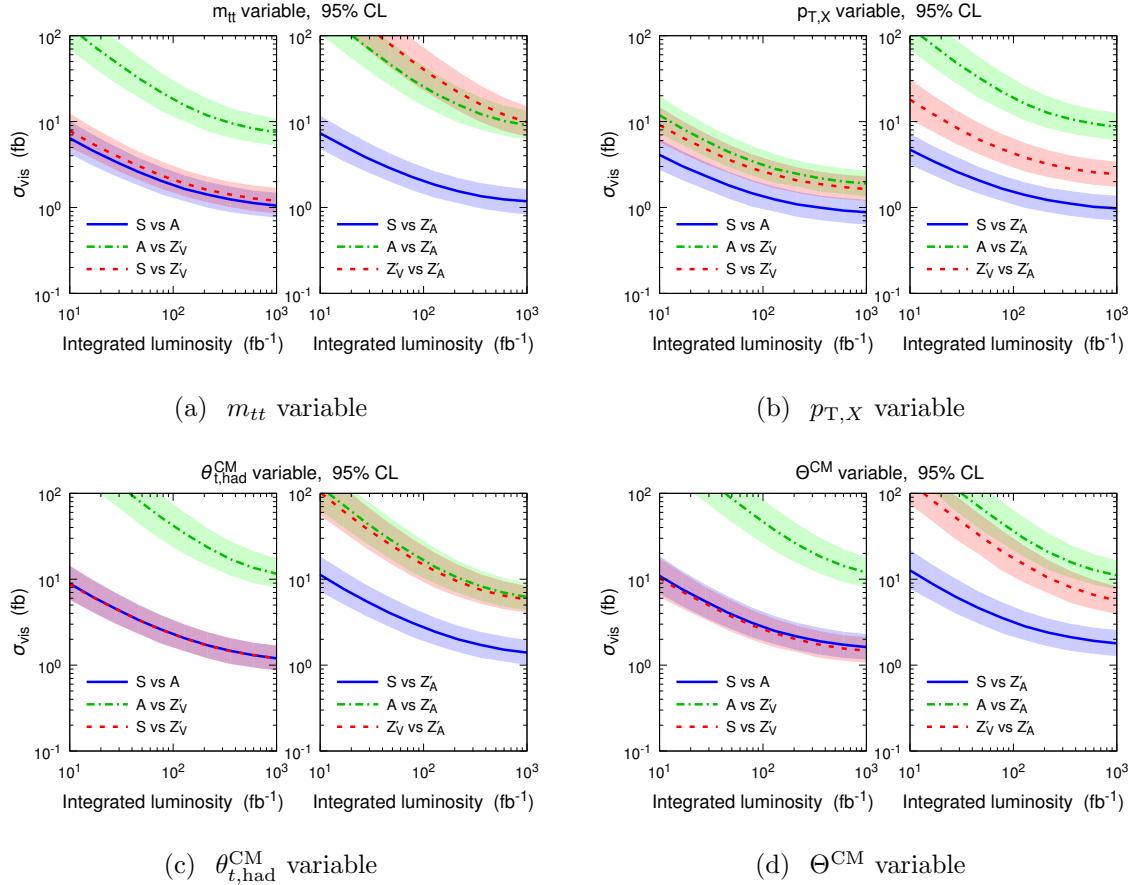
Figure 3.8 This figure shows the expected 95% CL exclusion limits on the visible cross section σ_{vis} as functions of the integrated luminosity at the 14 TeV LHC based on the variables m_{tt} (a), $p_{\mathrm{T},X}$ (b), $\theta_{t,\mathrm{had}}^{\mathrm{CM}}$ (c), and Θ^{CM} (d). The lines denote the median value of the limit, while the coloured bands denote the $\pm 1\sigma$ range. "s_1 vs s_2" corresponds to the exclusion of the signal hypothesis s_2 in favour of the signal hypothesis s_1, assuming both hypotheses yield the same visible cross section.

Chapter 4

Forward-Backward Asymmetry in NLO SMEFT

In the exploration of the physics at high energy scales, both hadron colliders and electron-positron collider are of great importance. One advantage of the LHC is its role in discovering heavy new particles beyond the SM. The existence of the Higgs boson with a non-zero vev has been confirmed by the LHC. However, the physical mechanism behind this non-zero vev is still mysterious. And therefore we need further experiments to explore the Higgs boson in great detail. Since the momentum of quarks at hadron colliders are described by parton distribution functions that can not be determined accurately, the LHC can not perform a measurement at an exact energy around the Higgs resonance. However, electron-positron colliders can perform such a measurement as the energy contributing to the hard process of the event is very precisely determined. Moreover, precision electroweak measurements performed at electron-positron colliders can set stringent limits on new physics. Several possible future colliders, i.e., `ILC` in Japan, `FCC-ee` in Europe, and `CEPC` in China, are expected to allow for measurements at higher center-of-mass energies compared to LEP, in an equally clean environment, thereby improving on the precision currently and previously achieved. Thus the precision electroweak observables, such as the effective Weinberg angle and the mass of W boson, could be measured more accurately in the future. As a result, constraints from such measurements can provide more information on possible extensions of the Standard Model. In Chapter

2, we have discussed the potential of the SMEFT in describing new physics at the high energy scale without knowing the fundamental theory behind the phenomena. In this chapter, we will study new physics in two processes, i.e., the $Z \to b\bar{b}$ decay and $e^+e^- \to b\bar{b}$ in the framework of dimension-six SMEFT up to one-loop.

The goal of this work is to calculate the forward-backward asymmetry for b-quarks in the $e^+e^- \to b\bar{b}$ process in the Dimension-six SMEFT. In the SM, the forward-backward asymmetry is very sensitive to higher order corrections, which will be illustrated in 4.8 for the $e^+e^- \to b\bar{b}$ case. We expect that this feature can be retained in the SMEFT framework. Moreover, we also calculate the one-loop amplitudes for $Z \to b\bar{b}$ process, whose diagrams are subsets of the former ones.

The Warsaw Basis will be adopted as the basis for the operators in our work. For the 59 baryon number conserving dimension-six operators in the Warsaw basis, parts of the one-loop anomalous dimension matrix has been calculated in [101–103], then a full calculation was performed for all the baryon number conserving dimension-six operators in [104–106], and further calculation for baryon number violating dimension-six operators can be found in [107].

The large-m_t limit will be adopted in the renormalisation procedure. In the large-m_t limit we assume $m_t \ll M_H$, and all the fermion masses except the t-quark mass can be neglected in the one-loop calculation to identify the leading-m_t corrections. However, the full mass dependence in the UV singular contributions will be kept. In the calculation of the NLO corrections of the four-fermion operators in the Warsaw Basis, we choose to keep the both the t-quark mass and b-quark mass in the amplitudes to check the cancellation of the UV divergences, though in the numerical calculation the mass of b-quark mass is neglected. The vanishing gauge couplings limit [108] is adopted as well, in which all the QCD one-loop corrections are ignored, and all the terms in the one-loop corrections that are proportional to the positive powers of $M_{W,Z}^2$ are also set to be zero, e.g., the counterterms which are proportional to M_Z^2 should be neglected in the vanishing gauge couplings limit. However, in the numerical calculation, we choose to work in the vanishing-m_b limit, in which all the terms including $M_{W,Z}$ will be preserved so that the results could be more accurate. Accordingly we will also check the cancellation of the UV divergences

which are proportional to M_Z^2 and M_W^2. A detailed introduction to the large-m_t limit and the vanishing-m_b limit can be found in A.2.

We will express all the amplitudes in the helicity form, where one diagram of the $e^- e^+ \to b\bar{b}$ process leads to four helicity amplitudes due to the four external fermions, while in the $Z \to b\bar{b}$ case, one diagram only generates two helicity amplitudes. In order to demonstrate the cancellation of UV divergence in detail, the $Zb\bar{b}$ case can be taken as a good example for simplicity's sake, since in the large-m_t limit, the renormalisation of the vertex Ze^+e^- is not be important, only the renormalisation of the vertex $Zb\bar{b}$ is considered in the renormalisation procedure.

As is shown in Chapter 2, the relations between different parameters in the SMEFT are very different from the SM case at tree-level, the NLO corrections depend on the input parameters as well. Before any calculation, a set of independent input parameters must be chosen. These parameters should all be physical quantities that can be measured directly by experiments. In our work, we choose the following input parameters set:

$$\bar{e}, M_Z, M_W, M_H, m_f, C_i \qquad (4.0.1)$$

4.1 Tree-Level Matrix Element

Since we set the electron mass to zero, the neutral Goldstone boson contribution vanishes in the SM. Therefore, the SMEFT contributions which generate this structure (scalar contributions) do not interfere with the SM and therefore arise at $O(1/\Lambda^2)$ and are thus neglected.

In general the tree-level matrix elements for $Z \to b\hat{b}$ can be written as

$$iM^{(6),0}(Z \to b\bar{b}) = -i \sum_{i=L,R} \bar{e}\bar{g}_i^b \left\langle \bar{b}_i \gamma^\mu b_i \right\rangle, \qquad (4.1.1)$$

in which we have denoted the Dirac structure in the amplitude with $\left\langle \bar{b}_i \gamma^\mu b_i \right\rangle$, which will be adopted in what follows. Specifically,

$$\left\langle \bar{b}_i \gamma^\mu b_i \right\rangle = \bar{u}(p_1)\gamma^\mu P_i v(p_2), \qquad (4.1.2)$$

where $\bar{u}(p_1)$ and $v(p_2)$ are the Dirac spinors. For $e^- e^+ \to b\bar{b}$, besides the interaction with bosons exchanging, there are also tree level contributions from Class 8 operators that is straight forward to read off:

$$
\begin{aligned}
& \left(C_{lq}^{(1)} + C_{lq}^{(3)} \right) \langle \bar{e}_L \gamma_\mu e_L \rangle \langle \bar{b}_L \gamma^\mu b_L \rangle, \\
& + C_{eb} \langle \bar{e}_R \gamma_\mu e_R \rangle \langle \bar{b}_R \gamma^\mu b_R \rangle, \\
& + C_{lb} \langle \bar{e}_L \gamma_\mu e_L \rangle \langle \bar{b}_R \gamma^\mu b_R \rangle, \\
& + C_{qe} \langle \bar{e}_R \gamma_\mu e_R \rangle \langle \bar{b}_L \gamma^\mu b_L \rangle.
\end{aligned}
\tag{4.1.3}
$$

Below are the tree-level matrix elements:

$$
\begin{aligned}
iM_{e^+ e^- \to \gamma \to b\bar{b}}^{(6),0} &= i \sum_{i,j=L,R} \frac{\bar{e}^2 Q^b Q^e}{\hat{s}} \langle \bar{e}_i \gamma_\mu e_i \rangle \langle \bar{e}_j \gamma^\mu b_j \rangle, \\
iM_{e^+ e^- \to Z \to b\bar{b}}^{(6),0} &= i \sum_{i,j=L,R} \frac{\bar{e}^2 \bar{g}_i^e \bar{g}_j^b}{\hat{s} - M_Z^2} \langle \bar{e}_i \gamma_\mu e_i \rangle \langle \bar{b}_j \gamma^\mu b_j \rangle, \\
iM_{e^+ e^- \to b\bar{b}}^{(6),0} &= i \sum_{i,j=L,R} C_{iijj} \langle \bar{e}_i \gamma_\mu e_i \rangle \langle \bar{b}_j \gamma^\mu b_j \rangle.
\end{aligned}
\tag{4.1.4}
$$

The couplings appearing in the above expressions are those which appear as effective couplings for the Z boson and photon couplings to fermions in the SMEFT. In addition, there are also contributions from four-fermion operators (denoted as C_{iijj}) which are not present in the SM.

The electromagnetic coupling $\bar{\alpha} = \bar{e}^2/4\pi$ appearing in the above expressions will eventually be included as input parameter. The electroweak couplings $\bar{g}_{i,j}^{e,b}$ appearing in the above expressions are modified by Wilson coefficients which directly alter $Z f \bar{f}$ couplings, and in addition through the Wilson coefficients which appear as a result of expressing observables in the broken phase of the theory with respect to a particular input parameter set. It is worth noting that the tree-level amplitudes appearing in 4.1.4 are correct when the electron mass is neglected. In this case, only these four Dirac structures are present in the SM. Consequently, we only consider SMEFT contributions which also generate these Dirac structures which result in non-vanishing interference contributions with the SM. The self interference of amplitudes with different Dirac structures, such as those generated by the Class 6 and scalar Class 8 operators, contribute to observables at $O(1/\Lambda^2)$ and are therefore neglected.

In [109], the electroweak couplings have been deduced in terms of barred quantities. However, we will do the renormalisation in the on-shell scheme which is suitable for the electroweak scale. As we can see, the renormalisation of the electroweak couplings $\bar{g}_{L,R}$ is directly connected to the renormalisation of the trigonometric function of the Weinberg angle. In the SM, $\hat{s}_w^2 = 1 - M_W^2/M_Z^2$, and the renormalisation constants are derived from this. In the SMEFT, the approach was the same which was why the quantity $\hat{s}_w$ is introduced, as this is derived from $1 - M_W^2/M_Z^2$ in SMEFT. Hence the renormalisation of $\hat{s}_w^2$ follows from the renormalisation of M_W^2 and M_Z^2 in the SMEFT. Actually, there is a shift between $\hat{s}_w^2$ and $\bar{s}_w^2$ since they are defined slightly differently. The shift can be found in [108] as

$$\bar{s}_w^2 = \hat{s}_w^2 - \frac{\hat{c}_w^2 \hat{v}_T^2}{2} \left(C_{HD} + 2\frac{\hat{s}_w}{\hat{c}_w} C_{HWB} \right). \tag{4.1.5}$$

After solving this equation, and neglecting the $O(\frac{1}{\Lambda^4})$ terms, the barred sine of the Weinberg angle can be obtained:

$$\bar{s}_w = \frac{\bar{g}_1}{\sqrt{\bar{g}_1^2 + \bar{g}_2^2}} + \frac{\bar{g}_2 (\bar{g}_2^2 - \bar{g}_1^2)}{(\bar{g}_1^2 + \bar{g}_2^2)^{\frac{3}{2}}} \hat{v}_T^2 C_{HWB}. \tag{4.1.6}$$

However, this expression is given in terms of barred quantities $\bar{g}_1$ and $\bar{g}_2$. In our notations, $\bar{g}_2$ can be directly written in terms of M_W and $\hat{v}_T$ by using the first equation of 2.1.14, both of which are renormalised in the on-shell scheme. As for $\bar{g}'$, we need to solve the second equation of 2.1.14 as a function of $\bar{g}_1$ and neglect the $O(\frac{1}{\Lambda^4})$ terms again. Thus we have the following expression of $\bar{g}_1$ and $\bar{g}_2$ in terms of input parameters

$$\bar{g}_1 = \frac{2\sqrt{M_Z^2 - M_W^2}}{\hat{v}_T} - 2M_W \hat{v}_T C_{HWB} - \frac{M_Z^2 \hat{v}_T}{2\sqrt{M_Z^2 - M_W^2}} C_{HD}$$

$$\bar{g}_2 = \frac{2M_W}{\hat{v}_T}. \tag{4.1.7}$$

We insert the first equation of 2.1.14 and 4.1.7 into 4.1.6, the trigonometric function of the Weinberg angle can also be written in terms of the hatted quantities

$$\bar{s}_w = \hat{s}_w - \frac{\hat{c}_w^2 \hat{v}_T^2}{4\hat{c}_w} C_{HD} - \frac{1}{2\hat{c}_w} C_{HWB}. \tag{4.1.8}$$

The final expression of $\bar{g}_{L,R}$ due to the redefinition of weak couplings could be deduced from 2.1.12, by which the neutral weak current could be written as

$$g_Z(T^3 - Q_f) = \sqrt{\bar{g}_1^2 + \bar{g}_2^2} \left(T^3 - Q_f \bar{s}_w \right) + \frac{\bar{g}_1 \bar{g}_2}{\sqrt{\bar{g}_1^2 + \bar{g}_2^2}} v_T^2 C_{HWB} \left(T^3 - Q_f \right). \tag{4.1.9}$$

The second part of 4.1.8 is straightforward to calculate, as $C_{HWB} \propto \frac{1}{\Lambda^2}$, the other EFT shifts could be neglected, and the barred quantities could be directly written as hatted quantities. As for the first part, we just need to insert 4.1.8 and 4.1.7 into the equation and combine it with the second part to get the final result. It turns out only C_{HWB} and C_{HD} are involved in, which contribute to the neutral weak coupling through the general form

$$
\begin{aligned}
\Delta g_L^f &= \frac{T^3 \hat{v}_T^2 \left(1 - 2\hat{s}_w\right)}{4\hat{c}_w} C_{HD} + \frac{I^3 \hat{v}_T^2 \hat{c}_w}{\hat{s}_w} C_{HWB} \\
\Delta g_R^f &= \frac{Q_f \hat{v}_T^2}{4\hat{c}_w \hat{s}_w},
\end{aligned}
\tag{4.1.10}
$$

which is a very simple form compared to the original expression. The expression for each fermion could be obtained by inserting their quantum numbers. The other shifts of the neutral weak coupling in SMEFT could be read off directly from [109], since they are expressed in terms of hatted quantity. As the set of input parameters is different, we need to replace some hatted quantities in their result with ours.

At last, in agreement with the results presented in [109], we find the following general expressions for the effective left-handed and right-handed Z boson couplings to fermions with $T^3 = -\frac{1}{2}$:

$$
\begin{aligned}
\bar{g}_R^f &= -\frac{\hat{s}_w}{\hat{c}_w} Q_f + \frac{\hat{v}_T^2}{2\hat{s}_w \hat{c}_w} \left(\frac{Q_f}{2} C_{HD} + C_{Hf} \right), \\
\bar{g}_L^f &= \bar{g}_R^f - \frac{I_{W,f}^3}{\hat{s}_w \hat{c}_w} + \frac{\hat{v}_T^2}{2\hat{s}_w \hat{c}_w} \left(\frac{I_{W,f}^3}{2} \left(\left(\frac{1}{\bar{s}_w^2} - 2 \right) C_{HD} - \frac{4\hat{c}_w}{\hat{s}_w} C_{HWB} \right) + C_{HL}^{(1)} + C_{HL}^{(3)} \right).
\end{aligned}
\tag{4.1.11}
$$

The general expressions for the effective left-handed and right-handed Z boson couplings to fermions with $T^3 = \frac{1}{2}$ can be obtained similarly:

$$
\begin{aligned}
\bar{g}_R^f &= -\frac{\hat{s}_w}{\hat{c}_w} Q_f + \frac{\hat{v}_T^2}{2\hat{s}_w \hat{c}_w} \left(\frac{Q_f}{2} C_{HD} + C_{Hf} \right), \\
\bar{g}_L^f &= \bar{g}_R^f - \frac{I_{W,f}^3}{\hat{s}_w \hat{c}_w} + \frac{\hat{v}_T^2}{2\hat{s}_w \hat{c}_w} \left(\frac{I_{W,f}^3}{2} \left(\left(\frac{1}{\bar{s}_w^2} - 2 \right) C_{HD} + \frac{4\hat{c}_w}{\hat{s}_w} C_{HWB} \right) + C_{HL}^{(1)} - C_{HL}^{(3)} \right).
\end{aligned}
\tag{4.1.12}
$$

In the last line, the notation $C_{HL}^{(1,3)}$ has been introduced for the Class 7 operators where L should be understood to refer to either the quark (q) or lepton (l) $SU(2)_L$ doublets. Explicitly, 4.1.11 and 4.1.12 lead to the following couplings for electrons,

b-quarks and t-quarks

$$
\bar{g}_R^e = \frac{\hat{s_w}}{\hat{c_w}} + \frac{\hat{v}_T^2}{2\hat{s_w}\hat{c_w}}\left(-\frac{1}{2}C_{HD} + C_{He}\right),
$$

$$
\bar{g}_L^e = \frac{-1 + 2\hat{s}_w^2}{2\hat{s_w}\hat{cw}} + \frac{\hat{v}_T^2}{2\hat{s_w}\hat{c_w}}\left(-\frac{1}{4\hat{s}_w^2}C_{HD} - \frac{\hat{c_w}}{\hat{s_w}}C_{HWB} + C_{Hl}^{(1)} + C_{Hl}^{(3)}\right),
$$

$$
\bar{g}_R^b = \frac{1}{3}\frac{\hat{s_w}}{\hat{c_w}} + \frac{\hat{v}_T^2}{2\hat{s_w}\hat{c_w}}\left(-\frac{1}{6}C_{HD} + C_{Hb}\right),
$$

$$
\bar{g}_L^b = \frac{-1 + \frac{2}{3}\hat{s}_w^2}{2\hat{s_w}\hat{cw}} + \frac{\hat{v}_T^2}{2\hat{s_w}\hat{c_w}}\left(\left(\frac{1}{3} - \frac{1}{4\hat{s}_w^2}\right)C_{HD} - \frac{\hat{c_w}}{\hat{s_w}}C_{HWB} + C_{Hq}^{(1)} + C_{Hq}^{(3)}\right),
$$

$$
\bar{g}_R^t = \frac{1}{3}\frac{\hat{s_w}}{\hat{c_w}} + \frac{\hat{v}_T^2}{2\hat{s_w}\hat{c_w}}\left(\frac{1}{3}C_{HD} + C_{Hu}\right),
$$

$$
\bar{g}_L^t = \frac{-1 + \frac{2}{3}\hat{s}_w^2}{2\hat{s_w}\hat{cw}} + \frac{\hat{v}_T^2}{2\hat{s_w}\hat{c_w}}\left(\left(-\frac{1}{6} + \frac{1}{4\hat{s}_w^2}\right)C_{HD} + \frac{\hat{c_w}}{\hat{s_w}}C_{HWB} + C_{Hq}^{(1)} - C_{Hq}^{(3)}\right).
$$

$$(4.1.13)$$

4.2 Renormalisation Procedure

In this section we cover the issue of renormalisation in the SMEFT framework. The on-shell scheme is adopted for mass, parameter, and wavefunction renormalisation which basically proceeds in the same way as in the SM. In addition, we choose to renormalise the Wilson coefficients in the $\overline{\text{MS}}$ scheme, a choice which is standard for EFT calculations.
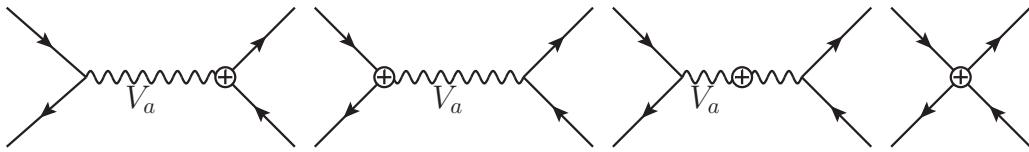
Figure 4.1 Examples of Counterterm diagrams for the $e^+e^- \to b\bar{b}$ process

The details of the on-shell renormalisation relevant for the current work have been previously been provided in [28, 110], and with the exception of the operator renormalisation, we follow the procedure outlined in this work. Essentially, one computes a set of two-point functions in the broken phase of the theory, and uses these results to renormalise a set of mass, parameters and external fields relevant for the process in question. In addition, the operator renormalisation is obtained from

the anomalous dimension matrix of the complete dimension-6 SMEFT operators in the unbroken phase [104–106]. These two ingredients allow to construct the tree-level UV counterterm amplitudes which are necessary to render the bare one-loop amplitudes finite. For the calculation of the process $e^+e^- \to b\bar{b}$, it is necessary to construct the counterterm amplitudes as depicted in 4.1. In the on-shell scheme, the counterterms associated to the external fields are cancelled by the insertion of the 1PI diagrams onto these legs. Note that as in the case of the LO calculation presented in the previous section, the electron mass is neglected throughout the one-loop calculation and consequently it is not necessary to consider the CT amplitudes which contain the exchange of a scalar (either the Higgs or neutral Goldstone boson). In fact, this simplifies the calculation somewhat, since in the end only the interference of vector-like Dirac structures contribute to the cross section. To construct these counterterm amplitudes it is necessary to renormalise electron and b-quark fields, electric charge, the left and right handed couplings of the Z boson with electrons and b-quarks, as well as the Z boson mass. In principle, the Feynman rules for the vertex and mass counterterms appearing in diagrams $(1-3)$ of 4.1 should individually contain renormalisation constants associated to the Z and A fields. However, these constants vanish when the diagrams are summed, as they do not appear as external fields, and it is therefore not necessary to consider wavefunction renormalisation of A and Z fields in the context of this work. Defining the renormalised fields and parameters in terms of the bare ones, which are indicated with the superscript 0, we have

$$
\begin{aligned}
f_L^0 &= \sqrt{Z_L^f} f_L = (1 + \delta Z_L^f) f_L, \\
f_R^0 &= \sqrt{Z_R^f} f_R = (1 + \delta Z_R^f) f_R, \\
M^0 &= M + \delta M, \\
\bar{e}^0 &= Z_{\bar{e}} \bar{e} = \bar{e} + \delta \bar{e}.
\end{aligned}
\tag{4.2.14}
$$

In the on-shell scheme, the renormalisation constants for the Z boson couplings to fermions are obtained from electric charge renormalisation constants as well as those associated to the sine of the weak mixing angle. It is therefore convenient to

also define counterterms associated to the weak mixing angle as

$$
\begin{aligned}
\hat{c}_w^0 &= \hat{c}_w + \delta\hat{c}_w, \, \hat{s}_w^0 = \hat{s}_w + \delta\hat{s}_w, \\
\hat{g}_L^{f,0} &= \hat{g}_L^f + \delta\hat{g}_L^f, \, \hat{g}_R^{f,0} = \hat{g}_R^f + \delta\hat{g}_R^f.
\end{aligned}
\tag{4.2.15}
$$

Note that the bare couplings $\bar{g}_{L,R}^{f,0}$ were previously defined in 4.1.13. Finally, we choose to renormalise the dimension-6 contributions by introducing counterterms for the Wilson coefficients as

$$
C_i^{(0)} = C_i(\mu) + \delta C_i(\mu).
\tag{4.2.16}
$$

Up to one-loop, we have

$$
C_i^0 = C_i(\mu) + \frac{\delta C_i(\mu)}{16\pi^2} = C_i(\mu) + \frac{1}{2\hat{\epsilon}}\frac{\delta C_i(\mu)}{16\pi^2}.
\tag{4.2.17}
$$

With these definitions, it is possible to obtain the necessary UV counterterm amplitudes by writing the bare tree-level amplitude 4.1.4 in terms of the renormalised fields and the UV renormalisation constants. Expanding this expression to first order in power of UV renormalisation constants, we find the following expression

$$
\begin{aligned}
M_{e^+e^-\to b\bar{b}}^{\text{CT}} = -i \sum_{i,/j=L,R} & \left(M^{LO}\left(e_i^+ e_i^- \to \gamma \to b_j \bar{b}_j\right) \left(\frac{1}{2}\left(\delta Z_e^i + \delta Z_b^j + h.c.\right) + \frac{\bar{e}}{e}\right), \right. \\
+ M^{LO}(e_i^+ e_i^- \to Z \to b_j \bar{b}_j) & \left(\frac{1}{2}\left(\delta Z_e^i + \delta Z_b^j + h.c.\right) + \frac{\bar{e}}{e} + \frac{\bar{g}_i^e}{g_i^e} + \frac{\bar{g}_j^b}{g_j^b} + \frac{\delta M_Z^2}{s - M_Z^2}\right) \\
+ M^{LO}(e_i^+ e_i^- \to b_j \bar{b}_j) & \left. \left(\frac{1}{2}\left(\delta Z_e^i + \delta Z_b^j + h.c.\right) + \frac{\delta C_{iijj}}{C_{iijj}}\right)\right).
\end{aligned}
\tag{4.2.18}
$$

Therefore, the full UV counterterm for dimension-4 and dimension-six contributions is computed as follows. The SM contribution is

$$
\begin{aligned}
M_{e^+e^-\to b\bar{b}}^{\text{CT},(4)} = -i \sum_{i,j=L,R} & M^{(4),0}\left(e_i^+ e_i^- \to \gamma \to b_j \bar{b}_j\right) \left(\frac{1}{2}(\delta Z_e^{i,(4)} + \delta Z_b^{j,(4)} + h.c.) + \frac{\bar{e}^{(4)}}{e}\right), \\
+ M^{(4),0}(e_i^+ e_i^- \to Z \to b_j \bar{b}_j) & \left(\frac{1}{2}\left(\delta Z_e^{i,(4)} + \delta Z_b^{j,(4)} + h.c.\right) \right. \\
+ \frac{\bar{e}}{e} + \frac{\bar{g}_i^{e,(4)}}{g_i^e} + \frac{\bar{g}_j^{b,(4)}}{g_j^b} & \left. + \frac{\delta M_Z^{2,(4)}}{s - M_Z^2}\right).
\end{aligned}
\tag{4.2.19}
$$

For the dimension-six contributions, in keeping with the expansion in $1/\Lambda^2$ one must include both the dimension-6 tree-level amplitudes multiplied by the SM renormalisation constants as well as SM tree-level amplitudes multiplied by dimension-6

renormalisation constants. This leads to the following general expression for the full dimension-six counterterm.

$$
\begin{aligned}
M_{e^+e^-\to b\bar{b}}^{\mathrm{CT},(6)} &= -i \sum_{i,j=L,R} M_{e_i^+e_i^-\to\gamma\to b_j\bar{b}_j}^{(4),0} \left(\frac{1}{2}\left(\delta Z_e^{i,(6)} + \delta Z_b^{j,(6)} + h.c. \right) + \frac{\bar{e}^{(6)}}{e} \right), \\
&+ M_{e_i^+e_i^-\to Z\to b_j\bar{b}_j}^{4,0} \left(\frac{1}{2}\left(\delta Z_e^{i,(6)} + \delta Z_b^{j,(6)} + h.c. \right) \right. \\
&\left. + \frac{\bar{e}^{(6)}}{e} + \frac{\bar{g}_i^{e,(6)}}{g_i^e} + \frac{\bar{g}_j^{b,(6)}}{g_j^b} + \frac{\delta M_Z^{2,(6)}}{s - M_Z^2} \right), \\
&+ M_{e_i^+e_i^-\to\gamma\to b_j\bar{b}_j}^{(6),0} \left(\frac{1}{2}\left(\delta Z_e^{i,(4)} + \delta Z_b^{j,(4)} + h.c. \right) + \frac{\bar{e}^{(4)}}{e} \right), \\
&+ M_{e_i^+e_i^-\to Z\to b_j\bar{b}_j}^{(6),0} \left(\frac{1}{2}\left(\delta Z_e^{i,(4)} + \delta Z_b^{j,(4)} + h.c. \right) \right. \\
&\left. + \frac{\bar{e}^{(4)}}{e} + \frac{\bar{g}_i^{e,(4)}}{g_i^e} + \frac{\bar{g}_j^{b,(4)}}{g_j^b} + \frac{\delta M_Z^{2,(4)}}{s - M_Z^2} \right), \\
&+ M_{e_i^+e_i^-\to b_j\bar{b}_j}^{(6),0} \left(\frac{1}{2}\left(\delta Z_e^{i,(4)} + \delta Z_b^{j,(4)} + h.c. \right) + \frac{\delta C_{iijj}}{C_{iijj}} \right).
\end{aligned}
\tag{4.2.20}
$$

Similarly to the $e^+e^- \to b\bar{b}$ case, The dimension-four SM contribution for the UV counterterm in the $Z \to b\bar{b}$ decay take a much simple form

$$
M_{Z\to b\bar{b}}^{\mathrm{CT},(4)} = M_{Z\to b_j\bar{b}_j}^{(4),0} \left(\frac{1}{2}\left(\delta Z_e^{i,(4)} + \delta Z_b^{j,(4)} + h.c. \right) + \frac{\bar{g}_i^{e,(4)}}{g_i^e} + \frac{\bar{g}_j^{b,(4)}}{g_j^b} \right).
\tag{4.2.21}
$$

And the dimension-6 counterterm could be expressed as

$$
\begin{aligned}
M_{Z\to b\bar{b}}^{\mathrm{CT},(6)} &= -i \sum_{i,j=L,R} M_{Z\to b\bar{b}}^{(4),0} \left(\frac{1}{2}\left(\delta Z_e^{i,(6)} + \delta Z_b^{j,(6)} + h.c. \right) + \frac{\bar{e}^{(6)}}{e} \right), \\
&+ M_{Z\to b_j\bar{b}_j}^{(4),0} \left(\frac{1}{2}\left(\delta Z_e^{i,(6)} + \delta Z_b^{j,(6)} + h.c. \right) + \frac{\bar{g}_i^{e,(6)}}{g_i^e} + \frac{\bar{g}_j^{b,(6)}}{g_j^b} \right).
\end{aligned}
\tag{4.2.22}
$$

Below we provide the wavefunction and mass renormalisation constants which are derived from two-point functions in the broken phase of the theory. In accordance with the approach in [108], we provide these results in t Hooft-Feynman gauge. They

read

$$\delta Z_b^{(4),L} = \frac{C_\epsilon}{v_T^2} \left[\frac{2}{\epsilon}(-m_b^2 - m_t^2) - \frac{3}{2}m_t^2 \right],$$

$$\delta Z_b^{(4),R} = \frac{C_\epsilon}{v_T^2} \frac{2m_b^2}{\epsilon},$$

$$\delta Z_b^{(6),L} = C_\epsilon \left[\frac{1}{\epsilon}\left(-m_b^2 \frac{C_{H,kin}}{v_T^2} + \frac{1}{4}m_b^2 C_{HD} + \frac{v_T}{\sqrt{2}m_b C_b H} \right. \right.$$

$$\left. \left. + m_b^2 C_H b + 2(m_t^2 - m_b^2)C_{Hq}^{(3)} + m_b m_t C_{Htb}) - m_t^2 C_{Hq}^{(3)} \right],$$

$$\delta Z_b^{(6),R} = \frac{C_\epsilon}{\epsilon} \left[-m_b^2 \frac{C_{H,kin}}{v_T^2} + \frac{1}{4}m_b^2 C_{HD} + \frac{v_T}{\sqrt{2}m_b C_b H} \right.$$

$$\left. -2m_b^2(C_{Hq}^{(1)} + C_{Hq}^{(3)}) \right],$$

$$\delta Z_e^{(4),L} = \delta Z_e^{(4),R} = \delta Z_e^{(6),L} = \delta Z_e^{(6),R} = 0,$$

$$\frac{\delta M_W^{(4)}}{M_W} = \frac{C_\epsilon}{v_T^2} \left[-\frac{1}{\epsilon}\left(N_c(m_b^2 + m_t^2) + m_{tau}^2 \right) - \frac{1}{2}N_c m_t^2 \right],$$

$$\frac{\delta M_W^{(6)}}{M_W} = C_\epsilon \left[-\frac{2}{\epsilon}\left(N_c m_b m_t C_{Htb} - N_c(m_b^2 + m_t^2)C_{Hq}^{(3)} \right) - N_c m_t^2 C_{Hq}^{(3)} \right],$$

$$\frac{\delta M_Z^{(4)}}{M_Z} = \frac{C_\epsilon}{v_T^2} \frac{1}{\epsilon}\left(N_c(m_b^2 + m_t^2) + m_\tau^2 \right),$$

$$\frac{\delta M_Z^{(6)}}{M_Z} = \frac{C_\epsilon}{\epsilon} \left[\frac{1}{4}\left(2N_c(m_b^2 + m_t^2) + 2m_\tau^2 + 3M_H^2 \right) C_{HD} + m_H^2 \hat{s}_w \hat{c}_w C_{HWB} \right.$$

$$\left. +2N_c \left(m_b^2 C_{Hb} - m_t^2 C_{Ht} - (m_b^2 - m_t^2)C_{Hq}^{(1)} - (m_b^2 + m_t^2)C_{Hq}^{(3)} \right) \right],$$

$$\frac{\delta \bar{e}^{(4)}}{\bar{e}} = 0,$$

$$\frac{\delta \bar{e}^{(6)}}{\bar{e}} = -\frac{C_\epsilon}{\epsilon} M_H^2 \hat{s}_w \hat{c}_w C_{HWB}.$$

(4.2.23)

From these results, and in addition the results for the anomalous dimension converted into the broken phase of the theory, it is possible to calculate all the remaining renormalisation constants require to construct the complete UV counterterm amplitudes valid in the large-m_t limit.

As can be seen from the counterterm amplitudes defined in 4.2.19 and 4.2.20, in addition to the renormalisation constants defined above, it is necessary to calculate those associated to the effective Z boson couplings. These can be calculated by expanding the couplings defined in 4.1.13 which were conveniently written in terms of hatted quantities. The renormalisation constants for these quantities are obtained from the W and Z boson mass renormalisation as

$$\frac{\delta \hat{c}_w}{\hat{c}_w} \equiv \frac{\delta M_W}{M_W} - \frac{\delta M_Z}{M_Z}, \frac{\delta \hat{s}_w}{\hat{s}_w} \equiv -\frac{\hat{s}_w^2}{\hat{s}_w^2} \frac{\delta \hat{c}_w}{\hat{c}_w},$$

$$\frac{\hat{v}_T}{\hat{v}_T} \equiv \frac{\delta M_W}{M_W} + \frac{\delta \hat{s}_w}{\hat{s}_w} - \frac{\delta \bar{e}}{\bar{e}}. \tag{4.2.24}$$

However, the quantities appear in the counters are s_w and v_T. Using the relation in [106], one can obtain

$$\frac{\delta v_T}{v_T} = \frac{\delta M_W}{M_W} + \frac{\delta \bar{s}_w}{\bar{s}_w} - \frac{\delta \bar{e}}{\bar{e}} - \frac{\hat{v}_T^2 \hat{c}_w}{2 \hat{s}_w} \delta C_{HWB}$$

$$- \frac{\hat{v}_T^2 \hat{c}_w}{2 \hat{s}_w} \left(\frac{\delta \hat{c}_w}{\hat{c}_w} - \frac{\delta \hat{s}_w}{\hat{s}_w} + 2 \frac{\delta \hat{v}_T}{\hat{v}_T} \right) C_{HWB},$$

$$\frac{\delta \bar{s}_w}{\bar{s}_w} = \frac{\delta \hat{s}_w}{\hat{s}_w} - \frac{\hat{v}_T^2 \hat{c}_w^2}{2 \hat{s}_w^2} \left(\frac{\delta \hat{c}_w}{\hat{c}_w} - \frac{\delta \hat{s}_w}{\hat{s}_w} + 2 \frac{\delta \hat{v}_T}{\hat{v}_T} \right) C_{HD} - \frac{\hat{v}_T^2 \hat{c}_w^2}{4 \hat{s}_w^2} \delta C_{HD} \tag{4.2.25}$$

$$- \frac{\hat{v}_T^2 \hat{c}_w}{2 \hat{s}_w} \left(\frac{\delta \hat{c}_w}{\hat{c}_w} - \frac{\delta \hat{s}_w}{\hat{s}_w} + 2 \frac{\delta \hat{v}_T}{\hat{v}_T} \right) C_{HWB} - \frac{\hat{v}_T^2 \hat{c}_w}{2 \hat{s}_w} \delta C_{HWB}.$$

The renormalisation constants for the left and right handed Z boson couplings defined in 4.2.15 can be found using these expressions. The SM expressions are

$$\delta \bar{g}_L^{(4),f} \equiv \delta \bar{g}_R^{(4),f} + I_{W,f}^3 \frac{N_c m_t^2 (1 - 2 \hat{s}_w^2)}{2 \hat{v}_T^2 \hat{s}_w \hat{c}_w},$$

$$\delta \bar{g}_R^{(4),f} \equiv Q^f \frac{N_c m_t^2}{2 \hat{v}_T^2 \hat{s}_w \hat{c}_w}. \tag{4.2.26}$$

The expressions for the dimension-6 counterterms are substantially longer, and we therefore choose to provide a more compact general expression

$$\delta \bar{g}_R^{(6),f} = -Q^f \frac{\hat{s}_w}{\hat{c}_w^3} \frac{\hat{s}_w^{(6)}}{\hat{s}_w} + \frac{\hat{v}_T^2}{2 \hat{s}_w \hat{c}_w} \left(\frac{Q^f}{2} \delta C_{HD} + \delta C_{Hf} \right)$$

$$+ \frac{\hat{v}_T^2}{2 \hat{s}_w \hat{c}_w} \left(2 \frac{\delta \hat{v}_T^{(4)}}{\hat{v}_T} + (-1 + \frac{\hat{s}_w^2}{\hat{c}_w^2}) \frac{\delta \hat{s}_w^{(4)}}{\hat{s}_w} \right) \left(\frac{Q_f}{2} C_{HD} + C_{Hf} \right),$$

$$\delta \bar{g}_L^{(6),f} = \delta \bar{g}_R^{(6),f} + \frac{I_{W,f}^3}{\hat{s}_w \hat{c}_w} (-1 + \frac{\hat{s}_w^2}{\hat{c}_w^2}) \frac{\hat{s}_w^{(6)}}{\hat{s}_w}$$

$$+ \frac{\hat{v}_T^2}{2 \hat{s}_w \hat{c}_w} \left(-\delta C_{Hf} + \delta C_{Hl}^{(1)} + \delta C_{Hl}^{(3)} + T_{W,f}^3 \left(\frac{\delta C_{HD}}{2 \hat{s}_w^2} + \frac{2 \hat{c}_w}{\hat{s}_w} \delta C_{HWB} \right) \right) \tag{4.2.27}$$

$$+ \frac{\hat{v}_T^2}{2 \hat{s}_w \hat{c}_w} (2 \frac{\delta \hat{v}_T^{(4)}}{\hat{v}_T} + (-1 + \frac{\hat{s}_w^2}{\hat{c}_w^2}) \frac{\delta \hat{s}_w^{(4)}}{\hat{s}_w}) \left(-C_{Hf} + C_{Hl}^{(1)} + C_{Hl}^{(3)} \right),$$

$$- T_{W,f}^3 \frac{2 \hat{v}_T^2}{\hat{s}_w^2} \left(\frac{\delta \hat{v}_T^{(4)}}{\hat{v}_T} - \frac{\delta \hat{s}_w^{(4)}}{\hat{s}_w^{(4)}} \right) C_{HWB}$$

$$+ T_{W,f}^3 \frac{\hat{v}_T^2}{2 \hat{s}_w \hat{c}_w} \left(\left(-1 + \frac{\hat{c}_w^2}{\hat{s}_w^2} \right) \frac{\delta \hat{v}_T^{(4)}}{\hat{v}_T} - \left(\frac{3}{2} \frac{\hat{c}_w^2}{\hat{s}_w^2} + \frac{1}{2} \frac{\hat{s}_w^2}{\hat{c}_w^2} \right) \frac{\delta \hat{s}_w^{(4)}}{\hat{s}_w^{(4)}} \right) C_{HD}.$$

We note that the SM results agree with those quoted in [111]. In the above equations we have defined the quantity

$$C_\epsilon = \left(\frac{\mu^2}{m_t^2}\right)^\epsilon = 1 - \epsilon \ln\left[\frac{m_t^2}{\mu^2}\right]. \tag{4.2.28}$$

4.3 The One-loop SM Counterterms

In the pure SM case, we will avoid giving the pure SM one-loop diagrams as well as the relevant amplitudes, since they are trivial. However, we will show how the counterterms are built from the renormalisation constants as an example. In what follows the symbol iijj will be adopt to mark helicity amplitudes that contribute to the $\langle \bar{e}_i \gamma_\mu e_i \rangle \langle \bar{b}_j \gamma^\mu b_j \rangle$ dirac structure, where $i, j = L, R$.

Thus we can express the specific tree level amplitudes for $e^+ e^- \to b\bar{b}$ process with a photon propagator as

$$\begin{aligned}
iM^{(4),0}_{e^+e^- \to \gamma \to b\bar{b}}(\text{LLLL}) &= i\frac{\bar{e}^{2,(4)} Q_b Q_e}{s} \langle \bar{e}_L \gamma_\mu e_L \rangle \langle \bar{b}_L \gamma^\mu b_L \rangle, \\
iM^{(4),0}_{e^+e^- \to \gamma \to b\bar{b}}(\text{LLRR}) &= i\frac{\bar{e}^{2,(4)} Q_b Q_e}{s} \langle \bar{e}_L \gamma_\mu e_L \rangle \langle \bar{b}_R \gamma^\mu b_R \rangle, \\
iM^{(4),0}_{e^+e^- \to \gamma \to b\bar{b}}(\text{RRLL}) &= i\frac{\bar{e}^{2,(4)} Q_b Q_e}{s} \langle \bar{e}_R \gamma_\mu e_R \rangle \langle \bar{b}_L \gamma^\mu b_L \rangle, \\
iM^{(4),0}_{e^+e^- \to \gamma \to b\bar{b}}(\text{RRRR}) &= i\frac{\bar{e}^{2,(4)} Q_b Q_e}{s} \langle \bar{e}_R \gamma_\mu e_R \rangle \langle \bar{b}_R \gamma^\mu b_R \rangle.
\end{aligned} \tag{4.3.29}$$

And the tree level amplitudes for $e^+ e^- \to b\bar{b}$ process with a Z propagator can be written as

$$\begin{aligned}
iM^{(4),0}_{e^+e^- \to Z \to b\bar{b}}(\text{LLLL}) &= i\frac{\bar{e}^{2,(4)} g_L^b g_L^e}{s - M_Z^2} \langle \bar{e}_L \gamma_\mu e_L \rangle \langle \bar{b}_L \gamma^\mu b_L \rangle \\
iM^{(4),0}_{e^+e^- \to Z \to b\bar{b}}(\text{LLRR}) &= i\frac{\bar{e}^{2,(4)} g_R^b g_L^e}{s - M_Z^2} \langle \bar{e}_L \gamma_\mu e_L \rangle \langle \bar{b}_R \gamma^\mu b_R \rangle \\
iM^{(4),0}_{e^+e^- \to Z \to b\bar{b}}(\text{RRLL}) &= i\frac{\bar{e}^{2,(4)} g_L^b g_R^e}{s - M_Z^2} \langle \bar{e}_R \gamma_\mu e_R \rangle \langle \bar{b}_L \gamma^\mu b_L \rangle \\
iM^{(4),0}_{e^+e^- \to Z \to b\bar{b}}(\text{RRRR}) &= i\frac{\bar{e}^{2,(4)} g_L^b g_L^e}{s - M_Z^2} \langle \bar{e}_R \gamma_\mu e_R \rangle \langle \bar{b}_R \gamma^\mu b_R \rangle.
\end{aligned} \tag{4.3.30}$$

Now we build the Z counterterms. Note that $\delta M_Z^2 = 2M_Z^2 \cdot \frac{\delta M_Z^{(4)}}{M_Z}$ can be neglected in the vanishing gauge couplings limit. So for the $e^+ e^- \to Z \to b\bar{b}$ process, in terms

of helicity states, the counterterms can be written as

$$
\begin{aligned}
M^{\text{CT},(4)}_{e^+e^-\to Z\to b\bar{b}}(\text{LLLL}) &= M^{(4),0}_{e^+e^-\to Z\to b\bar{b}}(\text{LLLL}) \\
&\left(\frac{\delta g^b_R}{g^b_R} + \frac{\delta g^e_R}{g^e_R} + \frac{1}{2}(2\delta Z^b_R) + 0\cdot\delta M^{(4)}_Z \cdot 2M^2_Z\frac{1}{s-M^2_Z}\right) \\
M^{\text{CT},(4)}_{e^+e^-\to Z\to b\bar{b}}(\text{RRLL}) &= M^{(4),0}_{e^+e^-\to Z\to b\bar{b}}(\text{RRLL}) \\
&\left(\frac{\delta g^b_L}{g^b_L} + \frac{\delta g^e_R}{g^e_R} + \frac{1}{2}(2\delta Z^b_L) + 0\cdot\delta M^{(4)}_Z \cdot 2M^2_Z\frac{1}{s-M^2_Z}\right) \\
M^{\text{CT},(4)}_{e^+e^-\to Z\to b\bar{b}}(\text{LLRR}) &= M^{(4),0}_{e^+e^-\to Z\to b\bar{b}}(\text{LLRR}) \\
&\left(\frac{\delta g^b_R}{g^b_R} + \frac{\delta g^e_L}{g^e_L} + \frac{1}{2}(2\delta Z^b_R) + 0\cdot\delta M^{(4)}_Z \cdot 2M^2_Z\frac{1}{s-M^2_Z}\right) \\
M^{\text{CT},(4)}_{e^+e^-\to Z\to b\bar{b}}(\text{RRRR}) &= M^{(4),0}_{e^+e^-\to Z\to b\bar{b}}(\text{RRRR}) \\
&\left(\frac{\delta g^b_L}{g^b_L} + \frac{\delta g^e_L}{g^e_L} + \frac{1}{2}(2\delta Z^b_R) + 0\cdot\delta M^{(4)}_Z \cdot 2M^2_Z\frac{1}{s-M^2_Z}\right).
\end{aligned}
\tag{4.3.31}
$$

And for the $e^+e^- \to \gamma \to b\bar{b}$ process, we have

$$
\begin{aligned}
M^{\text{CT}(4)}_{e^+e^-\to\gamma\to b\bar{b}}(\text{RRRR}) &= M^{(4),0}_{e^+e^-\to\gamma\to b\bar{b}}(\text{RRRR})\,\frac{1}{2}(2\delta Z^b_R), \\
M^{\text{CT}(4)}_{e^+e^-\to\gamma\to b\bar{b}}(\text{RRLL}) &= M^{(4),0}_{e^+e^-\to\gamma\to b\bar{b}}(\text{RRLL})\,\frac{1}{2}(2\delta Z^b_L), \\
M^{\text{CT}(4)}_{e^+e^-\to\gamma\to b\bar{b}}(\text{LLRR}) &= M^{(4),0}_{e^+e^-\to\gamma\to b\bar{b}}(\text{LLRR})\,\frac{1}{2}(2\delta Z^b_R), \\
M^{\text{CT}(4)}_{e^+e^-\to\gamma\to b\bar{b}}(\text{LLLL}) &= M^{(4),0}_{e^+e^-\to\gamma\to b\bar{b}}(\text{LLLL})\,\frac{1}{2}(2\delta Z^b_L).
\end{aligned}
\tag{4.3.32}
$$

4.4 The Class 8 Matrix Element

4.4.1 Bare matrix element

To calculate the matrix elements automatically, we need some `Mathematica` packages, including `FeynRules 2.0` [85], `FeynArts 3.9` [112], and `FormCalc 9.4` [113]. `FeynRules` is used to build the dimension-six SMEFT model file which includes all the information of the model. Then we can use `FeynArts` to read the model and to generate the amplitudes of different processes. Finally, `FormCalc` will be quoted to calculate the squared matrix elements.

In general, since only the third generation fermions are considered in the NLO corrections, all flavour indices will be dropped in what follows.
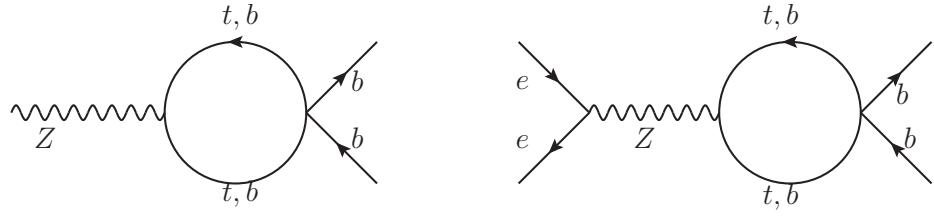
Figure 4.2 One-loop diagrams for $Z \to b\bar{b}$ and $e^+e^- \to b\bar{b}$ processes involving Class 8 operators

In the following calculation of one-loop integrals, the Passarino-Veltmann reduction scheme [114] is employed so that the bare matrix element can be expressed in terms of standard one-loop scalar integrals. It turns out there are only two scalar integrals involved in the Class 8 case, which can be divided into divergent parts and finite part as

$$A_0\left[m^2\right] = \frac{m^2}{\epsilon} + \hat{A}_0\left[m^2\right]$$
$$B_0\left[s, m_1^2, m_2^2\right] = \frac{1}{\epsilon} + \hat{B}_0\left[s, m_1^2, m^2\right],$$

(4.4.33)

in which the finite part can be given with scale-dependence as:

$$\hat{A}_0\left[m^2\right] = m^2 - m^2 \ln\left(\frac{m^2}{\mu^2}\right),$$

$$\hat{B}_0\left[s, m_1^2, m_2^2\right] = 2 - \ln\left(\frac{s}{\mu^2}\right) + \sum_i^{1,2}\left(\lambda_i \ln(\frac{\lambda_i - 1}{\lambda}) - \ln(\lambda_i - 1)\right),$$

(4.4.34)

where

$$\lambda_i = \frac{s - m_2^2 + m_1^2 \pm \sqrt{(s - m_2^2 + m_1^2) - 4sm_1^2}}{2s}.$$

(4.4.35)

According to the chiral feature, these amplitudes can be classified into 5 categories, they are $(\bar{L}L)(\bar{L}L)$, $(\bar{R}R)(\bar{R}R)$, $(\bar{L}L)(\bar{R}R)$, $(\bar{L}R)(\bar{L}R)$, and $(\bar{L}R)(\bar{R}L)$. However, it turns out that only the first three categories will contribute. In the one-loop calculation, only t-quarks and b-quarks in the loops are kept, while the other quarks and leptons are neglected. The loops in $Z \to b\bar{b}$ and $e^+e^- \to b\bar{b}$ are exactly the same, so the operators involved in these two processes are the same as well. The number of the operators that might take part in is limited to 11. These operators are $Q_{qq}^{(1)}, Q_{qq}^{(3)}, Q_d d, Q_{ud}^{(1)}, Q_{ud}^{(8)}, Q_{qu}^{(1)}, Q_{qu}^{(8)}, Q_{qd}^{(1)}, Q_{qd}^{(8)}, Q_{quqd}^{(1)}$ and $Q_{quqd}^{(8)}$. Some amplitudes just vanish, e.g., the trace of the $SU(3)$ generator $Tr\left(T^A\right) = 0$ will lead to their absence in the $Q_{qu}^{(8)}$ case. Besides, some operators only contribute to diagrams with scalar

Dirac structures, which can be neglected as well. At last, only six four-fermion operators contribute to non-scalar Dirac structures, which are $Q_{qq}^{(1)}$, $Q_{qq}^{(3)}$, Q_{dd}, $Q_{ud}^{(1)}$, $Q_{qu}^{(1)}$ and $Q_{qd}^{(1)}$. Actually, since the contribution from t-quark loops would be much bigger than that from the b-quark loops, we can neglect the b-quark loops for the purpose of simplification. But in the Class 8 case we will keep the b-quark loop diagrams and just set the mass of b-quarks to zero in the numerical calculation.

To start with, I will list the bare amplitude for each four-fermion operator and explain how they are generated. The amplitudes will be expressed in the helicity form, which will be very convenient for the following calculation. In the calculation below, according to the Wick's theorem, all possible contractions in the operators have to be included. Note that there are γ matrices in the four fermion operators, e.g., $Q_{qq}^{(1)} = (\bar{q}\gamma^\mu q)(\bar{q}\gamma_\mu q)$, in which I have omitted the flavor indices since we only consider the quarks in the third generation. The contraction operation will affect the position of the γ matrix in the amplitudes, which will lead to different Dirac structures. According to our calculation, there are two different kinds of Dirac structures, which are simply marked as structure (1) and structure (2), which will be explained in detail later.

In the calculation, we can use `FeynArts` to generate these diagram's amplitudes, but `FormCalc` is not able to handle the four-fermion vertexes generated by `FeynArts`. To solve this problem, a trick is needed. The idea is simple: for the first diagram of 4.2 with t-quarks in the loop, the relevant operators are those operators with two t-quarks and two b-quarks, e.g., $(\bar{u}_p\gamma_\mu u_r)(\bar{b}_s\gamma^\mu b_t)$. Since the final states are two b-quarks, the t-quarks must annihilate, which means each top quark must be contracted with a bottom quark. This leads to only one contraction structure, we denote it as structure (1). Now consider an auxiliary SM diagram 4.3(a) that can be dealt with in `FormCalc`. The only difference between this auxiliary diagram and the first diagram in 4.2 is that this diagram includes an extra Z boson propagator. Therefore, to obtain the expected EFT amplitude, we can use `FeynArts` to generate this SM amplitude and delete the Z propagator to get the EFT diagram. For the second diagram in 4.2 with b-quarks in the loop, the situation is more complex. The second diagram comes from operators with four b-quarks such as $(\bar{b}_p\gamma_\mu b_r)(\bar{b}_s\gamma^\mu b_t)$.
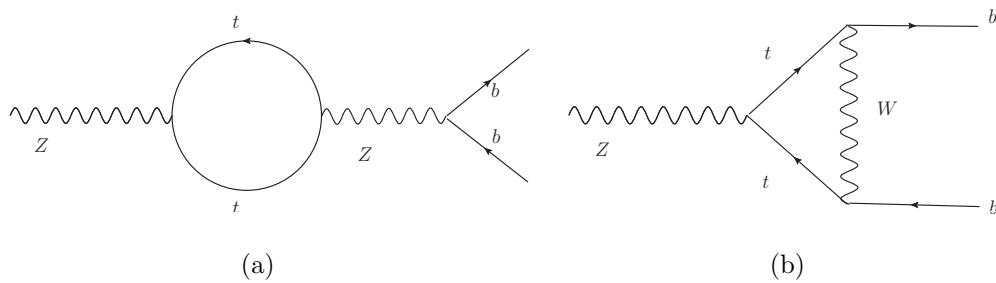
Figure 4.3 Two SM auxiliary diagrams that `FormCalc` can deal with for the $Z \rightarrow$ $b\bar{b}$ process

Since all particles in these operators are b-quarks, these operators could have two contraction structures. One structure is the same as that in the $(\bar{t}_p\gamma_\mu t_r)(\bar{b}_s\gamma^\mu b_t)$ case, which corresponds to the auxiliary diagram 4.3(a). While there is another contraction structure, marked as structure (2), corresponds to another pure SM auxiliary diagram 4.3(b). Note that the fermions in the loop of this SM diagram are t-quarks, in order to get the expected EFT amplitude, one should delete the extra W boson propagator and replace the t-quarks in the loop with b-quarks. Through these two auxiliary diagrams, `FormCalc` will be able to calculate the EFT amplitudes automatically.

We must stress that the relationship between each four-fermion operator and each diagram is not one-to-one, since these operators are not written in terms of particle states. Rather than using the original operators, we need to expand these operators into polynomials in terms of their third-generation particle states. Taking the $\bar{L}L\bar{R}R$ type operator $Q_{qq}^{(1)} = (\bar{q}_p\gamma_\mu q_r)(\bar{q}_s\gamma^\mu q_t)$ for example, The corresponding polynomial is $(\bar{t}\gamma_\mu t)(\bar{b}\gamma^\mu b) + (\bar{b}\gamma_\mu b)(\bar{b}\gamma^\mu b) + (\bar{b}\gamma_\mu b)(\bar{b}\gamma^\mu b)$. Notice that $(\bar{t}\gamma_\mu t)(\bar{b}\gamma^\mu b)$ and $(\bar{b}\gamma_\mu b)(\bar{t}\gamma^\mu t)$ only have one contraction way to generate $b\bar{b}$ final states, both of them belongs to structure (1). Together we can mark them as $2(\bar{t}_p\gamma_\mu t_r)(\bar{b}_s\gamma^\mu b_t)$ (1), where (1) means they belong to structure (1). While $(\bar{b}\gamma_\mu b)(\bar{b}\gamma^\mu b)$ has both contraction structures and each structure has one contraction way respectively. We can write down the corresponding polynomial as $2(\bar{b}\gamma_\mu b)(\bar{b}\gamma^\mu b)$ (1) $+ 2(\bar{b}\gamma_\mu b)(\bar{b}\gamma^\mu b)$ (2), these terms could be connected with the diagrams directly. For $\bar{R}R\bar{R}R$ operators, taking $Q_{ud}^{(1)}$ for example, the corresponding polynomial term should be $(\bar{t}\gamma_\mu t)(\bar{b}\gamma^\mu b)$ (1). For

$\bar{L}L\bar{R}R$ operators, taking $Q_{qd}^{(1)} = (\bar{q}_p\gamma_\mu q_r)\left(\bar{b}_s\gamma^\mu b_t\right)$ for example. The corresponding polynomial is $(\bar{t}\gamma_\mu t)\left(\bar{b}\gamma^\mu b\right) + \left(\bar{b}\gamma_\mu b\right)\left(\bar{b}\gamma^\mu b\right)$. The term $(\bar{t}\gamma_\mu t)\left(\bar{b}\gamma^\mu b\right)$ only have one contraction way, while the term $\left(\bar{b}\gamma_\mu b\right)\left(\bar{b}\gamma^\mu b\right)$ has two possible contraction ways. Note that the $\bar{b}b$ pairs in the left part of the operators are left-handed while the $\bar{b}b$ pairs in the right are right-handed, we have to distinguish diagrams with left-handed bottom quarks in the final states and diagrams with right-handed quarks in the final states. If these diagram belongs to structure (1), we mark diagrams with left handed fermions in the final states with (1L) and diagrams with right-handed fermions in the final states with (1R). Then we can write the polynomial of $Q_{qd}^{(1)}$ as $(\bar{t}\gamma_\mu t)\left(\bar{b}\gamma^\mu b\right)(1) + \left(\bar{b}\gamma_\mu b\right)\left(\bar{b}\gamma^\mu b\right)(1R) + \left(\bar{b}\gamma_\mu b\right)\left(\bar{b}\gamma^\mu b\right)(1L) + \left(\bar{b}\gamma_\mu b\right)\left(\bar{b}\gamma^\mu b\right)(2R) + \left(\bar{b}\gamma_\mu b\right)\left(\bar{b}\gamma^\mu b\right)(2L)$.

We summarize all the expansions in a table below in Table 4.1.

$Q_{qq}^{(1)}$	$2\,(\bar{t}\gamma_\mu t)\left(\bar{b}\gamma^\mu b\right)(1) + 2\left(\bar{b}\gamma_\mu b\right)\left(\bar{b}\gamma^\mu b\right)(1)$ $+2\left(\bar{b}\gamma_\mu b\right)\left(\bar{b}\gamma^\mu b\right)(2)$
$Q_{qq}^{(3)}$	$4\,(\bar{t}\gamma_\mu t)\left(\bar{b}\gamma^\mu b\right)(2) - 2\,(\bar{t}\gamma_\mu t)\left(\bar{b}\gamma^\mu b\right)(1)$ $+2\left(\bar{b}\gamma_\mu b\right)\left(\bar{b}\gamma^\mu b\right)(1) + 2\left(\bar{b}\gamma_\mu b\right)\left(\bar{b}\gamma^\mu b\right)(2)$
$Q_{ud}^{(1)}$	$(\bar{t}\gamma_\mu t)\left(\bar{b}\gamma^\mu b\right)(1)$
$Q_{ud}^{(8)}$	$\left(\bar{t}\gamma_\mu T^A t\right)\left(\bar{b}\gamma^\mu T^A b\right)(1)$
Q_{dd}	$2\left(\bar{b}\gamma_\mu b\right)\left(\bar{b}\gamma^\mu b\right)(1) + 2\left(\bar{b}\gamma_\mu b\right)\left(\bar{b}\gamma^\mu b\right)(2)$
$Q_{qu}^{(1)}$	$(\bar{t}\gamma_\mu t)\left(\bar{b}\gamma^\mu b\right)(1L)$
$Q_{qu}^{(8)}$	$\left(\bar{t}\gamma_\mu T^A t\right)\left(\bar{b}\gamma^\mu T^A b\right)(1L)$
$Q_{qd}^{(1)}$	$(\bar{t}\gamma_\mu t)\left(\bar{b}\gamma^\mu b\right)(1R)$ $+\left(\bar{b}\gamma_\mu b\right)\left(\bar{b}\gamma^\mu b\right)(1R) + \left(\bar{b}\gamma_\mu b\right)\left(\bar{b}\gamma^\mu b\right)(1L)$ $+\left(\bar{b}\gamma_\mu b\right)\left(\bar{b}\gamma^\mu b\right)(2R) + \left(\bar{b}\gamma_\mu b\right)\left(\bar{b}\gamma^\mu b\right)(2L)$
$Q_{qd}^{(8)}$	$\left(\bar{t}\gamma_\mu T^A t\right)\left(\bar{b}\gamma^\mu T^A b\right)(1L) +$ $\left(\bar{b}\gamma_\mu T^A b\right)\left(\bar{b}\gamma^\mu T^A b\right)(1R) + \left(\bar{b}\gamma_\mu T^A b\right)\left(\bar{b}\gamma^\mu T^A b\right)(1L)$ $+\left(\bar{b}\gamma_\mu T^A b\right)\left(\bar{b}\gamma^\mu T^A b\right)(2R) + \left(\bar{b}\gamma_\mu T^A b\right)\left(\bar{b}\gamma^\mu T^A b\right)(2L)$

Table 4.1 In the table, we expand the those Class 8 operators that contribute to NLO corrections for $Z \to b\bar{b}$ and $e^+e^- \to b\bar{b}$ processes in terms of the third-generation particle states.

I will organize this section as follows. First, the bare amplitudes of $Z \to b\bar{b}$ process will be given in a very detailed way, so that many subtleties can be manifested. And then the amplitudes of $e^+e^- \to b\bar{b}$ diagrams will be written into a more compact form.

In the $Z \to b\bar{b}$ process, for the $(\bar{L}L)(\bar{L}L)$ type operator $Q_{qq}^{(1)}$, the diagram with a t-quark loop only contributes to structure (1), the bare amplitude is

$$
\begin{aligned}
iM_{Z \to b\bar{b}}^{Q_{qq}^{(1)},1} = & -i\frac{2N_c \bar{e} C_{qq}^{(1)} \epsilon_Z^\mu}{36\pi^2} \langle \bar{b}_L \gamma_\mu b_L \rangle \left(g_L^t \left(M_Z^2 - 6m_t^2 \right) + 6g_L^t \hat{A}_0 \left[m_t^2 \right] \right. \\
& \left. + 3 \left(g_L^t m_t^2 - 3g_R^t m_t^2 - g_L^t M_Z^2 \right) \hat{B}_0 \left[M_Z^2, m_t^2, m_t^2 \right] \right) \\
& -i\frac{1}{\epsilon} \frac{2N_c \bar{e} C_{qq}^{(1)} \epsilon_Z^\mu}{12\pi^2} \langle \bar{b}_L \gamma_\mu b_L \rangle \left(\left(3g_L^t - 3g_R^t \right) m_t^2 - g_L^t M_Z^2 \right),
\end{aligned}
\tag{4.4.36}
$$

where g_L^t and g_R^t are the SM weak chiral couplings, the general form of SM weak chiral couplings are given in 1.2.47. And diagrams with b-quark loops include a structure (1) part and a structure (2) part, together they contribute

$$
\begin{aligned}
iM_{Z \to b\bar{b}}^{Q_{qq}^{(1)},2} = & -i\frac{2N_c \bar{e} C_{qq}^{(1)} \epsilon_Z^\mu}{36\pi^2} \langle \bar{b}_L \gamma_\mu b_L \rangle \epsilon^\mu \left(g_L^b \left(M_Z^2 - 6m_b^2 \right) + 6g_L^b \hat{A}_0 \left[m_b^2 \right] \right. \\
& \left. + 3 \left(g_L^b m_b^2 - 3g_R^t m_b^2 - g_L^b M_Z^2 \right) \hat{B}_0 \left[M_Z^2, m_b^2, m_b^2 \right] \right) \\
& -i\frac{1}{\epsilon} \frac{2N_c \bar{e} C_{qq}^{(1)} \epsilon_Z^\mu}{12\pi^2} \langle \bar{b}_L \gamma_\mu b_L \rangle \left((3g_L^b - 3g_R^b)m_b^2 - g_b^t M_Z^2 \right) \\
& -i\frac{2\bar{e} C_{qq}^{(1)} \epsilon_Z^\mu}{72\pi^2} \bar{b}_L \gamma_\mu b_L \epsilon^\mu \left(-15g_L^b m_b^2 + 9g_L^b m_b^2 + 4g_R^b M_Z^2 \right. \\
& \left. + 6g_L^b \hat{A}_0 \left[m_b^2 \right] + 3 \left(g_L^t m_t^2 - 3g_R^t m_t^2 - g_L^t M_Z^2 \right) \hat{B}_0 \left[M_Z^2, m_t^2, m_t^2 \right] \right) \\
& -i\frac{1}{\epsilon} \frac{2\bar{e} C_{qq}^{(1)} \epsilon_Z^\mu}{12\pi^2} \langle \bar{b}_L \gamma_\mu b_L \rangle \left((3g_L^b - 3g_R^b)m_b^2 - g_L^b M_Z^2 \right).
\end{aligned}
\tag{4.4.37}
$$

Note that for $(\bar{L}L)(\bar{L}L)$ type operators, the b-quarks in the final states must be left-handed.

From now on, we will avoid writing down the operators into the particle states for simplicity's sake. Similar to $Q_{qq}^{(1)}$, $Q_{qq}^{(3)}$ belongs to the $(\bar{L}L)(\bar{L}L)$ type operators as well. We sum up the all amplitudes of $Q_{qq}^{(3)}$ with two kinds contraction structures

as below:

$$
\begin{aligned}
iM_{Z\to b\bar{b}}^{Q_{qq}^{(3)}} = &-i\frac{-2N_c\bar{e}C_{qq}^{(3)}\epsilon_Z^\mu}{72\pi^2}\left\langle \bar{b}_L\gamma_\mu b_L\right\rangle \epsilon^\mu\left(g_L^t\left(M_Z^2-6m_t^2\right)+6g_L^t\hat{A}_0(m_t^2)\right. \\
&\left.+3\left(g_L^t m_t^2-3g_R^t m_t^2-g_L^t M_Z^2\right)\hat{B}_0\left[M_Z^2,m_t^2,m_t^2\right]\right) \\
&-i\frac{1}{\epsilon}\frac{-2N_c\bar{e}C_{qq}^{(3)}\epsilon_Z^\mu}{12\pi^2}\left\langle \bar{b}_L\gamma_\mu b_L\right\rangle\left(\left(3g_L^b-3g_R^b\right)m_t^2-g_L^t M_Z^2\right) \\
&-i\frac{4\bar{e}C_{qq}^{(3)}\epsilon_Z^\mu}{72\pi^2}<\bar{b}_L\gamma_\mu b_L>\epsilon^\mu\left(-15g_L^t m_t^2+9g_L^t m_t^2+4g_R^t M_Z^2+6g_L^t\hat{A}_0\left[m_t^2\right]\right. \\
&\left.+3(g_L^t m_t^2-3g_R^t m_t^2-g_L^t M_Z^2)\hat{B}_0\left[M_Z^2,m_t^2,m_t^2\right]\right) \\
&-i\frac{1}{\epsilon}\frac{4\bar{e}C_{qq}^{(3)}\epsilon_Z^\mu}{24\pi^2}\left\langle \bar{b}_L\gamma_\mu b_L\right\rangle\left(\left(3g_L^b-3g_R^b\right)m_b^2-g_L^b M_Z^2\right) \\
&-i\frac{2N_c\bar{e}C_{qq}^{(3)}\epsilon_Z^\mu}{72\pi^2}\left\langle \bar{b}_L\gamma_\mu b_L\right\rangle\epsilon^\mu\left(-15g_L^b m_b^2+9g_L^b m_b^2+4g_R^b M_Z^2+6g_L^t\hat{A}_0\left[m_b^2\right]\right. \\
&\left.+3\left(g_L^b m_b^2-3g_R^b m_b^2-g_L^b M_Z^2\right)\hat{B}_0\left[M_Z^2,m_b^2,m_b^2\right]\right) \\
&-i\frac{1}{\epsilon}\frac{2N_c\bar{e}C_{qq}^{(3)}\epsilon_Z^\mu}{12\pi^2}\left\langle \bar{b}_L\gamma_\mu b_L\right\rangle\left(\left(3g_L^b-3g_R^b\right)m_b^2-g_L^b M_Z^2\right) \\
&-i\frac{2\bar{e}C_{qq}^{(3)}\epsilon_Z^\mu}{72\pi^2}<\bar{b}_L\gamma_\mu b_L>\epsilon^\mu\left(-15g_L^b m_b^2+9g_L^b m_b^2+4g_R^b M_Z^2+6g_L^b\hat{A}_0\left[m_b^2\right]\right. \\
&\left.+3\left(g_L^b m_b^2-3g_R^b m_b^2-g_L^b M_Z^2\right)\hat{B}_0\left[M_Z^2,m_b^2,m_b^2\right]\right) \\
&-i\frac{1}{\epsilon}\frac{2\bar{e}C_{qq}^{(3)}\epsilon_Z^\mu}{12\pi^2}\left\langle \bar{b}_L\gamma_\mu b_L\right\rangle\left(\left(3g_L^b-3g_R^b\right)m_b^2-g_L^b M_Z^2\right).
\end{aligned}
\tag{4.4.38}
$$

Next we consider the $\left(\bar{R}R\right)\left(\bar{R}R\right)$ type operators, which only contribute to the diagrams with right-handed b-quarks in final states. For $Q_{ud}^{(1)}$, only a t-quark loop diagram with structure (1) can contribute:

$$
\begin{aligned}
iM_{Z\to b\bar{b}}^{Q_{ud}^{(1)}} = &-i\frac{N_c\bar{e}C_{ud}^{(1)}\epsilon_Z^\mu}{72\pi^2}\left\langle \bar{b}_R\gamma_\mu b_R\right\rangle \epsilon^\mu g_R^t\left(\left(M_Z^2-6m_t^2\right)+6g_R^t\hat{A}_0\left[m_t^2\right]\right. \\
&\left.+3\left(g_R^t m_t^2-3g_L^t m_t^2-g_R^t M_Z^2\right)\hat{B}_0\left[M_Z^2,m_t^2,m_t^2\right]\right) \\
&-i\frac{1}{\epsilon}\frac{2N_c\bar{e}C_{ud}^{(1)}\epsilon_Z^\mu}{24\pi^2}\left\langle \bar{b}_R\gamma_\mu b_R\right\rangle\left(\left(3g_R^b-3g_L^b\right)m_t^2-g_R^t M_Z^2\right).
\end{aligned}
\tag{4.4.39}
$$

For Q_{dd}, there are b-quark loops with structure (1) and structure (2), they contribute

as

$$
\begin{aligned}
iM_{Z\to b\bar{b}}^{Q_{dd}} = & -i\frac{2N_c\bar{e}C_{dd}\epsilon_Z^\mu}{72\pi^2}\left\langle\bar{b}_R\gamma_\mu b_R\right\rangle\epsilon^\mu\left(g_R^b\left(M_Z^2-6m_b^2\right)+6g_R^b\hat{A}_0\left[m_b^2\right]\right. \\
& \left. +3\left(g_R^b m_b^2-3g_L^b m_b^2-g_R^b M_Z^2\right)\hat{B}_0\left[M_Z^2,m_b^2,m_b^2\right]\right) \\
& -i\frac{1}{\epsilon}\frac{2N_c\bar{e}C_{dd}^{(1)}\epsilon_Z^\mu}{24\pi^2}\left\langle\bar{b}_R\gamma_\mu b_R\right\rangle\left(\left(3g_R^b-3g_L^b\right)m_b^2-g_R^b M_Z^2\right) \\
& -i\frac{2\bar{e}C_{dd}\epsilon_Z^\mu}{72\pi^2}\left\langle\bar{b}_R\gamma_\mu b_R\right\rangle\left(-15g_R^b m_b^2+9g_R^b m_b^2+4g_R^b M_Z^2+6g_L^b\hat{A}_0\left[m_b^2\right]\right. \\
& \left. +3\left(g_R^t m_b^2-3g_R^b m_b^2-g_R^b M_Z^2\right)\hat{B}_0\left[M_Z^2,m_b^2,m_b^2\right]\right) \\
& -i\frac{1}{\epsilon}\frac{2\bar{e}C_{dd}^{(1)}\epsilon_Z^\mu}{24\pi^2}\left\langle\bar{b}_R\gamma_\mu b_R\right\rangle\left(\left(3g_R^b-3g_L^b\right)m_b^2-g_R^b M_Z^2\right).
\end{aligned}
\tag{4.4.40}
$$

For the $\left(\bar{L}L\right)\left(\bar{R}R\right)$ type operators, the b-quarks in the final states could be left-handed or right-handed. For $Q_{qu}^{(1)}$, a t-quark loop with structure $(1L)$ lead to a amplitude with left-handed b-quarks in the final states:

$$
\begin{aligned}
iM_{Z\to b\bar{b}}^{Q_{qu}^{(1)}} = & -i\frac{N_c\bar{e}C_{qu}^{(1)}\epsilon_Z^\mu}{72\pi^2}\left\langle\bar{b}_L\gamma_\mu b_L\right\rangle\epsilon^\mu\left(g_R^t\left(M_Z^2-6m_t^2\right)+6g_R^t\hat{A}_0\left[m_t^2\right]\right. \\
& \left. +3\left(g_R^t m_t^2-3g_L^t m_t^2-g_R^t M_Z^2\right)\hat{B}_0\left[M_Z^2,m_t^2,m_t^2\right]\right) \\
& -i\frac{1}{\epsilon}\frac{N_c\bar{e}C_{qu}^{(1)}\epsilon_Z^\mu}{24\pi^2}\left\langle\bar{b}_L\gamma_\mu b_L\right\rangle\left(\left(3g_R^b-3g_L^b\right)m_t^2-g_R^t M_Z^2\right).
\end{aligned}
\tag{4.4.41}
$$

For the $Q_{qd}^{(1)}$ case, it turns out that only the structure (1) diagrams are non-vanishing. The corresponding amplitudes are

$$
\begin{aligned}
iM_{Z\to b\bar{b}}^{Q_{qd}^{(1)}} = & -i\frac{N_c\bar{e}C_{qd}^{(1)}\epsilon_Z^\mu}{72\pi^2}\left\langle\bar{b}_R\gamma_\mu b_R\right\rangle\epsilon^\mu\left(g_L^t\left(M_Z^2-6m_t^2\right)+6g_L^t\hat{A}_0\left[m_t^2\right]\right. \\
& \left. +3\left(g_L^t m_t^2-3g_R^t m_t^2-g_L^t M_Z^2\right)\hat{B}_0\left[M_Z^2,m_t^2,m_t^2\right]\right) \\
& -i\frac{1}{\epsilon}\frac{N_c\bar{e}C_{qd}^{(1)}\epsilon_Z^\mu}{24\pi^2}\left\langle\bar{b}_R\gamma_\mu b_R\right\rangle\left(\left(3g_L^t-3g_R^t\right)m_t^2-g_L^t M_Z^2\right) \\
& -i\frac{N_c\bar{e}C_{qd}^{(1)}\epsilon_Z^\mu}{72\pi^2}\left\langle\bar{b}_R\gamma_\mu b_R\right\rangle\epsilon^\mu\left(g_L^b\left(M_Z^2-6m_b^2\right)+6g_L^b\hat{A}_0\left[m_t^2\right]\right. \\
& \left. +3\left(g_L^b m_t^2-3g_R^b m_t^2-g_L^b M_Z^2\right)\hat{B}_0\left[M_Z^2,m_b^2,m_b^2\right]\right) \\
& -i\frac{1}{\epsilon}\frac{N_c\bar{e}C_{qd}^{(1)}\epsilon_Z^\mu}{24\pi^2}\left\langle\bar{b}_R\gamma_\mu b_R\right\rangle\left(\left(3g_L^t-3g_R^t\right)m_t^2-g_L^t M_Z^2\right) \\
& -i\frac{N_c\bar{e}C_{qd}\epsilon_Z^\mu}{72\pi^2}\left\langle\bar{b}_L\gamma_\mu b_L\right\rangle\epsilon^\mu\left(g_R^b\left(M_Z^2-6m_b^2\right)+6g_R^b\hat{A}_0\left[m_b^2\right]\right. \\
& \left. +3\left(g_R^b m_b^2-3g_L^b m_b^2-g_R^b M_Z^2\right)\hat{B}_0\left[M_Z^2,m_b^2,m_b^2\right]\right) \\
& -i\frac{1}{\epsilon}\frac{N_c\bar{e}C_{qd}^{(1)}\epsilon_Z^\mu}{24\pi^2}\left\langle\bar{b}_L\gamma_\mu b_L\right\rangle\left(\left(3g_R^b-3g_L^b\right)m_b^2-g_R^b M_Z^2\right),
\end{aligned}
\tag{4.4.42}
$$

In the case of $e^+e^- \rightarrow b\bar{b}$, the amplitudes are very similar to the amplitudes in $Z \rightarrow b\bar{b}$. Instead of writing down the amplitude for each diagram, we prefer to express them in a compact form. For this purpose, some notations need to be defined:

$$I_a^{1,i} = g_a^i \left(-6m_i^2 + s\right) + 6g_a^i \hat{A}_0[m_i^2],$$

$$I_a^{2,i} = 3\left(g_a^i m_i^2 - 3g_b^i m_i^2 - g_a^i s\right) \hat{B}_0[s, m_i^2, m_i^2],$$

$$I_a^{3,i} = -15g_a^i m_i^2 + 9g_b^i m_i^2 + 4g_a^i s + 6g_a^i \hat{A}_0\left[m_i^2\right],$$

$$I_a^{4,i} = 3\left(3g_a^i m_i^2 - 3g_b^i m_i^2 - g_a^i s\right),$$

(4.4.43)

where $a, b = L, R$ with $b \neq a$, and $i = t, b$. $g_{L,R}^{t,b}$ are the chiral neutral weak coupling constants. Using 4.4.43, the bare matrix element of $e^+e^- \rightarrow b\bar{b}$ in Class 8 can be written down in a simple way. Due to the different dirac structures, the bare matrix

element can be divided into 4 parts, in which the finite terms are

$$
iM^{\text{fin}}_{e^+e^-\to b\bar{b}}(\text{LLLL}) = -i \langle \bar{e}_L \gamma^\mu e_L \rangle \langle \bar{b}_L \gamma^\mu b_L \rangle \frac{g_L^e \bar{e}^2}{72\pi^2} \frac{1}{s - M_Z^2}
$$

$$
\left(2 \left(\left(I_L^{2,b} + I_L^{2,b} \right) C_{qq}^{(1)} + \left(I_L^{2,b} + I_L^{3,b} + 2 \left(I_L^{2,t} + I_L^{3,t} \right) \right) C_{qq}^{(3)} \right) \right.
$$

$$
+ N_c \left(\left(I_R^{1,b} + I_R^{2,b} \right) C_{qd}^{(1)} + 2 \left(I_L^{1,b} + I_L^{2,b} + I_L^{1,t} + I_L^{2,t} \right) C_{qq}^{(1)} \right.
$$

$$
\left. \left. +2(I_L^{1,b} + I_L^{2,b} - I_L^{1,t} - I_L^{2,t}) C_{qq}^{(3)} + \left(I_R^{1,t} + I_R^{2,t} \right) C_{qu}^{(1)} \right) \right),
$$

$$
iM^{\text{fin}}_{e^+e^-\to b\bar{b}}(\text{RRLL}) = -i \langle \bar{e}_R \gamma^\mu e_R \rangle \langle \bar{b}_L \gamma^\mu b_L \rangle \frac{g_R^e \bar{e}^2}{72\pi^2} \frac{1}{s - M_Z^2}
$$

$$
\left(2 \left(\left(I_L^{2,b} + I_L^{2,3} \right) C_{qq}^{(1)} + \left(I_L^{2,b} + I_L^{3,b} + 2 \left(I_L^{2,t} + I_L^{3,t} \right) \right) C_{qq}^{(3)} \right) \right.
$$

$$
+ N_c \left(\left(I_R^{1,B} + I_R^{2,b} \right) C_{qd}^{(1)} + 2 \left(I_L^{1,b} + I_L^{2,b} + I_L^{1,t} + I_L^{2,t} \right) C_{qq}^{(1)} \right.
$$

$$
\left. \left. +2 \left(I_L^{1,b} + I_L^{2,b} - I_L^{1,t} - I_L^{2,t} \right) C_{qq}^{(3)} + \left(I_R^{1,t} + I_R^{2,t} \right) C_{qu}^{(1)} \right) \right),
$$

$$
iM^{\text{fin}}_{e^+e^-\to b\bar{b}}(\text{LLRR}) = -i \langle \bar{e}_L \gamma^\mu e_L \rangle \langle \bar{b}_R \gamma^\mu b_R \rangle \frac{g_L^e \bar{e}^2}{72\pi^2} \frac{1}{s - M_Z^2}
$$

$$
\left(2 \left(I_R^{2,b} + I_R^{3,b} + \left(I_R^{1,b} + I_R^{2,b} \right) N_c \right) C_{dd} \right.
$$

$$
\left. + N_c \left(\left(I_L^{1,b} + I_L^{2,b} + I_L^{1,t} + I_L^{2,t} \right) C_{qd}^{(1)} + \left(I_R^{1,t} + I_R^{2,t} \right) C_{ud}^{(1)} \right) \right),
$$

$$
iM^{\text{fin}}_{e^+e^-\to b\bar{b}}(\text{RRRR}) = -i \langle \bar{e}_R \gamma^\mu e_R \rangle \langle \bar{b}_R \gamma^\mu b_R \rangle \frac{g_R^e \bar{e}^2}{72\pi^2} \frac{1}{s - M_Z^2}
$$

$$
\left(4 \left(I_R^{2,b} + I_R^{3,b} \right) C_{dd} + N_c \left(\left(I_L^{1,b} + I_L^{2,b} + I_L^{1,t} + I_L^{2,t} \right) C_{qd}^{(1)} + \left(I_R^{1,t} + I_R^{2,t} \right) C_{ud}^{(1)} \right) \right),
$$

$$
(4.4.44)
$$

and the UV divergent terms are

$$
iM^{\text{div}}_{e^+e^-\to b\bar b}(\text{LLLL}) = -i\,\langle \bar e_L\gamma^\mu e_L\rangle\,\langle \bar b_L\gamma^\mu b_L\rangle\,\frac{g_L^e\bar e^2}{72\pi^2}\frac{1}{s-M_Z^2}
$$

$$
\left(2\left(I_L^{4,b}C_{qq}^{(1)}+\left(I_L^{4,b}+2I_L^{4,t}\right)C_{qq}^{(3)}\right)\right.
$$

$$
\left.+N_c\left(I_R^{4,b}C_{qd}^{(1)}+2\left(I_L^{4,b}+I_L^{4,t}\right)C_{qq}^{(1)}+2\left(I_L^{4,b}-I_L^{4,t}\right)C_{qq}^{(3)}+I_R^{4,t}C_{qu}^{(1)}\right)\right)
$$

$$
iM^{\text{div}}_{e^+e^-\to b\bar b}(\text{RRLL}) = -i\,\langle \bar e_R\gamma^\mu e_R\rangle\,\langle \bar b_L\gamma^\mu b_L\rangle\,\frac{g_R^e\bar e^2}{72\pi^2}\frac{1}{s-M_Z^2}
$$

$$
\left(2\left(I_L^{4,b}C_{qq}^{(1)}+\left(I_L^{4,b}+2I_L^{4,t}\right)C_{qq}^{(3)}\right)\right.
$$

$$
\left.+N_c\left(I_R^{4,b}C_{qd}^{(1)}+2\left(I_L^{4,b}+I_L^{4,t}\right)C_{qq}^{(1)}+2\left(I_L^{4,b}-I_L^{4,t}\right)C_{qq}^{(3)}+I_R^{4,t}C_{qu}^{(1)}\right)\right) \qquad (4.4.45)
$$

$$
iM^{\text{div}}_{e^+e^-\to b\bar b}(\text{LLRR}) = -i\,\langle \bar e_L\gamma^\mu e_L\rangle\,\langle \bar b_R\gamma^\mu b_R\rangle\,\frac{g_L^e\bar e^2}{72\pi^2}\frac{1}{s-M_Z^2}
$$

$$
\left(2I_R^{4,b}\left(1+N_c\right)C_{dd}^{(1)}+N_c\left(\left(I_L^{4,b}+I_L^{4,t}\right)C_{qd}^{(1)}+I_R^{4,t}C_{ud}^{(1)}\right)\right),
$$

$$
iM^{\text{div}}_{e^+e^-\to b\bar b}(\text{RRRR}) = -i\,\langle \bar e_R\gamma^\mu e_R\rangle\,\langle \bar b_R\gamma^\mu b_R\rangle\,\frac{g_R^e\bar e^2}{72\pi^2}\frac{1}{s-M_Z^2}
$$

$$
\left(2I_R^{4,b}\left(1+N_c\right)C_{dd}^{(1)}+N_c\left(\left(I_L^{4,b}+I_L^{4,t}\right)C_{qd}^{(1)}+I_R^{4,t}C_{ud}^{(1)}\right)\right).
$$

4.4.2 Class 8 Counterterms and Renormalised Amplitudes

As is outlined in 1.4, UV poles need to be cancelled by the counterterms building through 4.2.22 and 4.2.20 respectively for $Z\to b\bar b$ and $e^+e^-\to b\bar b$ processes. Since we are not interested in corrections with leptons in the loop, the renormalisation of the couplings $g_{L,R}^e$ will not be considered here. Other counterterms could be calculated according to 4.2.23. However, the wavefunction renormalisation for the b-quark due to the Class 8 is not given in 4.2.23, which is needed in the counterterm.

Figure 4.4 The self energy diagrams for b-quarks involving Class 8 operators and QCD contribution

The wavefunction renormalisation for the b-quark together with the mass renor-

malisation can be found in [108], these renormalisation constants are

$$
\delta m_b^{(6)} = \frac{1}{\epsilon} \left[\frac{m_t^3}{2} \left((2N_c + 1) \left(C_{qtqb}^{(1)} + C_{qtqb}^{(1)*} \right) + c_{F,3} \left(C_{qtqb}^{(8)} + C_{qtqb}^{(8)*} \right) \right) \right.
$$
$$
\left. - 4m_b^3 \left(C_{qb}^{(1)} + c_{F,3} C_{qb}^{(8)} \right) \right] + \delta m_b^{fin}(\mu),
$$
$$
\delta m_b^{fin}(\mu) = \frac{m_t}{2} \hat{A}_0(m_t^2) \left((2N_c + 1) \left(C_{qtqb}^{(1)} + C_{qtqb}^{(1)*} \right) + c_{F,3} \left(C_{qtqb}^{(8)} + C_{qtqb}^{(8)*} \right) \right)
$$
$$
+ 2m_b \left(m_b^2 - 2\hat{A}_0(m_b^2) \right) \left(C_{qb}^{(1)} + c_{F,3} C_{qb}^{(8)} \right),
$$
$$
\delta Z_b^{L(6)} = \frac{1}{\epsilon} \left[-\frac{m_t^3}{m_b} \left((2N_c + 1) \left(C_{qtqb}^{(1)} + C_{qtqb}^{(1)*} \right) + c_{F,3} \left(C_{qtqb}^{(8)} + C_{qtqb}^{(8)*} \right) \right) \right]
$$
$$
+ \delta Z_b^{L,fin},
$$
$$
\delta m_b^{fin}(\mu) = -\frac{m_t}{m_b} \hat{A}_0(m_t^2) \left((2N_c + 1) \left(C_{qtqb}^{(1)} + C_{qtqb}^{(1)*} \right) + c_{F,3} \left(C_{qtqb}^{(8)} + C_{qtqb}^{(8)*} \right) \right)
$$
$$
\delta Z_b^{R(6)} = 0,
$$

$$(4.4.46)$$

in which we have omitted the lepton masses. The renormalisation constant of b-quark mass is also listed in 4.4.46, as it will be needed in the transformation procedure from on-shell scheme matrix element to the $\overline{\text{MS}}$ scheme one. And the wavefunction and mass renormalisation for the electron can be obtained by calculating the two-point function similarly as

$$
\delta m_e^{(6)} = \frac{1}{\epsilon} \left(-4m_e^3 C_{le} + N_c m_b^3 \left(C_{lebq} + C_{lebq}^* \right) + N_c m_t^2 \left(C_{leqt}^{(1)} + C_{letq}^* \right) \right) + \delta m_b^{\text{fin}}(e),
$$
$$
\delta m_e^{\text{fin}}(e) = 2m_e^2 \left(m_e^2 - \hat{A}_0 \left[m_e^2 \right] \right) C_{le} + N_c m_b \hat{A}_0 \left[m_b^2 \right] \left(C_{lebq} + C_{lebq}^* \right)
$$
$$
- N_c m_t \hat{A}_0(m_t^2) \left(C_{leqt} + C_{leqt}^* \right)
$$
$$
\delta Z_e^{L(6)} = 2N_c \frac{1}{\epsilon} \left(\frac{m_t^3}{m_e} \left(C_{leqt} - C_{leqt}^* \right) - \frac{m_b^3}{m_e} \left(C_{lebq} - C_{lebq}^* \right) \right) + \delta Z_e^{L,\text{fin}},
$$
$$
\delta m_e^{\text{fin}}(\mu) = 2N_c \left(-\frac{m_t}{m_e} \hat{A}_0 \left[m_t^2 \right] \left(C_{leqt} - C_{leqt}^* \right) - \frac{m_b}{m_e} \hat{A}_0 \left[m_b^2 \right] \left(C_{lebq} - C_{lebq}^* \right) \right)
$$
$$
\delta Z_e^{R(6)} = 0,
$$

$$(4.4.47)$$

in which the electron mass m_e can not set to zero since it appears in the denominators.

Observe 4.4.46 and 4.4.47, we can find that the real parts of the four-fermion Wilson coefficients only contribute to the mass renormalisation, while the imaginary parts only contribute to the fields wavefunction renormalisation. Since in our

assumption, the Wilson coefficients are real, the wavefunction renormalisation constants just vanish. Furthermore, the tree-level amplitudes of $Z \to b\bar{b}$ and $e^+e^- \to b\bar{b}$ processes have no mass terms, so we can conclude that there are no terms due to the mass renormalisation in the counterterm. It needs to be stressed that the wavefunction and mass renormalisation also occur in the SM, through a QCD interaction in the self-energy diagram as shown in 4.4. But it can be neglected in the vanishing gauge couplings limit. As a result, the wavefunction renormalisation and mass renormalisation of b-quark will not contribute to the counterterm at all.

Through 4.2.23, we know that the renormalisation of the electron charge does not contribute as well. The only source of the counterterm in Class 8 case is the renormalisation of the Wilson coefficients, which only contributes to the divergences. Therefore, we can conclude that the finite NLO corrections related to four-fermion EFT operators only come from the one-loop diagrams. Those UV divergent terms due to the one-loop diagrams are directly canceled by the counterterms arising from the Wilson coefficients renormalisation in Class 7 category. Extracting the pieces involving only four-fermion contributions in the vanishing gauge couplings limit to $\dot{C}_{Hq}^{(1)}$, $\dot{C}_{Hq}^{(3)}$ and $\dot{C}_{Hd}$ gives

$$
\dot{C}_{Hq}^1 = 2\frac{m_t^2 - m_b^2}{\hat{v}_t^2}\left(2\left(2N_c + 1\right)C_{qq}^{(1)} + 6C_{qq}^{(3)}\right) - 2\frac{m_t^2}{\hat{v}_t^2}2N_cC_{qu}^{(1)} + 2\frac{m_t^2}{\hat{v}_t^2}2N_cC_{qd}^{(1)},
$$

$$
\dot{C}_{Hq}^3 = -2\frac{m_t^2 + m_b^2}{\hat{v}_t^2}\left(2(2N_c - 1)C_{qq}^{(3)} + 2C_{qq}^{(1)}\right) - 2\frac{m_t^2}{\hat{v}_t^2}2N_cC_{qu}^{(1)} + 2\frac{m_t^2}{\hat{v}_t^2}2N_cC_{qd}^{(1)},
$$

$$
\dot{C}_{Hd} = 2\frac{m_b^2}{\hat{v}_t^2}4\left(N_c + 1\right)C_{dd} - 2\frac{m_t^2}{\hat{v}_t^2}2N_cC_{ud}^{(1)} + 2\frac{m_t^2 - m_b^2}{2}N_cC_{qu}^{(1)},
$$

$$(4.4.48)$$

in which all the flavour indices have been removed. In the Class 8 case, we also check the cancellation of UV divergent terms which are proportional to M_Z^2. Therefore we also list the gauge parts of these dotted Wilson Coefficients:

$$
\dot{C}_{Hq}^1 = \frac{8}{3}\left(2N_c + 1\right)g_1^2N_cy_Hy_qC_{qq}^{(1)} + 8g_1^2y_Hy_qC_{qq}^{(3)}
$$
$$
+ \frac{4}{3}N_cg_1^2N_cy_Hy_uC_{qu}^{(1)} + \frac{4}{3}N_cg_1^2N_cy_Hy_dC_{qd}^{(1)},
$$

$$
\dot{C}_{Hq}^3 = \frac{2}{3}g_2^2C_{qq}^{(1)} + \frac{2}{3}(2N_c - 1)g_2^2C_{qq}^{(3)},
$$

$$
\dot{C}_{Hd} = \frac{8}{3}\left(N_c + 1\right)g_1^2N_cy_Hy_dC_{dd} + +\frac{8}{3}N_cg_1^2N_cy_Hy_qC_{qd}^{(1)} + \frac{4}{3}N_cg_1^2N_cy_Hy_uC_{ud}^{(1)}.
$$

$$(4.4.49)$$

The details of the cancellation of UV divergence in the $Z \to b\bar{b}$ case can be found in A.3 in the Appendix. Cancellation of UV divergence in the $e^+e^- \to b\bar{b}$ case is very similar to former one, which will not be given in detail any more.

In order to convert the on-shell-scheme matrix element to the $\overline{\text{MS}}$-scheme one, we need to recover the μ-dependence of the one-loop matrix element, which could be done by shifting the scalar integrals by a μ-dependence logarithm. In the class 8 case, the one-point scalar integral and the two-point integral shift as

$$
\begin{aligned}
\hat{A}_0\left[m_i^2\right] &\to \hat{A}_0\left[m_i^2\right] - m_i^2 \ln\left[\frac{m_t^2}{\mu^2}\right] \\
\hat{B}_0\left[s, m_i^2, m_j^2\right] &\to \hat{B}_0\left[s, m_i^2, m_j^2\right] - \ln\left[\frac{m_t^2}{\mu^2}\right].
\end{aligned}
\tag{4.4.50}
$$

Furthermore, though the mass of electron is neglected in our assumption, the b-quark mass in the bare matrix element is the physical mass which is valid in the on-shell scheme but not the $\overline{\text{MS}}$ scheme. However, it is straightforward to derive the $\overline{\text{MS}}$ mass from the physical mass with the mass renormalisation of b-quark in hand. The relation between the $\overline{\text{MS}}$ mass and the physical mass for b-quarks are given as

$$
\bar{m}_b(\mu) = m_b + \delta m_b^{\text{fin}}(\mu).
\tag{4.4.51}
$$

Since δm_b^{fin} in 4.4.46 is also a function of the scalar integrals, the operation in 4.4.50 can also be used to recover the μ-dependence factor in the $\overline{\text{MS}}$ scheme. We need stress that the b-quark mass shift due to the $\overline{\text{MS}}$ scheme will not affect our results at all, as there is no counterterm due to the renormalisation of the mass of b-quark. If one just directly replaces m_b with $\bar{m}_b(\mu)$ in the one-loop amplitude, the $\delta m_b^{\text{fin}}(\mu)$ term will contribute to the $\frac{1}{\Lambda^4}$ order in the power counting of SMEFT, which can be neglected.

4.5   The Class 7 Matrix Element

As is shown above in 4.1, the operators in class 7 which contribute to the tree level correction of forward-backward asymmetry are $C_{Hl}^{(1)}$, $C_{Hl}^{(3)}$, C_{He}, $C_{Hq}^{(1)}, C_{Hq}^{(3)}$. A subset of Class 7 operators also contributes to the $Z \to b\bar{b}$ process through the diagrams shown in Fig. 4.5. Unlike the Class 8 case, we only keep the diagrams that contribute

(a) (b) (c) (d)

(e) (f) (g)
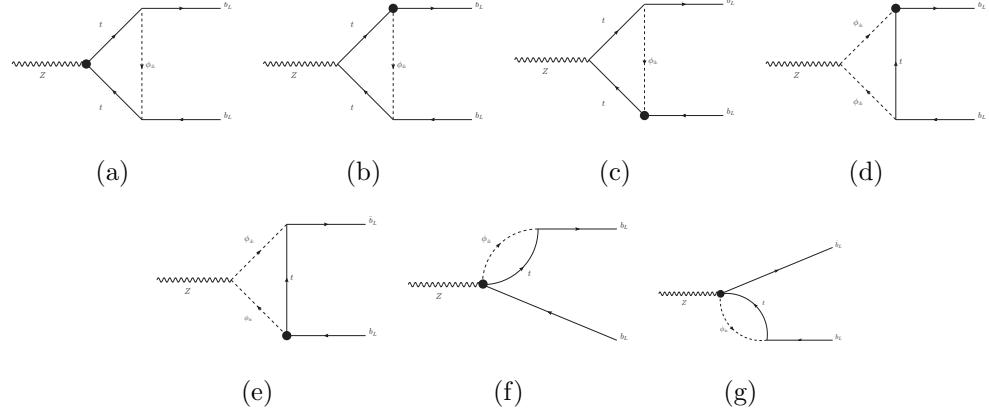
Figure 4.5 Class 7 one-loop diagrams for the $Z \to b\bar{b}$ process

to the m_t^2 terms, since they are dominating in the results. In this approximation, Only the operators $C_{Hq}^{(1)}$, $C_{Hq}^{(3)}$ and C_{Ht} in Class 7 will be involved. It turns out only the left-handed helicity amplitudes survive to contribute, therefore only $\bar{g}_L$ needs to be considered. For the first diagram 4.5(a), the SMEFT operators alter the $Zt\bar{t}$ coupling according to $\bar{g}_{(L,R)}^t$ in 4.1.13. The bare amplitude is

$$
iM_{Z \to b\bar{b}}^a = -i \frac{m_t^2 \bar{e} \epsilon_Z^\mu}{32\pi^2 \hat{c}_w \hat{s}_w M_Z^2} \left\langle \bar{b}_L \gamma_\mu b_L \right\rangle \left(C_{Ht} \left(M_Z^2 + 2 \left(m_t^2 - M_W^2 \right) \hat{B}_0 \left[m_b^2, m_t^2, M_W^2 \right] \right. \right.
$$
$$
- \left(2m_t^2 - 2M_W^2 + M_Z^2 \right) \hat{B}_0 \left[M_Z^2, m_t^2, m_t^2 \right] \right) + 2 \left(C_{Ht} \left(m_t^2 - M_W^2 \right)^2 \right.
$$
$$
\left. + \left(C_{Hq}^{(1)} - C_{Hq}^{(3)} \right) m_t^2 M_Z^2 \right) \hat{C}_0 \left[M_Z^2, m_b^2, m_b^2, m_t^2, m_t^2, M_W^2 \right] - M_Z^2 \frac{1}{\epsilon} C_{Ht} \right).
$$
$$
(4.5.52)
$$

It can be seen in the above amplitude that only C_{Ht} contributes to the UV divergence, while all the other three operators only contribute to the finite part. C_{Ht} does not appear in the born matrix element, it only contribute at the one-loop order. Note that $C_{Hq}^{(1)}$ and $C_{Hq}^{(1)}$ have opposite signs in 4.5.52, as in the $\bar{g}_L^t$.

In the cases of diagrams 4.5(b) 4.5(c), the EFT operators change the coupling

of the goldstone boson to two fermions. Together, these two diagrams contribute as

$$
\begin{aligned}
iM_{Z\to b\bar{b}}^{b,c} = -2i\frac{m_t^2\bar{e}C_{Hq}^{(3)}\epsilon_Z^\mu}{48\pi^2\hat{c}_w\hat{s}_w M_Z^2} \left\langle \bar{b}_L\gamma_\mu b_L\right\rangle &\Bigg(\left(-3\hat{c}_w^2 M_Z^2\right. \\
&+ \left(4m_t^2 - 4M_W^2 + M_Z^2\right)\hat{c}_w^2\right) \hat{B}_0[m_b^2, m_t^2, M_W^2] \\
&+ \hat{s}_w^2\left(M_Z^2 - \left(2m_t^2 - 2M_W^2 + M_Z^2\right)\hat{B}_0[M_Z^2, m_t^2 2, m_t^2]\right) \\
&+ \left(4\left(m_t^2 - M_W^2\right)^2\hat{s}_w^2 + m_t^2 M_Z^2\left(-3\hat{c}_w^2 + \hat{s}_w^2\right)\right)\hat{C}_0[M_Z^2, m_b^2, m_b^2, m_t^2, m_t^2, M_W^2] \\
&- \frac{1}{\epsilon}M_Z^2\left(3\hat{c}_w^2 + \hat{s}_w^2\right)\Bigg).
\end{aligned}
$$

(4.5.53)

The bare matrix element for the diagrams 4.5(d) and 4.5(e) is

$$
iM_{Z\to b\bar{b}}^{d,e} = 2i\frac{m_t^2\bar{e}C_{Hq}^{(3)}\epsilon_Z^\mu}{32\pi^2\hat{c}_w\hat{s}_w M_Z^2}\left\langle \bar{b}_L\gamma_\mu b_L\right\rangle\left(\hat{c}_w^2 - \hat{s}_w^2\right)
$$

$$
\left(\left(M_Z^2 - 2\left(m_t^2 - M_W^2\right)\hat{B}_0\left[m_b^2, m_t^2, M_W^2\right] + \left(2m_t^2 - 2M_W^2 + M_Z^2\right)\hat{B}_0[M_Z^2, M_W^2, M_W^2]\right.\right.
$$

$$
\left.\left.+2\left(m_t^4 + M_W^4 + m_t^2\left(-2M_W^2 + M_Z^2\right)\right)\hat{C}_0\left[m_b^2, M_Z^2, m_b^2, m_t^2, M_W^2, M_W^2\right]\right) + \frac{1}{\epsilon}M_Z^2\right).
$$

(4.5.54)

And the last two diagrams 4.5(f) and 4.5(g) contribute as

$$
iM_{Z\to b\bar{b}}^{f,g} = 2i\frac{m_t^2\bar{e}\hat{s}_w C_{Hq}^{(3)}\epsilon_Z^\mu}{8\pi^2\hat{c}_w M_Z^2}\left\langle \bar{b}_L\gamma_\mu b_L\right\rangle\left(\hat{B}_0\left[m_b^2, m_t^2, M_W^2\right] + \frac{1}{\epsilon}M_Z^2\right).
$$

(4.5.55)

Summing up all divergences above in the $Z\to b\bar{b}$ reaction, we have

$$
i\frac{\bar{e}m_t^2\epsilon_Z^\mu}{16\pi^2\hat{c}_w\hat{s}_w}\left(C_{Ht} + \left(6 + \frac{4}{3}\hat{s}_w^2\right)C_{Hq}^{(3)}\right)\left\langle \bar{b}_L\gamma_\mu b_L\right\rangle .
$$

(4.5.56)

The $e^+e^-\to b\bar{b}$ case is very similar to the $Z\to b\bar{b}$ one. We just simply write down the four corresponding bare amplitudes in the $e^+e^-\to b\bar{b}$ reaction, they are

$$
iM_{e^+e^-\to b\bar{b}}^a = -i\frac{\bar{\alpha}m_t^2}{16\pi s\hat{s}_w^2\hat{c}_w^2}\frac{1}{s - M_Z^2}
$$

$$
\left(C_{Ht}\left(s + 2\left(m_t^2 - M_W^2\right)\hat{B}_0\left[m_b^2, m_t^2, M_W^2\right] - \left(2m_t^2 - 2M_W^2 + s\right)\hat{B}_0\left[s, m_t^2, m_t^2\right]\right)\right.
$$

$$
+ 2(C_{Ht}(m_t^2 - M_W^2)^2 + \left(C_{Hq}^{(1)} - C_{Hq}^{(3)}\right)m_t^2 s)\hat{C}_0\left[S, m_b^2, m_b^2, m_t^2, m_t^2, M_W^2\right]
$$

$$
\left.- \frac{sC_{Ht}}{\epsilon}\right)\left(2\hat{s}_w^2\left\langle \bar{e}_L\gamma^\mu e_L\right\rangle\left\langle \bar{b}_L\gamma^\mu b_L\right\rangle - \left(\hat{c}_w^2 - \hat{c}_w^2\right)\left\langle \bar{e}_R\gamma^\mu e_R\right\rangle\left\langle \bar{b}_L\gamma^\mu b_L\right\rangle\right),
$$

(4.5.57)

$$iM^{b,c}_{e^+e^- \to b\bar{b}} = -2i\frac{\bar{\alpha}m_t^2 C_{Hq}^{(3)}}{24\pi s \hat{s}_w^2 \hat{c}_w^2}\frac{1}{s - M_Z^2}$$

$$\left(\left(-3\hat{c}_w^2 s + \left(4m_t^2 - 4M_W^2 + s\right)\hat{s}_w^2\right)\hat{B}_0\left[m_b^2, m_t^2, M_W^2\right] \right.$$

$$+ 2\hat{s}_w^2\left(s - \left(2m_t^2 - 2M_W^2 + s\right)\hat{B}_0\left[s, m_t^2, m_t^2\right]\right)$$

$$+ \left(-3\hat{c}_w^2 m_t^2 s + \left(4\left(m_t^2 - M_W^2\right)^2 + m_t^2 s\right)\hat{s}_w^2\right)\hat{C}_0\left[s, m_b^2, m_b^2, m_t^2, m_t^2, M_W^2\right]$$

$$\left. - \frac{s}{\epsilon}(3\hat{c}_w^2 + \hat{s}_w^2)\right)\left(2\hat{s}_w^2\left\langle\bar{e}_L\gamma^\mu e_L\right\rangle\left\langle\bar{b}_L\gamma^\mu b_L\right\rangle - \left(\hat{c}_w^2 - \hat{s}_w^2\right)\left\langle\bar{e}_R\gamma^\mu e_R\right\rangle\left\langle\bar{b}_L\gamma^\mu b_L\right\rangle\right),$$

$$(4.5.58)$$

$$iM^{d,e}_{e^+e^- \to b\bar{b}} = i\frac{\bar{\alpha}m_t^2 C_{Hq}^{(3)}}{8\pi s \hat{s}_w^2 \hat{c}_w^2}\frac{1}{s - M_Z^2}(\hat{c}_w^2 - \hat{s}_w^2)$$

$$\left(s + 2\left(-m_t^2 + M_W^2\right)\hat{B}_0\left[m_b^2, m_b^2, M_W^2\right] + \left(2m_t^2 - 2M_W^2 + s\right)\hat{B}_0\left[s, M_W^2, M_W^2\right]\right.$$

$$\left. + 2\left(\left(m_t^2 - M_W^2\right)^2 + m_t^2 s\right)\hat{C}_0\left[m_b^2, s, m_b^2, m_t^2, M_W^2, M_W^2\right] + \frac{s}{\epsilon}\right)$$

$$\left(2\hat{s}_w^2\left\langle\bar{e}_L\gamma^\mu e_L\right\rangle\left\langle\bar{b}_L\gamma^\mu b_L\right\rangle - \left(\hat{c}_w^2 - \hat{s}_w^2\right)\left\langle\bar{e}_R\gamma^\mu e_R\right\rangle\left\langle\bar{b}_L\gamma^\mu b_L\right\rangle\right),$$

$$(4.5.59)$$

and

$$iM^{f,g}_{e^+e^- \to b\bar{b}} = 2i\frac{\bar{\alpha}m_t^2 C_{Hq}^{(3)}}{4\pi \hat{c}_w^2}\frac{1}{s - M_Z^2}\left(\hat{B}_0\left[m_b^2, m_t^2, M_W^2\right] + \frac{1}{\epsilon}\right)$$

$$\left(2\hat{s}_w^2\left\langle\bar{e}_L\gamma^\mu e_L\right\rangle\left\langle\bar{b}_L\gamma^\mu b_L\right\rangle - \left(\hat{c}_w^2 - \hat{s}_w^2\right)\left\langle\bar{e}_R\gamma^\mu e_R\right\rangle\left\langle\bar{b}_L\gamma^\mu b_L\right\rangle\right).$$

$$(4.5.60)$$

As in the Class 8 case, the renormalisation of the Wilson coefficients only contributes to the divergent counterterm. Extracting the pieces involving only Class 7 contributions in the vanishing gauge coupling to $\dot{C}_{Hq}^{(1)}$, $\dot{C}_{Hq}^{(3)}$ and $\dot{C}_{Hd}$ gives

$$\dot{C}_{Hq}^1 = \frac{2m_t^2}{v_T^2}\left(-C_{Ht}4\left(\frac{N_c}{2} + 1\right)C_{Hq}^{(1)} - 9C_{Hq}^{(3)}\right)$$

$$\dot{C}_{Hq}^3 = -3\frac{2m_t^2}{v_T^2}C_{Hq}^{(1)} + 2\frac{2m_t^2}{v_T^2}\left(N_c + 1\right)C_{Hq}^{(3)}$$

$$\dot{C}_{Hd} = 0,$$

$$(4.5.61)$$

which could generate the following divergent counterterms:

$$i\frac{1}{\epsilon}\frac{\bar{e}m_t^2\epsilon_Z^\mu}{16\pi^2\hat{c}_w\hat{s}_w}\left(C_{Ht} + \left(7 - 2N_c\right)C_{Hq}^{(3)} - \left(1 + 2N_c\right)C_{Hq}^{(1)}\right)\left\langle\bar{b}_L\gamma_\mu b_L\right\rangle.$$

$$(4.5.62)$$

Following the renormalisation procedure in 4.2, there are still counterterms due to

$\frac{\delta \hat{v}_T^{(4)}}{\hat{v}_T}$, $\delta Z_b^{(4),L}$ and $\delta Z_b^{(6),L}$, which are

$$i \frac{\hat{v}_T^{(4),\text{div}}}{\hat{v}_T} = \frac{1}{\epsilon} \frac{-N_c m_t^2}{2 \hat{v}_T^2}$$

$$\delta Z_b^{(4),L,\text{div}} = \frac{1}{\epsilon} \frac{-m_t^2}{\hat{v}_T^2} \tag{4.5.63}$$

$$\delta Z_b^{(6),L,\text{div}} = \frac{1}{\epsilon} 2 m_t^2 C_{Hq}^{(3)}.$$

It is easy to check that the counterterms with N_c due to $\delta \frac{\hat{v}_T^{(4),div}}{\hat{v}_T}$ are responsible for cancelling the counterterms including N_c in 4.5.62. All other divergent counterterms directly cancel the divergences in the one-loop amplitude.

4.6 The Class 4 Matrix Element

In the large-m_t limit, there is only one operator C_{HWB} in Class 4 that can contribute to the NLO correction in both $Z \to b\bar{b}$ and $e^+ e^- \to b\bar{b}$ processes. These one-loop diagrams in the $Z \to b\bar{b}$ case are shown in Fig. 4.6.

$\quad$ (a) $\qquad\qquad$ (b) $\qquad\qquad$ (c) $\qquad\qquad$ (d)
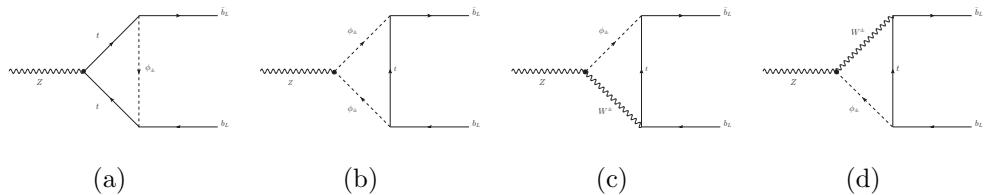
**Figure 4.6** $\quad$ Class 4 one-loop diagrams for the $Z \to b\bar{b}$ process

For the first diagram 4.6(a), the bare amplitude takes the form

$$i M_{Z \to b\bar{b}}^a = -i \frac{m_t^4 \bar{e} C_{HWB} \epsilon_Z^\mu}{16 \pi^2 \hat{s}_w^2} \hat{c}_w m_t^4 \hat{C}_0 \left[M_Z^2, m_b^2, m_b^2, m_t^2, m_t^2, M_W^2 \right] \left\langle \bar{b}_L \gamma_\mu b_L \right\rangle .$$

$$\tag{4.6.64}$$

For the second diagram 4.6(b), we have

$$iM^b_{Z\to b\bar{b}} = -i\frac{m_t^2\bar{e}C_{HWB}\epsilon_Z^\mu}{32\pi^2 M_Z^2\hat{s}_w^2}\hat{c}_w$$

$$\left(\left(M_Z^2 - 2\left(m_t^2 - M_W^2\right)\hat{B}_0\left[m_b^2, m_t^2, M_W^2\right] + \left(2m_t^2 - 2M_W^2 + M_Z^2\right)\hat{B}_0\left[M_Z^2, M_W^2, M_W^2\right]\right.\right.$$

$$\left.+2\left(m_t^4 + M_W^4 + m_t^2\left(-2M_W^2 + M_Z^2\right)\right)\hat{C}_0\left[m_b^2, M_Z^2, m_b^2, m_t^2, M_W^2, M_W^2\right]\right)$$

$$\left.+ M_Z^2\frac{1}{\epsilon}\right)\langle\bar{b}_L\gamma_\mu b_L\rangle.$$

$$(4.6.65)$$

The third and forth diagram will lead to a same amplitude, together they contribute as

$$iM^{c,d}_{Z\to b\bar{b}} = -2i\frac{m_t^2 M_Z^2\bar{e}C_{HWB}\epsilon_Z^\mu}{32\pi^2}\hat{c}_w\hat{c}_w\hat{C}_0\left[m_b^2, M_Z^2, m_b^2, m_t^2, M_W^2, M_W^2\right]\langle\bar{b}_L\gamma_\mu b_L\rangle.$$

$$(4.6.66)$$

For the $e^+e^- \to b\bar{b}$ case which is similar to the $Z \to b\bar{b}$ case, we just show the corresponding amplitudes as follows:

$$iM^a_{e^+e^-\to b\bar{b}} = -i\frac{m_t^4\bar{\alpha}C_{HWB}}{32\pi\hat{c}_w\hat{s}_w^3}\frac{1}{s - M_Z^2}\hat{C}_0\left[s, m_b^2, m_b^2, m_t^2, m_t^2, M_W^2\right]$$

$$\left(2\hat{s}_w^2\langle\bar{e}_L\gamma_\mu e_L\rangle\langle\bar{b}_L\gamma_\mu b_L\rangle + \left(\hat{s}_w^2 - \hat{c}_w^2\right)\langle\bar{e}_R\gamma_\mu e_R\rangle\langle\bar{b}_L\gamma_\mu b_L\rangle\right),$$

$$(4.6.67)$$

$$iM^b_{e^+e^-\to b\bar{b}} = -i\frac{m_t^2\bar{\alpha}C_{HWB}}{16\pi\hat{c}_w\hat{s}_w^3 s}\frac{1}{s - M_Z^2}$$

$$\left(\left(s - 2\left(m_t^2 - M_W^2\right)\hat{B}_0\left[m_b^2, m_t^2, M_W^2\right] + \left(2m_t^2 - 2M_W^2 + s\right)\hat{B}_0\left[s, M_W^2, M_W^2\right]\right.\right.$$

$$\left.+2\left(\left(m_t^2 + M_W^2\right)^2 + m_t^2 s\right)\hat{C}_0\left[m_b^2, s, m_b^2, m_t^2, M_W^2, M_W^2\right]\right)$$

$$\left.+ s\frac{1}{\epsilon}\right)\left(2\hat{s}_w^2\langle\bar{e}_L\gamma_\mu e_L\rangle\langle\bar{b}_L\gamma_\mu b_L\rangle + \left(\hat{s}_w^2 - \hat{c}_w^2\right)\langle\bar{e}_R\gamma_\mu e_R\rangle\langle\bar{b}_L\gamma_\mu b_L\rangle\right),$$

$$(4.6.68)$$

$$iM^{c,d}_{e^+e^-\to b\bar{b}} = -2i\frac{\bar{\alpha}sC_{HWB}}{16\pi\hat{c}_w\hat{s}_w}\frac{1}{s - M_Z^2}\hat{C}_0\left[m_b^2, s, m_b^2, m_t^2, M_W^2, M_W^2\right]$$

$$\left(2\hat{s}_w^2\langle\bar{e}_L\gamma_\mu e_L\rangle\langle\bar{b}_L\gamma_\mu b_L\rangle + \left(\hat{s}_w^2 - \hat{c}_w^2\right)\langle\bar{e}_R\gamma_\mu e_R\rangle\langle\bar{b}_L\gamma_\mu b_L\rangle\right).$$

$$(4.6.69)$$

Only one diagram contributes to the divergent term in the $Z \to b\bar{b}$ process as well as in the $e^+e^- \to b\bar{b}$ process. The one-loop UV divergencies for those two process can be directly read off from 4.6.65 and 4.6.68.

As usual, one source of divergent counterterms is the renormalisation of Wilson

coefficients. In the Class 4 case, only δC_{HWB} is involved:

$$\dot{C}_{HWB} = 2\frac{2m_t^2}{v_T^2}N_c C_{HWB}. \qquad (4.6.70)$$

Similar to the Class 7 case, the other divergent counterterms also arise from $\frac{\hat{v}_T^{(4)}}{\hat{v}_T}$, $\delta Z_b^{(4),L}$ and $\delta Z_b^{(6),L}$. The normal SM renormalisation constants $\frac{\hat{v}_T^{(4)}}{\hat{v}_T}$ and $\delta Z_b^{(4),L}$ are the same for Class 4 and Class 7 cases, while the EFT renormalisation constant $\delta Z_b^{(6),L}$ does not include any Class 4 Wilson Coefficient. We have

$$\delta Z_b^{(6),\text{div}} = 0. \qquad (4.6.71)$$

Since the divergent structure in the Class 4 case is simple for both processes, it is easy to check that the divergent counterterms due to $\frac{\delta \hat{v}_T^{(4)}}{\hat{v}_T}$ directly cancel the divergent counterterms due to $\dot{C}_{HWB}$, and the one-loop UV divergencies are cancelled by the counterterms due to $\delta Z_b^{(4),L}$.

4.7 G_F as an Input Parameter

In the above calculation, we express our calculations in terms of v_T that is deduced from the input parameter M_W. However, the measurement precision of M_W is not as good as G_F in the experiments. Consequently, it is better to replace M_W with G_F in the set of input parameters in the numeric calculation. To be more specific, we need to express the vacuum expectation value v_T in terms of G_F. Correspondingly, the tree-level relation 2.1.18 has to be extended to its one-loop form. In [108], such a relation is given as

$$\frac{1}{\sqrt{2}}\frac{1}{v_T^2}(1 + \Delta r) = G_F + R^{(6)}, \qquad (4.7.72)$$

where Δr represents for the finite non-QED radiative corrections to muon decay in terms of two-point functions [115]. In the vanishing gauge couplings limit,

$$\Delta r = 2\left(\frac{\delta M_W}{M_W} - \frac{\delta v_T}{v_T}\right). \qquad (4.7.73)$$

By using the relations in 4.2.23 one can obtain Δr at the one-loop order, the specific expression of Δr can be found in [108]. And $R^{(6)}$ is the finite correction arising from

the SMEFT contribution, including a tree-level part and a one-loop part. The tree level part could be deduced from 2.1.18, which is

$$\Delta R^{(6,0)} = -\sqrt{2}C_{Hl}^{(3)} + \frac{\sqrt{2}}{2}C_{ll},$$
(4.7.74)

in which the favour indices are dropped. The one-loop part can be found in the large-m_t limit in [108]. Dropping the redundant flavour indices, it can be written as

$$\Delta R^{(6,1)} = \frac{\sqrt{2}N_c m_t^2}{v_T^2}C_{lq}^{(3)} - \frac{1}{\sqrt{2}}\left(\dot{C}_{Hl}^{(3)} - \dot{C}_{ll}^{(3)}\right)\ln\left(\frac{m_t^2}{\mu^2}\right),$$
(4.7.75)

where the μ dependence has been restored by the RG equations. For convenience's sake, we can divide a general amplitude in dimension-six SMEFT into four parts as

$$M_{(e^+e^-\to b\bar{b})}^{(6)} = \bar{v}(p_e)\gamma^\mu u(p_{\bar{e}})\bar{u}(p_b)\gamma_\mu v(p_{\bar{b}})\left(A^{(4,0)} + A^{(6,0)} + A^{(4,1)} + A^{(6,1)}\right),$$
(4.7.76)

where $A^{(4,0)}$ is the tree-level pure SM part, $A^{(4,1)}$ is the one-loop SM part, $A^{(6,0)}$ is the tree-level EFT part and $A^{(6,1)}$ is the one-loop EFT part. For each SM diagram, each vertex will contribute to a v_T^{-1}, which is equal to $G_F^{1/2}$. Accordingly, $A^{(6,0)}$ and $A^{(6,1)}$ will receive shifts as follows:

$$A^{(6,0)} \to A^{(6,0)} + \delta A_{G_F}^{(6,0)}$$
$$A^{(6,1)} \to A^{(6,1)} + \delta A_{G_F}^{(6,1)},$$
(4.7.77)

in which the shifts could be computed as

$$\delta A_{G_F}^{(6,0)} = A^{(4,0)}\frac{\Delta R^{(6,0)}}{G_F}$$
$$\delta A_{G_F}^{(6,1)} = A^{(4,0)}\frac{\Delta R^{(6,1)}}{G_F} + A^{(4,1)}\frac{2\Delta R^{(6,0)}}{G_F}.$$
(4.7.78)

4.8 Phenomenology and Numerical Results

In this section we focus on the $e^+e^- \to b\bar{b}$ process. In the following numerical calculations, input parameters are chosen as $\alpha = 1/127.91$ $m_t = 173.3$ GeV, $m_Z = 91.1875$ GeV $m_H = 125.0$ GeV, $G_F = 1.16638 \cdot 10^{-5}$ GeV^{-2}, $\Gamma_Z = 2.4952$ GeV [13], and the physical scale is chosen as $\mu = \mu_t \sim m_t$, in which case the large logarithms arising from the one-loop matrix elements are absorbed into the Wilson coefficients

$C_i(\mu_t)$. According to the RG equations, one can obtain the following relation of Wilson Coefficients for different energy scales:

$$C_i(\mu_t) = C_i(\Lambda) + \frac{1}{2}\frac{1}{16\pi^2}\dot{C}_i(\Lambda)\ln\left[\frac{\mu_t^2}{\Lambda^2}\right], \tag{4.8.79}$$

through which the numerical results obtained at the scale μ_t could be transformed to the result at the new physics scale Λ on the assumption that Λ does not exceed μ_t by several orders of magnitude. The specific form of each $\dot{C}_i$ at one loop has been given in [104–106]. Benefiting from this approach, our following numerical result could be used to test new physics models at the scale Λ.

The following calculation is up to one loop and $1/\Lambda^2$, which means the self-interference of the pure EFT terms that are proportional to $1/\Lambda^4$ are neglected. In order to constrain the values of the Wilson coefficients, one should compute the predictions for specific observables. To began with, the squared Matrix elements of $e^+e^- \to b\bar{b}$ process should be calculated. In the SMEFT, the squared matrix elements could be decomposed into SM part and EFT part, in which the SM part can be written as

$$\left|M^{(4)}\right|^2 = M^{(4,0),*} \cdot M^{(4,0)} + 2M^{(4,0),*} \cdot M^{(4,1)}, \tag{4.8.80}$$

and similarly the EFT part can be written as

$$\left|M^{(6)}\right|^2 = 2M^{(4,0),*} \cdot M^{(6,0)} + 2M^{(4,1),*} \cdot M^{(6,0)} + 2M^{(4,0),*} \cdot M^{(6,1)}. \tag{4.8.81}$$

The total squared matrix elements should be the sum of these two parts:

$$\left|M^{\text{SMEFT}}\right|^2 = |M^{(4)}|^2 + |M^{(6)}|^2. \tag{4.8.82}$$

For the $e^+e^- \to b\bar{b}$ process, neglecting the mass of electron, the general differential cross-section can be expressed as

$$d\sigma = \frac{\sqrt{1 - \frac{4m_b^2}{s}}|M|^2 d\cos\theta}{8\pi s} \tag{4.8.83}$$

To make the suppression of dimension-6 contributions more explicit, we define the dimensionless Wilson Coefficient as

$$C_i(\mu_t) \equiv \frac{\widetilde{C}_i(\mu_t)}{\Lambda^2}. \tag{4.8.84}$$

In terms of the dimensionless Wilson Coefficients, the tree-level general differential cross section $d\sigma/dc_\theta \left(e^+ e^- \to b\bar{b}\right)$ which is the massive version of equation 4.2

of [109] can be expressed as:

$$\frac{1}{N_c}\frac{d\sigma}{dc_\theta} = \frac{\left(\bar{e}^4 Q_b^2 Q_e^2 \beta \left(2 + \left(-1 + c_\theta^2\right)\beta^2\right)\right)}{32\pi s} + \frac{\bar{e}^2 N_c Q_b Q_e \beta}{64\pi\Lambda^2}$$

$$\left[2\left(\widetilde{C}_{eb} + \widetilde{C}_{lb} + \widetilde{C}_{qe}\right) + 2c_\theta\beta\left(\widetilde{C}_{eb} - \widetilde{C}_{lb} - \widetilde{C}_{qe}\right) - \left(\widetilde{C}_{eb} + \widetilde{C}_{lb} + \widetilde{C}_{qe}\right)\beta^2(1 - c_\theta^2)\right.$$

$$\left. + \left(\widetilde{C}_{lq}^{(1)} + \widetilde{C}_{lq}^{(3)}\right)\left(2 + 2c_\theta\beta - \beta^2 + c_\theta^2\beta^2\right)\right]$$

$$+ \frac{\bar{e}^4 Q_b Q_e \beta \bar{\chi}(s)}{128\pi}\left[\bar{g}_L^b\left(\bar{g}_R^e\left(2 - 2c_\theta\beta - \beta^2 + c_\theta^2\beta^2\right) + \bar{g}_L^e\left(2 + 2c_\theta\beta - \beta^2 + c_\theta^2\beta^2\right)\right)\right.$$

$$\left. + \bar{g}_R^b\left(\bar{g}_L^e\left(2 - 2c_\theta\beta - \beta^2 + c_\theta^2\beta^2\right) + \bar{g}_R^e\left(2 + 2c_\theta\beta - \beta^2 + c_\theta^2\beta^2\right)\right)\right]$$

$$+ \frac{s\beta}{128\pi\Lambda^4}\left[\widetilde{C}_{eb}^2 + \widetilde{C}_{lb}^2 + 2\widetilde{C}_{eb}\widetilde{C}_{qe} + \widetilde{C}_{qe}^2 + 2c_\theta\widetilde{C}_{eb}^2\beta - 2c_\theta\widetilde{C}_{lb}^2\beta - 2c_\theta\widetilde{C}_{qe}^2\beta + c_\theta^2\widetilde{C}_{eb}^2\beta^2\right.$$

$$\left. + c_\theta^2\widetilde{C}_{lb}^2\beta^2 - 2\widetilde{C}_{eb}\widetilde{C}_{qe}\beta^2 + c_\theta^2\widetilde{C}_{qe}^2\beta^2 + \left(\widetilde{C}_{lq}^{(1)} + c_\theta\widetilde{C}_{lq}^{(1)}\beta\right)^2 + \left(\widetilde{C}_{lq}^{(3)} + c_\theta\widetilde{C}_{lq}^{(3)}\beta\right)^2\right.$$

$$\left. - 2\widetilde{C}_{lq}^{(3)}\widetilde{C}_{lb}(-1 + \beta^2) + 2\widetilde{C}_{lq}^{(1)}\left(\widetilde{C}_{lb} - \widetilde{C}_{lb}\beta^2 + \widetilde{C}_{lq}^{(3)}(1 + c_\theta\beta)^2\right)\right]$$

$$+ \frac{\bar{e}^2 s\bar{\chi}(s)}{128\pi\Lambda^2}\beta\left[\bar{g}_L^b\left(\bar{g}_R^e\left(\widetilde{C}_{eb} - \widetilde{C}_{eb}\beta^2 + \widetilde{C}_{qe}(-1 + c_\theta\beta)^2\right)\right.\right.$$

$$\left. + \bar{g}_L^e\left(\widetilde{C}_{lb} - \widetilde{C}_{lb}\beta^2 + \widetilde{C}_{lq}^{(1)}(1 + c_\theta\beta)^2 + \widetilde{C}_{lq}^{(3)}(1 + c_\theta\beta)^2\right)\right)$$

$$+ \bar{g}_R^b\left(\bar{g}_L^e\left(\widetilde{C}_{lq}^{(1)} + \widetilde{C}_{lq}^{(3)} - \widetilde{C}_{lq}^{(1)}\beta^2 - C_{lq}^{(3)}\beta^2 + \widetilde{C}_{lb}(-1 + c_\theta\beta)^2\right)\right.$$

$$\left.\left. + \bar{g}_R^e\left(\widetilde{C}_{qe} - \widetilde{C}_{qe}\beta^2 + \widetilde{C}_{eb}(1 + c_\theta\beta)^2\right)\right)\right]$$

$$+ \frac{\bar{e}^4 Q_b Q_e \beta \chi(s)}{128\pi}\left[\bar{g}_L^e\bar{g}_R^b(-1 + c_\theta\beta)^2 + \bar{g}_L^b\bar{g}_R^e(-1 + c_\theta\beta)^2 + \bar{g}_L^b\bar{g}_L^e\right.$$

$$(1 + c_\theta\beta)^2 + \bar{g}_R^b\bar{g}_R^e(1 + c_\theta\beta)^2 - \bar{g}_L^b\bar{g}_L^e\left(-1 + \beta^2\right)$$

$$\left. - \bar{g}_L^e\bar{g}_R^b\left(-1 + \beta^2\right) - \bar{g}_L^b\bar{g}_R^e\left(-1 + \beta^2\right) - \bar{g}_R^b\bar{g}_R^e\left(-1 + \beta^2\right)\right]$$

$$+ \frac{\bar{e}^2\beta s\chi(s)}{128\pi\Lambda^2}\left[\widetilde{C}_{lb}\bar{g}_L^b\bar{g}_L^e + \widetilde{C}_{lb}\bar{g}_L^e\bar{g}_R^b + \widetilde{C}_{eb}\bar{g}_L^b\bar{g}_R^e + \widetilde{C}_{qe}\bar{g}_L^b\bar{g}_R^e + \widetilde{C}_{eb}\bar{g}_R^b\bar{g}_R^e + \widetilde{C}_{qe}\bar{g}_R^b\bar{g}_R^e\right.$$

$$- 2c_\theta\widetilde{C}_{lb}\bar{g}_L^e\bar{g}_R^b\beta - 2c\widetilde{C}_{qe}\bar{g}_L^b\bar{g}_R^e\beta + 2c_\theta\widetilde{C}_{eb}\bar{g}_R^b\bar{g}_R^e\beta - \widetilde{C}_{lb}\bar{g}_L^b\bar{g}_L^e\beta^2 + c_\theta^2\widetilde{C}_{lb}\bar{g}_L^e\bar{g}_R^b\beta^2$$

$$- \widetilde{C}_{eb}\bar{g}_L^b\bar{g}_R^e\beta^2 + c_\theta^2\widetilde{C}_{qe}\bar{g}_L^b\bar{g}_R^e\beta^2 + c_\theta^2\widetilde{C}_{eb}\bar{g}_R^b\bar{g}_R^e\beta^2 - \widetilde{C}_{qe}\bar{g}_R^b\bar{g}_R^e\beta^2$$

$$\left. + \widetilde{C}_{lq}^{(1)}\bar{g}_L^e\left(\bar{g}_R^b - \bar{g}_R^b\beta^2 + \bar{g}_L^b(1 + c_\theta\beta)^2\right) + C_{lq}^{(3)}\bar{g}_L^e\left(\bar{g}_R^b - \bar{g}_R^b\beta^2 + \bar{g}_L^b(1 + c_\theta\beta)^2\right)\right]$$

$$+ \frac{\bar{e}^4\beta\chi(s)\bar{\chi}(s)}{128\pi}\left[-2\bar{g}_L^b\bar{g}_R^b\left(\bar{g}_L^{e,2} + \bar{g}_R^{e,2}\right)\left(-1 + \beta^2\right) + \bar{g}_L^{b,2}\left(\bar{g}_R^{e,2}(-1 + c_\theta\beta)^2\right.\right.$$

$$\left.\left. + (\bar{g}_L^e + c_\theta\bar{g}_L^e\beta)^2\right) + \bar{g}_R^{b,2}\left(\bar{g}_L^{e,2}(-1 + c_\theta\beta)^2 + (\bar{g}_R^e + c_\theta\bar{g}_R^e\beta)^2\right)\right],$$

$$(4.8.85)$$

where $\beta = \sqrt{1 - \frac{m_b^2}{s}}$, c_θ is the scattering angle we have encountered in 1.3 and

$$\chi(s) = \frac{s}{s - M_Z^2 + \omega(s)^2} \tag{4.8.86}$$

is the propagator at the Z peak obtained by using the Breit-Wigner formula, in which the Breit-Wigner distribution is denoted as $\omega(s)$. Note that in 4.8.85, terms proportional to $\frac{1}{\Lambda^4}$ are kept, which will be dropped in the following numerical calculations.

4.8.1 The Forward-Backward Asymmetry at Z peak

The complete forward-backward asymmetry at Z peak in dimension-six SMEFT includes the pure SM contribution and the EFT contribution. The SM result could be directly computed by evaluating 1.3.61. In order to compare the contribution from LO and NLO diagrams, we need to calculate the ratio of the NLO SM cross-section and the LO SM cross-section, it is

$$\frac{d\sigma^{(4,1)}}{d\sigma^{(4,0)}} = -0.0627827, \tag{4.8.87}$$

and the ratio of NLO SM forward-backward asymmetry and LO SM forward-backward asymmetry can be obtained similarly as

$$\frac{A_{fb}^{(4,1)}}{A_{fb}^{(4,0)}} = -0.297382. \tag{4.8.88}$$

It can be seen from 4.8.87 that the NLO corrections only alter the LO cross-section by a few percents, but alter the LO forward-backward asymmetry by dozens of percents. Therefore we can conclude that in the SM, the NLO order contribution plays a very important role in the determination of the forward-backward asymmetry.
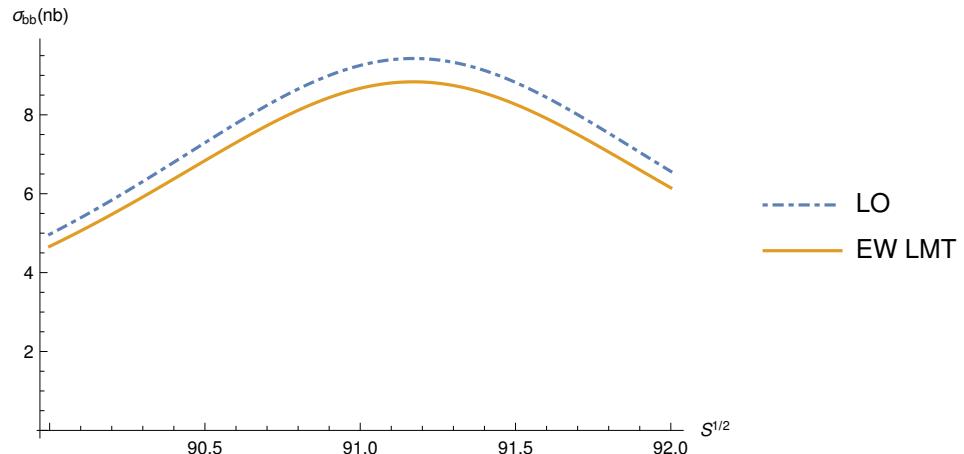
Figure 4.7   The cross section in the large-m_t limit at LO and EW NLO for the $e^+e^- \to b\bar{b}$ process
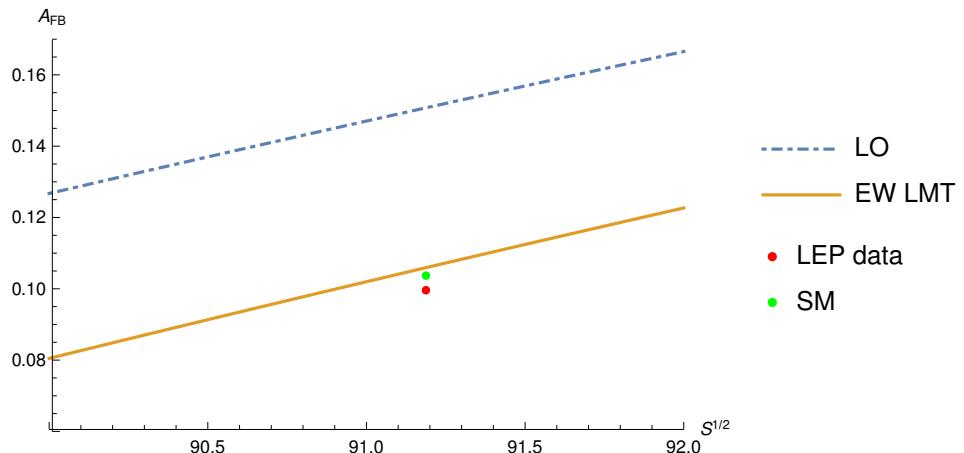
Figure 4.8   The forward-backward Asymmetry in the large-m_t limit in the SM for the $e^+e^- \to b\bar{b}$ process

From Fig. 4.8 we can see that the NLO SM value of the forward-backward asymmetry at Z peak in the large-m_t limit is very close to the SM prediction, which means the physical scale μ_t is a reasonable scale in predicting the forward-backward asymmetry at the electroweak scale. The shift of forward-backward asymmetry due to the SMEFT operators could be generally expressed as

$$\delta A_{fb}^{(6)} = \frac{\sigma_{Asym}^{(4)}}{\sigma_{Sym}^{(4)}} \left(-\frac{\sigma_{Sym}^{(6)}}{\sigma_{Sym}^{(4)}} \right) + \frac{\sigma_{Asym}^{(6)}}{\sigma_{Sym}^{(4)}}, \tag{4.8.89}$$

in which we have defined

$$\sigma_{Asym}^{(d)} = \int_0^1 \frac{d\sigma^{(d)}}{d\Omega}d\Omega - \int_{-1}^0 \frac{d\sigma^{(d)}}{d\Omega}, \quad \sigma_{Sym}^{(d)} = \int_0^1 \frac{d\sigma^{(d)}}{d\Omega}d\Omega + \int_{-1}^0 \frac{d\sigma^{(d)}}{d\Omega}, \quad (4.8.90)$$

where $d = 4, 6$.

Inserting the values of input parameters, we can obtain the numerical result of the LO EFT correction to the cross-section at Z peak in dimension-six SMEFT:

$$\begin{aligned}
\delta\sigma^{(6,0)} = \frac{1}{\Lambda^2} \Big(&2.17337 \cdot 10^6 \widetilde{C}_{Hb} + 1.00681 \cdot 10^6 \widetilde{C}_{He} - 1.25168 \cdot 10^6 \widetilde{C}_{Hl}^{(1)} \\
&-1.17991 \cdot 10^6 \widetilde{C}_{Hl}^{(3)} - 1.30399 \cdot 10^6 \widetilde{C}_{Hq}^{(1)} - 1.30399 \cdot 10^6 \widetilde{C}_{Hq}^{(3)} + 511.365 C_{lq}^{(1)} \\
&+511.365 \widetilde{C}_{lq}^{(3)} + 5.11365 \cdot 10^2 \widetilde{C}_{eb} + 5.11365 \cdot 10^2 \widetilde{C}_{lb} - 3.58804 \cdot 10^4 \widetilde{C}_{ll} \\
&+5.11365 \cdot 10^2 \widetilde{C}_{qe} + 1.89214 \cdot 10^6 \widetilde{C}_{HD} + 4.77194 \cdot 10^6 \widetilde{C}_{HWB} \Big).
\end{aligned} \quad (4.8.91)$$

And the NLO numerical EFT corrections are

$$\begin{aligned}
\delta\sigma^{(6,1)} = \frac{1}{\Lambda^2} \Big(&1.33936 \cdot 10^4 \widetilde{C}_{Hb} + 2.68963 \cdot 10^4 \widetilde{C}_{He} + 2.46264 \cdot 10^4 \widetilde{C}_{Hl}^{(1)} \\
&+1.68147 \cdot 10^5 \widetilde{C}_{Hl}^{(3)} - 1.88730 \cdot 10^4 \widetilde{C}_{Hq}^{(1)} - 6.04193 \cdot 10^4 \widetilde{C}_{Hq}^{(3)} + 7.98682 \cdot 10^2 \widetilde{C}_{lq}^{(1)} \\
&+3.39398 \cdot 10^6 \widetilde{C}_{lq}^{(3)} + 2.38262 \widetilde{C}_{eb} + 2.38262 \widetilde{C}_{lb} - 7.17605 \cdot 10^4 \widetilde{C}_{ll} \\
&+79.8682 \widetilde{C}_{qe} - 2.6339 \cdot 10^4 \widetilde{C}_{HD} + 1.87414 \cdot 10^2 \widetilde{C}_{Ht} + 1.04460 \cdot 10^5 \widetilde{C}_{HWB} \\
&1.60261 \cdot 10^4 \widetilde{C}_{qq}^{(1)} - 1.74154 \cdot 10^4 \widetilde{C}_{qq}^{(3)} + 4.23562 \cdot 10^2 \widetilde{C}_{dd}^{(1)} + 1.92525 \cdot 10^2 \widetilde{C}_{ud}^{(1)} \\
&-1.10309 \cdot 10^3 \widetilde{C}_{qu}^{(1)} - 2.17381 \cdot 10^3 \widetilde{C}_{qd}^{(1)} \Big).
\end{aligned}$$

$$(4.8.92)$$

Through 4.8.91 and 4.8.92, we find that as in the SM case, roughly speaking, the cross-section due to the NLO calculation changes the tree-level EFT correction only by a few percents except for the $C_{lq}^{(3)}$ term, which receive a shift due to $\Delta R^{(6,1)}$, which is a reasonable result that could be directly seen from 4.1.4.

According to the order in perturbative theory and power order in EFT, the complete forward-backward asymmetry in the dimension-six SMEFT can be divided into four parts:

$$\delta A_{fb}^{SMEFT} = A_{fb}^{(4,0)} + A_{fb}^{(4,1)} + \delta A_{fb}^{(6,0)} + \delta A_{fb}^{(6,1)}, \quad (4.8.93)$$

in which the tree-level EFT numerical correction is

$$
\begin{aligned}
\delta A_{fb}^{(6,0)} = \frac{1}{\Lambda^2} \Big(&-6.72941 \cdot 10^3 \widetilde{C}_{Hb} - 9.22652 \cdot 10^4 \widetilde{C}_{He} - 8.46914 \cdot 10^4 \widetilde{C}_{Hl}^{(1)} \\
&-9.62913 \cdot 10^4 \widetilde{C}_{Hl}^{(3)} - 7.99348 \cdot 10^3 \widetilde{C}_{Hq}^{(1)} - 7.99348 \cdot 10^3 \widetilde{C}_{Hq}^{(3)} + 36.6943 \widetilde{C}_{lq}^{(1)} \\
&+1.72582 \cdot 10^4 \widetilde{C}_{lq}^{(3)} + 36.6943 \widetilde{C}_{eb} - 48.9561 \widetilde{C}_{lb} + 5.79993 \cdot 10^3 \widetilde{C}_{ll} \\
&-48.9561 \widetilde{C}_{qe} + 1.40548 \cdot 10^5 \widetilde{C}_{HD} + 1.73060 \cdot 10^5 \widetilde{C}_{HWB} \Big) .
\end{aligned}
\tag{4.8.94}
$$

Using the result in 4.8.81, we find the total EFT numerical correction up to NLO for A_{fb} is

$$
\begin{aligned}
\delta A_{fb}^{(6)} &= \delta A_{fb}^{(6,0)} + \delta A_{fb}^{(6,1)} \\
&= \frac{1}{\Lambda^2} \Big(-6.70038 \cdot 10^3 \widetilde{C}_{Hb} - 9.16456 \cdot 10^4 \widetilde{C}_{He} - 7.99811 \cdot 10^4 \widetilde{C}_{Hl}^{(1)} \\
&\quad -6.75213 \cdot 10^4 \widetilde{C}_{Hl}^{(3)} - 5.37357 \cdot 10^3 \widetilde{C}_{Hq}^{(1)} - 5.67248 \cdot 10^3 \widetilde{C}_{Hq}^{(3)} + 37.1437 \widetilde{C}_{lq}^{(1)} \\
&\quad +1.72587 \cdot 10^4 \widetilde{C}_{lq}^{(3)} + 36.6659 \widetilde{C}_{eb} + 1.40547 \cdot 10^5 \widetilde{C}_{HD} + 1.1627 \widetilde{C}_{Ht} \\
&\quad +1.60080 \cdot 10^5 \widetilde{C}_{HWB} - 48.9847 \widetilde{C}_{lb} - 6.22994 \cdot 10^3 \widetilde{C}_{ll} - 49.6197 \widetilde{C}_{qe} \\
&\quad 99.4018 \widetilde{C}_{qq}^{(1)} - 1.08018 \cdot 10^2 \widetilde{C}_{qq}^{(3)} - 12.7867 \widetilde{C}_{dd}^{(1)} - 5.81193 \widetilde{C}_{ud}^{(1)} \\
&\quad -6.84184 \widetilde{C}_{qu}^{(1)} + 29.4381 \widetilde{C}_{qd}^{(1)} \Big) .
\end{aligned}
\tag{4.8.95}
$$

To show the impacts of Wilson coefficients on the forward-backward asymmetry in the SMEFT, we perform a chi-squared analysis. According to our numerical results, the contributions from different Wilson coefficients have huge gaps from each other, so a global fit will be not appropriate. Alternatively, we analyse each Wilson coefficient respectively. According to [13], the SM fit value of A_{fb} is 0.1038, and the measurement value of A_{fb} is 0.0992 ± 0.0016. Accordingly, the chi-squared of $A_{fb}^{(6)}$ can be defined as

$$
A_{fb}^{(6)} = \delta A_{fb}^{(6)} + 0.1038,
$$

$$
\Delta X_{A_{fb}^{(6)}}^2 = \frac{\left(A_{fb}^{(6)} - 0.0992 \right)^2}{(0.0016)^2} .
\tag{4.8.96}
$$

All the plots according to the chi-squared analysis are given as what follows.

(a) $\Lambda = 500$ GeV

(b) $\Lambda = 500 GeV$

(c) $\Lambda = 500$ GeV

(d) $\Lambda = 500$ GeV

(e) $\Lambda = 500$ GeV

(f) $\Lambda = 500$ GeV

(g) $\Lambda = 500$ GeV

(h) $\Lambda = 500$ GeV
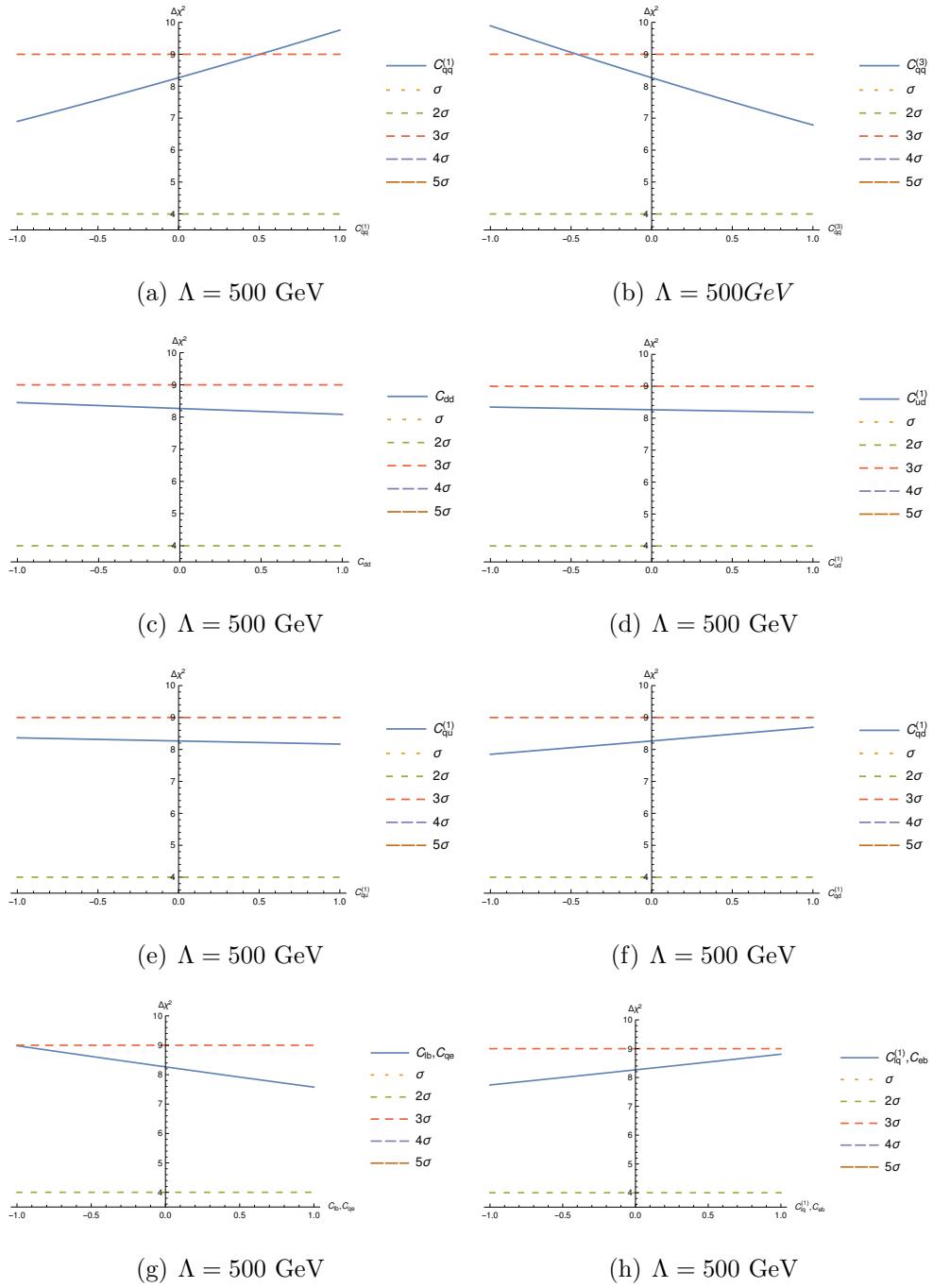
Figure 4.9 The chi-squared of A_{fb} for four-fermion Wilson coefficients

(a) $\Lambda = 500$ GeV

(b) $\Lambda = 1.0$ TeV

(c) $\Lambda = 1.5$ TeV

(d) $\Lambda = 2.0$ TeV
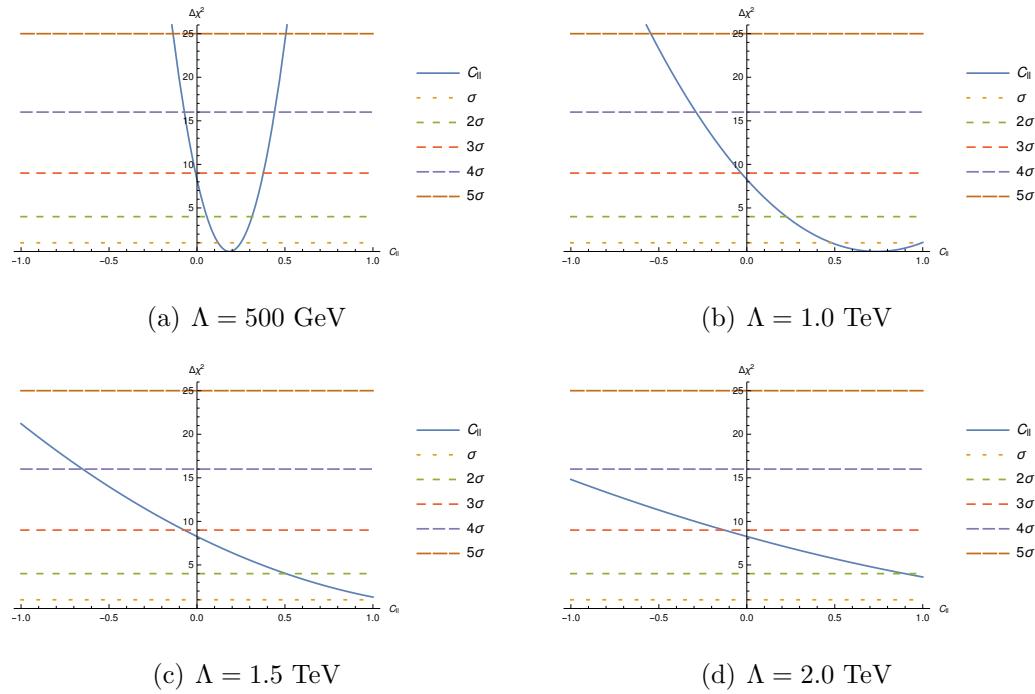
Figure 4.10   The chi-squared of A_{fb} for C_{ll}

(a) $\Lambda = 500$ GeV

(b) $\Lambda = 1.0$ TeV

(c) $\Lambda = 1.5$ TeV

(d) $\Lambda = 2.0$ TeV
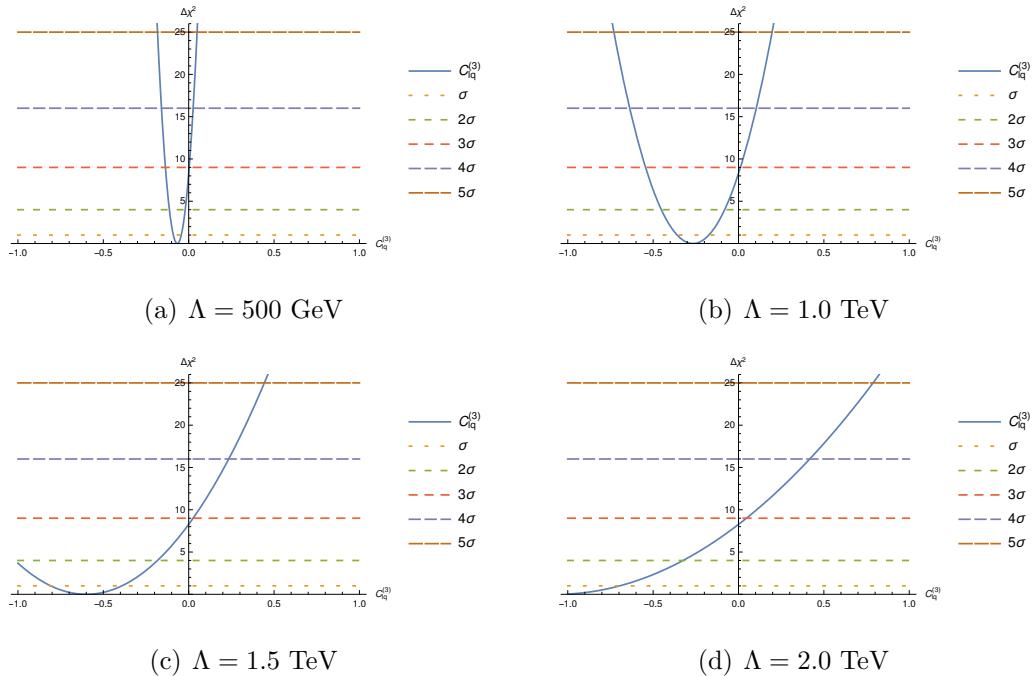
Figure 4.11 The chi-squared of A_{fb} for $C_{lq}^{(3)}$

(a) $\Lambda = 500$ GeV

(b) $\Lambda = 1.0$ TeV

(c) $\Lambda = 1.5$ TeV

(d) $\Lambda = 2.0$ TeV
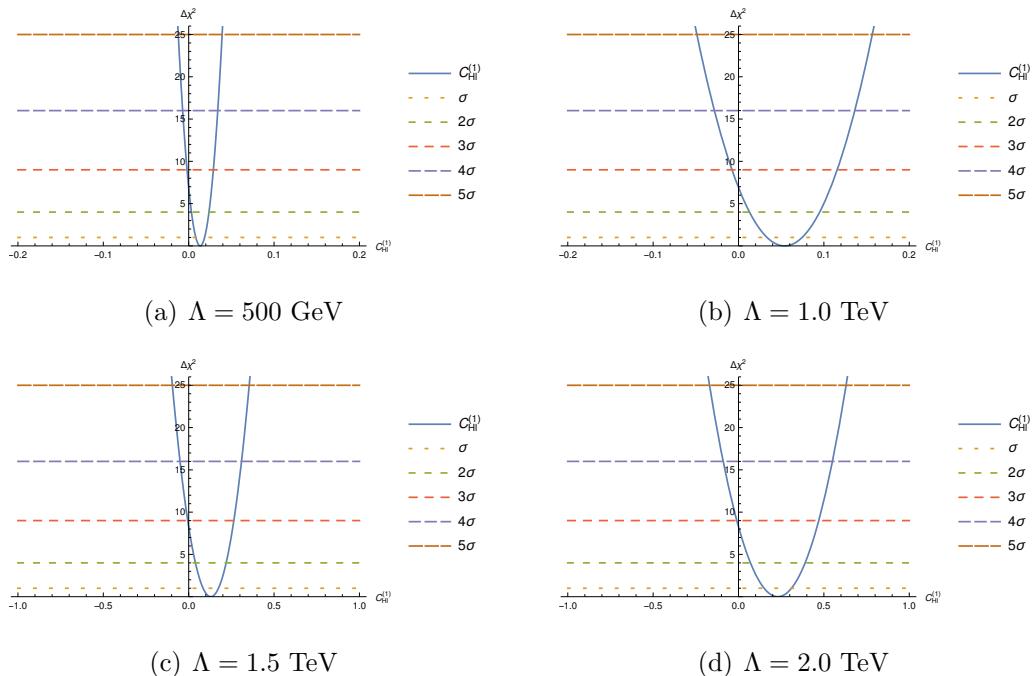
Figure 4.12 The chi-squared of A_{fb} for $C_{Hl}^{(1)}$

(a) $\Lambda = 500$ GeV

(b) $\Lambda = 1.0$ TeV

(c) $\Lambda = 1.5$ TeV

(d) $\Lambda = 2.0$ TeV
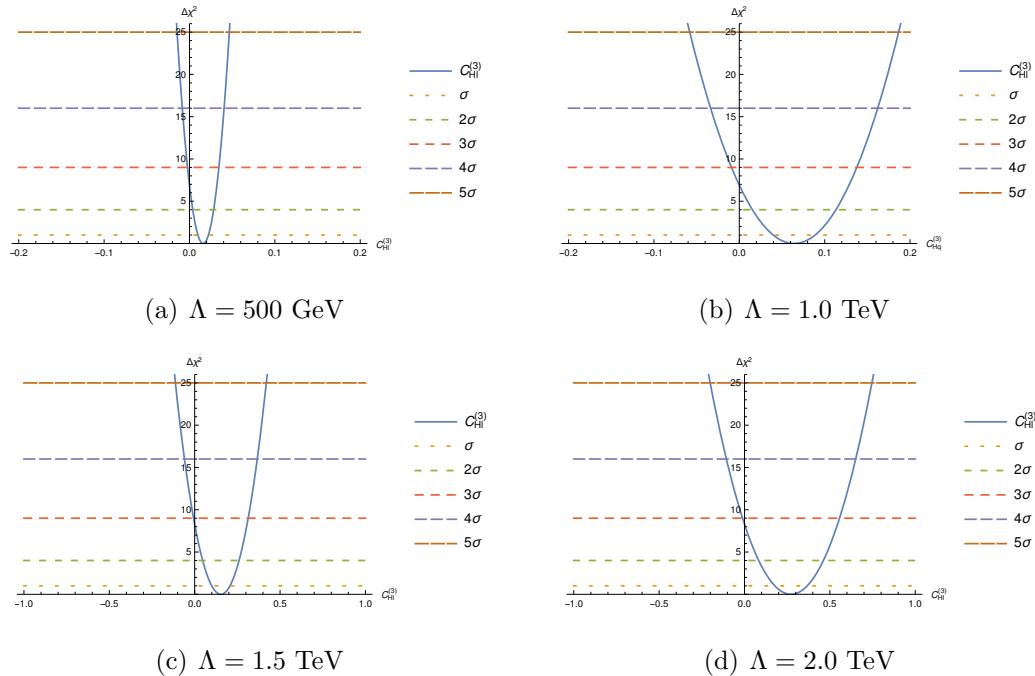
Figure 4.13 The chi-squared of A_{fb} for $C_{Hl}^{(3)}$

(a) $\Lambda = 500$ GeV

(b) $\Lambda = 1.0$ TeV

(c) $\Lambda = 1.5$ TeV

(d) $\Lambda = 2.0$ TeV
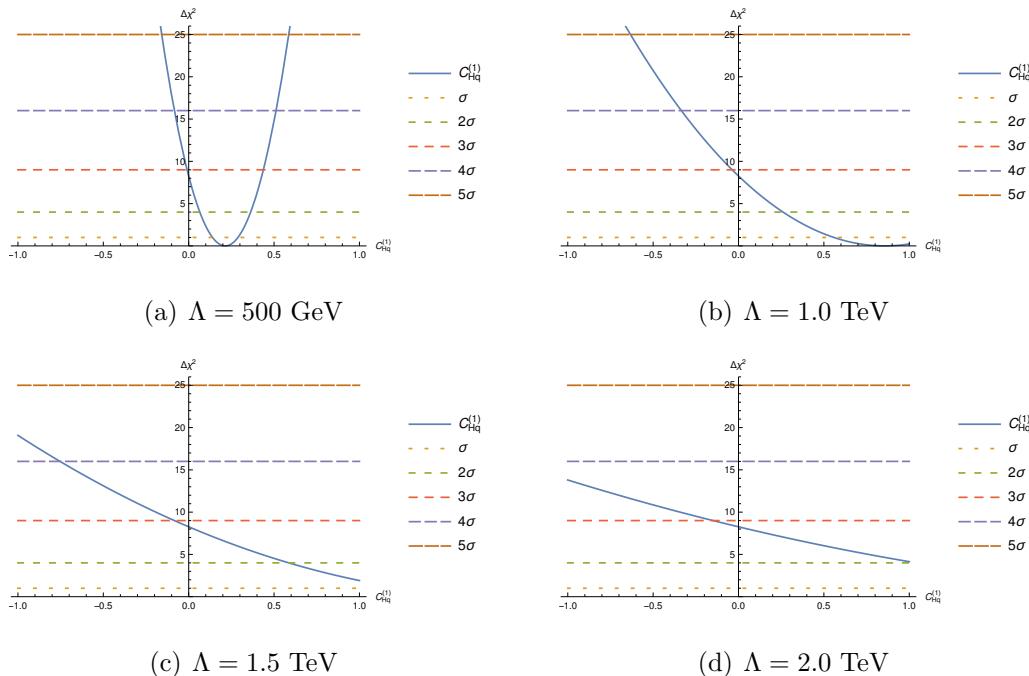
Figure 4.14 The chi-squared of A_{fb} for $C_{Hq}^{(1)}$

(a) $\Lambda = 500$ GeV

(b) $\Lambda = 1.0$ TeV

(c) $\Lambda = 1.5$ TeV

(d) $\Lambda = 2.0$ TeV
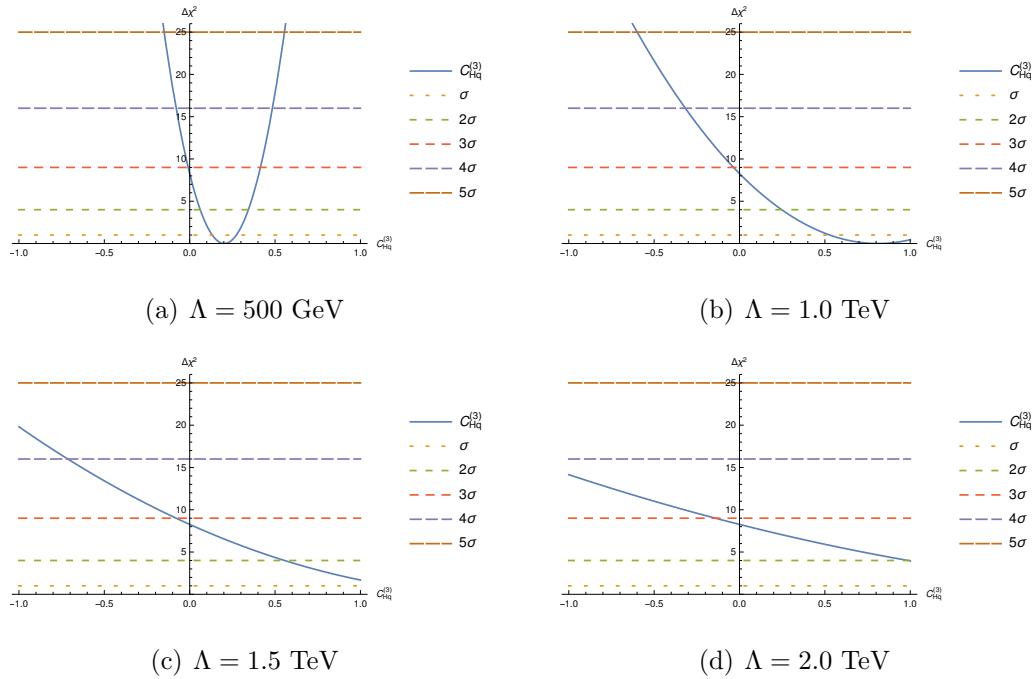
Figure 4.15 The chi-squared of A_{fb} for $C_{Hq}^{(3)}$

(a) $\Lambda = 500$ GeV

(b) $\Lambda = 1.0$ TeV

(c) $\Lambda = 1.5$ TeV

(d) $\Lambda = 2.0$ TeV
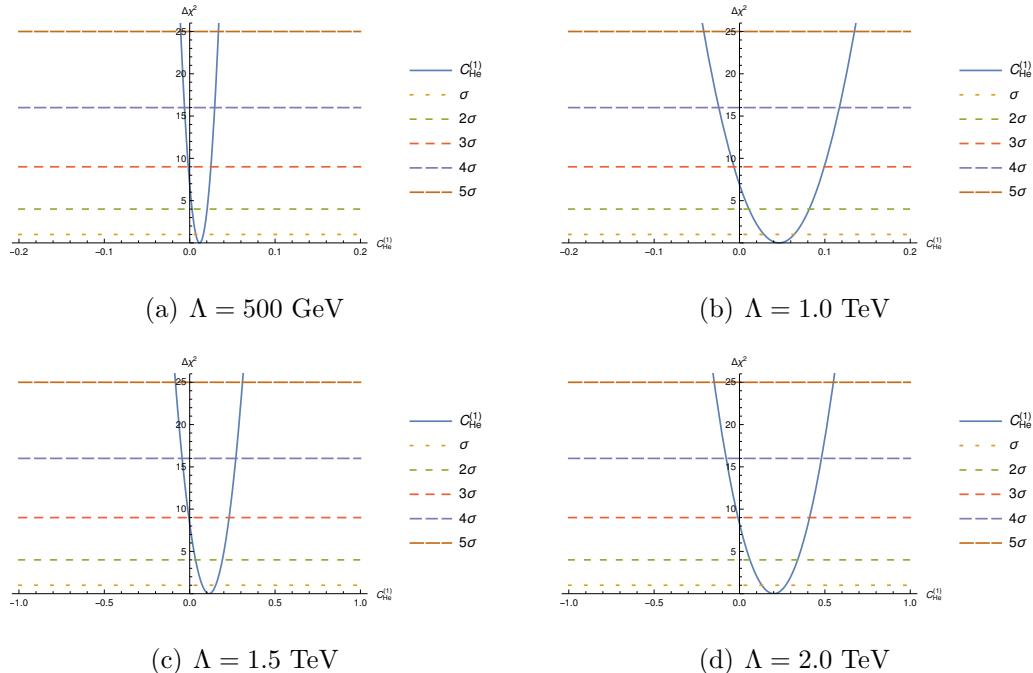
Figure 4.16 The chi-squared of A_{fb} for $C_{He}^{(1)}$

(a) $\Lambda = 500$ GeV

(b) $\Lambda = 1.0$ TeV

(c) $\Lambda = 1.5$ TeV

(d) $\Lambda = 2.0$ TeV
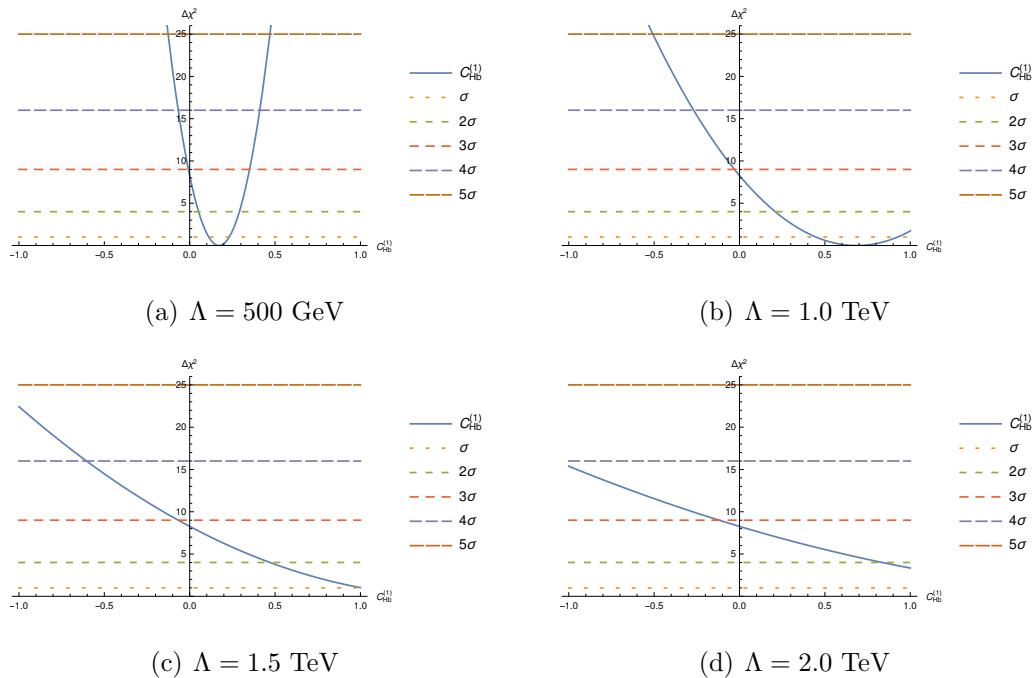
Figure 4.17 The chi-squared of A_{fb} for $C_{Hb}^{(1)}$

(a) $\Lambda = 500$ GeV

(b) $\Lambda = 1.0$ TeV

(c) $\Lambda = 1.5$ TeV

(d) $\Lambda = 2.0$ TeV
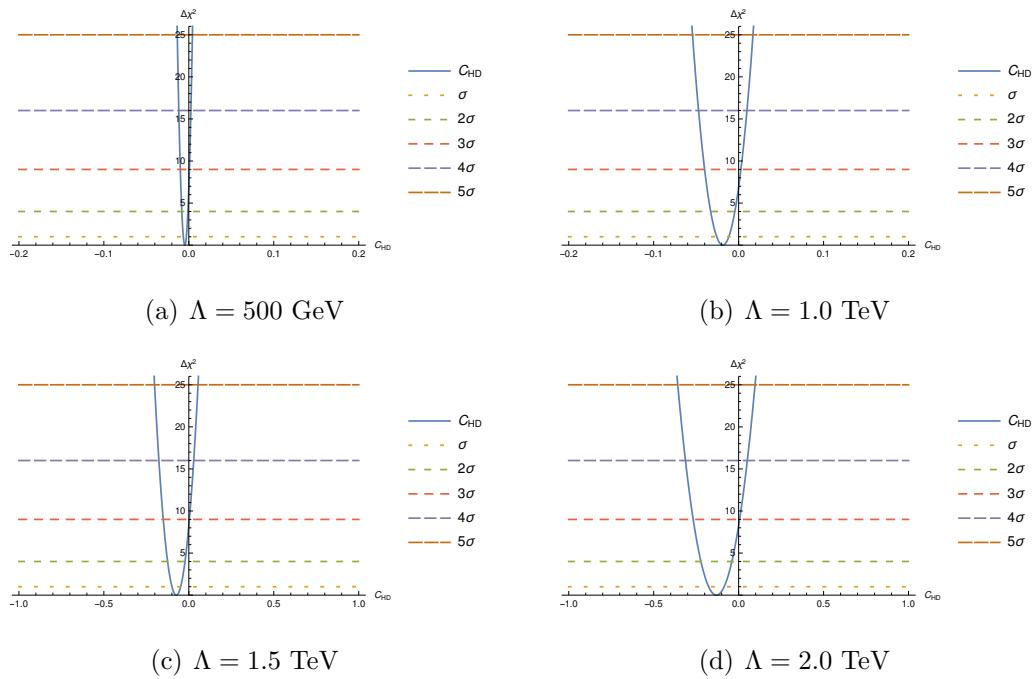
Figure 4.18 The chi-squared of A_{fb} for C_{HD}

(a) $\Lambda = 500$ GeV

(b) $\Lambda = 1.0$ TeV

(c) $\Lambda = 1.5$ TeV

(d) $\Lambda = 2.0$ TeV
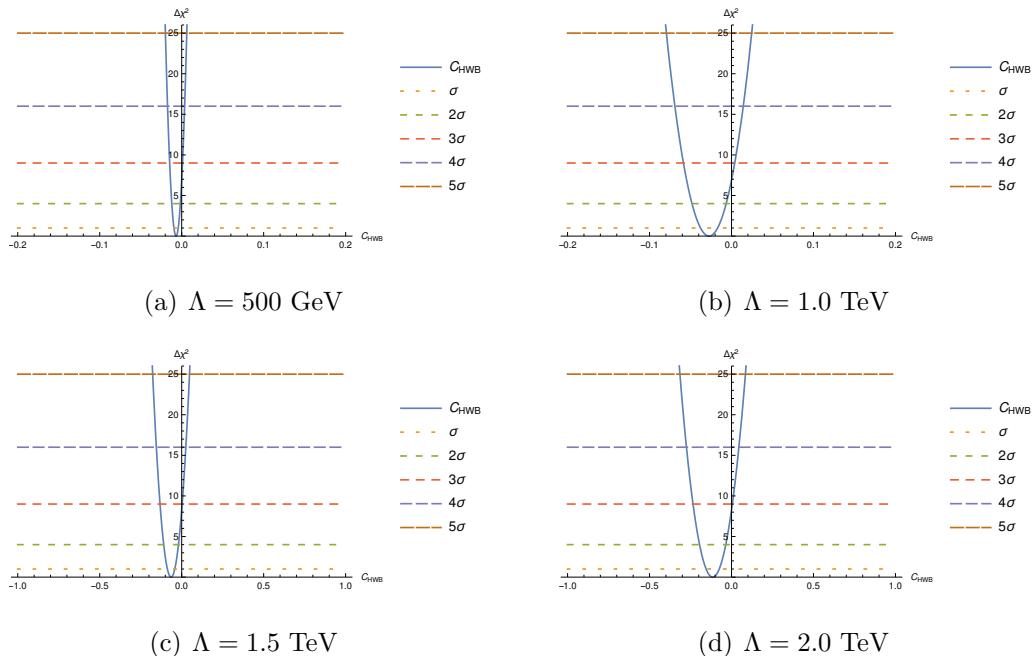
Figure 4.19 The chi-squared of A_{fb} for C_{HWB}

In these plots we choose to vary each Wilson Coefficient from $-1 \to 1$ for four fixed values of Λ, in which see how each Wilson Coefficient affects the A_{fb}. Generally speaking, the EFT corrections due the Class 8 operators are much smaller compared to the Class 7 and Class 4 contributions, however, C_{ll} and $C_{lq}^{(3)}$ are exceptions, since their influences on A_{fb} receive extra tone-up due to their influences on the input parameter G_F. Therefore in the plots of Fig. 4.9 for the four-fermion Operators except C_{ll} and $C_{lq}^{(3)}$, only the $\Lambda = 500$ GeV case is given, since in the other three cases the influences of these Class 8 Wilson coefficients are very small. Moreover, the influence of the Class 7 Wilson coefficient C_{Ht} which only contributes at the NLO is too small so that it is even not obvious in the $\Lambda = 500$ GeV case, therefore the plots of C_{Ht} are absent. For all the other Wilson coefficients, the corrections could be clearly seen even in the $\Lambda = 2.0$ TeV case.

4.8.2 The EFT Effects on The $e^+e^- \to b\bar{b}$ Cross-Section

In this section, we focus on the EFT corrections of the cross-section of the $e^+e^- \to b\bar{b}$ process for different energy scales up to one-loop. As in 4.8.1, we perform a full analysis for each Wilson Coefficient respectively. However, there are several

hundreds of plots all together, so we decide to only choose several interesting typical plots in the case $\Lambda = 1.0$ TeV. Generally, the Wilson Coefficients involved can be divided into three categories. The first category includes the Wilson Coefficients that contribute both at LO and NLO. Accordingly, C_{Hb}, C_{He}, $C_{Hl}^{(1)}$, $C_{Hl}^{(3)}$, $C_{Hq}^{(1)}$ and $C_{Hq}^{(3)}$ belong to this category. C_{Ht} that only takes part in the one-loop contribution and C_{ll} can also be grouped into this category, the reason of which will be explained later soon. The second category includes the four-fermion Wilson coefficients which only contribute at the tree-level, i.e. C_{lb}, C_{eb}, C_{qe}, $C_{lq}^{(1)}$ and $C_{lq}^{(3)}$. And the four-fermion Wilson coefficients which only contribute at one-loop belongs to the third category, which include $C_{qq}^{(1)}$, $C_{qq}^{(3)}$, C_{dd}, $C_{ud}^{(1)}$, $C_{qu}^{(1)}$ and $C_{qd}^{(1)}$. We choose only one typical Wilson Coefficient in each category, they are $C_{qq}^{(1)}$, C_{eb} and $C_{Hq}^{(1)}$ respectively. In the following plots, four typical values of $\sqrt{s}$ are selected for each Wilson Coefficient, they are 500 GeV, 1.0 TeV, 1.5 TeV and 2.0 TeV.

(a) $\sqrt{s} = 500$ GeV

(b) $\sqrt{s} = 1.0$ TeV

(c) $\sqrt{s} = 1.5$ TeV

(d) $\sqrt{s} = 2.0$ TeV
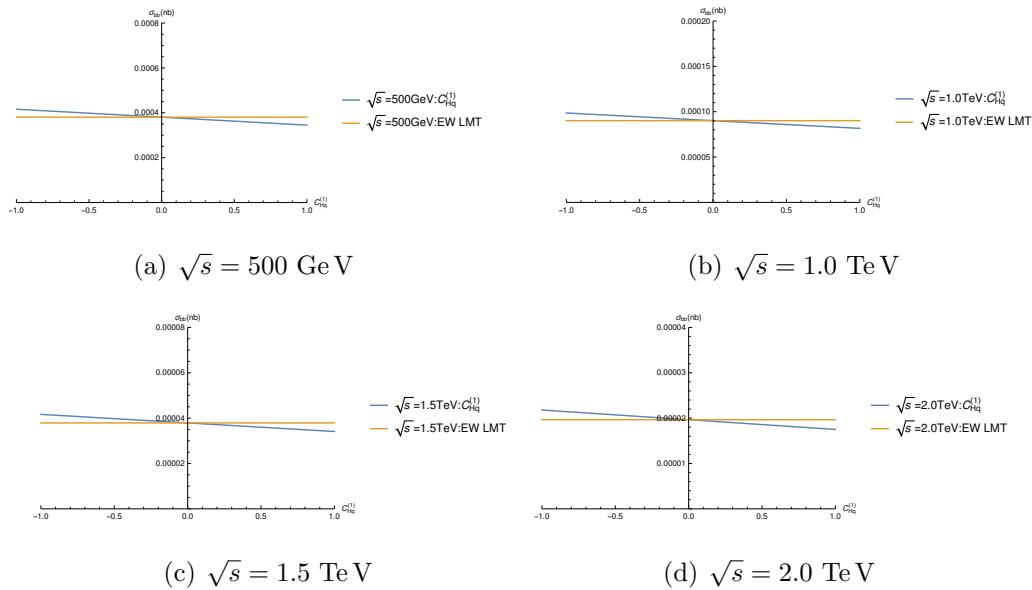
Figure 4.20 The cross-sections for $C_{Hq}^{(1)}$ for four different $\sqrt{s}$ when $\Lambda = 1.0$ TeV for the $e^+ e^- \to b\bar{b}$ process

(a) $\sqrt{s} = 500$ GeV

(b) $\sqrt{s} = 1.0$ TeV

(c) $\sqrt{s} = 1.5$ TeV

(d) $\sqrt{s} = 2.0$ TeV
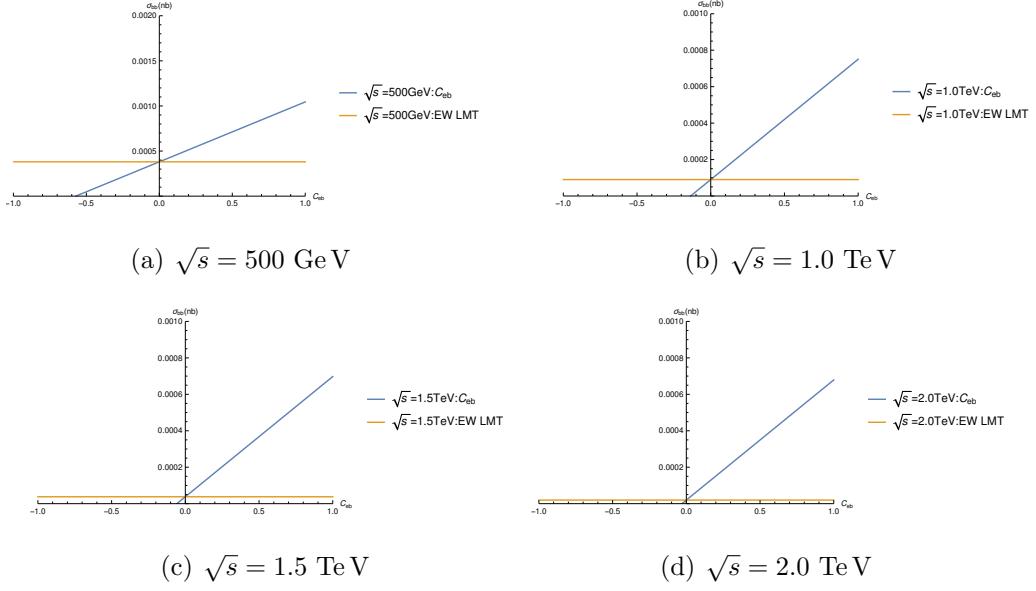
Figure 4.21   The cross-sections for C_{eb} for four different $\sqrt{s}$ when $\Lambda = 1.0$ TeV for the $e^+e^- \rightarrow b\bar{b}$ process

(a) $\sqrt{s} = 500$ GeV

(b) $\sqrt{s} = 1.0$ TeV

(c) $\sqrt{s} = 1.5$ TeV

(d) $\sqrt{s} = 2.0$ TeV
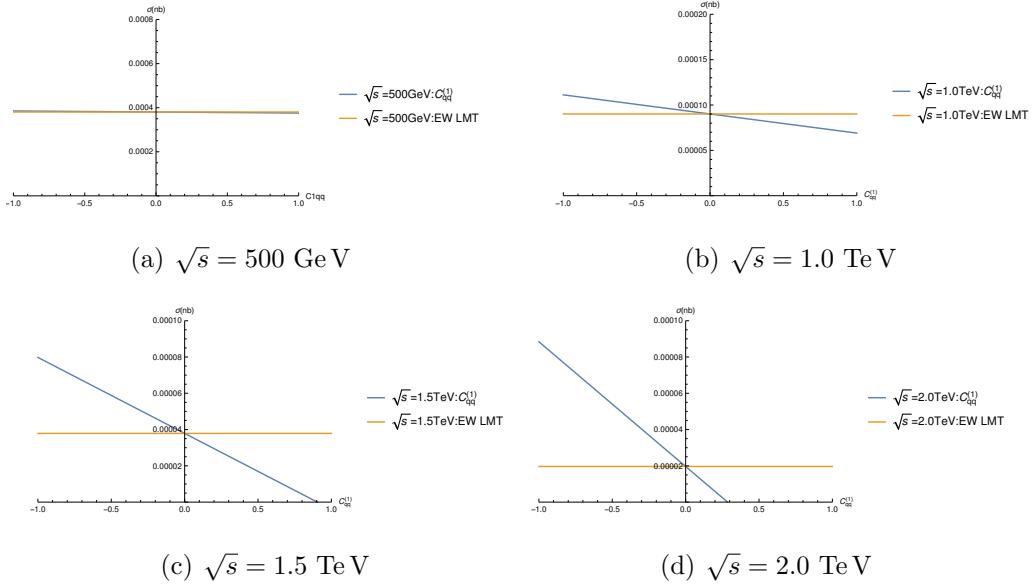
**Figure 4.22**   The cross-sections for $C_{qq}^{(1)}$ for four different $\sqrt{s}$ when $\Lambda = 1.0$ TeV for the $e^+e^- \rightarrow b\bar{b}$ process

In Fig. 4.20, we can see that for $C_{Hq}^{(1)}$ the ratio of EFT shift and the SM prediction is roughly kept unchanged for different $\sqrt{s}$. The other Wilson Coefficients in this category generate similar plots. In these plots, the EFT corrections are always

smaller than the SM values. Note that the topologies of relevant diagrams are the exactly the same as some of the SM diagrams both at LO and one-loop NLO. As a result, with the increment of $\sqrt{s}$, the decrease of the cross-section due to these Wilson Coefficients will be similar to the SM case as well. Recall that the one-loop diagram of C_{Ht} also has the same topology as the one of the SM one-loop diagram, and the $\delta A_{G_F}^{(6,0)}$ and $\delta A_{G_F}^{(6,1)}$ are directly built from the SM amplitudes, both C_{Ht} and C_{ll} can be grouped into this category. Moreover, the cross-section for $C_{Hq}^{(1)}$ also receives a shift from $\delta A_{G_F}^{(6,1)}$, but that does not change the basic feature mentioned above.

In Fig. 4.21, we find that as the energy increases, the ratio of EFT shift and the SM prediction gets larger too. This is not hard to understand since the scattering amplitudes due to these four-fermion Wilson Coefficients are not suppressed by $1/s$ or $1/(s - M_Z^2)$. In this category, the cross-section for $C_{lq}^{(1)}$ also receives a shift due to $\delta A_{G_F}^{(6,1)}$ which behaves similarly like the tree level SM cross-section. However, when $\sqrt{s}$ is large enough, the contribution from the tree level four-fermion interaction will be dominating since it is not suppressed by $1/s$ or $1/(s - M_Z^2)$.

In Fig. 4.22, one can observe similar curves as in Fig. 4.21, though the magnitude of the ratio is not as large as the former one. Generally speaking, the NLO cross-section corrections due to these four-fermion Wilson Coefficients in this category are much smaller than the corrections due to those four-fermion Wilson Coefficients that contribute at tree-level. All the diagrams due to these Wilson Coefficients share the same topology that does not appears in the SM case. As a result, the plots are similar for different Wilson Coefficients in this category. It is worth to emphasize that the correction due to $C_{qq}^{(3)}$ will change the sign when $\sqrt{s}$ increases to a certain value. This behaviour originates from the minus sigh appearing in the expansion of the operator $Q_{qq}^{(3)}$ which can be found in Table 4.1. The correction due to $C_{qq}^{(3)}$ includes contributions from both structure (1) and structure (2). Actually, we find that the amplitudes due to these two different structures behave differently when $\sqrt{s}$ changes.

Chapter 5

Conclusions

In this thesis, we mainly investigate the applications of two kinds of Effective Field Theories, namely a Simplified Model for $t\bar{t}X$ interactions and the dimension-six Standard Model Effective Field theory. To start with, a brief review of the Standard Model is given in Chapter 1, including an introduction to two processes in SM which are inextricably linked with the research in Chapter 4. In chapter 2, a general introduction to effective field theories is given followed by the detailed introduction of these two effective field theories mentioned above.

In Chapter 3, a simplified model is adopted to investigate the searches for $t\bar{t}X$ production at the LHC are sensitive to a new resonance X coupled to the third generation quarks. If X is discovered, a further measurement of its parity and spin will be essential for revealing the underlying new physics scenario. In this work we assumed a class of simplified models to describe the couplings between X and the third generation quarks, with X being a scalar, pseudoscalar, vector, or axial vector. Then we sought kinematic variables that are helpful for determining parity and spin quantum numbers and investigated the expected sensitivity through detailed simulations. We have proposed four parton-level variables which exhibit different shapes for different models. Two of them are defined in the $t\bar{t}X$ CM frame. Therefore, using them requires a nearly full reconstruction of two tops and the resonance X, which can be achieved in the semi-leptonic channel. We have carried out the reconstruction procedure based on simulations in this channel and estimated the LHC sensitivity for discovery. We constructed the detector-level counterparts of the parton-level

119

variables and observed that their distributions preserve the important features for discrimination between the different simplified models. A CL_s hypothesis test has been performed to evaluate the sensitivity of discrimination separately based on each variables. We found that the scalar is the easiest one to be distinguished from others while the hardest case is to discriminate between the pseudoscalar and the axial vector. Further improvements to our analysis could be made by utilising jet substructure techniques to suppress the background more, and to allow a more accurate attribution of the b-jets used in the top and X reconstruction. It would also be interesting to perform a combined analysis of leptonic and semi-leptonic final states to see the ultimate sensitivity of the LHC. We leave this for future work.

In chapter 4, we mainly investigate the $e^+e^- \to b\bar{b}$ process up to NLO in the framework dimension-six SMEFT. Numerical analysis is provided for the forward-backward asymmetry and the cross-section, we explored the $Z \to b\bar{b}$ process as well without the numerical results. Firstly, we calculate the LO amplitudes for the two processes. In the LO calculation, we expressed the effective left-handed and right-handed Z boson couplings to fermions in terms of the bare quantities in the SM. In order to compute the EFT corrections up to NLO, we choose to perform the wavefunction, mass, and electric charge renormalisation in the on-shell scheme, while the operator renormalisation was done in the MS scheme. Following the renormalisation procedure in the SM, we found the way to build the counterterms for the two processes in the SMEFT. The one-loop renormalised matrix elements for Class 8, Class 7, and Class 4 were then obtained, in which step, we have shown how the cancellations of UV divergences occur. The cancellation of UV divergences was illustrated in a detailed way for the $Z \to b\bar{b}$ process, which could be extended to the $e^+e^- \to b\bar{b}$ process straightforwardly. In the NLO Class 8 case, only the operators altering the Z boson couplings to fermions were calculated up to NLO, since their contributions will dominate on the Z resonance. Finally, the numerical results of the forward-backward asymmetry and the cross-section of the $e^+e^- \to b\bar{b}$ process were obtained. We computed the forward-backward asymmetry at Z peak in the SMEFT for Wilson coefficients defined at the scale $\mu = m_t$, which is a reasonable choice for observables measured at the electroweak scale. Then the cross-

sections for different Wilson Coefficients defined at the same scale were calculated, whose numerical results can be translated by RG equations into their high-energy forms at $\mu = \Lambda_{NP}$, where Λ_{NP} is the scale for the new physics. According to the numerical results, the corrections to cross-section due to the NLO contribution are not obvious on the Z resonance, which could be neglected compared to the LO's contribution within the current experimental precision. However, the NLO corrections to the forward-backward asymmetry in the SMEFT are important and can not be neglected, especially for the Class 7 operators. The forward- backward asymmetry is mostly sensitive to the Class 7 operators, C_{ll}, $C_{lq}^{(3)}$, C_{HWB} and C_{HD}. And the cross-section is mostly sensitive to those four-fermion Wilson coefficients which contribute at tree-level. Extending SMEFT calculations to NLO will improve the accuracy of the theoretical predictions, which will become increasingly important in the future.

Appendix A

Basic and Auxiliary Results

A.1 Independent Dimension-six Operators in the Warsaw Basis

The 59 baryon number conserving operators in the Warsaw Basis [36] of dimension-six operators are listed in this section.

Class 1: X^3	
Q_G	$f^{ABC}G_\mu^{A\nu}G_\nu^{B\rho}G_\rho^{C\mu}$
$Q_{\widetilde{G}}$	$f^{ABC}\widetilde{G}_\mu^{A\nu}G_\nu^{B\rho}G_\rho^{C\mu}$
Q_W	$\epsilon^{IKJ}W_\mu^{I\nu}W_\nu^{K\rho}W_\rho^{J\mu}$
$Q_{\widetilde{W}}$	$\epsilon^{ABC}\widetilde{W}_\mu^{I\nu}W_\nu^{K\rho}W_\rho^{J\mu}$

Class 2: H^6	
Q_H	$(H^\dagger H)^3$

Class 3: H^4D^2	
$Q_{H\Box}$	$(H^\dagger H)\Box(H^\dagger H)$
Q_{HD}	$(H^\dagger D^\mu H)(H^\dagger D_\mu H)$

Class 4: X^2H^2	
Q_{HG}	$H^\dagger H G_{\mu\nu}^A G^{A\mu\nu}$
$Q_{H\widetilde{G}}$	$H^\dagger H \widetilde{G}_{\mu\nu}^A G^{A\mu\nu}$
Q_{HW}	$H^\dagger H W_{\mu\nu}^I W^{I\mu\nu}$
$Q_{H\widetilde{W}}$	$H^\dagger H \widetilde{W}_{\mu\nu}^I W^{I\mu\nu}$
Q_{HB}	$H^\dagger H W_{\mu\nu} W^{\mu\nu}$
$Q_{H\widetilde{B}}$	$H^\dagger H \widetilde{B}_{\mu\nu} B^{\mu\nu}$
Q_{HWB}	$H^\dagger \tau^I H W_{\mu\nu}^I B^{\mu\nu}$
$Q_{H\widetilde{W}B}$	$H^\dagger \tau^I H \widetilde{W}_{\mu\nu}^I B^{\mu\nu}$

Class 5: $\phi^2H^3 + h.c.$	
Q_{eH}	$(H^\dagger H)(\bar{l}_p e_r H)$
Q_{uH}	$(H^\dagger H)(\bar{q}_p u_r \widetilde{H})$
Q_{eH}	$(H^\dagger H)(\bar{q}_p d_r H)$

Class 6: $\phi^2XH + h.c.$	
Q_{eW}	$(\bar{l}_p \sigma^{\mu\nu} e_r)\tau^I H W_{\mu\nu}^I$
Q_{eB}	$(\bar{l}_p \sigma^{\mu\nu} e_r) H B_{\mu\nu}$
Q_{uG}	$(\bar{q}_p \sigma^{\mu\nu} T^A u_r)\widetilde{H} G_{\mu\nu}^A$
Q_{uW}	$(\bar{q}_p \sigma^{\mu\nu} u_r)\tau^I \widetilde{H} W_{\mu\nu}^I$
Q_{uB}	$(\bar{q}_p \sigma^{\mu\nu} u_r)\widetilde{H} B_{\mu\nu}$
Q_{dG}	$(\bar{q}_p \sigma^{\mu\nu} T^A d_r) H G_{\mu\nu}^A$
Q_{dW}	$(\bar{q}_p \sigma^{\mu\nu} d_r)\tau^I H W_{\mu\nu}^I$
Q_{dB}	$(\bar{q}_p \sigma^{\mu\nu} d_r) H B_{\mu\nu}$

Class 7: ϕ^2H^2D	
$Q_{Hl}^{(1)}$	$(H^\dagger i\overleftrightarrow{D}_\mu H)(\bar{l}_p \gamma^\mu l_r)$
$Q_{Hl}^{(3)}$	$(H^\dagger i\overleftrightarrow{D}_\mu H)(\bar{l}_p \tau^I \gamma^\mu l_r)$
Q_{He}	$(H^\dagger i\overleftrightarrow{D}_\mu H)(\bar{e}_p \gamma^\mu e_r)$
$Q_{Hq}^{(1)}$	$(H^\dagger i\overleftrightarrow{D}_\mu H)(\bar{q}_p \gamma^\mu q_r)$
$Q_{Hq}^{(3)}$	$(H^\dagger i\overleftrightarrow{D}_\mu H)(\bar{q}_p \tau^I \gamma^\mu q_r)$
Q_{Hu}	$(H^\dagger i\overleftrightarrow{D}_\mu H)(\bar{u}_p \gamma^\mu u_r)$
Q_{Hd}	$(H^\dagger i\overleftrightarrow{D}_\mu H)(\bar{d}_p \gamma^\mu d_r)$
Q_{Hud}	$i(\widetilde{H}^\dagger \overleftrightarrow{D}_\mu H)(\bar{u}_p \gamma^\mu d_r)$

Class 8: $(\bar{L}L)(\bar{L}L)$	
Q_{ll}	$(\bar{l}_p\gamma_\mu l_r)(\bar{l}_s\gamma^\mu l_t)$
$Q_{qq}^{(1)}$	$(\bar{q}_p\gamma_\mu q_r)(\bar{q}_s\gamma^\mu q_t)$
$Q_{qq}^{(3)}$	$(\bar{q}_p\gamma_\mu \tau^I q_r)(\bar{q}_s\gamma^\mu \tau^I q_t)$
$Q_{lq}^{(1)}$	$(\bar{l}_p\gamma_\mu l_r)(\bar{q}_s\gamma^\mu q_t)$
$Q_{lq}^{(3)}$	$(\bar{l}_p\gamma_\mu \tau^I l_r)(\bar{q}_s\gamma^\mu \tau^I q_t)$

Class 8: $(\bar{L}L)(\bar{R}R)$	
Q_{le}	$(\bar{l}_p\gamma_\mu l_r)(\bar{e}_s\gamma^\mu e_t)$
Q_{lu}	$(\bar{l}_p\gamma_\mu l_r)(\bar{u}_s\gamma^\mu u_t)$
Q_{ld}	$(\bar{l}_p\gamma_\mu l_r)(\bar{d}_s\gamma^\mu d_t)$
$Q_{qe}^{(1)}$	$(\bar{q}_p\gamma_\mu q_r)(\bar{u}_s\gamma^\mu u_t)$
$Q_{qu}^{(1)}$	$(\bar{q}_p\gamma_\mu q_r)(\bar{u}_s\gamma^\mu u_t)$
$Q_{qu}^{(8)}$	$(\bar{q}_p\gamma_\mu T^A q_r)(\bar{u}_s\gamma^\mu T^A u_t)$
$Q_{qd}^{(1)}$	$(\bar{q}_p\gamma_\mu q_r)(\bar{d}_s\gamma^\mu d_t)$
$Q_{qd}^{(8)}$	$(\bar{q}_p\gamma_\mu T^A q_r)(\bar{d}_s\gamma^\mu T^A d_t)$

Class 8: $(\bar{L}R)(\bar{R}L)$	
Q_{ledq}	$(\bar{l}_p^j e_r)(\bar{d}_s q_{tj})$

Class 8: $(\bar{R}R)(\bar{R}R)$	
Q_{ee}	$(\bar{e}_p\gamma_\mu e_r)(\bar{e}_s\gamma^\mu e_t)$
Q_{uu}	$(\bar{u}_p\gamma_\mu u_r)(\bar{u}_s\gamma^\mu u_t)$
Q_{dd}	$(\bar{d}_p\gamma_\mu d_r)(\bar{d}_s\gamma^\mu d_t)$
$Q_{eu}^{(1)}$	$(\bar{e}_p\gamma_\mu e_r)(\bar{u}_s\gamma^\mu u_t)$
Q_{ed}	$(\bar{e}_p\gamma_\mu e_r)(\bar{d}_s\gamma^\mu d_t)$
$Q_{ud}^{(1)}$	$(\bar{u}_p\gamma_\mu u_r)(\bar{d}_s\gamma^\mu d_t)$
$Q_{ud}^{(8)}$	$(\bar{u}_p\gamma_\mu T^A u_r)(\bar{d}_s\gamma^\mu T^A d_t)$

Class 8: $(\bar{L}R)(\bar{L}R)$	
$Q_{quqd}^{(1)}$	$(\bar{q}_p^j u_r)\epsilon_{jk}(\bar{q}_s^k d_t)$
$Q_{quqd}^{(8)}$	$(\bar{q}_p^j T^A u_r)\epsilon_{jk}(\bar{q}_s^k T^A u_t)$
$Q_{lequ}^{(1)}$	$(\bar{l}_p^j e_r)\epsilon_{jk}(\bar{q}_s^k u_t)$
$Q_{lequ}^{(8)}$	$(\bar{l}_p^j T^A e_r)\epsilon_{jk}(\bar{q}_s^k T^A u_t)$

A.2 Large-m_t Limit and Vanishing-m_b Limit

The large-m_t procedure can be found in [108]. I will also give a introduction here according to our calculations. In order to determine the large-m_t corrections in the one-loop diagrams, all fermion masses but the masses of top quark have to be neglected in the integrals appearing in the one-loop scattering amplitudes. The details of taking large-m_t procedure could be illustrated by explaining the calculation of following one-loop SMEFT diagram in the $Z \to b\bar{b}$ reaction, in which process the SM contribution the will be neglected. Three Class 7 operators are involved, in which $C_{Hq}^{(1)}$ and $C_{Hq}^{(1)}$ alter the left-handed coupling and C_{Ht} alter the right-handed coupling. The coupling of the quarks to the Goldstone bosons is also affected by the Class 7 operators, but they are not considered here for simplification. In the flavour symmetry limit, the amplitude of the above diagrams in the Feynman gauge can be expressed as:

$$
\begin{aligned}
iA = i\frac{2e}{v_T^2} \int \frac{d^d l}{2\pi^d} \bar{u}(p_b) \Bigg(& (m_b P_L - m_t P_R) \frac{1}{(l - p_b)^2 - M_W^2} \\
& \frac{\slashed{l} + m_t}{l^2 - m_t^2} \frac{v_T^2}{2} \left(\left(C_{Hq}^{(1)} - C_{Hq}^{(3)} \right) P_L + C_{Ht} P_R \right) \\
& \frac{\left(\slashed{l} - \slashed{p}_b - \slashed{p}_{\bar{b}} \right) + m_t}{(l - p_b - p_{\bar{b}})^2 - m_t^2} (m_t P_L - m_b P_R) \Bigg) v(p_{\bar{b}}) \epsilon_Z^\mu,
\end{aligned}
\tag{A.2.1}
$$

where we have replaced the bare vev $\hat{v}_t$ with v_T, since the difference only arise at the order Λ^4, thus can be neglected. Again, all the couplings are written in the broken phase. In the following calculations, we set $m_b \to 0$ in the large-m_t limit. For convenience, the amplitude can be split into finite part and divergent part as

$$
iA = i\frac{e}{16\pi^2 v_T^2} \bar{u}(p_b) v(p_{\bar{b}}) \epsilon_Z^\mu \left(A^{\text{fin}} + A^{\text{div}} \right).
\tag{A.2.2}
$$

The amplitude has been given in 4.5.52, it turns out that the left-handed coupling vanishes in the divergent part, only C_{Ht} is left in the divergent part:

$$
iA^{\text{div}} = \frac{1}{\epsilon} M_Z^2 m_t^2 C_{Ht}.
\tag{A.2.3}
$$

And the finite amplitude can be reduced by using the scalar integrals:

$$
\begin{aligned}
iA^{fin} = -\bigg(& C_{Ht} \left(M_Z^2 + 2 \left(m_t^2 - M_W^2 \right) \hat{B}_0 \left[m_b^2, m_t^2, M_W^2 \right] \right. \\
& - \left(2m_t^2 - 2M_W^2 + M_Z^2 \right) \hat{B}_0 \left[M_Z^2, m_t^2, m_t^2 \right] \bigg) + 2 \left(C_{Ht} \left(m_t^2 - M_W^2 \right)^2 \right. \\
& + \left(C_{Hq}^{(1)} + C_{Hq}^{(3)} \right) m_t^2 M_Z^2 \bigg) \hat{C}_0 [M_Z^2, m_b^2, m_b^2, m_t^2, m_t^2, M_W^2] \bigg),
\end{aligned}
\tag{A.2.4}
$$

where only the finite parts of these integrals are reserved, which are marked as "hatted" symbols. There are two kinds of scalar integrals apearing in the above expression: scalar two-point integral and three-point integral. Actually, scalar one-point integral will also be needed to calculate Class 8 one-loop corrections, which is denoted as $A\left[m_i^2\right]$, usually with $i = t, b$ in our case. The scalar one-point integral is very simple:

$$
A_0 = \frac{m_i^2}{\epsilon} + \hat{A}_0 m_i^2 = \frac{m_i^2}{\epsilon} + m_i^2 \left(1 + \ln \left[\frac{m_i^2}{\mu^2} \right] \right).
\tag{A.2.5}
$$

In the large-mt limit, we can simply have $\hat{A}_0 9 m_i^2 0 = 0$. For the other scalar integrals, the general result of these integrals should be expanded into a series of $1/m_t$ and taking the limit $m_t \to \infty$. According the parameters apearing in the integral, there are two general cases for the scalar two-point integral:

$$
\begin{aligned}
\lim_{m_t \to \infty} \hat{B}_0 \left[m_1^2, m_t^2, m_2^2 \right] &= 1 + \frac{1}{m_t^2} \left(\frac{m_1^2}{2} + m_2^2 \ln \left[\frac{m_2^2}{m_t^2} \right] \right) - \ln \left[\frac{m_t^2}{\mu^2} \right] \\
\lim_{m_t \to \infty} \hat{B}_0 \left[m_1^2, m_t^2, m_t^2 \right] &= \frac{m_1^2}{6 m_t^2} - \ln \left[\frac{m_t^2}{\mu^2} \right].
\end{aligned}
\tag{A.2.6}
$$

Furthermore, there are usually gauge boson mass terms like M_W and M_Z appearing in the integral. In the vanishing gauge couplings limit, the positive powers of gauge boson masses could also be neglected together with the fermion masses with exception of the top-quark mass. In such a way, the two-point integral could be simplified a lot. Now we write down the two two-point integrals in A.2.4:

$$
\lim_{m_t \to \infty} \hat{B}_0 \left[m_b^2, m_t^2, M_W^2 \right] = 1 - \ln \left[\frac{m_t^2}{\mu^2} \right], \quad \lim_{m_t \to \infty} \hat{B}_0 \left[M_Z^2, m_t^2, m_t^2 \right] = 0 - \ln \left[\frac{m_t^2}{\mu^2} \right]
\tag{A.2.7}
$$

. For the three-point integral that are related to the triangle one-loop diagrams, the large-mt reduction could be done in a similar way. Now we consider the integral in A.2.4:

$$
\lim_{m_t \to \infty} \hat{C}_0 [M_Z^2, m_b^2, m_b^2, m_t^2, m_t^2, M_W^2] \to \lim_{m_t \to \infty} \hat{C}_0 \left[0, 0, 0, m_t^2, m_t^2, 0 \right]
\tag{A.2.8}
$$

. Then we find that the finite part of the amplitude that we consider here can take a very simple form:

$$A^{\text{fin}} = \left(-2 \left(C_{Hq}^{(1)} + C_{Hq}^{(3)} \right) + C_{Ht} \left(1 + \ln \left[\frac{m_t^2}{\mu^2} \right] \right) \right) v_T^2 \qquad \text{(A.2.9)}$$

.

For convenience, we sum up those integrals we might encounter in the calculation of one-loop amplitudes in the $e^+e^- \to b\bar{b}$:

$$\hat{B}_0 \left[b, m_b^2, m_t^2 \right] = 1 - \ln \left[\frac{m_t^2}{\mu^2} \right] + \left(\frac{b}{2} - \frac{m_b^2}{m_t^2} \ln \left[\frac{m_t^2}{\mu^2} \right] \right),$$

$$\hat{B}_0 \left[s, m_t^2, m_t^2 \right] = \frac{b}{6m_t^2} - \ln \left[\frac{m_t^2}{\mu^2} \right],$$

$$\hat{B}_0 \left[M_W^2, m_b^2, m_t^2 \right] = 1 - \frac{m_b^2}{m_t^2} \ln \left[\frac{m_t^2}{m_b^2} \right] - \ln \left[\frac{m_t^2}{\mu^2} \right] + \frac{1}{2} \frac{M_W^2}{m_t^2},$$

$$\hat{B}_0 \left[m_b^2, m_t^2, a^2 b \right] = 1 + \frac{1}{m_t^2} \left(\frac{m_b^2}{2} + b \ln \left[\frac{1}{m_t^2} \right] \right) - \ln \left[\frac{m_t^2}{\mu^2} \right],$$

$$\dot{\hat{B}}_0 \left[m_b^2, m_t^2, b \right] = 1 + \left(m_b^2 + 0 \left(b \ln [b] + \frac{b}{m_t^2} \ln \left[\frac{1}{m_t^2} \right] \right) \right) - \ln \left[\frac{m_t^2}{\mu^2} \right],$$

$$\dot{\hat{B}}_0 \left[m_b^2, m_t^2, b \right] = \frac{1}{2m_t^2},$$

$$\dot{\hat{B}}_0 \left[m_b^2, m_t^2, a^2 b \right] = \frac{1}{2m_t^2}, \qquad \text{(A.2.10)}$$

$$\hat{B}_0 \left[a^2 b, m_b^2, m_t^2 \right] = 1 - \ln \left[\frac{m_t^2}{\mu^2} \right] + \left(\frac{b}{2} - \frac{m_b^2}{m_t^2} \ln \left[\frac{m_t^2}{m_b^2} \right] \right),$$

$$\hat{B}_0 \left[b, m_t^2, m_t^2 \right] = \frac{b}{6m_t^2} - \ln \left[\frac{m_t^2}{\mu^2} \right],$$

$$\hat{B}_0 \left[m_H^2, a^2 M_W^2, a^2 M_W^2 \right] = \hat{B}_0 [m_H^2, M_W^2, M_W^2] - \ln \left[\frac{m_H^2}{\mu^2} \right],$$

$$\dot{\hat{B}}_0 \left[m_H^2, m_t^2, m_t^2 \right] = \frac{1}{6m_t^2}$$

$$C_0 \left[s, m_b^2, m_b^2, m_t^2, m_t^2, m_W^2 \right] = -\frac{1}{m_t^2} - \frac{1}{12} \frac{s}{m_t^2},$$

$$C_0 \left[m_b^2, s, m_b^2, m_b^2, M_W^2, M_W^2 \right] = -\frac{1}{m_t^2} \left(1 + i\pi + \ln \left[\frac{m_t^2}{s} \right] \right),$$

However, in the numerical calculation, we would choose the vanishing-m_b limit rather than the large-m_t limit. In such a case, we set the mass of bottom-quark as zero together with the other non-t-quark masses, but keeping the masses of gauge bosons. The scalar integrals in the calculation of one-loop diagrams in the $e^+e^- \to b\bar{b}$

process in the vanishing-m_b limit are listed below:

$$\lim_{m_b \to 0} \hat{B}_0 \left[m_b^2, m_t^2, M_W^2 \right] = 1 + \left(M_W^2 \left(m_t^2 + M_W^2 \right) \ln \left[\frac{m_t^2}{\mu^2} \right] \right) - \ln \left[\frac{m_t^2}{mu^2} \right],$$

$$\lim_{m_b \to 0} \hat{B}_0 \left[s, m_t^2, m_t^2 \right] = \frac{s}{6m_t^2} - \ln \left[\frac{m_t^2}{\mu^2} \right],$$

$$\lim_{m_b \to 0} \hat{C}_0 \left[s, m_b^2, m_b^2, m_t^2, m_2^{\cdot} M_W^2 \right] = -\frac{1}{m_t^4} (12m_t^2 + 12M_W^2 + s + 12M_W^2 \ln \left[\frac{M_W^2}{m_t^2} \right]),$$

$$\lim_{m_b \to 0} \hat{B}_0 \left[s, M_W^2, M_W^2 \right] = 2 - \frac{m_t^2}{\mu^2} + \frac{m_t^2}{s} - \ln \left[\frac{1+z^2}{4} \right] + izln \left[\frac{i+z}{-i+z} \right],$$

$$\lim_{m_b \to 0} \hat{C}_0 \left[m_b^2, s, m_b^2, m_2^{\cdot} M_W^2, M_W^2 \right] = \frac{1}{m_t^2} \left(-1 + \frac{M_W^2}{m_t^2} + iz \ln \left[-\frac{-2M_W^2 + s + izs}{2M_W^2} \right] \right),$$

$$\text{(A.2.11)}$$

in which $z = \sqrt{\frac{4M_W^2}{s} - 1}$.

A.3 Cancellation of UV Divergence for Class 8 Operators in the $Z \to b\bar{b}$ Process

In the following I will show how to build the counterterms and how they cancel the UV divergence for the $Z \to b\bar{b}$ process. All the One-loop UV divergent terms and Counterterms for each Wilson Coefficient could be obtained from 4.4. For simplicity's sake, I just show the original form of the one-loop UV divergent terms and the corresponding counterterms. For convenience, we denote the Hyper charge as y_i and the Yukawa coupling as Y_i for a particle i in this section, where the Hyper charge of Higgs is $y_H = 1/2$.

Secondly we consider the $\bar{L}L\bar{L}L$ operators. For $Q_{qq}^{(1)}$, three kinds of diagrams are included, we will list their UV divergent terms respectively. According to 4.4, the UV divergent term of $2(\bar{t}\gamma_\mu)(\bar{b}\gamma^\mu b)(1)$ is

$$- 2i \frac{1}{\epsilon} \epsilon_Z^\mu \left\langle \bar{b}_L \gamma^\mu b_L \right\rangle \frac{\bar{e}N_c \left[2 \left(g_L^t - g_R^t \right) m_t^2 - \frac{2}{3} g_L^t M_Z^2 \right]}{16\pi^2 2\hat{s}_w \hat{c}_w} C_{qq}^{(1)}$$

$$= -2i \frac{1}{\epsilon} \epsilon_Z^\mu \left\langle \bar{b}_L \gamma^\mu b_L \right\rangle \frac{\bar{e}2N_c m_t^2}{16\pi^2 2\hat{s}_w \hat{c}_w} C_{qq}^{(1)} \qquad \text{(A.3.12)}$$

$$- 2i \frac{1}{\epsilon} \epsilon_Z^\mu \left\langle \bar{b}_L \gamma^\mu b_L \right\rangle \frac{\bar{e}N_c (\frac{-1}{3}) M_Z^2 + \bar{e}N_c (\frac{4}{9}) s^2 M_Z^2}{16\pi^2 2\hat{s}_w \hat{c}_w} C_{qq}^{(1)}.$$

For $2(\bar{b}\gamma_\mu b)(\bar{b}\gamma^\mu b)(1)$, the UV divergent term is

$$
\begin{aligned}
&- 2i\frac{1}{\epsilon}\epsilon_Z^\mu \left\langle \bar{b}_L\gamma^\mu b_L \right\rangle \frac{\bar{e}N_c\left[2\left(g_L^b - g_R^b\right)m_b^2 - \frac{2}{3}g_L^b M_Z^2\right]}{16\pi^2 2\hat{s}_w\hat{c}_w}C_{qq}^{(1)} \\
&= -2i\frac{1}{\epsilon}\epsilon_Z^\mu \left\langle \bar{b}_L\gamma^\mu b_L \right\rangle \frac{-\bar{e}2N_c m_b^2}{16\pi^2 2\hat{s}_w\hat{c}_w}C_{qq}^{(1)} \\
&- 2i\frac{1}{\epsilon}\epsilon_Z^\mu \left\langle \bar{b}_L\gamma^\mu b_L \right\rangle \frac{\bar{e}N_c M_Z^2 + \bar{e}N_c(\frac{-2}{9})s^2 M_Z^2}{16\pi^2 2\hat{s}_w\hat{c}_w}C_{qq}^{(1)}.
\end{aligned}
\tag{A.3.13}
$$

For $2(\bar{b}\gamma_\mu b)(\bar{b}\gamma^\mu b)(2)$, the UV divergent term is

$$
\begin{aligned}
&- 2i\frac{1}{\epsilon}\epsilon_Z^\mu \left\langle \bar{b}_L\gamma^\mu b_L \right\rangle \frac{\bar{e}\left[2(g_L^b - g_R^b)m_b^2 - \frac{2}{3}g_L^b M_Z^2\right]}{16\pi^2 2\hat{s}_w\hat{c}_w}C_{qq}^{(1)} \\
&= -2i\frac{1}{\epsilon}\epsilon_Z^\mu \left\langle \bar{b}_L\gamma^\mu b_L \right\rangle \frac{-\bar{e}2m_b^2}{16\pi^2 2\hat{s}_w\hat{c}_w}C_{qq}^{(1)} \\
&- 2i\frac{1}{\epsilon}\epsilon_Z^\mu \left\langle \bar{b}_L\gamma^\mu b_L \right\rangle \frac{\bar{e}M_Z^2 + \bar{e}(\frac{-2}{9})s^2 M_Z^2}{16\pi^2 2\hat{s}_w\hat{c}_w}C_{qq}^{(1)}.
\end{aligned}
\tag{A.3.14}
$$

Summing the above divergent terms up, we have

$$
\begin{aligned}
&- 2i\frac{1}{\epsilon}\epsilon_Z^\mu \left\langle \bar{b}_L\gamma^\mu b_L \right\rangle \frac{\bar{e}2N_c m_t^2}{16\pi^2 2\hat{s}_w\hat{c}_w}C_{qq}^{(1)} \\
&- 2i\frac{1}{\epsilon}\epsilon_Z^\mu \left\langle \bar{b}_L\gamma^\mu b_L \right\rangle \frac{-\bar{e}2N_c m_b^2}{16\pi^2 2\hat{s}_w\hat{c}_w}C_{qq}^{(1)} \\
&- 2i\frac{1}{\epsilon}\epsilon_Z^\mu \left\langle \bar{b}_L\gamma^\mu b_L \right\rangle \frac{-\bar{e}2m_b^2}{16\pi^2 2\hat{s}_w\hat{c}_w}C_{qq}^{(1)} \\
&- 2i\frac{1}{\epsilon}\epsilon_Z^\mu \left\langle \bar{b}_L\gamma^\mu b_L \right\rangle \frac{\bar{e}N_c(\frac{2}{9})\hat{s}_w^2 M_Z^2}{16\pi^2 2\hat{s}_w\hat{c}_w}C_{qq}^{(1)} \\
&- 2i\frac{1}{\epsilon} \left\langle \bar{b}_L\gamma^\mu b_L \right\rangle \frac{\bar{e}M_Z^2 + \bar{e}(\frac{-2}{9})\hat{s}_w^2 M_Z^2}{8\pi^2 2\hat{s}_w\hat{c}_w}C_{qq}^{(1)}.
\end{aligned}
\tag{A.3.15}
$$

Following the renormalisation procedure in 4.2, we can obtain the counterterms for $Q_{qq}^{(1)}$, they are

$$
\begin{aligned}
i\delta = {}&i\frac{1}{2}\frac{1}{\epsilon}\epsilon_Z^\mu \left\langle \bar{b}_L\gamma^\mu b_L \right\rangle \frac{\bar{e}v_T^2\left(4N_c Y_t^2\right)}{16\pi^2 2\hat{s}_w\hat{c}_w}C_{qq}^{(1)} \\
&+ i\frac{1}{2}\frac{1}{\epsilon}\epsilon_Z^\mu \left\langle \bar{b}_L\gamma^\mu b_L \right\rangle \frac{\bar{e}v_T^2\left(-4N_c Y_b^2\right)}{16\pi^2 2\hat{s}_w\hat{c}_w}C_{qq}^{(1)} \\
&+ i\frac{1}{2}\frac{1}{\epsilon}\epsilon_Z^\mu \left\langle \bar{b}_L\gamma^\mu b_L \right\rangle \frac{\bar{e}v_T^2\left(-4Y_b^2\right)}{16\pi^2 2\hat{s}_w\hat{c}_w}C_{qq}^{(1)} \\
&+ i\frac{1}{2}\frac{1}{\epsilon}\epsilon_Z^\mu \left\langle \bar{b}_L\gamma^\mu b_L \right\rangle \frac{\bar{e}v_T^2\frac{16}{3}N_c g_1^2 y_H y_q}{16\pi^2 2\hat{s}_w\hat{c}_w}C_{qq}^{(1)} \\
&+ i\frac{1}{2}\frac{1}{\epsilon}\epsilon_Z^\mu \left\langle \bar{b}_L\gamma^\mu b_L \right\rangle \frac{e v_T^2\frac{8}{3}g_1^2 y_H y_q}{16\pi^2 2\hat{s}_w\hat{c}_w}C_{qq}^{(1)} \\
&+ i\frac{1}{2}\frac{1}{\epsilon}\epsilon_Z^\mu \left\langle \bar{b}_L\gamma^\mu b_L \right\rangle \frac{\bar{e}v_T^2\frac{2}{3}g_2^2}{16\pi^2 2\hat{s}_w\hat{c}_w}C_{qq}^{(1)}.
\end{aligned}
\tag{A.3.16}
$$

For the $Q_{qq}^{(3)}$ operator, four types one loop diagrams are included. We simply list the UV Divergent parts of the amplitudes and the relevant counterterms. The UV divergent term arising from $4(\bar{t}\gamma_\mu t)(\bar{b}\gamma^\mu b)(2)$ is

$$
\begin{aligned}
&-4i\frac{1}{\epsilon}\epsilon_Z^\mu \left\langle \bar{b}_L\gamma^\mu b_L \right\rangle \frac{\bar{e}\left[2\left(g_L^t - g_R^t\right)m_t^2 - \frac{2}{3}g_L^t M_Z^2\right]}{16\pi^2 2\hat{s}_w\hat{c}_w}C_{qq}^{(3)}\\
&-4i\frac{1}{\epsilon}\epsilon_Z^\mu \left\langle \bar{b}_L\gamma^\mu b_L \right\rangle \frac{\bar{e}2m_t^2}{16\pi^2 2\hat{s}_w\hat{c}_w}C_{qq}^{(3)}\\
&-4i\frac{1}{\epsilon}\epsilon_Z^\mu \left\langle \bar{b}_L\gamma^\mu b_L \right\rangle \frac{e(\frac{-1}{3})M_Z^2 + \bar{e}\left(\frac{4}{9}\right)\hat{s}_w^2 M_Z^2}{16\pi^2 2\hat{s}_w\hat{c}_w}C_{qq}^{(3)}.
\end{aligned}
\tag{A.3.17}
$$

in which the UV divergent part due to $-2(\bar{t}\gamma_\mu t)(\bar{b}\gamma^\mu b)(1)$ is

$$
\begin{aligned}
&2i\frac{1}{\epsilon}\epsilon_Z^\mu \left\langle \bar{b}_L\gamma^\mu b_L \right\rangle \frac{\bar{e}N_c\left[2\left(g_L^t - g_R^t\right)m_t^2 - \frac{2}{3}g_L^t M_Z^2\right]}{16\pi^2 2\hat{s}_w\hat{c}_w}C_{qq}^{(3)}\\
&= 2i\frac{1}{\epsilon}\epsilon_Z^\mu \left\langle \bar{b}_L\gamma^\mu b_L \right\rangle \frac{\bar{e}2N_c m_t^2}{16\pi^2 2\hat{s}_w\hat{c}_w}C_{qq}^{(3)}\\
&+ 2i\frac{1}{\epsilon}\epsilon_Z^\mu \left\langle \bar{b}_L\gamma^\mu b_L \right\rangle \frac{\bar{e}N_c(\frac{-1}{3})M_Z^2 + \bar{e}N_c(\frac{4}{9})\hat{s}_w^2 M_Z^2}{16\pi^2 2\hat{s}_w\hat{c}_w}C_{qq}^{(3)},
\end{aligned}
\tag{A.3.18}
$$

the UV divergent part due to $2(\bar{b}\gamma_\mu b)(\bar{b}\gamma^\mu b)(1)$ is

$$
\begin{aligned}
&-2i\frac{1}{\epsilon}\epsilon_Z^\mu \left\langle \bar{b}_L\gamma^\mu b_L \right\rangle \frac{\bar{e}N_c\left[2\left(g_L^b - g_R^b\right)m_b^2 - \frac{2}{3}g_L^b M_Z^2\right]}{16\pi^2 2\hat{s}_w\hat{c}_w}C_{qq}^{(3)}\\
&= -2i\frac{1}{\epsilon}\epsilon_Z^\mu \left\langle \bar{b}_L\gamma^\mu b_L \right\rangle \frac{-\bar{e}2N_c m_b^2}{16\pi^2 2\hat{s}_w\hat{c}_w}C_{qq}^{(3)}\\
&-2i\frac{1}{\epsilon}\epsilon_Z^\mu \left\langle \bar{b}_L\gamma^\mu b_L \right\rangle \frac{\bar{e}N_c M_Z^2 + \bar{e}N_c\left(\frac{-2}{9}\right)\hat{s}_w^2 M_Z^2}{16\pi^2 2\hat{s}_w\hat{c}_w}C_{qq}^{(3)},
\end{aligned}
\tag{A.3.19}
$$

and the UV divergent part due to $2(\bar{b}_p\gamma_\mu b)(\bar{b}_s\gamma^\mu b)(2)$ is

$$
\begin{aligned}
&-2i\frac{1}{\epsilon}\epsilon_Z^\mu \left\langle \bar{b}_L\gamma^\mu b_L \right\rangle \frac{\bar{e}\left[2\left(g_L^b - g_R^b\right)m_b^2 - \frac{2}{3}g_L^b M_Z^2\right]}{16\pi^2 2\hat{s}_w\hat{c}_w}C_{qq}^{(3)}\\
&= -2i\frac{1}{\epsilon}\epsilon_Z^\mu \left\langle \bar{b}_L\gamma^\mu b_L \right\rangle \frac{-\bar{e}2m_b^2}{16\pi^2 2\hat{s}_w\hat{c}_w}C_{qq}^{(3)}\\
&-2i\frac{1}{\epsilon}\epsilon_Z^\mu \left\langle \bar{b}_L\gamma^\mu b_L \right\rangle \frac{\bar{e}M_Z^2 + \bar{e}N_c\left(\frac{-2}{9}\right)\hat{s}_w^2 M_Z^2}{16\pi^2 2\hat{s}_w\hat{c}_w}C_{qq}^{(3)}.
\end{aligned}
\tag{A.3.20}
$$

Adding all these UV divergent parts up, we can obtain the total UV divergent terms

for $Q_{qq}^{(3)}$, they are

$$
\begin{aligned}
& - 2i\frac{1}{\epsilon}\epsilon_Z^\mu \left\langle \bar{b}_L\gamma^\mu b_L \right\rangle \frac{-\bar{e}2N_c m_t^2}{16\pi^2 2\hat{s}_w\hat{c}_w}C_{qq}^{(3)} \\
& - 2i\frac{1}{\epsilon}\epsilon_Z^\mu \left\langle \bar{b}_L\gamma^\mu b_L \right\rangle \frac{-\bar{e}2N_c m_b^2}{16\pi^2 2\hat{s}_w\hat{c}_w}C_{qq}^{(3)} \\
& - 4i\frac{1}{\epsilon}\epsilon_Z^\mu \left\langle \bar{b}_L\gamma^\mu b_L \right\rangle \frac{\bar{e}2 m_t^2}{16\pi^2 2\hat{s}_w\hat{c}_w}C_{qq}^{(3)} \\
& - 2i\frac{1}{\epsilon}\epsilon_Z^\mu \left\langle \bar{b}_L\gamma^\mu b_L \right\rangle \frac{-\bar{e}2 m_b^2}{16\pi^2 2\hat{s}_w\hat{c}_w}C_{qq}^{(3)} \\
& - 2i\frac{1}{\epsilon}\epsilon_Z^\mu \left\langle \bar{b}_L\gamma^\mu b_L \right\rangle \frac{\bar{e}N_c(\frac{2}{3}M_Z^2) + \bar{e}N_c(\frac{-2}{3})\hat{s}_w^2 M_Z^2}{16\pi^2 2\hat{s}_w\hat{c}_w}C_{qq}^{(3)} \\
& - 2i\frac{1}{\epsilon}\epsilon_Z^\mu \left\langle \bar{b}_L\gamma^\mu b_L \right\rangle \frac{\bar{e}(\frac{-1}{3}M_Z^2) + \bar{e}N_c(\frac{2}{3})\hat{s}_w^2 M_Z^2}{16\pi^2 2\hat{s}_w\hat{c}_w}C_{qq}^{(3)}.
\end{aligned}
\tag{A.3.21}
$$

The corresponding counterterms for $Q_{qq}^{(3)}$ are

$$
\begin{aligned}
i\delta = & -i\frac{1}{2}\frac{1}{\epsilon}\epsilon_Z^\mu \left\langle \bar{b}_L\gamma^\mu b_L \right\rangle \frac{-\bar{e}v_T^2\left(-4N_c Y_t^2\right)}{16\pi^2 2\hat{s}_w\hat{c}_w}C_{qq}^{(3)} \\
& + i\frac{1}{2}\frac{1}{\epsilon}\epsilon_Z^\mu \left\langle \bar{b}_L\gamma^\mu b_L \right\rangle \frac{\bar{e}v_T^2\left(8Y_t^2\right)}{16\pi^2 2\hat{s}_w\hat{c}_w}C_{qq}^{(3)} \\
& + i\frac{1}{2}\frac{1}{\epsilon}\epsilon_Z^\mu \left\langle \bar{b}_L\gamma^\mu b_L \right\rangle \frac{-\bar{e}v_T^2\left(4N_c Y_b^2\right)}{16\pi^2 2\hat{s}_w\hat{c}_w}C_{qq}^{(3)} \\
& + i\frac{1}{2}\frac{1}{\epsilon}\epsilon_Z^\mu \left\langle \bar{b}_L\gamma^\mu b_L \right\rangle \frac{-\bar{e}v_T^2\left(4Y_b^2\right)}{16\pi^2 2\hat{s}_w\hat{c}_w}C_{qq}^{(3)} \\
& + i\frac{1}{2}\frac{1}{\epsilon}\epsilon_Z^\mu \left\langle \bar{b}_L\gamma^\mu b_L \right\rangle \frac{\bar{e}v_T^2 8N_c g_1^2 y_H y_q}{16\pi^2 2\hat{s}_w\hat{c}_w}C_{qq}^{(3)} \\
& + i\frac{1}{2}\frac{1}{\epsilon}\epsilon_Z^\mu \left\langle \bar{b}_L\gamma^\mu b_L \right\rangle \frac{\bar{e}N_c v_T^2\frac{4}{3}g_2^2}{16\pi^2 2\hat{s}_w\hat{c}_w}C_{qq}^{(3)} \\
& i\frac{1}{2}\frac{1}{\epsilon}\epsilon_Z^\mu \left\langle \bar{b}_L\gamma^\mu b_L \right\rangle \frac{\bar{e}v_T^2\frac{-2}{3}g_2^2}{16\pi^2 2\hat{s}_w\hat{c}_w}C_{qq}^{(3)},
\end{aligned}
\tag{A.3.22}
$$

which exactly cancel the UV terms.

Secondly we consider the $\bar{R}R\bar{R}R$ operators. For $Q_{ud}^{(1)}$, there is only one diagram involved, which corresponds to $(\bar{t}\gamma_\mu t)(\bar{b}\gamma^\mu b)(1)$. The UV divergent amplitudes of this diagram are

$$
\begin{aligned}
& - i\frac{1}{\epsilon}\epsilon_Z^\mu \left\langle \bar{b}_R\gamma^\mu b_R \right\rangle \frac{\bar{e}N_c\left[2\left(g_R^t - g_L^t\right)m_t^2 - \frac{2}{3}g_R^t M_Z^2\right]}{16\pi^2 2\hat{s}_w\hat{c}_w}C_{ud}^{(1)} \\
& = -i\frac{1}{\epsilon}\epsilon_Z^\mu \left\langle \bar{b}_R\gamma^\mu b_R \right\rangle \frac{-\bar{e}2N_c m_t^2}{16\pi^2 2\hat{s}_w\hat{c}_w}C_{ud}^{(1)} \\
& - i\frac{1}{\epsilon}\epsilon_Z^\mu \left\langle \bar{b}_R\gamma^\mu b_R \right\rangle \frac{\bar{e}N_c(\frac{4}{9}\hat{s}_w^2 M_Z^2)}{16\pi^2 2\hat{s}_w\hat{c}_w}C_{ud}^{(1)},
\end{aligned}
\tag{A.3.23}
$$

and the corresponding counterterms are

$$i(\frac{1}{2})\frac{1}{\epsilon}\epsilon_Z^\mu \left\langle \bar{b}_R\gamma^\mu b_R \right\rangle \frac{\bar{e}v_T^2 \left(-2N_c Y_t^2\right)}{16\pi^2 2\hat{s}_w\hat{c}_w}C_{ud}^{(1)}$$

$$i(\frac{1}{2})\frac{1}{\epsilon}\epsilon_Z^\mu \left\langle \bar{b}_R\gamma^\mu b_R \right\rangle \frac{\bar{e}v_T^2 \frac{4}{3}N_c g_1^2 y_H y_t}{16\pi^2 2\hat{s}_w\hat{c}_w}C_{ud}^{(1)}. \tag{A.3.24}$$

For Q_{dd}, there are two diagrams involved, which correspond $2(\bar{b}\gamma_\mu b)(\bar{b}_s\gamma^\mu b)(1)$ and
$2(\bar{b}\gamma_\mu b)(\bar{b}\gamma^\mu b)(1)$. The one-loop UV part for $2(\bar{b}\gamma_\mu b)(\bar{b}\gamma^\mu b)(1)$ is

$$-2i\frac{1}{\epsilon}\epsilon_Z^\mu \left\langle \bar{b}_R\gamma^\mu b_R \right\rangle \frac{\bar{e}N_c \left[2\left(g_R^b - g_L^b\right)m_b^2 - \frac{2}{3}g_R^b M_Z^2\right]}{16\pi^2 2\hat{s}_w\hat{c}_w}C_{dd}$$

$$= -2i\frac{1}{\epsilon}\epsilon_Z^\mu \left\langle \bar{b}_R\gamma^\mu b_R \right\rangle \frac{-\bar{e}2N_c m_b^2}{16\pi^2 2\hat{s}_w\hat{c}_w}C_{dd} \tag{A.3.25}$$

$$-2i\frac{1}{\epsilon}\epsilon_Z^\mu \left\langle \bar{b}_R\gamma^\mu b_R \right\rangle \frac{-\bar{e}N_c \left(\frac{4}{9}\hat{s}_w^2 M_Z^2\right)}{16\pi^2 2\hat{s}_w\hat{c}_w}C_{dd},$$

whose corresponding counterterms are

$$i\frac{1}{2}\frac{1}{\epsilon}\epsilon_Z^\mu \left\langle \bar{b}_R\gamma^\mu b_R \right\rangle \frac{\bar{e}v_T^2 \left(-4N_c Y_b^2\right)}{16\pi^2 2\hat{s}_w\hat{c}_w}C_{dd}$$

$$+i\frac{1}{2}\frac{1}{\epsilon}\epsilon_Z^\mu \left\langle \bar{b}_R\gamma^\mu b_R \right\rangle \frac{\bar{e}v_T^2 \frac{8}{3}N_c g_1^2 y_H y_b}{16\pi^2 2\hat{s}_w\hat{c}_w}C_{dd}. \tag{A.3.26}$$

And the UV part for $2(\bar{b}\gamma_\mu b)(\bar{b}\gamma^\mu b)(2)$ is

$$-2i\frac{1}{\epsilon}\epsilon_Z^\mu \left\langle \bar{b}_R\gamma^\mu b_R \right\rangle \frac{\bar{e}\left[2\left(g_L^b - g_L^b\right)m_b^2 - \frac{2}{3}g_R^b M_Z^2\right]}{16\pi^2 2\hat{s}_w\hat{c}_w}C_{dd}$$

$$= -2i\frac{1}{\epsilon}\epsilon_Z^\mu \left\langle \bar{b}_R\gamma^\mu b_R \right\rangle \frac{-\bar{e}2m_b^2}{16\pi^2 2\hat{s}_w\hat{c}_w}C_{dd} \tag{A.3.27}$$

$$-2i\frac{1}{\epsilon}\epsilon_Z^\mu \left\langle \bar{b}_R\gamma^\mu b_R \right\rangle \frac{\bar{e}(\frac{4}{9}\hat{s}_w^2 M_Z^2)}{16\pi^2 2\hat{s}_w\hat{c}_w}C_{dd},$$

whose corresponding counterterms are

$$i\frac{1}{2}\frac{1}{\epsilon}\epsilon_Z^\mu \left\langle \bar{b}_R\gamma^\mu b_R \right\rangle \frac{\bar{e}v_T^2(-2Y_b^2)}{16\pi^2 2\hat{s}_w\hat{c}_w}C_{dd}$$

$$+i\frac{1}{2}\frac{1}{\epsilon}\epsilon_Z^\mu \left\langle \bar{b}_R\gamma^\mu b_R \right\rangle \frac{\bar{e}v_T^2 \frac{8}{3}N_c g_1^2 y_H y_b}{16\pi^2 2\hat{s}_w\hat{c}_w}C_{dd}. \tag{A.3.28}$$

At last we consider the $(\bar{L}L)(\bar{R}R)$. For the operator $Q_{qu}^{(1L)}$, only one type of
diagram are included. For its expanded operator $(\bar{t}\gamma_\mu t)(\bar{b}\gamma^\mu b)(1)$, the UV divergent
term is

$$-i\frac{1}{\epsilon}\epsilon_Z^\mu \left\langle \bar{b}_L\gamma^\mu b_L \right\rangle \frac{\bar{e}N_c \left[2\left(g_R^t - g_L^t\right)m_t^2 - \frac{2}{3}g_R^t M_Z^2\right]}{16\pi^2 2\hat{s}_w\hat{c}_w}C_{qu}^{(1)}$$

$$= -i\frac{1}{\epsilon}\epsilon_Z^\mu \left\langle \bar{b}_L\gamma^\mu b_L \right\rangle \frac{-\bar{e}2N_c m_t^2}{16\pi^2 2\hat{s}_w\hat{c}_w}C_{qu}^{(1)} \tag{A.3.29}$$

$$-i\frac{1}{\epsilon}\epsilon_Z^\mu \left\langle \bar{b}_L\gamma^\mu b_L \right\rangle \frac{\bar{e}N_c(\frac{4}{9}\hat{s}_w^2 M_Z^2)}{16\pi^2 2\hat{s}_w\hat{c}_w}C_{qu}^{(1)},$$

and the corresponding counterterms are

$$
\begin{aligned}
& i\frac{1}{2}\frac{1}{\epsilon}\epsilon_Z^\mu \left\langle \bar{b}_L \gamma^\mu b_L \right\rangle \frac{\bar{e}v_T^2\left(-2N_cY_t^2\right)}{16\pi^2 2\hat{s}_w\hat{c}_w}C_{qu}^{(1)} \\
& + i\frac{1}{2}\frac{1}{\epsilon}\epsilon_Z^\mu \left\langle \bar{b}_L \gamma^\mu b_L \right\rangle \frac{\bar{e}v_T^2 \frac{4}{3}N_c g_1^2 y_H y_t}{16\pi^2 2\hat{s}_w\hat{c}_w}C_{qu}^{(1)}.
\end{aligned}
\tag{A.3.30}
$$

For the operator $Q_{qd}^{(1)}$, five types of diagrams are included. According to the calculation, the amplitudes of two diagrams with structure (2) are zero. So only these types of operators are left to deal with, their expanded operators are $(\bar{t}\gamma_\mu t)(\bar{b}\gamma^\mu b)(1) + (\bar{b}\gamma_\mu b)(\bar{b}\gamma^\mu b)(1L) + (\bar{b}\gamma_\mu b)(\bar{b}\gamma^\mu b)(1R)$. For $(\bar{t}\gamma_\mu t)(\bar{b}\gamma^\mu b)(1)$, the one-loop UV divergent amplitude is

$$
\begin{aligned}
& -i\frac{1}{\epsilon}\epsilon_Z^\mu \left\langle \bar{b}_R \gamma^\mu b_R \right\rangle \frac{\bar{e}N_c\left[2\left(g_L^t - g_R^t\right)m_t^2 - \frac{2}{3}g_L^t M_Z^2\right]}{16\pi^2 2\hat{s}_w\hat{c}_w}C_{qd}^{(1)} \\
& = -i\frac{1}{\epsilon}\epsilon_Z^\mu \left\langle \bar{b}_R \gamma^\mu b_R \right\rangle \frac{\bar{e}2N_c m_t^2}{16\pi^2 2\hat{s}_w\hat{c}_w}C_{qd}^{(1)} \\
& - i\frac{1}{\epsilon}\left\langle \bar{b}_R \gamma^\mu b_R \right\rangle \frac{\bar{e}N_c(\frac{-1}{3})M_Z^2 + \bar{e}N_c(\frac{4}{9})\hat{s}_w^2 M_Z^2}{16\pi^2 2\hat{s}_w\hat{c}_w}C_{qd}^{(1)}.
\end{aligned}
\tag{A.3.31}
$$

For $(\bar{b}\gamma_\mu b)(\bar{b}\gamma^\mu b)(1R)$, the one-loop UV divergent amplitude is

$$
\begin{aligned}
& -i\frac{1}{\epsilon}\epsilon_Z^\mu \left\langle \bar{b}_R \gamma^\mu b_R \right\rangle \frac{\bar{e}N_c\left[2\left(g_L^b - g_R^b\right)m_b^2 - \frac{2}{3}g_L^b M_Z^2\right]}{16\pi^2 2\hat{s}_w\hat{c}_w}C_{qd}^{(1)} \\
& = -i\frac{1}{\epsilon}\epsilon_Z^\mu \left\langle \bar{b}_R \gamma^\mu b_R \right\rangle \frac{-\bar{e}2N_c m_b^2}{16\pi^2 2\hat{s}_w\hat{c}_w}C_{qd}^{(1)} + \\
& - i\frac{1}{\epsilon}\epsilon_Z^\mu \left\langle \bar{b}_R \gamma^\mu b_R \right\rangle \frac{\bar{e}N_c(\frac{1}{3})M_Z^2 + \bar{e}N_c(\frac{-2}{9})\hat{s}_w^2 M_Z^2}{16\pi^2 2\hat{s}_w\hat{c}_w}C_{qd}^{(1)}.
\end{aligned}
\tag{A.3.32}
$$

The diagrams for A.3.31 and A.3.32 both include right-handed b-quarks in the loop. The sum of these two UV terms is

$$
\begin{aligned}
& -i\frac{1}{\epsilon}\epsilon_Z^\mu \left\langle \bar{b}_R \gamma^\mu b_R \right\rangle \frac{\bar{e}2N_c m_t^2}{16\pi^2 2\hat{s}_w\hat{c}_w}C_{qd}^{(1)} \\
& -i\frac{1}{\epsilon}\epsilon_Z^\mu \left\langle \bar{b}_R \gamma^\mu b_R \right\rangle \frac{-\bar{e}2N_c m_b^2}{16\pi^2 2\hat{s}_w\hat{c}_w}C_{qd}^{(1)} \\
& -i\frac{1}{\epsilon}\epsilon_Z^\mu \left\langle \bar{b}_R \gamma^\mu b_R \right\rangle \frac{\bar{e}N_c(\frac{2}{9})\hat{s}_w^2 M_Z^2}{16\pi^2 2\hat{s}_w\hat{c}_w}C_{qd}^{(1)},
\end{aligned}
\tag{A.3.33}
$$

which will be cancelled by the following counterterms:

$$
\begin{aligned}
& i\frac{1}{2}\frac{1}{\epsilon}\epsilon_Z^\mu \left\langle \bar{b}_R \gamma^\mu b_R \right\rangle \frac{\bar{e}v_T^2\left(2N_cY_t^2\right)}{16\pi^2 2\hat{s}_w\hat{c}_w}C_{qd}^{(1)} \\
& + i\frac{1}{2}\frac{1}{\epsilon}\epsilon_Z^\mu \left\langle \bar{b}_R \gamma^\mu b_R \right\rangle \frac{\bar{e}v_T^2\left(-2N_cY_b^2\right)}{16\pi^2 2\hat{s}_w\hat{c}_w}C_{qd}^{(1)} \\
& + i\frac{1}{2}\frac{1}{\epsilon}\epsilon_Z^\mu \left\langle \bar{b}_R \gamma^\mu b_R \right\rangle \frac{\bar{e}v_T^2 \frac{8}{3}N_c g_1^2 y_H y_q}{16\pi^2 2\hat{s}_w\hat{c}_w}C_{qd}^{(1)}.
\end{aligned}
\tag{A.3.34}
$$

For $(\bar{b}\gamma_\mu b)(\bar{b}\gamma^\mu b)(1L)$, the one-loop UV divergent amplitudes is

$$
\begin{aligned}
&- i\frac{1}{\epsilon}\epsilon_Z^\mu \left\langle \bar{b}_L \gamma^\mu b_L \right\rangle \frac{\bar{e}N_c \left[2\left(g_R^b - g_L^b\right)m_b^2 - \frac{2}{3}g_R^b M_Z^2\right]}{16\pi^2 2\hat{s}_w \hat{c}_w} C_{qd}^{(1)} \\
&= -i\frac{1}{\epsilon}\epsilon_Z^\mu \left\langle \bar{b}_L \gamma^\mu b_L \right\rangle \frac{\bar{e}2N_c m_b^2}{16\pi^2 2\hat{s}_w \hat{c}_w} C_{qd}^{(1)} \\
&- i\frac{1}{\epsilon}\epsilon_Z^\mu \left\langle \bar{b}_L \gamma^\mu b_L \right\rangle \frac{\bar{e}N_c(\frac{-2}{9})\hat{s}_w^2 M_Z^2}{16\pi^2 2\hat{s}_w \hat{c}_w} C_{qd}^{(1)},
\end{aligned} \tag{A.3.35}
$$

whose corresponding diagram include left-handed b-quarks in the loop, will be cancelled by the following counterterms

$$
\begin{aligned}
&i\frac{1}{2}\frac{1}{\epsilon}\epsilon_Z^\mu \left\langle \bar{b}_L \gamma^\mu b_L \right\rangle \frac{\bar{e}v_T^2 \left(2N_c Y_b^2\right)}{16\pi^2 2\hat{s}_w \hat{c}_w} C_{qd}^{(1)} \\
&+ i\frac{1}{2}\frac{1}{\epsilon}\epsilon_Z^\mu \left\langle \bar{b}_L \gamma^\mu b_L \right\rangle \frac{\bar{e}v_T^2 \frac{4}{3}N_c g_1^2 y_H y_b}{16\pi^2 2\hat{s}_w \hat{c}_w} C_{qd}^{(1)}.
\end{aligned} \tag{A.3.36}
$$

Bibliography

[1] Steven Weinberg. A Model of Leptons. <u>Phys. Rev. Lett.</u>, 19:1264–1266, 1967.

[2] Abdus Salam. Weak and Electromagnetic Interactions. <u>Conf. Proc.</u>, C680519:367–377, 1968.

[3] S. L. Glashow. Partial Symmetries of Weak Interactions. <u>Nucl. Phys.</u>, 22:579–588, 1961.

[4] Michael E Peskin. <u>An introduction to quantum field theory</u>. CRC Press, 2018.

[5] Chen-Ning Yang and Robert L Mills. Conservation of isotopic spin and isotopic gauge invariance. <u>Physical review</u>, 96(1):191, 1954.

[6] Murray Gell-Mann. Symmetries of baryons and mesons. <u>Physical Review</u>, 125(3):1067, 1962.

[7] Stephen F King. Neutrino mass models. <u>Reports on Progress in Physics</u>, 67(2):107, 2003.

[8] J Van Bladel. Lorenz or lorentz? <u>IEEE Antennas and Propagation Magazine</u>, 33(2):69–69, 1991.

[9] Peter W Higgs. Broken symmetries and the masses of gauge bosons. <u>Physical Review Letters</u>, 13(16):508, 1964.

[10] Lev Borisovich Okun. <u>Leptons and quarks</u>. Elsevier, 2013.

[11] DALLAS C Kennedy. The electroweak polarization asymmetry: A guided tour. Technical report, 1988.

[12] Hideki Yukawa. On the interaction of elementary particles. i. Proceedings of the Physico-Mathematical Society of Japan. 3rd Series, 17:48–57, 1935.

[13] C Patrignani, Particle Data Group, et al. Review of particle physics. Chinese physics C, 40(10):100001, 2016.

[14] Ziro Maki, Masami Nakagawa, and Shoichi Sakata. Remarks on the unified model of elementary particles. Progress of Theoretical Physics, 28(5):870–880, 1962.

[15] Gideon Alexander, J Allison, N Altekamp, K Ametewee, KJ Anderson, S Anderson, S Arcelli, S Asai, D Axen, G Azuelos, et al. A measurement of the charm and bottom forward-backward asymmetries using D mesons at LEP. Zeitschrift für Physik C Particles and Fields, 73(3):379–395, 1997.

[16] Gregory Breit and Eugene Wigner. Capture of slow neutrons. Physical review, 49(7):519, 1936.

[17] Benjamín Grinstein and Christopher W Murphy. Bottom-quark forward-backward asymmetry in the standard model and beyond. Physical review letters, 111(6):062003, 2013.

[18] Debajyoti Choudhury, Rohini M Godbole, Saurabh D Rindani, and Pratishruti Saha. Top polarization, forward-backward asymmetry, and new physics. Physical Review D, 84(1):014023, 2011.

[19] M Beccaria, G Macorini, G Panizzo, and C Verzegnassi. New Physics signals from measurable polarization asymmetries at LHC. Physics Letters B, 730:149–154, 2014.

[20] Enrico Fermi. Versuch einer theorie der β-Strahlen. i. Zeitschrift für Physik, 88(3-4):161–177, 1934.

[21] Toichiro Kinoshita. Mass singularities of Feynman amplitudes. Journal of Mathematical Physics, 3(4):650–677, 1962.

[22] Tsung-Dao Lee and Michael Nauenberg. Degenerate systems and mass singularities. Physical Review, 133(6B):B1549, 1964.

[23] Martinus Veltman et al. Regularization and renormalization of gauge fields. Nuclear Physics B, 44(1):189–213, 1972.

[24] Wolfgang Pauli and Felix Villars. On the invariant regularization in relativistic quantum theory. Reviews of Modern Physics, 21(3):434, 1949.

[25] CG Bollini and JJ Giambiagi. Dimensional renorinalization: The number of dimensions as a regularizing parameter. Il Nuovo Cimento B (1971-1996), 12(1):20–26, 1972.

[26] Kenneth G Wilson and John Kogut. The renormalization group and the ϵ expansion. Physics Reports, 12(2):75–199, 1974.

[27] M Böhm, H Spiesberger, and W Hollik. On the 1-loop renormalization of the electroweak standard model and its application to leptonic processes. Fortschritte der Physik, 34(11):687–751, 1986.

[28] Ansgar Denner. Techniques for the calculation of Electroweak radiative corrections at the one-loop level and results for W-physics at LEP 200. Fortschritte der Physik, 41(4):307–420, 1993.

[29] Gerard't Hooft. Dimensional regularization and the renormalization group. Nuclear Physics: B, 61:455–468, 1973.

[30] William A. Bardeen, A. J. Buras, D. W. Duke, and T. Muta. Deep inelastic scattering beyond the leading order in asymptotically free gauge theories. Phys. Rev., D18:3998, 1978.

[31] Georges Aad, T Abajyan, B Abbott, J Abdallah, S Abdel Khalek, AA Abdelalim, O Abdinov, R Aben, B Abi, M Abolins, et al. Observation of a new particle in the search for the Standard Model Higgs boson with the ATLAS detector at the LHC. Physics Letters B, 716(1):1–29, 2012.

[32] Serguei Chatrchyan, Vardan Khachatryan, Albert M Sirunyan, Armen Tumasyan, Wolfgang Adam, Ernest Aguilo, T Bergauer, M Dragicevic, J Erö, C Fabjan, et al. Observation of a new boson at a mass of 125 GeV with the CMS experiment at the LHC. Physics Letters B, 716(1):30–61, 2012.

[33] Brian Henning, Xiaochuan Lu, and Hitoshi Murayama. How to use the Standard Model effective field theory. Journal of High Energy Physics, 2016(1):23, 2016.

[34] Ta-Pei Cheng, Ling-Fong Li, and Ta-Pei Cheng. Gauge theory of elementary particle physics. 1984.

[35] Steven Weinberg. Baryon-and lepton-nonconserving processes. Physical Review Letters, 43(21):1566, 1979.

[36] Bohdan Grzadkowski, M Iskrzyński, Mikolaj Misiak, and Janusz Rosiek. Dimension-six terms in the standard model lagrangian. Journal of High Energy Physics, 2010(10):85, 2010.

[37] Stephen P Martin. A supersymmetry primer. Adv. Ser. Direct. High Energy Phys, 21(515):1–153, 2010.

[38] Paul Langacker. Grand unified theories and proton decay. Physics Reports, 72(4):185–385, 1981.

[39] Nima Arkani-Hamed, Gordon L Kane, Jesse Thaler, and Lian-Tao Wang. Supersymmetry and the LHC inverse problem. Journal of High Energy Physics, 2006(08):070, 2006.

[40] Jay Hubisz, Joseph Lykken, Maurizio Pierini, and Maria Spiropulu. Missing energy look-alikes with 100 pb^{-1} at the CERN LHC. Physical Review D, 78(7):075008, 2008.

[41] Andreas Albert, Martin Bauer, Jim Brooke, Oliver Buchmueller, David G Cerdeño, Matthew Citron, Gavin Davies, Annapaola de Cosa, Albert De Roeck, Andrea De Simone, et al. Towards the next generation of simplified Dark Matter models. Physics of the dark universe, 16:49–70, 2017.

[42] Jalal Abdallah, Henrique Araujo, Alexandre Arbey, Adi Ashkenazi, Alexander Belyaev, Joshua Berger, Celine Boehm, Antonio Boveia, Amelia Brennan, Jim Brooke, et al. Simplified models for dark matter searches at the LHC. Physics of the Dark Universe, 9:8–23, 2015.

[43] Hao Zhang, Qing-Hong Cao, Chuan-Ren Chen, and Chong Sheng Li. Effective dark matter model: relic density, CDMS II, Fermi LAT and LHC. Journal of High Energy Physics, 2011(8):18, 2011.

[44] Maria Beltran, Dan Hooper, Edward W Kolb, Zosia AC Krusberg, and Tim M-P Tait. Maverick dark matter at colliders. Journal of High Energy Physics, 2010(9):37, 2010.

[45] Jessica Goodman, Masahiro Ibe, Arvind Rajaraman, William Shepherd, Tim MP Tait, and Hai-Bo Yu. Constraints on light Majorana dark matter from colliders. Physics Letters B, 695(1):185–188, 2011.

[46] LJ Hall and Lisa Randall. Weak-scale effective supersymmetry. Physical review letters, 65(24):2939, 1990.

[47] B Sekhar Chivukula and Howard Georgi. Composite-technicolor standard model. Physics Letters B, 188(1):99–104, 1987.

[48] Andrzej J Buras, P Gambino, M Gorbahn, S Jäger, and L Silvestrini. Universal unitarity triangle and physics beyond the standard model. Physics Letters B, 500(1-2):161–167, 2001.

[49] Giudice D'Ambrosio, GF Giudice, G Isidori, and A Strumia. Minimal flavour violation: An effective field theory approach. Nuclear Physics B, 645(1-2):155–187, 2002.

[50] AA Abdo, Markus Ackermann, Marco Ajello, B Anderson, WB Atwood, M Axelsson, Luca Baldini, J Ballet, Guido Barbiellini, D Bastieri, et al. Fermi large area telescope measurements of the diffuse gamma-ray emission at intermediate galactic latitudes. Physical Review Letters, 103(25):251101, 2009.

[51] Alessandro Cesarini, Francesco Fucito, Andrea Lionetto, Aldo Morselli, and Piero Ullio. The galactic center as a dark matter gamma-ray source. Astroparticle Physics, 21(3):267–285, 2004.

[52] Tim Linden. The characterization of the Gamma-Ray signal from the central Milky Way: A compelling case for annihilating Dark Matter. In AAS/High Energy Astrophysics Division, volume 14, 2014.

[53] Prateek Agrawal, Brian Batell, Patrick J Fox, and Roni Harnik. WIMPs at the galactic center. Journal of Cosmology and Astroparticle Physics, 2015(05):011, 2015.

[54] Francesca Calore, Ilias Cholis, Christopher McCabe, and Christoph Weniger. A tale of tails: dark matter interpretations of the fermi GeV excess in light of background model systematics. Physical Review D, 91(6):063003, 2015.

[55] Céline Bœhm, Matthew J Dolan, and Christopher McCabe. Interpretation of the galactic center excess of gamma rays with heavier dark matter particles. Physical Review D, 90(2):023531, 2014.

[56] Céline Bœhm, Matthew J Dolan, Christopher McCabe, Michael Spannowsky, and Chris J Wallace. Extended gamma-ray emission from Coy Dark Matter. Journal of Cosmology and Astroparticle Physics, 2014(05):009, 2014.

[57] Asher Berlin, Dan Hooper, and Samuel D McDermott. Simplified dark matter models for the galactic center gamma-ray excess. Physical Review D, 89(11):115022, 2014.

[58] Dan Hooper. Z mediated dark matter models for the Galactic Center gamma-ray excess. Physical Review D, 91(3):035025, 2015.

[59] Oliver Buchmüller, Matthew J Dolan, and Christopher McCabe. Beyond effective field theory for dark matter searches at the LHC. Journal of High Energy Physics, 2014(1):25, 2014.

[60] Oliver Buchmueller, Matthew J Dolan, Sarah A Malik, and Christopher McCabe. Characterising dark matter searches at colliders and direct detection

experiments: vector mediators. Journal of High Energy Physics, 2015(1):37, 2015.

[61] Sarah A Malik, Christopher McCabe, Henrique Araujo, Alexander Belyaev, Céline Bœhm, Jim Brooke, Oliver Buchmueller, Gavin Davies, Albert De Roeck, Kees de Vries, et al. Interplay and characterization of dark matter searches at colliders and in direct detection experiments. Physics of the Dark Universe, 9:51–58, 2015.

[62] Matthew R Buckley, David Feld, and Dorival Goncalves. Scalar simplified models for dark matter. Physical Review D, 91(1):015017, 2015.

[63] Philip Harris, Valentin V Khoze, Michael Spannowsky, and Ciaran Williams. Constraining dark sectors at colliders: beyond the effective theory approach. Physical Review D, 91(5):055009, 2015.

[64] Qian-Fei Xiang, Xiao-Jun Bi, Peng-Fei Yin, and Zhao-Huan Yu. Searches for dark matter signals in simplified models at future hadron colliders. Physical Review D, 91(9):095020, 2015.

[65] Ulrich Haisch and Emanuele Re. Simplified dark matter top-quark interactions at the LHC. Journal of High Energy Physics, 2015(6):78, 2015.

[66] Jonathan Kozaczuk and Travis AW Martin. Extending LHC coverage to light pseudoscalar mediators and coy dark sectors. Journal of High Energy Physics, 2015(4):46, 2015.

[67] Nathaniel Craig, Francesco D'Eramo, Patrick Draper, Scott Thomas, and Hao Zhang. The hunt for the rest of the Higgs bosons. Journal of High Energy Physics, 2015(6):137, 2015.

[68] Mirkoantonio Casolino, Trisha Farooque, Aurelio Juste, Tao Liu, and Michael Spannowsky. Probing a light CP-odd scalar in di-top-associated production at the LHC. The European Physical Journal C, 75(10):498, 2015.

[69] Lev Davidovich Landau. On the angular momentum of a system of two photons. In Dokl. Akad. Nauk Ser. Fiz., volume 60, pages 207–209, 1948.

[70] Chen-Ning Yang. Selection rules for the dematerialization of a particle into two photons. Physical Review, 77(2):242, 1950.

[71] Peter Cox, Anibal D Medina, Tirtha Sankar Ray, and Andrew Spray. Novel collider and dark matter phenomenology of a top-philic Z. Journal of High Energy Physics, 2016(6):1–28, 2016.

[72] LHC searches for heavy neutral Higgs bosons with a top jet substructure analysis, author=Chen, Ning and Li, Jinmian and Liu, Yandong, journal=Physical Review D, volume=93, number=9, pages=095013, year=2016, publisher=APS.

[73] Stefania Gori, Ian-Woo Kim, Nausheen R Shah, and Kathryn M Zurek. Closing the wedge: search strategies for extended Higgs sectors with heavy flavor final states. Physical Review D, 93(7):075038, 2016.

[74] Nathaniel Craig, Jan Hajer, Ying-Ying Li, Tao Liu, and Hao Zhang. Heavy Higgs bosons at low tan β: from the LHC to 100 TeV. Journal of High Energy Physics, 2017(1):18, 2017.

[75] Chiara Arina, Mihailo Backović, Eric Conte, Benjamin Fuks, Jun Guo, Jan Heisig, Benoît Hespel, Michael Krämer, Fabio Maltoni, Antony Martini, et al. A comprehensive approach to dark matter studies: exploration of simplified top-philic models. Journal of High Energy Physics, 2016(11):111, 2016.

[76] Matthew R Buckley and Dorival Gonçalves. Boosting the direct CP measurement of the Higgs-Top coupling. Physical review letters, 116(9):091801, 2016.

[77] Matthew R Buckley and Dorival Goncalves. Constraining the strength and CP structure of dark production at the LHC: The associated top-pair channel. Physical Review D, 93(3):034003, 2016.

[78] Gregory Mahlon and Stephen Parke. Angular correlations in top quark pair production and decay at hadron colliders. Physical Review D, 53(9):4886, 1996.

[79] Ulrich Haisch, Anthony Hibbs, and Emanuele Re. Determining the structure of dark-matter couplings at the LHC. Physical Review D, 89(3):034009, 2014.

[80] Federico Demartin, Fabio Maltoni, Kentarou Mawatari, Ben Page, and Marco Zaro. Higgs characterisation at NLO in QCD: CP properties of the top-quark Yukawa interaction. The European Physical Journal C, 74(9):3065, 2014.

[81] Mihailo Backović, Michael Krämer, Fabio Maltoni, Antony Martini, Kentarou Mawatari, and Mathieu Pellen. Higher-order QCD predictions for dark matter production at the LHC in simplified models with s-channel mediators. The European Physical Journal C, 75(10):482, 2015.

[82] John Ellis, Dae Sung Hwang, Kazuki Sakurai, and Michihisa Takeuchi. Disentangling Higgs-top couplings in associated production. Journal of High Energy Physics, 2014(4):4, 2014.

[83] Daniele Alves, Nima Arkani-Hamed, Sanjay Arora, Yang Bai, Matthew Baumgart, Joshua Berger, Matthew Buckley, Bart Butler, Spencer Chang, Hsin-Chia Cheng, et al. Simplified models for LHC new physics searches. Journal of Physics G: Nuclear and Particle Physics, 39(10):105005, 2012.

[84] Matthew J Dolan, Philip Harris, Martin Jankowiak, and Michael Spannowsky. Constraining CP-violating Higgs sectors at the LHC using gluon fusion. Physical Review D, 90(7):073008, 2014.

[85] Adam Alloul, Neil D Christensen, Céline Degrande, Claude Duhr, and Benjamin Fuks. FeynRules 2.0A complete toolbox for tree-level phenomenology. Computer Physics Communications, 185(8):2250–2300, 2014.

[86] Johan Alwall, R Frederix, S Frixione, V Hirschi, Fabio Maltoni, Olivier Mattelaer, H-S Shao, T Stelzer, P Torrielli, and M Zaro. The automated computation of tree-level and next-to-leading order differential cross sections, and their matching to parton shower simulations. Journal of High Energy Physics, 2014(7):79, 2014.

[87] Celine Degrande, Claude Duhr, Benjamin Fuks, David Grellscheid, Olivier Mattelaer, and Thomas Reiter. UFO–the universal FeynRules output. Computer Physics Communications, 183(6):1201–1214, 2012.

[88] Patrick De Causmaecker, Raymond Gastmans, Walter Troost, and Tai Tsun Wu. Multiple bremsstrahlung in gauge theories at high energies (i). general formalism for quantum electrodynamics. Nuclear Physics B, 206(1):53–60, 1982.

[89] Glennys R Farrar and Filippo Neri. How to calculate 35 640 O(α^5) feynman diagrams in less than an hour. Physics Letters B, 130(1-2):109–114, 1983.

[90] Frits A Berends and W Giele. The six-gluon process as an example of Weyl-van der Waerden spinor calculus. Nuclear Physics B, 294:700–732, 1987.

[91] Hermann Weyl. The theory of groups and quantum mechanics. Courier Corporation, 1950.

[92] Sérgio Ferraz Novaes and D Spehler. Weyl-van der Waerden spinor technique for spin-32 fermions. Nuclear Physics B, 371(3):618–636, 1992.

[93] Gregory Mahlon and Stephen J Parke. Spin correlation effects in top quark pair production at the LHC. Physical Review D, 81(7):074024, 2010.

[94] Niccolo Moretti, Petar Petrov, Stefano Pozzorini, and Michael Spannowsky. Measuring the signal strength in ttH with $H \to bb$. Physical Review D, 93(1):014019, 2016.

[95] Torbjörn Sjöstrand, Stephen Mrenna, and Peter Skands. PYTHIA 6.4 physics and manual. Journal of High Energy Physics, 2006(05):026, 2006.

[96] J De Favereau, Christophe Delaere, Pavel Demin, Andrea Giammanco, Vincent Lemaitre, Alexandre Mertens, Michele Selvaggi, Delphes 3 Collaboration, et al. DELPHES 3: a modular framework for fast simulation of a generic collider experiment. Journal of High Energy Physics, 2014(2):57, 2014.

[97] Matteo Cacciari, Gavin P Salam, and Gregory Soyez. The anti-kt jet clustering algorithm. Journal of High Energy Physics, 2008(04):063, 2008.

[98] Thomas Junk. Confidence level computation for combining searches with small statistics. Nuclear Instruments and Methods in Physics Research Section A: Accelerators, Spectrometers, Detectors and Associated Equipment, 434(2-3):435–443, 1999.

[99] Georges Aad, B Abbott, J Abdallah, O Abdinov, R Aben, M Abolins, OS AbouZeid, H Abramowicz, H Abreu, R Abreu, et al. Study of the spin and parity of the Higgs boson in diboson decays with the ATLAS detector. The European Physical Journal C, 75(10):476, 2015.

[100] Vardan Khachatryan, AM Sirunyan, Armen Tumasyan, Wolfgang Adam, Thomas Bergauer, M Dragicevic, J Erö, M Friedl, R Frühwirth, VM Ghete, et al. Constraints on the spin-parity and anomalous HVV couplings of the Higgs boson in proton collisions at 7 and 8 TeV. Physical Review D, 92(1):012004, 2015.

[101] J Elias-Miró, JR Espinosa, E Masso, and A Pomarol. Renormalization of dimension-six operators relevant for the Higgs decays $h \to \gamma\gamma, \gamma Z$. Journal of High Energy Physics, 2013(8):33, 2013.

[102] J Elias-Miro, JR Espinosa, E Masso, and A Pomarol. Higgs windows to new physics through $D = 6$ operators: constraints and one-loop anomalous dimensions. Journal of High Energy Physics, 2013(11):66, 2013.

[103] Joan Elias-Miró, Christophe Grojean, Rick S Gupta, and David Marzocca. Scaling and tuning of EW and Higgs observables. Journal of High Energy Physics, 2014(5):19, 2014.

[104] Elizabeth E Jenkins, Aneesh V Manohar, and Michael Trott. Renormalization group evolution of the standard model dimension six operators. i: formalism and λ dependence. Journal of High Energy Physics, 2013(10):87, 2013.

[105] Elizabeth E Jenkins, Aneesh V Manohar, and Michael Trott. Renormalization group evolution of the standard model dimension six operators ii: Yukawa dependence. Journal of High Energy Physics, 2014(1):35, 2014.

[106] Rodrigo Alonso, Elizabeth E Jenkins, Aneesh V Manohar, and Michael Trott. Renormalization group evolution of the standard model dimension six operators iii: gauge coupling dependence and phenomenology. Journal of High Energy Physics, 2014(4):1–47, 2014.

[107] Rodrigo Alonso, Hsi-Ming Chang, Elizabeth E Jenkins, Aneesh V Manohar, and Brian Shotwell. Renormalization group evolution of dimension-six baryon number violating operators. Physics Letters B, 734:302–307, 2014.

[108] Rhorry Gauld, Benjamin D Pecjak, and Darren J Scott. One-loop corrections to $h \to bb$ and $h \to \tau\tau$ decays in the Standard Model Dimension-6 EFT: four-fermion operators and the large-mt limit. Journal of High Energy Physics, 2016(5):80, 2016.

[109] Laure Berthier and Michael Trott. Towards consistent electroweak precision data constraints in the SMEFT. Journal of High Energy Physics, 2015(5):24, 2015.

[110] Bernd A Kniehl and Apostolos Pilaftsis. Mixing renormalization in Majorana neutrino theories. Nuclear Physics B, 474(2):286–308, 1996.

[111] Mathias Butenschön, Frank Fugel, and Bernd A Kniehl. Two-loop electroweak correction of $\mathcal{O}(G_F M_t^2)$ to the Higgs-boson decay into photons. Nuclear Physics B, 772(1-2):25–48, 2007.

[112] Thomas Hahn. Generating Feynman diagrams and amplitudes with FeynArts 3. Computer Physics Communications, 140(3):418–431, 2001.

[113] Thomas Hahn and M Perez-Victoria. Automated one-loop calculations in four and D dimensions. Computer Physics Communications, 118(2-3):153–165, 1999.

[114] Giampiero Passarino and M Veltman. One-loop corrections for e^+e^- annihilation into $\mu^+\mu^-$ in the weinberg model. Nuclear Physics B, 160(1):151–207, 1979.

[115] A Sirlin. Radiative corrections in the $SU(2)_L \times U(1)$ theory: a simple renormalization framework. Physical Review D, 22(4):971, 1980.